HHS Public Access

Author manuscript

Chem Soc Rev. Author manuscript; available in PMC 2022 July 05.

Published in final edited form as:

Chem Soc Rev. 2021 July 05; 50(13): 7436–7495. doi:10.1039/d0cs01096k.

NBD-based synthetic probes for sensing small molecules and proteins: design, sensing mechanisms and biological applications

Chenyang Jiang[†,a], **Haojie Huang**[†,a], **Xueying Kang**[†,a], **Liu Yang**[†,b], **Zhen Xi**[c], **Hongyan Sun**[b,d], **Michael D. Pluth**[e], **Long Yi**[a]

[a]State Key Laboratory of Organic–Inorganic Composites and Beijing Key Lab of Bioprocess, Beijing University of Chemical Technology (BUCT), Beijing 100029, China.

[b]Department of Chemistry and Center of Super-Diamond and Advanced Films (COSDAF), City University of Hong Kong, 83 Tat Chee Avenue, Kowloon, Hong Kong, China.

[c]State Key Laboratory of Elemento-Organic Chemistry and Department of Chemical Biology, College of Chemistry, National Pesticide Engineering Research Center, Collaborative Innovation Center of Chemical Science and Engineering, Nankai University, Tianjin 300071, China.

[d]Key Laboratory of Biochip Technology, Biotech and Health Centre, Shenzhen Research Institute of City University of Hong Kong, Shenzhen 518057, China

[e]Department of Chemistry and Biochemistry, Materials Science Institute, Knight Campus for Accelerating Scientific Impact, Institute of Molecular Biology, University of Oregon, Eugene, OR 97403, USA.

Abstract

Compounds with a nitrobenzoxadiazole (NBD) skeleton exhibit prominent useful properties including environmental sensitivity, high reactivity toward amines and biothiols (including H_2S) accompanied by distinct colorimetric and fluorescent changes, fluorescence-quenching ability, and small size, all of which facilitate biomolecular sensing and self-assembly. Amines are important biological nucleophiles, and the unique activity of NBD ethers with amines has allowed for site-specific protein labelling and for the detection of enzyme activities. Both H_2S and biothiols are involved in a wide range of physiological processes in mammals, and misregulation of these small molecules is associated with numerous diseases including cancers. In this review, we focus on NBD-based synthetic probes as advanced chemical tools for biomolecular sensing. Specifically, we discuss the sensing mechanisms and selectivity of the probes, the design strategies for multi-reactable multi-quenching probes, and the associated biological applications of these important constructs. We also highlight self-assembled NBD-based probes and outline future directions for NBD-based chemosensors. We hope that this comprehensive review will

zhenxi@nankai.edu.cn, hongysun@cityu.edu.hk, pluth@uoregon.edu, yilong@mail.buct.edu.cn.
[†]These authors contributed equally to this work

Conflicts of interest

The authors declare no competing financial interests.

facilitate the development of future probes for investigating and understanding different biological processes and aid the development of potential theranostic agents.

1. Introduction

4-Chloro-7-nitro-2,1,3-benzoxadiazole (NBD-Cl) was first developed by Ghosh and Whitehouse as a fluorogenic reagent for sensing amino acids and other amines in 1968.[1] Since then, compounds with an NBD skeleton have been widely employed for various applications in biochemistry and chemical biology.[2–5] The emission wavelength of *N*-monoalkyl NBD amines (NBD-NHR) is typically above 420 nm,[6–8] and the fluorescence derives from intramolecular charge transfer (ICT) transitions.[9] In NBD-NHR compounds, the amino group and the strong electron-withdrawing nitro group are the ICT donor and acceptor, respectively. In general, donor–acceptor (or push–pull) type dipolar fluorophores emit strongly in organic solvents but poorly in aqueous media.[10] Furthermore, hydrogen bonding between the 2-oxa-1,3-diazole of NBD and water molecules can provide nonradiative deactivation pathways, which often results in lower quantum yields (Φ) for NBD-NHR species in aqueous solution.[11] The water-solubility, environmental sensitivity, and small size of NBD-NHR fluorophores provide prominent advantages that facilitate biomolecular interactions[12] and self-assembly[13] in buffers and even in live systems.

For other NBD derivatives, the emission properties largely depend on the ICT donors (Fig. 1). For example, both NBD-Cl and oxygen-substituted ethers (NBD-OR) are non-fluorescent due to the poor inductive electron-donating ability of Cl and O atoms. The sulfur-substituted thioether (NBD-SR) and aryl-substituted amines (NBD-NHAr) also contain poor electron-donating groups, and exhibit very weak fluorescence.[14] NBD-based *N,N*-dialkyl-substituted amines (NBD-NRR′) can be partly protonated at physiological pH (*e.g.* the pK_a of 1-methyl piperizine is ~9),[15] which leads to relatively weak ICT and a corresponding weak fluorescence.[16,17] For example, the quantum yield of NBD-NMe_2 (Φ = 0.008) in water is much lower than that of NBD-NHMe (Φ = 0.04).[11] Therefore, these NBD derivatives can be used as quenching groups in probe design because of their inherent weak fluorescence and the fluorescent quenching ability of the NBD nitro group. In NBD-based compounds, the strong electron-withdrawing nitro group increases the electrophilicity of the carbon at the 4-position. As a result, NBD derivatives with suitable leaving groups can undergo nucleophilic aromatic substitution (S_NAr) reactions with nucleophiles to ligate the NBD fluorophore to the reactive nucleophile. This general approach has been leveraged to develop different sensing motifs for biological nucleophiles.

Species like NBD-X (X = F, Cl, Br) are highly reactive toward amines,[4,18] thiols,[19] cysteine sulfenic acids,[20] and tyrosine hydroxyl groups.[21] These reactions are typically accompanied by distinct colorimetric and/or fluorescent changes. Specific examples and classes of these types of reactivity will be covered in detail later in this review. Highlighting the versatility of NBD-based systems to differentiate between different nucleophiles and provide different optical outcomes, we highlight a few introductory examples here. For example, NBD electrophiles can react with biological nucleophiles to give different responses (Fig. 2). Although both contain sulfhydryl groups, RSH and H_2S nucleophiles react with NBD-

Cl or NBD-SR compounds to give different optical responses, with H_2S generating a characteristic purple color due to the formation of NBD-SH.[22] More generally, NBD-OR and NBD-NRR′ species also show high reactivity toward biothiols (including H_2S) and amines, resulting in distinct colorimetric and fluorescent changes (Fig. 2).[23–25] In addition, NBD-O/SR motifs are specially designed to differentiate between biothiols by leveraging the S-to-N intramolecular Smiles rearrangement after initial S_NAr substitution.[24,25] These simple examples highlight the ability of NBD-based systems to differentiate between SH and NH nucleophiles in complex systems. In addition, significant progress has been made in fluorogenic enzyme assays[26] and in site-specific protein labelling[27] based on the transformation of non-fluorescent NBD-OR to fluorescent NBD-NHR derivatives. In total, NBD-based synthetic probes have been widely used for sensing specific small molecules and proteins and constitute an important class of small molecule chromophores used for biological investigations.

We note that general approaches for biolabelling using NBD-Cl were reviewed previously in reviews published between 1994 and 2008.[3–5] More focused reviews on the thiolysis of NBD amines and ethers[28] and NBD dyes for H_2S sensing have been reported more recently,[29] but these reviews do not cover the broader design strategies of the NBD-based synthetic probes. In addition, significant progress related to NBD-based tool development has occurred in the last decade, which includes broad areas ranging from protein and small molecule sensing to self-assembly, which have not been reviewed comprehensively. In the present review, we provide an in-depth coverage of NBD-based synthetic probes as five major sections: (1) H_2S-specific probes based on cleavage of C–N bonds; (2) thiol probes based on cleavage of C–O/S/Se bonds; (3) multi-reactable multi-quenching probes; (4) probes for sensing or labelling proteins; (5) self-assembled probes. We also highlight and compare the sensing mechanisms and properties of different NBD-based probes, and suggest key future directions and unmet needs for NBD-based chemosensors. We anticipate that this review will help readers gain a clear understanding of contemporary design strategies, sensing mechanisms, and potential applications of NBD-based synthetic probes in chemical biology and materials science.

2. NBD-Based H_2S probes based on cleavage of C–N bonds

H_2S is the third gasotransmitter along with NO and CO and is involved in many physiological and pathological processes.[30–34] Endogenous H_2S in mammals can be enzymatically produced from Cys and Hcy by the primary enzymes cystathionine γ-lyase (CSE), cystathionine-β-synthase (CBS) and 3-mercaptopyruvate sulfurtransferase (3-MST)/cysteine aminotransferase (CAT).[35–39] Low levels of H_2S show cytoprotective effects,[30,32] whereas high concentrations of H_2S are cytotoxic.[40,41] As an example of these activities, up-regulation of H_2S levels in the liver is related to TNF-α-induced insulin resistance and aggravates diabetes.[42] Endogenous H_2S or low level of exogenous H_2S can exhibit pro-cancer effects, whereas exposure to higher levels of H_2S for long periods can lead to cancer cell death.[43–45] Colon cancer and ovarian cancer cells are reported to overexpress CBS to produce H_2S, which contributes to tumor growth, proliferation, angiogenesis and vasodilation, thereby providing blood and nutrients to the tumor.[46–50] CSE is overexpressed in breast cancer and gastric cancer cells, leading to the proliferation and migration

of cancer cells.[51–53] Due to its complex activities in many diseases, the physiological characteristics of H_2S and the molecular mechanisms by which H_2S is involved need further thorough investigation. Taken together these activities support the need for development and refinement of chemical tools for H_2S detection *in vivo* or in related complex environments.[28,29,34]

Many different research groups have developed chemical tools to investigate H_2S, and a number of these tools are based on NBD chromophores. For example, Pluth and co-workers demonstrated that NBD-Cl and related NBD-derived electrophiles reacted with H_2S to form both $(NBD)_2S$ and NBD-SH and characterized the mechanism of the reactions.[22] The efficacy of these NBD probes was demonstrated in buffer and serum with associated submicromolar detection limits. Furthermore, the formation of the purple of NBD-SH enables the colorimetric detection of H_2S by the naked eye (Fig. 3). In 2013, Yi and coworkers designed a fluorescence resonance energy transfer (FRET) probe (Fig. 4) that is cleavaged by H_2S to produce fluorescent coumarin[23] and colorimetric NBD-SH.[22] Consequently, we as well as others reported a series of fluorescent probes *via* H_2S-specific thiolysis of NBD amines.[54–80] The following sections highlight the sensing mechanisms, design strategies, and biological applications of these NBD-based H_2S probes.

2.1 Probes with emission wavelength shorter than NBD

For fluorescent probes with emission wavelength shorter than NBD, both FRET and photo-induced electron transfer (PET) mechanisms can quench the fluorophore. In these systems, the NBD moiety acts as both the FRET acceptor and the PET quencher (Fig. 4a). Normally, these probes exhibit a large off–on response upon activation because of the dual FRET-PET quenching effects, which significantly reduces the background fluorescence in the off state.

As an example of this approach, Yi, Xi, and coworkers developed H_2S probe **1**, which was the first such probe based on C–N bond cleavage.[23] Probe **1** has a Stokes shift, limit of detection (LOD), and fluorescent turn-on of 75 nm, 9 μM, and 45-fold at 480 nm, respectively. The product amine **1a**, which is released after the reaction with H_2S, has a relatively low quantum yield ($\Phi < 0.02$). Xi, Yi, and coworkers optimized this system by using density functional theory (DFT) calculations to rationally design julolidine-fused coumarin-NBD probe **2** (Fig. 4b).[54] When compared with **1**, the second-generation probe **2** demonstrates a larger fluorescence enhancement (200-fold at 496 nm), lower LOD (0.9 μM), and longer fluorescence life-time (τ) of the amine product **2a** (6.27 ns compared 3.53 ns of **1a**). Moreover, **2** demonstrates excellent selectivity for H_2S over competing analytes and showed good biocompatibility. This probe was successfully employed to image H_2S in live cells and zebrafish. These examples highlight the ability to tune the different components of NBD-based systems to generate a brighter fluorophore (**2a**, $\Phi = 0.81$) to enhance the properties of NBD-based H_2S probes.

The connection between the NBD-piperazinyl moiety and other fluorophores was modified to generate fluorescent probes **3–13** (Fig. 4c). When the emission of the ligated fluorophore does not overlap with the NBD emission profile, these compounds produce a ratiometric response to H_2S.[29] For example, You, Sun, and coworkers developed ratiometric probe **3** based on acridone and NBD fluorophores. Probe **3** exhibited a significant enhancement in

emission ratio (F_{427}/F_{552}), which was accompanied by a visual color change (yellow to blue under UV light) in the presence of micromolar H_2S (Fig. 4).[55] Probe **3** also has excellent selectivity and a low LOD (0.19 μM), which was successfully used for detecting H_2S in different samples including monosodium glutamate, beer, and environmental water as well as bioimaging in *Daphnia magna* organisms.[55]

The high energy excitation of **3** (380 nm) may be phototoxic to live systems, but related two-photon (TP) probes that are excited with near-infrared (NIR) light are also available. The TP approach allows for deeper penetration and less photodamage in biosamples[56,57] and has emerged as an important tool for *in vivo* 3D imaging in biomedical research. To this end, the NBD-based TP probe **4**, which has a TP excitation at 780 nm, was developed by Jiang and Tang for detection of H_2S in live cells.[58] Probe **4** is highly selective for H_2S, displays a 29-fold off–on response at 468 nm, has a LOD of 24 nM, and functions over the pH range 6.0–9.0. The TP cross section ($\Phi\delta$) of **4** upon reaction with H_2S is about 40 GM at 780 nm, which is comparable to other small-molecule TP probes.[56]

Romieu and coworkers reported water-soluble NBD-based probe **5**, which uses 3-(2-benzimidazolyl)-7-hydroxycoumarin as the fluorophore.[59] Probe **5** was reported to react with S^{2-} and SO_3^{2-} but not with NaSH in pH 7.4 buffer. This reported selectivity toward S^{2-} over HS^- is likely incorrect because both Na_2S and NaSH equilibrate to the same sulfide species in solution (~80% HS^- and 20% H_2S in aqueous buffer (pH 7.4)).[60] Moreover, in a recent thorough analysis May and coworkers highlighted that free S^{2-} does not exist in aqueous solution.[61] In addition, other NBD-based probes show high selectivity for HS^- over SO_3^{2-},[62–64] which brings into question the reported selectivity for **5**.[59] For example, water-soluble probe **6**, which is the click product of alkyne-containing NBD and azido-coumarin,[62] rapidly reacts with H_2S using either Na_2S or NaSH in buffer (pH 7.4) as expected. The selectivity studies of **6** demonstrate reactivity with H_2S even in the presence of SO_3^{2-}/HSO_3^-. Importantly, this probe was used to monitor H_2O_2-induced H_2S generation in yeast cells for the first time.

In addition to blue and cyan coumarins, green-emitting fluorophores including fluorescein and phthalimide have also been used to develop NBD-based H_2S probes.[63,64] Yi, Xi, and coworkers developed fluorescein-NBD probe **7**, which demonstrates high selectivity toward H_2S with a 65-fold off–on fluorescence response at 530 nm upon reaction with H_2S.[63] When HEK293 cells were treated with exogenous H_2O_2 followed by probe **7**, a fluorescent increase was observed, implying that H_2O_2 could induce endogenous H_2S production. Similarly, Sureshkumar and coworkers designed H_2S-specific fluorescent probe **8** using a napthalimide scaffold.[64] Probe **8** is highly specific for sulfide over sulfite, sulfate, and biothiols, and exhibits a 36-fold off–on response at 540 nm with a LOD of 0.016 μM. Probe **8** was successfully applied for monitoring H_2S in various water samples.

Endogenous small molecules are generated in many organelles, including the lysosome, mitochondria, and endoplasmic reticulum (ER). These organelles can be readily targeted by different strategies to deliver small-molecule probes to these subcellular localles.[65–67] The thiolysis of NBD amines has also been employed to develop the organelle-targeted H_2S fluorescent probes **9–13** (Fig. 4c). This design strategy depends on the conjugation

of both an organelle-targetable moiety and an NBD amine onto one fluorophore. Yi, Xi, and coworkers developed ratiometric fluorescent probe **9** for visualization of H_2S in lysosomes using an appended morpholine group.[68] Probe **9** demonstrates a 300-fold ratiometric fluorescence increase (F_{415}/F_{560}) and a 49-fold intensity enhancement at 415 nm upon reaction with H_2S. Lysosome-targeted probe **9** is water-soluble, highly selective, and non-cytotoxic. Li and coworkers reported TP fluorescent probe **10** that employs a dual lock system (dual PET process and dual reaction sites), which was also targeted to the lysosome.[69] Probe **10** demonstrates a 72-fold off–on response at 536 nm after reaction with H_2S. Accordingly, probe **10** was successfully used for precisely tracking and detecting endogenous H_2S in the lysosomes of live cells and tissue.

In 2015, Yoon and coworkers developed NBD-based probe **11** by using triphenylphosphinium (TPP) as a mitochondrial targeting moiety (Fig. 4c).[70] Probe **11** demonstrates a 68-fold fluorescence enhancement at 528 nm, a LOD of 2.46 μM, low cytotoxicity, and good selectivity towards H_2S. Similarly, the TPP-ligated probe **12** was also developed by Wei, Li, and coworkers for selective imaging of mitochondrial H_2S in live cells.[71] Probe **12** provides a ratiometric response for H_2S using a coumarin with a fluorescence signal that does not overlap with the NBD emission. The probe demonstrates high selectivity, fast response to H_2S, a 58-fold turn-on at 415 nm, low cytotoxicity, and suitability for imaging in live cells.[71]

To detect H_2S in the ER, Song, Chen, and coworkers reported NBD-based probe **13** by using the methyl sulfonamide group as the ER targeting moiety (Fig. 4c).[72] Probe **13** demonstrates high selectivity and good sensitivity for H_2S, and low cytotoxicity. Moreover, **13** can be used for imaging of H_2S in the ER of live cells, even with the relatively small fluorescence enhancement (6.5-fold) at 490 nm.[73]

Although the NBD-piperazinyl motif in many of the above probes is only minimally fluorescent at 550 nm, the turn-on dynamic range of probes **1–12** can be quite high (13–200 fold). This large fluorescence turn-on is likely due to the FRET-PET dual-quenching effects, which significantly reduce the background fluorescence of these probes in their off state. Additionally, using brighter fluorophores should further increase the observed fluorescence turn-on, which should in turn increase the sensitivity for H_2S detection. Even when the emission of the fluorophore occurs at a short wavelength and does not overlap with the NBD emission, such as in probes **3**, **9**, and **12**, a ratiometric signal is observed. Despite this useful ratiometric response, the high energy excitation wavelength required for these probes may limit their biocompatibility due to phototoxicity. Although a number of NBD-based probes have been developed with specific organelle-targeting groups, the H_2S-specific thiolysis of NBD amines normally is inefficient below pH 5.0, which may significantly reduce the efficacy of these compounds in acidic subcellular compartments.[58,70,72]

2.2 Probes with emission wavelength longer than NBD

In general, NBD-based probes with emission wavelengths longer than NBD are quenched by PET, so the distance between the fluorophore and NBD is important for controlling the quenching efficiency (Fig. 5a). For example, using rhodamine as a fluorophore, Yi, Xi, and

coworkers developed probe **14**,[74] which demonstrates a 4.5-fold fluorescence enhancement at 589 nm after reaction with H_2S and can be used to detect H_2S in live cells and mice. By converting the *N,N*-diethylamino groups of rhodamine B to azetidinyl groups, Xi, Yi, and coworkers further developed second-generation rhodamine-NBD dyad **15**, which demonstrates a 19-fold fluorescence enhancement at 585 nm upon reaction with H_2S.[63] Moreover, **15** is highly selective for H_2S, water-soluble, minimally cytotoxic and can be used to monitor mitochondrial H_2S in live cells and zebrafish.

Using the dansyl fluorophore, Yin, Liu, and coworkers developed colorimetric and turn-on fluorescent probe **16**.[75] The probe is highly selective for H_2S, water-soluble, biocompatible, and cell-permeable. Probe **16** demonstrates a 5-fold fluorescence enhancement at 594 nm and was used to detect H_2S in live cells. The relatively small turn-on response for probes **14** and **16** may be due to the fact that PET is the sole quenching mechanism in these systems.

To enhance the quenching effect, probes with direct connection of NBD to the reporting fluorophore were developed.[76,77] For example, Zhao and coworkers synthesized methylene blue-based fluorescent probe **17**, which demonstrates a 60-fold fluorescence enhancement at 684 nm after reaction with H_2S, a LOD of 0.43 μM, and is highly selective.[76] Moreover, probe **17** shows minimal cytotoxicity and can be used for cell imaging. Guo, Lv, and coworkers reported probe **18**, which combines a rhodamine moiety and NBD amine (Fig. 5b).[77] Thiolysis of the NBD amine moiety of **18** by H_2S releases the ring-opened rhodamine, leading to a 160-fold fluorescence enhancement at 565 nm and a low LOD (48 nM). Probe **18** demonstrates a fast response (k_2 = 26.7 M^{-1} s^{-1}), good selectivity for H_2S, good biocompatibility, and can be used to visualize H_2S in live cells.

Continuing to shift the emission profile toward the red region of the spectrum, NIR fluorescent probes with emission in the region of 650 to 900 nm have been developed. These probes have several advantages including high signal-to-noise ratios and deep tissue penetration.[78,79] To this end, a series of NIR H_2S probes based on the thiolysis of NBD amines have been developed.[80–85] Using a red-shifted rhodamine derivative, Yi, Xi, and coworkers developed probe **19**,[80] which demonstrates a 10-fold fluorescence enhancement at 660 nm, a fast response to H_2S (k_2 = 29.8 M^{-1} s^{-1}), and a bright fluorescence product (Φ = 0.29) after reaction with H_2S. Moreover, probe **19** is water-soluble, cell-permeable, and highly selective and sensitive for H_2S in live cells. Similarly, Jiang, Tan, and coworkers developed dicyanoisophorone-based NIR fluorescent probe **20** for H_2S detection in cancer cells and liver tissues.[81] The probe demonstrates a 19-fold fluorescence enhancement at 670 nm, a large Stokes shift (186 nm), is highly selective, and has a LOD of 0.03 μM. Compared with probes **17** and **18**, probes **19** and **20** demonstrate smaller fluorescence responses upon reaction with H_2S, which is likely due to the weaker PET effect because of the longer distance between NBD and the fluorophore.

Cyanine dyes with longer excitation and emission wavelengths have also been employed to develop NBD-based H_2S probes.[82–84] Yi, Zhang, and coworkers reported probe **21**, which demonstrates an 87-fold fluorescence enhancement at 796 nm (with excitation at 730 nm) upon reaction with H_2S.[82] Probe **21** shows high selectivity and high sensitivity toward H_2S and is water-soluble, cell-permeable, minimally cytotoxic, and can be used to monitor

endogenous H_2S in live cells and mice (Fig. 5c and d). Probe **21** was used to demonstrate that (1) D-Cys induces endogenous H_2S production to enhance angiogenesis *in vitro*; (2) D-Cys enhances H_2S production in the liver in mice; and (3) intratumoral H_2S in murine tumor models can be visualized by NIR fluorescence imaging. These results highlight that NBD-based probes can serve as efficient tools for the detection of endogenous H_2S in live animals and even for cancer diagnosis. Similarly, the Yang group and Wang group developed NIR fluorescent probes **22** and **23** for H_2S detection, which have a 50-fold enhancement at 800 nm and a 58-fold enhancement at 830 nm, respectively, upon reaction with H_2S.[83,84] Both probes have excellent selectivity for H_2S over other biologically relevant analytes and were successfully applied for NIR imaging. For example, probe **23** was successfully used to monitor D-Cys-induced H_2S production in cancer cells and mice. Based on their NIR emission, good selectivity and fluorescence response profiles, probes **21–23** are useful tools for detecting cellular H_2S in live animals.

Using a shorter distance between the fluorophore and NBD group can lead to stronger PET quenching and result in a larger turn-on fluorescence response. This design approach was clearly demonstrated by Ge, Gao, and coworkers who developed H_2S probes **24** and **25**, which are based on an azonia-cyanine skeleton.[85] Probe **24** has a 4.5-fold turn-on at 660 nm, a 178 nM LOD, and localizes to the mitochondria. Probe **25** has a 17-fold turn-on at 639 nm, a 9.6 nM LOD, and localizes to the lysosome.

In total, NBD-based probes **14–25** show very good selectivity for H_2S over competing analytes and good fluorescence enhancements in the pH range 5.0–9.0. These probes highlight two primary strategies to improve the fluorescence response, namely: (1) using bright fluorophores, and (2) reducing the distance between the fluorophore and NBD. The longer wavelength emission of the NIR probes is particularly useful for enabling H_2S detection in tissues and live mammals where greater tissue penetration is required.

2.3 Turn-off and dual-signal H_2S detection

Because NBD amines have a weak yellow fluorescence in aqueous buffer, probes that lack an attached fluorophore can be used to provide a turn-off fluorescence response as well as a colorimetric response due to formation of NBD-SH upon the reaction with H_2S (Fig. 6). Yi, Qiu, and coworkers synthesized compounds **26–34** as part of a structure–function investigation into how the amine identity impacts H_2S reactivity and selectivity.[16] The piperidyl- and piperazinyl-based NBD probes **27** and **28** react efficiently with micromolar H_2S in buffer (pH 7.4), whereas **29**, which contains a piperazinyl-based nitrobenzothiadiazole (NBD(S)), shows much slower thiolysis. Low reactivity toward H_2S was also observed for thiolysis of ethylamino-, ethanolamino- and anilino-based NBD probes (**26**, **30–33**). Acetylpiperazinyl-containing NBD **34** was used to efficiently detect H_2S by the naked eye and was also used for paper-based H_2S detection. Similarly, Yan and coworkers developed related probes **35–37** to investigate how the piperazine ring governs the reactivity and selectivity of NBD amines towards H_2S (Fig. 6b).[86] Probes **36** and **37** show no response toward H_2S, whereas probe **35** displays faster reactivity toward H_2S. These results also suggest that the piperazinyl-NBD derivatives could be used to develop turn-off H_2S

probes. In general, most NBD-NHR compounds used in biological settings should be stable due to the presence of only micromolar endogenous H_2S *in vivo*.[16,34]

Recently, Zhang, Liu, and coworkers used **38** and $[Ru(bpy)_3]^{2+}$-doped silica nanoprobes to develop a dual fluorescent and electrochemiluminescent (ECL) detection system for H_2S.[87] H_2S reacts with **38** to provide a turn-off fluorescence response and to release the secondary amine. This released amine then participates in electron transfer to Ru at the electrode surface to enhance the ECL signal. This work broadens the design strategy of NBD-based probes for H_2S detection in ECL systems.

Photoacoustic (PA) imaging combines diffusive optical and focused ultrasound detection, offering high contrast in deep tissue.[88] Because the functional imaging depth of a fluorescence-based method is relatively low, PA-based systems offer an attractive approach for *in vivo* detection of H_2S. To this end, Sun, Wang, and coworkers developed NBD-based probes **39–41** for dual-modal fluorescence and PA imaging of H_2S (Fig. 7b).[89] Probe **41** demonstrates a high fluorescence on-off response rate (k_2 = 4 M^{-1} s^{-1}) and excellent selectivity for H_2S over other biothiols, and works as an activatable PA probe because of the strong absorption of NBD-SH. Furthermore, **41** was successfully used to detect H_2S within a 1 mm depth in mice, which highlights the benefits of the PA approach. In addition, this work suggests that NBD-based probes could be used for fluorescent and PA dual-modal detection of H_2S *in vivo*.

2.4 H_2S-Triggered prodrug release

In addition to using the H_2S-specific thiolysis of NBD amines to develop fluorescent probes, the reactivity can also be used to design H_2S-triggered prodrug release because many drugs contain free amines (Fig. 8). As a proof-of-concept study, Yi, Xi, and coworkers employed NBD-capped ciprofloxacin **42** as a H_2S-triggered prodrug in 2019.[90] Activation of the prodrug by H_2S and release of ciprofloxacin (k_2 = 12.0 M^{-1} s^{-1}) are accompanied by a 62-fold fluorescence enhancement at 415 nm. The prodrug release has very good selectivity for activation by H_2S and can be used for localized release of ciprofloxacin in the presence of micromolar H_2S, which was leveraged for the effective killing of *E. coli* (Fig. 8c). The concentration-dependent inhibition of bacterial growth indicates that **42** is weakly inhibited below 0.1 μM, but the addition of H_2S or L-Cys significantly increases the observed inhibition. The minimum inhibitory concentration of the combination of **42** and H_2S (50 μM Na_2S or 5 mM L-Cys) is about 30 nM, which resulted in *E. coli* cell death within 12 h.[90] Based on the H_2S-specific thiolysis of NBD amines, it is likely that other drugs (*e.g.* norfloxacin, chloroquine, thiazide, Fig. 8d) could also be employed to develop H_2S-triggered prodrugs in the future.

3. NBD-based probes based on cleavage of C–O/S/Se bonds

3.1 Thiolysis of NBD ethers for detection of H_2S

Building from the success of thiolysis of NBD amines for H_2S detection, NBD ethers have also been used to develop H_2S-responsive probes (Fig. 9a).[24] In 2014, Yi and coworkers developed probes **43** and **44** based on dual-NBD-capped fluorescein and naphthofluorescein,

respectively. Probe **43** demonstrates over a 1000-fold fluorescence enhancement at 514 nm upon reaction with H_2S at pH 7.4, but shows relatively low selectivity towards H_2S over biothiols. Probe **44**, however, exhibits better selectivity toward H_2S over biothiols (Fig. 9b), but with a slower thiolysis rate. Probe **43** responds to H_2S over the pH range 5.9 to 8.5, whereas probe **44** responds better under weakly alkaline conditions (Fig. 9c). Comparing the chemical structures of the both probes, we surmise that the electron-withdrawing oxygen at the meta-position enhances the reactivity of the electrophilic NBD ether in **43**.[24]

A series of H_2S fluorescent probes, **45–54**, have been developed that are based on the thiolysis of NBD ethers. Building from work by Feng and coworkers who used the introduction of an aldehyde group into 2,4-dinitrophenyl (DNB) ether-based probes to enhance the reaction response toward H_2S,[91a] a similar strategy was used for the development of NBD-based H_2S probes **45** and **46**.[91b] When compared to probe **45**, probe **46** exhibits a much faster reaction with H_2S (under 60 s) (Fig. 9d). Moreover, probe **45** is unstable in solutions above pH 7.0, whereas probe **46** can function over a broader pH range. Probe **46** can also be used for imaging of H_2S in live cells with low cytotoxicity.

Using the NBD ether of 3-hydroxyflavone, Hou and coworkers developed colorimetric and fluorescent probe **47** for H_2S detection.[92] The probe demonstrates a high sensitivity and selectivity for H_2S with a large Stokes shift (146 nm). The addition of H_2S to probe **47** results in a green fluorescence and a corresponding color change from colorless to pink due to the formation of NBD-SH. Furthermore, this probe displays a rapid fluorescence response to H_2S and was used to detect H_2S in live cells.

Yang, Li, and coworkers reported TP fluorescent probe **48** by using the NBD ether of 7-hydroxycoumarin.[93] This probe demonstrates high sensitivity for H_2S (LOD: 0.12 μM) and a fast response time (about 2 min). Moreover, the probe was used to image H_2S in live cells and fresh tissues by TP confocal microscopy. In addition, probe **48** was used to measure the endogenous H_2S level in different viscera, and also to indicate the primary distribution of endogenous H_2S in the brain, liver, and lungs.

Chang and coworkers developed NBD-dansyl dyad **49** for chromogenic and fluorogenic detection of sulfide and azide anions.[94] In a water rich system (H_2O/THF = 99 : 1, v/v), probe **49** reacts primarily with hydrosulfide ions, owing to the sulfide-selective cleavage of the NBD–OSO_2Ar bond, yielding the pink-colored NBD-SH and fluorescent dansyl acid. When under water deficient conditions (H_2O/THF = 10 : 90, v/v), probe **49** reacts with both azide and sulfide anions, due to the cleavage of the NBD–OSO_2Ar bond to yield either NBD-N_3 (for azide ions) or NBD-SH (for sulfide ions). This observed impact of water on selectivity was not affected by other anions in solution.[94]

Adding to the fluorophore conjugates of NBD-based fluorescent probes, a number of BODIPY constructs have also been developed, including compounds **50–52** (Fig. 9d). BODIPY fluorophores benefit from high brightness and good photostability, and unlike fluorescein-based fluorophores are pH insensitive.[95,96] Shao and coworkers developed probe **50**, which was characterized by X-ray single-crystal analysis. Probe **50** demonstrates high sensitivity (LOD of 2.6 μM), a 150-fold fluorescence enhancement at 510 nm upon reaction

with H_2S, and a smaller response to Cys or GSH.[97] Probe **50** shows a linear response to H_2S over the 1–200 μM concentration range and was applied to image H_2S in live cells. Yin, Huo, and coworkers developed probes **51** and **52** which are based on the same BODIPY platform but contain one or two NBD motifs, respectively.[98] Probe **52** demonstrates longer excitation and emission wavelengths in the NIR range because of the larger conjugation than that of probe **51**. Probes **51** and **52** demonstrate 150-fold and 170-fold fluorescence enhancement at 587 nm and at 674 nm, respectively, and were used to image biological H_2S in cells and zebrafish.

Feng and coworkers developed NIR fluorescent probe **53** for selective detection of H_2S over biothiols.[99] Upon thiolysis of the probe by H_2S, a 40-fold fluorescence turn-on signal at 744 nm was observed with a low LOD (26 nM) and a significant Stokes shift (166 nm). Moreover, probe **53** was successfully used for bioimaging of H_2S in live cells and mice. Similarly, Zhou, Zhang, and coworkers developed NIR fluorescent probe **54**,[100a] which demonstrates a 121-fold fluorescence enhancement at 630 nm and fast response (completed within 5 min) upon reaction with H_2S. Probe **54** was used to monitor H_2S in red wine samples and to image H_2S in HeLa cells and athymic mice. Although **54** was reported to have high sensitivity toward H_2S,[100a] Sheng, Zhu, and coworkers later reported the cross-reactivity of **54** with biothiols.[100b] In this system, Cys/Hcy and GSH/H_2S can be identified by two separated fluorescence emission channels under single wavelength excitation. These results, taken together with our experiences[24,29] as well as others work in the field, suggest that thiolysis of NBD ethers does not provide the same level of specificity toward H_2S as that observed from the thiolysis of NBD amines. Considering that GSH is commonly present in millimolar intracellular levels, NBD-OR based probes should be used with caution in complex systems or *in vivo* because the fluorescence response may be due to GSH-induced thiolysis of the NBD ether rather than the desired response to H_2S.[100b]

Even without an attached fluorophore, NBD-ester/ether derivatives can also be used for colorimetric H_2S detection due to the formation of NBD-SH (Fig. 9e).[101,102] A series of simple probes **55a–55c** were developed by Chang and coworkers as sulfide- and azide-selective optical probes.[101] These probes demonstrate a colorimetric response for sulfide ions, and both chromogenic and fluorogenic signaling for azide ions by producing NBD-OH. The series of NBD-ether probes **56a–56d** was developed by Fan and coworkers for selective quantification of H_2S by LC-MS/MS.[102] The thiolysis of NBD ethers demonstrates good retention on common chromatographic columns and high instrument response. Probe **56b** was the most selective among the tested probes, whereas probe **56d** was reported to react efficiently with biothiols by Pu, Tu, and coworkers.[103] For the S_NAr substitution reaction, the aryl ether is a better leaving group than the alkyl ether. Because of this factor, alkyl-*O*-NBD **56b** should have slower thiolysis reactivity and generate higher selectivity than that of aryl-*O*-NBD **56d**. When compared with the methylene blue assay (MBA), H_2S measurement using **56b** matches the sensitivity and linearity of the MBA method, shows better selectivity, and shows higher repeatability.

Although the thiolysis of NBD ethers is less selective for H_2S than the hydrolysis of NBD amines, a number of NBD-OR based probes have very high dynamic ranges (*e.g.* over 1000-fold turn-on) due to more efficient fluorescence quenching by incorporating multiple

NBD ethers in a fluorophore. For example, probe **43** results in over a 1000-fold turn-on for H_2S. Such probes may be particularly useful for environments in which high sensitivity for H_2S is needed, especially if there are not competing thiols present. Again, we remind readers that the high levels of intracellular GSH may result in activation of NBD-OR probes,[104,105] which may complicate interpretation of the results from this class of fluorescent probes for H_2S in live organisms. However, these highly reactive NBD-OR derivatives have been used in different contexts to develop fluorescent probes for thiols as indicated below.

3.2 Thiolysis of NBD ethers for detection and differentiation of biothiols

Biothiols including GSH, Cys, and Hcy are involved in redox homeostasis as well as various mammalian physiological processes.[104] GSH is the most abundant biothiol in cells and can be generated from Cys by the consecutive actions of glutamate cysteine ligase (GCL) and GSH synthetase (GS).[106–108] Hcy is condensed with serine to generate cystathionine *via* CBS and then converted to Cys upon subsequent reaction with CSE.[109–111] Through these pathways, the concentrations of biothiols are in dynamic equilibrium in live systems, and abnormal levels of biothiols are associated with the pathology of many dieases.[112–123] For example, accumulating evidence suggests that Cys deficiency can contribute to various diseases, including stunting, lethargy, skin lesions, liver damage, and hair depigmentation,[112] whereas excess Cys is associated with diseases including rheumatoid arthritis, motor neuron disease, Parkinson's disease, and Alzheimer's disease.[113,114] Similarly, a decrease in GSH levels can cause or be related to various diseases, including neurodegenerative diseases, cystic fibrosis, cancer, liver damage, schizophrenia, and bipolar disorder.[115–120] Notably, the concentration of GSH in some tumors is known to be much higher than that in normal tissues.[121,122] Elevated Hcy levels can also endanger human health, and overaccumulation of Hcy in the blood results in hyperhomocysteinemia (HHcy).[123,124] In addition, high levels of Hcy are found in non-alcoholic fatty liver disease, coronary artery disease, early pregnancy loss, Alzheimer's disease, neural tube defects, chronic kidney disease (CKD), and bone disease.[125–134] Furthermore, the pathology of some diseases is associated with abnormal concentration of two or more different biothiols, such as liver disease[118,125] and Alzheimer's disease.[114,119,130] Based on these diverse roles, the development of chemical tools that enable the simultaneous detection and differentiation of different biothiols has applications in various disease states.

The thiolysis of NBD ethers has also been applied to differentiate and detect biothiols (Fig. 10–13). After the initial S_NAr reaction between Cys/Hcy and the NBD electrophile, the resultant NBD-thioether undergoes an intermolecular Smiles rearrangement to generate fluorescent NBD-NHR compounds. GSH or H_2S, neither of which have a pendant nucleophilic amine, reacts with NBD electrophiles but cannot undergo the subsequent intramolecular Smiles rearrangement. Therefore, they will only generate thioether products, which have different optical properties from the NBD-NHR products (Fig. 10). For example, Shao, Wang, and coworkers developed probe **57** for detection of Cys/Hcy over GSH.[135] The probe is non-fluorescent until addition of Hcy or Cys, which results in a 30-fold and 14-fold fluorescence enhancement at 542 nm for the two thiols, respectively. Using a similar approach, Hu, Wang, and coworkers developed probe **58** by fusing non-fluorescent

tetrahydro[5]-helicene and NBD for the simultaneous discrimination of Hcy/Cys, H_2S, and GSH in aqueous solution.[136] Upon reaction with H_2S, probe **58** is not fluorescent, but shows an absorbance at 548 nm corresponding to NBD-SH. Treatment of **58** with Cys/Hcy, however, results in a fluorescence response at 536 nm, which allows for the differentiation between H_2S, Cys/Hcy, and GSH.

If the emission wavelength of the fluorophore used in the NBD-*O*-fluorophore motif is similar to that of the NBD-NHR product (~540 nm), then only one emission profile is observed upon reaction with thiols (Fig. 11). Using this approach, Sheng and coworkers developed fluorescent probe **59** by preparing the NBD adduct of 4-hydroxy-1,8-naphthalimide.[137] The probe demonstrates single emission at 550 nm in the presence of Cys, Hcy, or GSH, but cannot be used to differentiate these thiols. Probe **59** was successfully used to image biothiols in live cells and zebrafish. In addition, the probe is sufficiently sensitive to distinguish cancer cells from normal cells *via* imaging.

Using a pyrimidine-based TP fluorophore, Li and coworkers developed probe **60** for detection of biothiols and sulfide both *in vitro* and *in vivo*.[138] The probe demonstrates a single emission at 550 nm in the presence of either thiol or H_2S and exhibits good sensitivity and a large Stokes shift. The probe can be used to detect biothiols and H_2S in live cells, mice brain slices, and zebrafish *via* TP excitation at 760 nm. Importantly, changes of oxidative stress levels in HeLa cells can be monitored by probe **60**. Similarly, Zeng and coworkers developed probe **61**, which gives one emission peak with different intensities upon reaction with thiols.[139] All thiols can react with **61** to produce a non-fluorescent NBD thioether (such as NBD-SG, $\Phi = 0.0047$) and to release the fluorophore, which is relatively low brightness ($\Phi = 0.0106$) at 574 nm. For Cys/Hcy, however, the intramolecular Smiles rearrangement occurs to form bright NBD-NH-Cys ($\Phi = 0.263$) and NBD-NH-Hcy ($\Phi = 0.376$) at 543 nm, resulting in the differentiation of Cys/Hcy over other thiols and amino acids. In addition, **61** demonstrates a fast (a few minutes) and sensitive (16 nM) response toward Hcy and can be used for imaging Hcy in live cells.

If the emission of a fluorophore used in an NBD-*O*-fluorophore system has different optical properties than NBD-NHR, then the probe can generate either a single- or dual-emission response for GSH/H_2S or Cys/Hcy, respectively. In 2014, Pluth and Hammers presented a dual-fluorophore fragmentation strategy (Fig. 12) for ratiometric determination of relative H_2S and Cys/Hcy concentrations.[140] Probe **62** is non-fluorescent (Fig. 13) and can be activated upon reaction with Cys/Hcy to generate a fluorescence response from both coumarin (449 nm) and NBD (549 nm). The reaction with H_2S generates coumarin and non-fluorescent NBD-SH. Because both reactions with Cys/Hcy and H_2S release coumarin, this released fluorophore can function as an internal standard. This approach allows for the ratiometric measurement of NBD-NHR *versus* NBD-SH, and thus the Cys/Hcy to H_2S concentration ratios with a sigmoidal response curve. Probe **62** demonstrates a rapid response (<1 min) and is selective for sulfhydryl-containing nucleophiles over other reactive sulfur, oxygen, and nitrogen species. Additionally, **62** was demonstrated to differentiate and report on different oxidative stress stimuli in simulated sulfur pools containing H_2S, Cys, and cystine.

Other related NBD-coumarin fluorescent probes have been reported in succession (Fig. 13).[141–143] To study biothiols in organelles, Pu, Tu, and coworkers developed lysosome-targeted fluorescent probe **63** for discriminative detection of Cys/Hcy and GSH *via* a dual-emission response.[141] Probe **63** demonstrates a fast fluorescence response, a low LOD toward biothiols, and low cytotoxicity. Probe **63** was used to detect and discriminate between Cys/Hcy and GSH/H_2S in live cells. Lin and coworkers reported lysosome-targetable probe **64** for distinguishing biothiols by bioimaging in cells and zebrafish.[142] Interestingly, the fluorescence intensity at 565 nm of the probe after reaction with Cys at pH 5 is much larger than that of other species. Therefore, the probe can not only detect biothiols under physiological conditions, but can also distinguish Cys from Hcy/GSH and H_2S *via* a dual-color mode due to the weakly acidic environment (pH ~ 5) of lysosomes. In addition, the probe was used to differentiate Cys from Hcy/GSH and H_2S in a zebrafish model. To extend the emission wavelength, Yin and coworkers developed probe **65** for discrimination of Cys/Hcy and GSH/H_2S, along with the colorimetric detection of H_2S.[143] Probe **65** reacts with Cys/Hcy to produce two fluorescence emissions at 486 nm and 550 nm, whereas it generates single emission at 486 nm for GSH/H_2S. Furthermore, probe **65** can selectively distinguish Cys/Hcy and GSH/H_2S in live cells.

Fluorophores containing intramolecularly hydrogen-bonded structures can generate excited-state intramolecular proton transfer (ESIPT) tautomers upon irradiation, resulting in a large bathochromic shift in emission.[144] Using these types of fluorophores, a series of ESIPT-based NBD-OR probes **66–69** were developed.[145–149] In 2015, Yi, Liu, and coworkers developed probes **66a** and **66b** by using 2-(2′-hydroxyphenyl)benzothiazole (HBT) and 2-(2′-hydroxy-3′-methoxyphenyl)benzothiazole (HMBT) to generate the corresponding NBD ethers, respectively.[145] The fluorescence enhancement of the probes upon thiol treatment was found to be 115-fold at 460 nm and 33-fold at 485 nm for **66a** and **66b**, respectively. The reaction rate of **66a** with Cys is calculated to be 74.4 M^{-1} s^{-1}, which is much faster than that of **43**.[23] This difference may be due to the intermolecular hydrogen bonding effect between thiols and nitrogen at the benzothiazole moiety.[146] Although HBT is one of the most often used ESIPT fluorophores, it has a UV excitation and a relatively low fluorescence quantum yield. Therefore, Yi and coworkers rationally designed the NBD-based probe **67** by using: (1) a combination of an ESIPT fluorophore and an electron-withdrawing group for faster reaction with biothiols; (2) a combination of HBT with a coumarin motif for longer excitation and emission wavelength.[146] As expected, probe **67** demonstrates a fast response toward Cys with k_2 up to 616.7 M^{-1} s^{-1}, which is faster than that of probe **66a**. Additionally, **67** is cell-permeable and can be used for imaging of thiols in live yeast cells. Similarly, using a new ESIPT fluorophore, Zha and coworkers developed probe **68** for the detection of Cys/Hcy and GSH.[147] Probe **68** demonstrates a large Stokes shift, high sensitivity, low cytotoxicity, and good cell permeability. Furthermore, the probe provides a 100-fold fluorescence enhancement at 520 nm upon reaction with Cys in buffer within 2.5 min. Probe **68** was applied for imaging thiols in A549 cells and xenograft mouse tumor tissues.

Based on phenanthroimidazole fluorophores, Lu, Fan, and coworkers developed two ESIPT-based probes **69a** and **69b** for separative detection of biothiols, respectively.[148,149] In the

presence of Cys/Hcy, probe **69a** demonstrates two fluorescence emissions at 480 nm and 550 nm upon excitation at 365 nm and 470 nm, respectively. In comparison, addition of GSH to the probe only leads to blue fluorescence at 480 nm.[148] Probe **69a** was successfully used to simultaneously distinguish endogenous biothiols in live cells and zebrafish models. Unlike **69a**, probe **69b** shows a smaller emission response for Hcy at 550 nm.[149]

Using perylene diimide (PDI) derivatives as the fluorophore, Singh and coworkers developed NBD-based ratiometric probe **70** for discriminative detection of H_2S and Cys.[150] Probe **70** demonstrates a fluorescence signal at 660 nm, which decreases after the addition of Cys and shifts to a new emission maximum at 537 nm. After the reaction of **70** with H_2S, the characteristic absorptions of PDI-OH (λ_{max} = 680 nm) and NBD-SH (λ_{max} = 550 nm) are observed, as well as the decrease of emission intensity at 537 nm. The probe can be used for fluorescence imaging of H_2S and Cys in cells and for fabrication of logic gates based on different responses toward H_2S and Cys.

By using longer wavelength fluorophores, the thiolysis of NBD ethers can be employed to develop off–on fluorescent probes for Cys/Hcy detection in the red and NIR range of the spectrum.[151–170] In 2015, Ma, Li, and coworkers developed probe **71** for discrimination of Cys from GSH by combining resorufin and NBD.[151] The probe, which displays distinct emission patterns for Cys and GSH at single excitation wavelength, can be used for simultaneous determination of Cys and GSH in human plasma. Recently, the same probe was used to develop paper-based analytical devices based on color changes from light yellow to red after the thiolysis reaction.[152] The color intensities of such system increase linearly in the 0.04 to 70 μM Cys concentration range with a LOD of 16 nM.

Similarly, Fan and coworkers developed probe **72** using a dicyanomethylenedifuran-based fluorophore and NBD ether.[153] Nucleophilic addition of GSH produces a single emission response at 610 nm (λ_{ex} = 570 nm), and in the case of Cys/Hcy results in two emission maxima at 547 nm (λ_{ex} = 470 nm) and 610 nm. Probe **72** enables dual-channel imaging of Cys/Hcy and GSH in live cells and *Daphnia magna*. Song, Liu, and coworkers developed probe **73** for the discriminative detection of Cys/Hcy and GSH in live cells.[154] Due to the methylation of the pyridine moiety in chromenoquinoline (CQ) derivatives, the CQ dye exhibits a red emission at 610 nm with similar excitation and comparable quantum yield of NBD-NHR. Probe **73** reacts with biothiols to provide a fast, selective, and sensitive response to produce two emissions under a single-wavelength excitation. Using a 3-hydroxyflavone derivative, Song and coworkers developed probe **74** which can detect GSH with a single emission response at 621 nm (λ_{ex} = 458 nm) and, Cys/Hcy with double emission maxima at 545 nm and 621 nm.[155] Probe **74** was used to detect and differentiate GSH and Cys/Hcy in live cells with single wavelength excitation. Using Nile red as the fluorophore, Ye, Gao, and coworkers developed NBD-based probe **75** for discriminating thiols and H_2S.[156] After reaction of **75** with biothiols, increases in absorbance are observed at different wavelengths (sulfide at 560 nm, Cys at 475 nm, and GSH at 425 nm). A dual-channel fluorescence response is achieved at 543 nm and 636 nm after reaction with Cys/Hcy, whereas reaction with GSH/H_2S only results in a fluorescence enhancement at 636 nm. Additionally, probe **75** produces a rapid response to these thiols and can be applied for bioimaging. Yin and coworkers developed fluorescent probe **76** for discrimination of biothiols.[157] The thiolysis

of **76** results in fluorescence emission at 625 nm for GSH, and at 550 nm and 625 nm for Cys/Hcy. Furthermore, **76** can be used to detect thiols in live cells, zebrafish, and model plant *Arabidopsis thaliana*. Probe **54**, which had been developed for selective detection of H_2S,[100a] can also detect Cys/Hcy at both 543 nm and 643 nm under single wavelength excitation.[100b] This probe shows low cytotoxicity and can be applied for bioimaging of biothiols in live cells and zebrafish.

In a related approach to obtain bright probes with long emission wavelengths, BODIPY-based probes based on NBD ethers have also been developed for the specific detection of biothiols.[158–163] For example, Song, Liu, and coworkers synthesized probe **77** by using an iminocoumarin borate complex as the fluorophore and NBD ether as the electrophile.[158] A strongly donating tetrahydroquinoxaline group was also introduced to enhance ICT and to increase the emission wavelength of the fluorophore. The reaction of **77** with Cys/Hcy results in two emissions at 565 nm and 630 nm under 490 nm excitation, whereas the reaction with GSH gives a single emission at 630 nm. Probe **77** was successfully used for bioimaging in live cells and zebrafish. Bao, Zeng, and coworkers developed probe **78** to detect Cys and GSH in human plasmas and live cells.[159] Upon reaction with GSH, probe **78** releases the indole-BODIPY fluorophore, resulting in a 30-fold fluorescence enhancement at 635 nm, whereas reaction with Cys results in two emissions at 540 nm and 635 nm.

Qian and Xia developed dual-armed BODIPY-based fluorescent probe **79** for detection of biothiols.[160] This probe, which has a TP excitation at 800 nm ($\Phi\delta$ = 198.5 GM), reacts with thiols to generate a strong fluorescence enhancement at 660 nm. Probe **79** demonstrates high sensitivity and selectivity for biothiols, and was successfully applied for live-cell imaging.

Zhao and coworkers developed NIR fluorescent probe **80** using an NBD moiety and a BODIPY fluorophore linked through a self-immolative linker.[161] The probe selectively responds to biothiols with a fluorescence enhancement up to 20-fold at 685 nm when excited at 620 nm. This probe is able to differentiate H_2S/GSH and Cys/Hcy using different fluorescent channels corresponding to the BODIPY and NBD-NHR emission profiles. Probe **80** was successfully used to image GSH in live cells and mice.

Zeng and coworkers developed water-soluble NIR fluorescent probe **81**, which contains two morpholine groups to enhance water-solubility.[162] Compared with probe **78**, BODIPY-based probe **81** has a longer emission wavelength at 735 nm due to the extended conjugation. Probe **81** can be used to monitor Cys through two well-resolved emissions at 735 nm (λ_{ex} = 650 nm) and 540 nm (λ_{ex} = 466 nm). The probe demonstrates good brightness, photostability, a low LOD (22 nM), and low cytotoxicity. Probe **81** was successfully used to distinguish Cys and GSH by fluorescence imaging in live cells.

Using aza-BODIPY as the fluorophore, Zhao, Liu, and coworkers developed NBD-based NIR fluorescent probe **82** for multicolor discrimination of Cys/Hcy and GSH in live cells.[163] The aza-BODIPY has long emission wavelength (>700 nm), which facilitates deep penetration *in vivo* with less photodamage.[96] Probe **82** is almost non-fluorescent until reaction with a thiol, after which there is a strong emission at 730 nm (λ_{ex} = 670

nm). In addition, the fluorescence spectra of aza-BODIPY and the NBD-NHR product are completely separated, which is beneficial for multicolor imaging of Cys/Hcy in live cells.

Beyond these BODIPY derivatives, other NIR fluorophores have also been employed to develop NBD-OR probes for thiol detection in live systems.[164–169] Zhao and coworkers, and Zhu and coworkers independently reported the same probe **83** with different sensing behaviors,[164] just like that for probe **54**.[100] In one report,[164a] the addition of Hcy induces significant fluorescence enhancement at both 549 nm and 697 nm, whereas Cys/GSH results in fluorescence at only 697 nm. The observed selectivity may be due to the faster response toward Hcy and higher quantum yield of NBD-NH-Hcy than that of other biothiols, which is similar to probe **61**.[139] The probe was used for discriminative detection of Hcy and Cys/GSH in live cells. In another report,[164b] probe **83** was exploited for the simultaneous detection of H_2S and GSH. The probe exhibits an emission at 672 nm with LODs of 13.2 nM (H_2S) and 112 nM (GSH). Using this system, probe **83** was successfully applied to image H_2S and GSH in HepG2 cells and zebrafish. The authors did not test the NBD-NHR emission for Cys/Hcy,[164b] and the excitation wavelengths for the dicyanoisophorone-based fluorophore in two papers are 560 nm[164a] and 480 nm,[164b] respectively. Although the NBD ether should be prone to thiolysis by all biothiols as seen in probes **62–82**, more studies are needed to clarify the properties of **83** in the future.

Gu, Wang, and coworkers developed the related dicyanoisophorone-based probe **84** for detection of biothiols.[165] Probe **84** demonstrates good selectivity and sensitivity and can differentiate between Cys/Hcy and GSH with dual fluorescence signals, rather than by providing a unique response toward Hcy as in **83**.[164a] Moreover, probe **84** shows low cytotoxicity and was used for imaging in live cells and mice.

Hemicyanine-containing based NBD-based fluorescent probes **85–87** have also been prepared and benefit from the high stability and NIR emission profile of this class of dyes.[166–168] For example, Liu, Zeng, and coworkers developed probe **85** for differentiating between Cys and GSH.[166] Probe **85** demonstrates weak fluorescence ($\Phi = 0.011$), but a significant fluorescence enhancement is observed at 702 nm ($\Phi = 0.065$, 670 nm excitation) upon reaction with thiols. In addition, the reaction with Cys/Hcy results in emission at 540 nm due to formation of NBD-NHR as expected. Probe **85** was used to monitor Cys and GSH in live cells and human plasma. Similarly, Wu, Zeng, and coworkers developed probe **86** by using a cyanine-based fluorophore.[167] After treatment with biothiols, the fluorophore is released, resulting in an emission at 716 nm, and an emission near 550 nm due to formation of NBD-NHR from Cys/Hcy. Probe **86** was applied to measure Cys/Hcy and GSH levels in live cells and in human serum samples. Both probes **85** and **86** only produce a small response toward H_2S at high concentration (1 mM) at 702 nm and 716 nm, respectively.[166,167] In our experience, as well as other's work on the thiolysis of NBD ethers,[23,100,140] H_2S is a better nucleophile than biothiols and reacts more quickly with NBD electrophiles than potential thiol reactants. One explanation of the observed lack of fluorescence response toward H_2S in **85** is that at high concentrations, H_2S may react directly with the Michael acceptor motifs in the semiheptamethine cyanine, which would quench the fluorescence of the dye. Further studies are needed for compounds **85** and **86** to determine whether lower concentration of H_2S (<100 μM) inhibits the fluorescence response

toward other thiols and also to identify the reaction product of these probes with H_2S at higher concentrations of H_2S.

Qian and coworkers developed water-soluble NIR probe **87** for discrimination of biothiols *via* dual-channel emissions.[168] The reaction of the probe with Cys/Hcy results in fluorescence enhancement at 540 nm and 702 nm, whereas the reaction with GSH alone only results in emission at 702 nm. This probe was used for tracking Cys/Hcy and GSH in aqueous solution at wide pH from 4 to 10 and in live cells. The reaction of **87** and H_2S was not tested.[168]

Using a hybrid chromenylium-cyanine (CC) fluorophore, Lin and coworkers developed fluorescent probe **88** for efficiently discriminating Cys/Hcy from GSH/H_2S using a dual-channel detection method.[169] The CC fluorophore has a high fluorescence quantum yield, high molar absorption coefficient, long excitation and emission wavelengths, and good stability under physiological conditions.[170] Additionally, the CC fluorophore is not degraded by H_2S, and probe **88** reacts with H_2S to give strong CC fluorescence.[169] This outcome is different from the observed reactivity with hemicyanine probes.[166,167] Upon addition of Cys/Hcy, probe **88** generates significant fluorescence enhancement at 544 nm and 707 nm, whereas reaction with GSH/H_2S only increases the response at 707 nm. The quantum yields for NBD-NH-Cys or NBD-NH-Hcy in this system were determined to be 0.1016 or 0.0697, respectively.[169] Probe **88** was also successfully applied to distinguish between Cys/Hcy and GSH/H_2S in live cells. Notably, the thiolysis response of probe **88** toward H_2S is faster than toward biothiols, which is consistent with the observed reactivity of other NBD-based probes.[23,100,140]

Overall, the thiolysis of NBD ethers has been used broadly to develop single- and dual-channel fluorescent probes for multicolor imaging of biothiols and H_2S. Although the design strategy is similar, the probes have different properties because of different fluorophores, which result in different reactivities, selectivities, and optical properties. In general, H_2S reacts faster than biothiols with NBD ethers.[23,100,140,169] Therefore, less reactive NBD ethers are often more suitable for the development of selective H_2S probes, whereas more reactive NBD ethers can be used as more general biothiol probes. For systems that use a dual-channel detection approach for Cys/Hcy, a large difference in wavelength between the fluorophore and NBD-NHR product is beneficial, which minimizes signal overlap and facilitates high selectivity. Because the reaction between Cys/Hcy and NBD ethers results in formation of fluorescent NBD-NHR with emission maxima near 540 nm, the differential reactivities for Cys and Hcy can in some cases lead to differentiation between these similar thiols. Many of the developed NBD-OR thiol probes have not been tested with H_2S, which is an important potentially competing analyte for thiol probes, although it is present at much lower concentrations than common biological thiols. Moreover, H_2S may react directly with certain fluorophores, especially if they have potentially electrophilic, Michael acceptor sites.

3.3 Thiolysis of NBD ethers for specific detection of Cys or Hcy

Effective differentiation and tracking of Cys or Hcy over other biothiols remains a challenge due to structural and reactivity similarities with related molecules. To address this challenge, Sun, Zhu, and coworkers developed the two dual-site probes **89** and **90** by installing an

acrylic ester group onto the NBD ether linked *via* a flexible chain.[171] The acrylate moiety functions as a classical Michael receptor for Cys.[172] These probes demonstrate a unique sensing mechanism for Cys that relies on Michael addition of the thiol to the acrylic ester followed by ammonolysis of the NBD ether rather than the ester bond (Fig. 14). Fluorescence spectra of the probes show a strong enhancement at 560 nm in the presence of Cys, whereas reaction with Hcy/GSH results in only a slight fluorescence response within 30 min. Compared with probe **90**, which has three methylene units, probe **89** with a glycol linker demonstrates better selectivity for Cys over other biothiols within 30 min. At longer reaction times, the selectivity of probe **89** is decreased, but can be used to quantify all biothiols if extended reaction times (3 h) are used. Although the intramolecular aminolysis of the NBD ether by Hcy and GSH is slow, the NBD amine reaction products were confirmed by HPLC (Fig. 14c) and mass spectrometry and are consistent with the fluorescence results.

Recently, Kim and coworkers compared the reactivity and selectivity of several NBD ethers with different aromatic substitutions at the 4-position toward biothiols (Fig. 15a).[173] Only probe **91b** displays a selective fluorescence response toward Cys, which was complete within 10 min (Fig. 15b and c). In this system, the reaction rate of the thiolysis of NBD ethers can be modulated by using the electron-deficient pentafluoro-substituted aromatic ring. Moreover, **91b** demonstrates a low LOD (0.12 ppm), low cytotoxicity, a TP excitation, and the ability to target the ER.

Probe **91b** was successfully applied to monitor Cys level in human primary glioblastoma multiforme (GBM) cell lines (U87MG), GBM patient-derived primary cultured cell line (SNU4098), a GBM xenograft mouse model, and human clinical biopsy GBM samples. GBM cell lines treated with **91b** show a bright fluorescence under a confocal laser scanning microscopy (CLSM). Similarly, Cys levels can be monitored at the GBM-site of a xenograft mouse model using the fluorescence tissue imaging system (FTIS) and TP microscopy (TPM) (Fig. 15d and e). Furthermore, the probe can distinguish the GBM site of patients from the healthy control through fluorescence analysis of the tissue samples (Fig. 15f). Probe **91b** also demonstrates promising applications such as the straightforward screening of GBM in excisional biopsy brain tissues, which could be a potential approach to replace the current complex protocols. In addition to diagnostic applications, the NBD-based probe alone or related nanoparticle hybrids have the potential for applications in image-guided tumor resection.

In addition to differentiating Cys from other thiols, NBD-ether probes can also be used for the specific detection of Hcy from other thiols. For example, Tang, Li, and coworkers developed dual-emission fluorescent probe **92** for the rapid detection of Cys and Hcy at pH 6–9 (Fig. 16).[174] Probe **92** is quenched by the NBD moiety through the PET effect, and dual fluorescence responses are observed at 543 nm and 592 nm after reaction with Cys/Hcy at pH 7.4. However, the reactivity of **92** with Hcy is much higher than with Cys at pH 10. Probe **92** was successfully applied to monitor the level of Hcy in live cells. As presented above, NBD-OR probes show the potential to specifically identify a single biothiol by modulating the group linking the NBD ether.

3.4 Other NBD probes based on cleavage of C–S/Se/N bonds

Joining their NBD ether counterparts, both NBD thioethers and NBD selenoethers can also be used for the selective detection of biothiols. In 2013, Pluth and coworkers reported NBD thioether probes for the colorimetric detection of H_2S.[22] In addition, this system demonstrated that such probes could react with thiols to form an intermediate NBD thioether that maintained reactivity toward biothiols and H_2S (Fig. 17a). In addition, this approach means that thiols may not be irreversibly consumed in such systems, which has been further leveraged through different approaches to generate analyte-replacement sensing systems.[175]

In 2014, Wang and coworkers reported NBD-SCN (**93**) for the specific detection of Cys and Hcy due to the formation of NBD-NHR.[176] Probe **93** reacts quickly with Cys (within 20 s) and Hcy (within 10 min) and can be used for selective detection of Cys/Hcy in live cells. By adjusting substituent groups at the 4-position, similar single-emission probes **94–98** were reported with tunable reactivities and selectivities (Fig. 17b).[177–181] Shao and coworkers developed probe **94** (Φ = 0.003), which reacts with Cys to produce a 100-fold fluorescent enhancement at 540 nm (Φ = 0.072) within 20 min.[177] In addition, the reaction rate of **94** with Cys is much faster than with Hcy at pH 7.4, with a difference in rate of up to 13.8-fold. The probe exhibits very low cytotoxicity and was applied to image Cys in live cells. In contrast to *p*-thiocresol NBD **94**, Shao, Xu, and coworkers reported *p*-aminothiophenol NBD **95** that demonstrates a similar fluorescence response toward Cys or Hcy.[178] Moreover, gold nanoclusters (AuNCs) with carboxyl groups were conjugated with amino groups in **95** to develop AuNCs-**95** for ratiometric detection of Cys/Hcy. In this system, the emission at 540 nm gradually increases with increasing concentrations of Cys or Hcy, while the emission at 630 nm of AuNCs remains constant. The AuNCs-**95** composite provides a ratiometric fluorescence response, high specificity, good solubility, and a useful detection limit. This system was used for imaging intracellular Cys/Hcy.

Using 4,6-dimethoxy-2-pyrimidinylthioether, Wang and coworkers developed NBD-based probe **96** for Cys/Hcy detection.[179] Probe **96** is non-fluorescent (Φ = 0.003), and treatment with Cys or Hcy results in a 78-fold fluorescent enhancement at 547 nm (Φ = 0.124) or a 113-fold fluorescent enhancement at 547 nm (Φ = 0.171), respectively. Probe **96** reacts with Cys faster than with Hcy, with LODs for Cys and Hcy of 95 nM and 138 nM, respectively. Treatment of **96** with GSH does not produce a fluorescence response, but rather provides a change in the absorption spectra, which suggests that a thiol-exchange reaction is occurring. This probe is minimally cytotoxic and can be used to image Cys/Hcy in various cell lines.[179] The same group also developed probe **97** by using thiazole thioether for Cys/Hcy detection.[180] Dong, Zhang, and coworkers developed probe **98** using a benzothiazole thioether.[181] The probe demonstrates high selectivity and sensitivity toward Cys/Hcy, low toxicity, and is suitable for fluorescent imaging in live cells. Both probes **97** and **98** can react with Cys faster than with Hcy.[180,181] Overall, the reaction rates of these NBD thioethers toward Cys/Hcy can be tuned by using different substituents.

Inspired by the dual-channel detection of Cys/Hcy from NBD ether,[140] Yi, Xi, and coworkers designed and synthesized probes **99–101** for selective detection of Cys/Hcy.[182,183] Probe **100** was unstable,[182] but probe **99** exhibited good stability and rapid

detection of Cys/Hcy in aqueous buffer. Moreover, **99** avoids the interference of GSH due to the accessibility of the transformation between NBD-SR adducts. Yi, Xi, and coworkers further developed red-emitting NBD-*S*-rhodamine probe **101**, which produces dual-emission signals at 590 nm and 547 nm in the presence of Cys/Hcy, but only at 590 nm for GSH/H_2S.[183] Probe **101** was successfully used for discriminative imaging of intracellular GSH and Cys/Hcy.

Recently, Yuan, Yin, and coworkers developed dual-channel probe **102** for differentiation of Cys/Hcy and GSH in live cells and mice.[184] Prior to activation, the probe is not fluorescent due to PET quenching from the NBD moiety. The sensing mechanism for discriminating between GSH and Cys/Hcy is shown in Fig. 18a. The probe responds to GSH with a 45-fold NIR enhancement at 810 nm (excitation at 720 nm), and to Cys/Hcy with only yellow emission at 550 nm (excitation at 470 nm) due to the weak fluorescence of **102-NH-Cys** or **102-NH-Hcy**.[185] These reactions can be completed within 1 h (Fig. 18b and c). Probe **102** is an excellent tool for the NIR detection of GSH in the presence of other thiols, and has distinct advantages over NBD-based probes **81–88** that all react with Cys, Hcy, and GSH to generate a NIR fluorescence response. Notably, probe **102** is suitable for visualizing exogenous and endogenous biothiols in live cells (Fig. 18d).

Considering that GSH is overexpressed in some cancer cells,[121,122] probe **102** was applied for tumor imaging in mammary cancer cells in xenograft mice. The fluorescence signal observed in the tumor was significantly higher than that observed in other organs (heart, spleen, lung, and kidney), and strong signals in the liver and intestine may be due to the enterohepatic circulation and metabolism of the probe (Fig. 18e). The extracted tumors from mice showed strong fluorescence in both the NIR and yellow light channels (Fig. 18f). Furthering the biological significance, the probe is used to image GSH in acute liver injury mice models (Fig. 18g). The relative fluorescence intensity in the ethanol injection group is smaller than that of the PBS injection group (Fig. 18h). Therefore, the probe can be used for *in vivo* imaging of solid tumors as well as detection of acute liver injury, which highlights potential clinical value of the NBD-based probe.

In summary, there are significantly fewer fluorescent probes based on NBD thioethers than based on NBD ethers. One attractive feature of the thiolysis of NBD thioethers for investigating reactive sulfur species is that a thiol is released during cleavage of the NBD-thioether, which should help to minimize interference with redox homeostasis when compared to NBD-ether probes. Much like NBD-ether probes, specific detection of a single biothiol can be achieved by tuning substituents on NBD thioethers, such as probe **94** for Cys and probe **102** for GSH.

In addition to NBD ether/thioether compounds, NBD selenoethers may also provide a potential avenue for the development of fluorescent probes. To the best of our knowledge, Chang and coworkers reported the only NBD-selenoether based probe **103** (Fig. 19a).[186] The sensing mechanism was based on H_2S-mediated cleavage of the selenoether bond,[186b] resulting in a color change from yellow to pink NBD-SH.[22] It was reported that probe **103** had excellent selectivity compared with NBD ether and thioether, however the same probe was also used for malononitrile identification with similar pink signal (Fig. 19a).[187] For

malonitrile detection, potential interference by H_2S or several transition metal ions could be circumvented by copper precipitation and EDTA coordination, respectively. To explore the possibility of NBD selenoethers as *in vivo* fluorescent probes, the selectivity and reactivity for alkyl-substituted compounds may be further investigated in the future.

Zhang and coworkers developed the simple and chemically reversible fluorescent probe **104** for sensing different redox states.[188a] The probe demonstrates weak fluorescence due to the PET effect from the Se atom, but treatment with HOCl results in a 32-fold fluorescent enhancement at 544 nm within 10 s. This increase in fluorescence can be reversed by the addition of GSH. This reversible redox cycle can be repeated several times. In addition, the probe can be used to reversibly monitor the redox status of live cells. NBD-based probes have also been used for the reversible sensing of metal ions (*e.g.* Zn(II) ion), which have recently been reviewed elsewhere.[188b]

In 2013, Chen and coworkers developed NBD-N_3 **105** as a colorimetric and fluorescent probe for rapid and selective detection of H_2S in live cells (Fig. 20a).[189] After H_2S treatment, probe **105** demonstrates a colorimetric change from pale-yellow to deep-yellow and a large fluorescence enhancement at 550 nm. Absorbance spectra of the reaction show new peaks at 468 nm and 540 nm, which may be attributed to the production of fluorescent NBD-NH_2 (reduction reaction) and colorimetric NBD-SH (substitution reaction), respectively. In addition, live cell imaging confirmed the practicality of **105** for fluorescent detection of biological H_2S.

Using 4-nitrobenzo-2-thia-1,3-diazole (NBD(S)), Yoon, Yin, and coworkers rationally designed and synthesized probe **106** for selective detection of Cys over Hcy (Fig. 20b).[190] The *p*-amino group in **106** suggests that the properties of the probe can be changed at acidic pH values. Interestingly, this probe reacts with both Cys and Hcy at pH 7.4, but only with Cys at pH 6.0, along with a significant fluorescence enhancement at 535 nm. The probe is water-soluble, non-cytotoxic, highly selective for Cys, and suitable for bioimaging in live cells. Selective imaging of Cys in live cells was achieved by **106** at pH 6.0. This work also suggests that modification of the NBD moiety may be an efficient strategy to tune the reactivities and selectivities of fluorescent probes to provide better chemical tools.

4. NBD-based multi-reactable multi-quenching fluorescent probes

4.1 Dual-reactable H_2S fluorescent probes

The sensitivity of fluorescent probes can be evaluated by measuring the LOD, which is typically defined as $3\sigma/k$, where σ is the standard deviation for multiple fluorescence tests of the probe solution in the absence of analyte, and k is the slope of the fluorescence of the probe *versus* the analyte concentration.[191] To lower the LOD, one approach is to install multiple quenchers into one fluorophore, which would decrease the background fluorescence of the probe and subsequently decrease the σ value. This approach should also increase the fluorescent enhancement after release of the quenching groups and subsequently increase the k value. As a result, the multi-quenching probe should demonstrate a low LOD and high sensitivity.

Because endogenous biothiols are present at millimolar concentrations in live systems, it is important to also enhance the selectivity of H_2S fluorescent probes so that H_2S can be recognized even in the presence of a large excess of other thiols. To this end, attachment of multi-reactable groups that have different reaction mechanisms for the same analyte can often be used to improve the selectivity of the probe. In these systems, if a competing reactant (*e.g.* GSH) reacts with one of the reactable groups (*e.g.* nucleophilic or redox reactions), the remaining unreacted group can still quench the fluorophore. Therefore, the competing analyte cannot generate a significant fluorescence response in the absence of suitable concentrations of the desired analyte.

As a proof-of-concept study, Yi, Xi, and coworkers prepared the dual-reactable and dual-quenching probe **107** as well as its control probes **107a** and **107b** (single-reactable probes with the same fluorophore and reaction group as that of **107**).[192] As shown in Fig. 21a, the napthalimide fluorophore in probe **107** is attached with two quenching groups, NBD and azide, which have FRET/PET and ICT effects, respectively. Probe **107** can react with H_2S *via* two different reaction types (nucleophilic and redox reactions), resulting in a 54.8-fold turn-on fluorescence at 540 nm and a 21.6-fold selectivity for H_2S over Cys. The high selectivity and sensitivity of **107** enabled its use for sensing H_2S in live cells. Compared with the control probes **107a** and **107b**, probe **107** demonstrates higher and multiplicative fluorescent turn-on and better selectivity (Fig. 21a). We propose that this multiplication effect may also be a viable approach to increase the sensitivity and selectivity for different analytes using an analogous approach of appending multiple reaction sites.

The FRET/PET-ICT multi-quenching probe **108** based on thiolysis of DNB ether and NBD amine was developed by Yi, Xi, and coworkers in 2015 (Fig. 21b).[193] This probe demonstrates a >2000-fold fluorescence turn-on at 455 nm upon reaction with H_2S and better water-stability than that of single-reactable control probes in PBS buffer (pH 7.4). The probe can be used for imaging of endogenous H_2S in live cells. This probe, however, was not highly selective for H_2S over biothiols, which may be due to the interference of competing nucleophilic substitutions.

Subsequently, Xi, Yi, and coworkers developed dual-reactable probes **109** and **110** that incorporate both nucleophilic and redox activated H_2S sensing motifs, which generated a highly selective and sensitive probe.[194] As expected, the coumarin emission is highly quenched in both probes due to the FRET/PET-ICT multi-quenching effects. These probes demonstrate significant fluorescence enhancement at 460 nm after reaction with H_2S, with a 3150-fold turn-on for **109** and a 4010-fold turn-on for **110**. To the best of our knowledge, **110** has the largest reported fluorescence turn-on of reported H_2S fluorescent probes. The LOD of **109** and **110** for H_2S is calculated to be 27 nM and 24 nM, respectively. Both probes demonstrate higher selectivity toward H_2S than their corresponding single-reactable probes. The selectivity of probe **110** for 100 μM H_2S over 5 mM GSH or 100 μM SO_3^{2-} can reach 228-fold or 1000-fold, respectively, which is much higher than that of single-reactable NBD-based probes **1–13**. These large fold values highlight the advantages of these dual-reactable probes.

Probe **110** was further applied for high-throughput screening of CBS inhibitors. These studies revealed that the drug sparfloxacin can inhibit H_2S biosynthesis *in vitro* with half maximal inhibitory concentration (IC_{50}) of 133.7 μM. Other tested compounds with moderate inhibition potency included Cys derivatives, quinolones, methacrylic acid, and hydroxylamine.[194] Bioimaging experiments using probe **110** also revealed the suppression of L-Cys-induced H_2S production by sparfloxacin in live HEK293 cells. In addition, probe **110** was used for tracing the D-Cys-induced endogenous H_2S in live cells and zebrafish.

Apart from coumarin derivatives, other fluorophores can also be used to develop dual-reactable H_2S probes. For example, Li, Wei, and coworkers developed rhodamine-based dual-reactable fluorescent probe **111** to detect mitochondrial H_2S (Fig. 21b).[195] After reaction with H_2S, probe **111** demonstrates a 40-fold fluorescence enhancement at 565 nm, whereas the corresponding single-reactable probes show about 9.5-fold or 2.9-fold enhancement under the same conditions. Probe **111** can be used for fast, highly selective and sensitive detection of mitochondrial H_2S in live cells and mice.

Taken together, these examples highlight the generality of the dual-reactable strategy for preparing highly selective and sensitive H_2S probes. This strategy has also been used to develop other probes in detection of H_2S,[196] biothiols,[197–199] Cys,[200] and HOCl.[201–203] For example, Zhang, Sun, and coworkers developed a dual-reactable fluorescent probe with a 4600-fold fluorescent enhancement at 530 nm after reaction with HOCl,[201] which is the largest reported fluorescence turn-on of reported HOCl fluorescent probes. Furthermore, we propose that such multi-reactable multi-quenching strategy can be further used to develop many highly efficient fluorescent probes for the detection of different analytes.

4.2 Multi-reactable probe for distinguishing biothiols

4.2.1 Probes for dual-channel imaging.—

Different NBD receptors can be employed to develop multi-reactable probes to differentiate different biothiols.[204–211] For example, Yi, Sun, and coworkers installed the NBD amine motif and the NBD thioether/ether motif onto one coumarin fluorophore to construct dual-reactable probes **112** and **113** (Fig. 22).[204] Both probes demonstrate almost no background fluorescence due to dual-quenching effects from the both NBD moieties, but show a strong blue fluorescence of coumarin upon reaction with H_2S. The fluorescence enhancement of probe **112**, however, is low (<3 fold) in the presence of Cys/Hcy/GSH, which may be due to slower thiolysis of the NBD thioether moiety. Compared with **112**, probe **113** demonstrates a much larger fluorescence response for biothiols. In the case of Cys/Hcy, the generated NBD thioether undergoes a Smiles rearrangement to generate the fluorescent NBD-NHR, while the coumarin still shows very weak fluorescence, which can be further used to sense H_2S. In the case of GSH, two non-fluorescent fragments, namely coumarin-NBD and NBD-SG, are produced from **113**. NBD-SG can be further activated by Cys/Hcy to form fluorescent NBD-NHR. This reactivity allows for the simultaneous discrimination of H_2S and Cys/Hcy from a single probe in the presence of GSH using a dual-emission strategy.

Chen, Song, and coworkers developed dual-reactable probe **114** for detection of H_2S and Cys/Hcy without interference from GSH.[205] The probe contains two quenchers, the NBD

thioether and azido moieties that can be thiolyzed and reduced by H_2S, respectively (Fig. 23). The probe generates different fluorescence responses for H_2S (blue), Cys/Hcy (yellow), and GSH (no fluorescence). The probe showed low cytotoxicity and was used to selectively detect Cys/Hcy and H_2S in live cells *via* dual-channel imaging. Notably, probe **114** can still detect H_2S after thiolysis of the NBD thioether by biothiols, which is similar to that of probe **113**. Furthermore, using different combinations of NBD thioether/ether/amine and other receptors (also quenchers) should be useful for developing multi-reactable probes with different types of sensing mechanisms.

Sheng and coworkers developed naphthofluorescein-based fluorescent probe **115** with NBD ether and acrylate reactive sites (Fig. 24).[206] Naphthofluorescein is a bright NIR fluorophore with two hydroxyl groups that can be functionalized to include two different reaction sites onto a single fluorescent probe. Probe **115** can react initially with Cys/Hcy to produce the fluorescent NBD-NHR and the acrylate can also be cleaved by Cys/Hcy to provide naphthofluorescein. As a result, reaction with Cys/Hcy can trigger a significant fluorescence enhancement in both yellow and NIR regions. In the case of GSH, however, the non-fluorescent NBD-SG product is formed. In addition, the reaction of GSH with the acrylate group results in a much weaker fluorescence than that of naphthofluorescein. Therefore, probe **115** can be used to visualize Cys/Hcy in two different emission channels.

Shang, Wang, and coworkers also reported another strategy for separating biothiols and H_2S by conjugating two fluorophores through a disulfide bond with a functional NBD amine (Fig. 25).[207] Probe **116** is inherently non-fluorescent due to the ICT process for both coumarin and resorufin as well as additional quenching of the coumarin by the FRET/PET effects from NBD. For this probe, the NBD amine can be cleaved by H_2S, and the disulfide bond between coumarin and resorufin can be cleaved by nucleophiles like biothiols. The cleavage of the disulfide linkage triggers the release of resorufin through a quinone methide intermediate as well as piperazine–coumarin through lactonization of the persulfide species. As a result, both the fluorophores are released to generate a fluorescence enhancement at 467 nm (125-fold) and at 588 nm (83-fold) after reaction with H_2S. Reaction with Cys, Hcy, or GSH results in a 65, 65 and 70-fold enhancement at 588 nm, respectively. In addition, further treatment of mixtures of probe **116** and biothiols with H_2S results in blue emission for Cys/Hcy but not for GSH. Taken together, probe **116** can distinguish between H_2S and biothiols, and also detect Cys/Hcy and GSH through two well-defined emission bands. Moreover, probe **116** has high water-solubility and low cytotoxicity, and can simultaneously monitor H_2S, Cys/Hcy, and GSH *via* dual-channel imaging. This work provides an effective strategy for investigating the functions of different biothiol species in biological systems.

4.2.2 Probes for triple-channel imaging.—

In 2017, Lin and coworkers developed hybrid fluorescent dyad **117**, which contains a hydroxyphenyl benzothiazole merocyanine (HBTMC) fluorophore connected to an NBD ether for triple-channel imaging.[208] As shown in Fig. 26, the HBTMC moiety serves as a recognition unit for H_2S, and the NBD ether moiety is the recognition unit for Cys/Hcy. Probe **117** is non-fluorescent, which is likely due to the protected hydroxyl NBD chromophore and associated quenching of the HBTMC moiety by the NBD group. The reaction of **117** with Cys/Hcy cleaves the NBD ether,

releasing the red HBTMC, and generating the green NBD-NHR. The reaction of **117** with GSH generates non-fluorescent NBD-SG and the HBTMC fluorophore. If **117** reacts with the more nucleophilic H_2S, the ether bond will also be cleaved to yield the non-fluorescent NBD-SH, and the C=N double bond of the HBTMC chromophore would be attacked to afford the blue-emissive HBTMC-SH derivative. Therefore, **117** can discriminate Cys/Hcy, GSH, and H_2S with three different sets of fluorescence signals in three channels. For example, treatment with Cys/Hcy induced a 53.4/57.6- and 32.2/32.9-fold enhancement at 546 nm and 609 nm, respectively; treatment with GSH induced a 33.6-fold enhancement at 609 nm; and treatment with H_2S induced a 52.7-fold enhancement at 485 nm.[208] Further DFT studies reveal that the response emission of probe **117** to biothiols is regulated by the PET and ICT effects, and HBTMC-SH has a larger energy difference between the lowest unoccupied molecular orbital (LUMO) and highest occupied molecular orbital (HOMO) than that of HBTMC.

In addition, upon addition of high, non-physiologically relevant concentrations of H_2S (5 mM) to the mixture of **117** and Cys/Hcy, both the green and red emissions gradually bleach, with the appearance of a signal in the blue channel.[208] The authors suggest that the NBD-NH-Cys/Hcy may react with H_2S to produce NBD-SH, however, it is also possible that at these high concentrations of H_2S, nitro group reduction in NBD-NHR by H_2S becomes competitive. As expected, addition of excessive H_2S to **117** in the presence of GSH resulted in an increase in blue emission, and concomitant weakening of the red emission. As shown in Fig. 26b and c, probe **117** can discriminate between cellular Cys/Hcy, GSH, and H_2S with three different sets of signals *via* three-color fluorescence imaging. The cationic **117** is primarily localized to the mitochondria and enables the cellular imaging of mitochondrial biothiols. The excellent performance of **117** in three-channel fluorescence imaging suggests that the probe can be applied to simultaneously discriminate biothiols from each other and sequentially sense Cys/Hcy/GSH and H_2S in various physiological and pathological processes.

Song and coworkers developed probe **118** by conjugating a capped tetrahydroquinoxaline coumarin precursor with an NBD-*O*-modified 7-hydroxycoumarin to generate a three-color emission system that is compatible with bioimaging in live systems (Fig. 27a).[209] When reacting with biothiols, the NBD ether in **118** is cleaved to generate the blue coumarin derivative, and non-fluorescent NBD-SG or fluorescent NBD-NH-Cys/Hcy. H_2S reacts with both azido and NBD-ether reactive sites in **118** to generate blue-emissive hydroxycoumarin and red-emissive tetrahydroquinoxaline coumarin. Therefore, **118** can produce three different signal patterns upon reaction with Cys/Hcy (490 nm and 559 nm), GSH (490 nm), and H_2S (490 nm and 618 nm). The probe was successfully used to distinguish Cys/Hcy, GSH, and H_2S in live cells with good selectivity and sensitivity. Furthermore, probe **118** was used for the discriminative detection of Cys/Hcy, GSH, and H_2S in live organisms (zebrafish, Fig. 27b) for the first time.

Using a similar approach, Song and coworkers reported fluorescent probe **119** by using a DNB-functionalized tetrahydroquinoxaline coumarin precursor which was developed to simultaneously detect Cys/Hcy, GSH/H_2S, and thiophenol.[210a] DNB has been widely used as a receptor for both H_2S[91a,210b,c] and thiophenols.[210d] The NBD ether can be cleaved

by all five tested thiol substrates to release the blue-emitting coumarin derivatives and to produce the fluorescent NBD-NH-Cys/Hcy adduct. In contrast, the DNB ether is only reactive toward thiophenol but is inert toward Cys/Hcy/GSH/H_2S under the conditions investigated (50 μM H_2S, 20 min reaction). Although there are many H_2S-selective fluorescent probes based on thiolysis of the DNB ether, this expected reaction does not appear to occur in **119**.[210a] Therefore, only thiophenol leads to the release of both blue-emissive hydroxycoumarin and red-emissive tetrahydroquinoxaline coumarin from probe **119**. Together, the simultaneous differentiation of Cys/Hcy, GSH/H_2S, and thiophenol can be realized by using a single probe species **119** (Fig. 28).

Lin and coworkers developed a multifunctional logic gate based on triple-channel fluorescent probe **120**.[211] The probe contains coumarin, NBD, and flavylium chromophores, but only exhibits red emission of the flavylium dye (Fig. 29a). The reaction of probe **120** with Cys/Hcy produces a free hydroxyl coumarin derivative and the fluorescent NBD-NH-Cys/Hcy, with blue (453 nm), yellow (554 nm) and red (658 nm) emissions. For GSH, the probe generates blue and red emissions *via* thiolysis of the NBD ether. The reaction of probe **120** with H_2S also releases a free hydroxy coumarin derivative, but the flavylium moiety can be attacked by HS^-, resulting in only blue emission. Thus, the triad **120** can simultaneously discriminate between Cys/Hcy, GSH, and H_2S through three different sets of fluorescence signals.

Using the four different reporting patterns from probe **120** (black-black-red, blue-yellow-red, blue-black-red and blue-black-black) in the absence or presence of small molecules, these outputs can be translated into logic operations including OR, TRANSFER, INH, NOT, and YES logic gates (Fig. 29b). For example, probe **120** generates the OR logic operation when using the 453 nm emission as the output and Cys/Hcy, GSH and H_2S as the inputs, because the probe exhibits a strong blue emission toward any of these small molecules. As an example of a two-input logic gate, the 554 nm emission is used as the output, and the probe performs as the INH logic operation by using the Cys/Hcy and H_2S couple as the inputs. Similarly, the NOT logic can be generated using H_2S as the input and taking the fluorescence emission at 658 nm as the output, because the red fluorescence is quenched by any combination of biothiols and H_2S. This work provides an efficient strategy for constructing multiple-input molecular logic gates.

Shi, Chang, and coworkers developed mitochondria-targeted three-channel probe **121** for specific detection of biothiols and HOCl in live cells.[212] Probe **121** contains NBD and rhoadamine hydrazide for Cys/Hcy and HOCl detection, respectively, as well as an imidazolium group to target the mitochondria (Fig. 30). Probe **121** reacts with HOCl to generate a red fluorescence at 580 nm. Upon reaction with GSH or Cys/Hcy, probe **121** generates a yellow fluorescence for NBD-NH-Cys/Hcy, and a blue fluorescence at 450 nm due to the release of 7-hydroxycoumarin, which can react with HOCl to generate an additional red fluorescence. Due to its good cell permeability and biocompatibility, the probe was successfully used for selectively sensing these small molecules in live cancer cells.

In summary, the development of unimolecular probes for multiplex imaging is important approach to generating chemical tools for biomedical research. The multi-reactable probes **112–121** provide examples and strategies for designing single-molecule fluorescent probes for simultaneous detection of multiple biological species. The approach of combining different reactivities into one probe platform overcomes some of the disadvantages of using multiple probes with different spatiotemporal distributions within the same system.[212] In addition, this work also highlights the utility of NBD as an important platform in the development of multi-reactable probes.

4.3 Probe based on photo- and chemically-activated reactions

Other types of reactions can also be used with NBD motifs to develop multi-reactable probes. For example, Pu, Tu, and coworkers reported probe **122** based on both photochemical and chemical reactions, which can be used for simultaneous detection and discrimination of biothiols.[213] As shown in Fig. 31, the probe contains a diarylethene moiety that can undergo reversible structural changes, resulting in different colors after excitation with different light sources. Probe **122O** reacts with all biothiols to produce the fluorescent NBD-NH-Cys/Hcy or non-fluorescent NBD-SG. When Cys is added to the closed-ring isomer **122C**, a dark pink color forms that is different from the light green color for Hcy and GSH, which may be due to the different thiolysis reactivities of **122O** and **122C**. Taking advantage of the photochromic properties of the diarylethene moiety and the different fluorescence properties of NBD derivatives, **122** can be used as a robust tool to differentiate Cys, Hcy, and GSH simultaneously. Moreover, a logic gate can be constructed based on the colorimetric and fluorescent readout of probe **122**.[213]

4.4 Probe based on enzymatic- and chemically-activated reactions

Dual-reactable probes based on both chemical and enzymatic reactions have been rarely reported. In 2019, Xi, Yi, Li, and coworkers reported the rational design and preparation of dual-reactable fluorescent probes **123** and **124** for detection of both H_2S and human NAD(P)H:quinone oxidoreductase 1 (hNQO1) in live cells (Fig. 32).[214] Both H_2S and hNQO1 are potential cancer biomarkers, and the response of these two biomarkers to oxidative stress remains largely unknown. A trimethyl-lock containing quinone propionic acid (Q_3PA) moiety and the NBD amine were used as a triggering groups for hNQO1 and H_2S, respectively. The coumarin and naphthalimide fluorophores are highly quenched by PET effect from the Q_3PA moiety as well as FRET effect from the NBD moiety. After reaction with both H_2S and hNQO1, probes **123** and **124** generate a significant fluorescence turn-on at 465 nm (220-fold) and 535 nm (400-fold), respectively, which further supports the high efficiency of the dual-quenching strategy. When compared with probe **123**, probe **124** displays a larger fluorescent response and higher selectivity for the dual-activation from H_2S and hNQO1. In addition, probe **124** was successfully applied to differentiate the endogenous levels of H_2S and activation of hNQO1 in HT29 and HepG2 cells from those in FHC, HCT116, and HeLa cells (Fig. 32c). Probe **124** was also used to demonstrate that endogenous H_2S and hNQO1 can be generated in live cells when cells suffer from acute oxidative stress caused by exogenous H_2O_2. These studies suggest that synergistic antioxidant effects of H_2S and hNQO1 may contribute to reducing oxidative

stress in live cells *via* the Nrf2 pathway, which can subsequently trigger the expression of hNQO1 directly and improve endogenous H_2S levels indirectly by controlling GSH (Fig. 32d).[214] The above results clearly demonstrate the strengths of this dual reporter system, including the significant off–on response, ability to distinguish cancer cells with both cancer biomarkers, and ability to investigate the crosstalk of different analytes. Such dual-reactable probes provide a number of advantages over single-analyte detection probes, including: (1) avoiding inhomogeneous intracellular distribution from different probes; (2) providing an enhanced off–on response due to the dual-quenching effects; and (3) enabling a simple method to investigate the cooperative relationship of different analytes.

5. NBD-Based probes for sensing proteins

5.1 Direct aminolysis of NBD-OR probes

Chemical tools for protein modifications are important for structural analysis and for functional investigation of proteins.[215–217] In general, lysine (Lys) residues are the most common targets for functionalization due to the relative abundance and its strong nucleophilicity. Moreover, there are many chemoselective reactions available for labelling primary amines.[218–220] One general design strategy for site-specific fluorogenic labelling of proteins is based on the reaction between a non-fluorescent NBD ether and accessible Lys amino group near a ligand binding site on the target protein, leading to the formation of fluorescent NBD-NHR adducts (Fig. 33a).[27,221] In addition, NBD ethers are also used in fluorogenic enzyme assays, especially for the detection of enzymes involved in the post-translational modifications (PTMs) of Lys.[222] Lys residues can undergo different types of PTMs.[223–225] For example, Lys acylation (Kac) levels are closely associated with numerous diseases, including neurological disorders,[226] cancers,[227–229] and cardiovascular disease.[230,231] Through enzymatic reaction, the free Lys residue in the fluorogenic probe can be released, which can undergo intramolecular reaction with NBD ether with turn-on fluorescence, enabling the detection of enzymatic activity. As a whole, NBD-based probes are now playing increasingly important roles in developing tools to better understand protein functions and interactions in cellular environments.

5.1.1 Site-specific fluorescent labelling of targeted proteins.—The reaction between an NBD-*O*-ligand probe and the amino group of Lys results in site-specific fluorescent labelling of the target protein.[27] The small size of the NBD group minimizes the impact of the ligand–protein interactions. Additionally, during such aminolysis of the NBD ether, the ligand moiety from the original NBD-*O*-ligand construct is released, which enables traceless fluorescent labelling of the target protein (Fig. 33a). To test this concept, Sodeoka and coworkers employed biotin–avidin as a ligand–protein pair (Fig. 33b), where Lys 111 (K111) of avidin near the biotin-binding site may react with the NBD-*O*-biotin probes. The group designed probes **125a–125h** with different linker lengths (Fig. 33c). Among the probes, **125f** and **125h** demonstrated the best labelling efficiency. Such NBD-based labelling requires the specific ligand–protein interaction and is not influenced by non-target proteins, providing a powerful method for selective fluorescence labelling of target proteins.

Subsequently, Sodeoka and coworkers employed the NBD-ether probes for intermolecular protein labelling in live cells. As shown in Fig. 33d, TSPO, an 18 kDa translocator protein, is mainly located on the outer mitochondrial membrane and is closely associated with VDAC (a 32 kDa voltage-dependent anion channel) and ANT (a 30 kDa adenine nucleotide translocase).[232,233] The TSPO-multiprotein complex was labelled with NBD-ether probes **126** and **127** bearing a TSPO ligand *N,N*-dialkyl-2-phenylindol-3-ylglyoxylamide (PIGA, Fig. 33d and e).[234] The *in vitro* labelling of mitochondria revealed that both probes reproducibly labelled two proteins with 32 and 28 kDa. Using two-dimensional polyacrylamide gel electrophoresis (2D PAGE) analysis, specific fluorescent labelling at 32 kDa was identified with probe **127** (Fig. 33f), which is assigned as VDAC. Another TSPO partner, ANT, however, was not labelled by this strategy, which is likely due to the lack of a Lys near the binding site of ANT for the labelling reaction.[27] The probe was successfully used to image the PIGA–TSPO interaction in live cells (Fig. 33g). Furthermore, probe **127** specifically labelled mitochondrial proteins (Fig. 33h), which is consistent with the localization of TSPO. These data suggest that the strategy allows for selective labelling and visualization of ligand-interacting proteins in live cells. Compared to other labelling strategies that require expression of genetically engineered proteins, this method is facile and allows direct labelling of native target proteins. One limitation of this method, however, is the requirement of a Lys residue at an appropriate position near the binding site for the direct aminolysis of NBD-OR probes.

Similarly, this NBD-based labelling was used successfully to label proteins in native membranes.[221] The smoothened receptor (SMO) is a frizzled G protein-coupled receptor (GPCR) that mediates the hedgehog signalling pathway.[235] To fluorescently label SMO, Tao, Zhao, and coworkers developed a series of NBD-based affinity probes to selectively label the K395 residue (Fig. 34). The ligand anchor fragment is derived from a potent SMO antagonist skeleton.[221] These probes, which have various modifications in the ligand skeleton and different linker lengths between the anchor fragment and NBD moiety, were synthesized to evaluate the labelling efficiency of SMO *via* fluorescence enhancement. A highly efficient probe **128i** was identified and further used to confirm the specificity of SMO labelling at the K395 residue. This probe also worked well for the on-membrane labelling of SMO, despite the fact that a side reaction occurred between the probe and the primary amine of the membrane lipid. The observed side reaction may be due to the hydrophobic interactions of the probe and the lipid. Therefore, highly selective ligand–protein interactions are required to design NBD-*O*-ligand probes for selective protein labelling in live cells.

5.1.2 Fluorogenic enzyme assays.—Fluorescent probes **129–136** were designed for enzymatic assays which make use of direct aminolysis of NBD ethers (Fig. 35–40). For example, Waters and coworkers developed a strategy to selectively label trimethyl lysine (Kme3) histone peptides for histone deacetylase (HDAC) assays.[231] Because most Kme3 residues are 4–5 amino acid residues away from another Lys residue in histones,[236] a receptor binding to the Kme3 residue can help place the NBD ether near a nucleophilic Lys in the target peptide to facilitate subsequent NBD labelling (Fig. 35a). To this end, NBD-based probe **129** was developed with a trisulfonated calix-[4]-arene as the Kme3 receptor (Fig. 35b).[222] The probe demonstrates a significant turn-on fluorescence at 520

nm in the presence of a Kme3 histone peptide and shows >5 fold selectivity in covalent labelling over the unmethylated Lys peptide (Fig. 35c). Using the substrates K4me3K9ac and K27acK36me3 peptides, the designed probe provides measurable turn-on fluorescence for assaying the HDAC activity (Fig. 35d). In addition, the presence of inhibitor significantly reduced the fluorescence enhancement during the enzymatic reaction (Fig. 35e), which suggests that this probe has potential for inhibitor screening. This work represents the first example of receptor-directed affinity labelling and broadens the scope of PTM detection by NBD-based probes.

Lysine acetylation is important for the regulation of intracellular processes and is catalyzed by lysine acetyltransferases (KATs).[237] Development of fluorescent probes for detecting the activity of KAT is useful for expanding the general understanding of KAT biological functions.[238] To this end, Zheng and coworkers reported three “turn-on” fluorescent probes **130–132** (Fig. 36) for development of a simple mix-and-read method for detecting KAT activity.[239] As shown in Fig. 36, the 3-azidopropanoyl group can be transferred to the substrate peptides *via* the KAT-catalyzed acylation. A subsequent bioorthogonal reaction with alkynyl-NBD results in an alkyne–azide clicked product, which will undergo an intramolecular nucleophilic substitution to generate a fluorescent NBD-NHR unit. Therefore, such assay can be used to sense the KAT-mediated acylation. This mix-and-read fluorogenic strategy does not require enzymatic coupling or product separation, which significantly reduces the complexity of the assay and enhances the throughput capacity.

In 2016, Sun and coworkers developed activity-based fluorescent probe **133a** (Fig. 37a), which contains the Kac residue and an NBD-ether for sensing deacetylation activity.[26] Upon enzymatic cleavage of the Kac, the released free amine reacts intramolecularly with the NBD ether to generate an NBD-NHR product with an associated turn-on fluorescence response (Fig. 37b). This turn-on can be up to 50-fold at 545 nm, which is larger than other reported single-step HDAC fluorescent probes. The probe is capable of determining the IC_{50} value of tenovin-6 (Fig. 37c), a known inhibitor of Sirtuin 2 (SIRT2). Building on these results, Sun and coworkers further designed dual-purpose fluorescent probe **133b** using a diazirine photo-crosslinker for protein labelling. Probe **133b** not only reports on the deacetylation activity, but also can fluorescently label target proteins such as SIRT1 and SIRT2 in a complex proteome environment (Fig. 37d).[26] The probes may provide useful tools for screening HDAC inhibitors and facilitate chemical proteomic study for epigenetics.

To investigate the potential enzymatic activity of SIRT2 toward Lys lipoylation, Sun, Hao, Zhang, and coworkers developed single-step fluorogenic probe **134** to report delipoylation activity in a continuous manner (Fig. 38a).[240] The study revealed that SIRT2 leads to significant delipoylation of probe **134**, resulting in a 60-fold fluorescence enhancement at 545 nm (Fig. 38b). Further detailed kinetic study with lipoylated peptides revealed that the delipoylation activity of SIRT2 (Fig. 38c) is about 400-fold higher than that of SIRT4, which is the only mammalian enzyme with known delipoylation activity. In addition, **134** is the first example of a single-step fluorescent probe developed for rapid assay of delipoylation activity, which can be useful for understanding the roles of Lys lipoylation in biology and medicine.

Yi, Li, Xiao, and coworkers developed a FRET-based NIR fluorescent probe **135** for assaying SIRT1 activity, which is an important member of HDACs.[241] As shown in Fig. 39, probe **135** contains a non-fluorescent NBD ether and an NIR fluorophore. The NBD ether in **135** can be converted to fluorescent NBD-NHR through intramolecular substitution after a deacetylation reaction with SIRT1. In addition, intramolecular FRET between the donor NBD-NHR and the NIR fluorophore occurs to generate a significant NIR fluorescence enhancement, which should minimize the interference in live systems in the process of SIRT1 detection. Thus, this probe not only detects SIRT1 *in vitro*, but also allows NIR imaging of SIRT1 activity in live cells.

Apart from using the direct reaction of amines released from enzymatic reactions to cleave NBD ethers, the trimethyl lock moiety can be used to unmask amino groups to react with NBD ether and produce fluorescence. Using acetylated trimethyl lock precursors, this approach can be used to develop systems to measure esterase activity.[242] To this end, Obika and coworkers developed probe **136** that contains an NBD ether and an acetylated trimethyl lock (Fig. 40). After esterase treatment and conversion of the acetyl group to a hydroxyl group, a rapid lactonization of the trimethyl lock moiety releases an amino group, which subsequently undergoes an intramolecular reaction to generate the fluorescent NBD-NHR. Probe **136** was used to detect porcine liver esterase activity *in vitro*.

5.2 Intermolecular interactions of NBD-amine probes and proteins

The emission of NBD amines is sensitive to the local environment, with lower fluorescence responses in polar and protic environments, and larger fluorescence responses in hydrophobic microenvironments. Moreover, the small size of the NBD moiety should not significantly affect the binding affinity of the parent ligand. As a result, NBD-modified lipid probes have be widely used for studies of lipid interactions, membrane fusion and assembly mechanisms in the last three decades.[243–250] On the other hand, lipid binding of NBD-modified protein probes can also result in significant fluorescence enhancement to study protein–membrane interactions.[251] Beyond the NBD-*N*-lipid probes, NBD-*N*-ligand probes can bind to hydrophobic domains of protein-of-interest (POI) accompanied by significant off–on fluorescence response (Fig. 41a), which can be used to study protein–ligand interactions and to develop fluorogenic enzyme assays.

5.2.1 Protein-small-molecule binding.—

Ali and coworkers investigated the interaction of NBD-based olanzapine derivative **137** with human serum albumin (HSA) *via* various spectroscopic and molecular docking methods (Fig. 41).[252] With successive additions of HSA protein, a gradual fluorescence enhancement of probe **137** was observed, and the maximum emission wavelength blue-shifted from yellow (555 nm) to green (533 nm). In addition, when compared to the free probe in aqueous solution, the average fluorescence lifetime values of HSA-**137** are increased. These can be due to increased motional constraint imposed by the rigid and nonpolar microenvironment within HSA, which subsequently limits accessible non-radiative decay processes of NBD. The binding of **137** to HSA was also indicated by a molecular docking study. All of these data supported that probe **137** is a useful tool for sensing protein–ligand interactions.

The NBD-*N*-ligand probes can also be used to sense proteins in live cells *via* wash-free imaging techniques. For example, Li and coworkers developed NBD-based agonists **138a–138c** for sensing of α1-adrenergic receptors (α1-ARs).[253] These probes, which contain NBD and phenylephrine linking *via* different lengths of carbon chains (Fig. 42a), demonstrate low quantum yields (< 0.06) in PBS buffer. Specifically, probe **138a** is up to 30-fold brighter in acetonitrile than in PBS, highlighting the environmental sensitivity of the probe. In addition, probe **138a** demonstrates a better binding affinity to α1-ARs than that of **138b** and **138c** with shorter linkers. Therefore, probe **138a** was successfully applied for monitoring the dynamic process of α1-AR internalization using real-time and wash-free imaging (Fig. 42b). Moreover, the *Renilla* luciferase (RLuc)-tagged α1-ARs can oxidize coelenterazine (CTZ) to generate bioluminescence at 480 nm to excite the NBD fluorophore (Fig. 42c) *via* a bioluminescence resonance energy transfer (BRET) mechanism. This BRET assay *via* the NBD-based probes (Fig. 42d) may be useful for high-throughput screening of α1-AR agonists and antagonists in the future.

NBD-*N*-ligand probes have also been investigated to image organelle-specific proteins (Fig. 43). For example, Taliani and coworkers synthesized a series of probes **139a–140** based on PIGAs as the ligands for binding mitochondrial TSPO.[234,254,255] Probes **139a** and **139b**, which have shorter ethylene chain linkers, demonstrate a moderate affinity toward TSPO. Whereas probes **139c–139f** with longer chain linkers demonstrate nanomolar binding affinities. This difference likely derives from the flexibility of the longer linker, which is more complementary than the shorter linker to the lipophilic pocket of the receptor binding site. On the other hand, the electron-withdrawing fluorine in the 4′-position slightly increases in the affinity toward TSPO. Subsequently, probe **139f** was chosen and used to specifically label TSPO in the mitochondria in C6 glioma cells. Probe **140** was also developed for irreversible labelling of TSPO through covalent linking of the isothiocyanate group to the receptor protein.[255] This probe was demonstrated to selectively and covalently label TSPO at a cellular level. Using 4-phenyquinazoline-2-carboxylic acid as the TSPO ligand, Taliani, Castellano, and coworkers also developed probes **141a–141b** for specifically labelling the TSPO in live cells.[256] Probe **141a** has a high binding affinity, attractive spectroscopic properties, and suitability for mitochondrial imaging (Fig. 43c).

Recently, Li, Sheng, and coworkers developed NBD-based probes **142a–142c** (Fig. 44a) for visualization of prenyl-binding protein (PDEδ) in live cells and tissues.[257] The PDEδ protein binds, solubilizes, and maintains the spatial organization of prenylated GTPases (*e.g.* Ras) in the cytosol.[258,259] The Φ values of **142a–142c** are 0.02–0.05 in PBS (pH 7.4), which increases to 0.28–0.31 in DMSO, highlighting the environment-sensitive turn-on property. Upon addition of PDEδ, the fluorescence intensities of probe **142c** increase by 6.6-fold at 555 nm. Live cell imaging showed that probes **142a–142c** exhibit stronger fluorescence in human pancreatic carcinoma cell lines (Capan-1) due to the overexpression of PDEδ than that of HEK293T cell lines. In addition, Capan-1 tumor slices treated with probes **142b–142c** showed stronger fluorescence than that of the deltazinone (a PDEδ inhibitor) pretreatment group or the normal mouse skin tissue slices (Fig. 44b). Taken together, these NBD-based probes are useful tools for investigating the physiological and pathological roles of the PDEδ protein.

To explore tools for *in situ* imaging of *Arabidopsis* histidine kinases (AHKs, cytokinin receptors), Spíchal, Plíhal, Benková, and coworkers developed probe **143** by attaching an NBD amine to the N9 position of isopentenyladenine (iP, a natural cytokinin).[260] Docking simulations suggest that the probe could bind with the active sites of all AHKs with micromolar affinity. Fluorescence images of plant cells treated with **143** support the ER as an organelle with affinity to the probe (cytokinin) (Fig. 44c). In addition, co-localization studies further revealed that the probe could accumulate in subcellular vesicles and plasma membrane (PM), implying that the cytokinin receptors may enter endo-membrane trafficking systems and also localize to the PM.[260b] This work highlights the utility of NBD-based probes in studying protein localization and functions in plants.

NBD-based probes using peptide ligands can also provide a robust strategy for sensing target proteins. For example, Tamaura and coworkers developed peptide probe **144**,[261] which is based on the interaction of leucine zipper (ZIP) peptides.[262] As shown in Fig. 45a, probe **144** interacts strongly with the peptide **A**/**B**, which led to a significant fluorescent enhancement and change from yellow (536 nm) to green (505 nm). In addition, **144** was used to image a membrane protein fusion with the peptide **A**/**B**. This ZIP tag-probe pair provides a method to facilitate the real-time and wash-free imaging of target proteins in live cells.

Epithelial cell adhesion molecule (EpCAM) is a hallmark of circulating tumor cells (CTCs).[263] To identify CTCs from blood, Shiba, Uzawa, and coworkers developed a series of NBD-based peptide probes **145a–145g** for sensing EpCAM-expressing cells.[264] Ep114, an EpCAM-binding peptide, was functionalized by replacing an amino acid with an NBD-modified aminophenylalanine (Fig. 45b). The probes **145b** and **145c** retain the binding ability of Ep114 and can specifically label EpCAM-expressing CTCs for fluorescence detection, which might be useful for aiding CTC diagnosis.

NBD-*N*-ligand probes can be designed to have a turn-off response by installing a quenching group near the protein binding site (Fig. 46a). Urano and coworkers developed fluorescent probe **146**, which reports integrin activity, by using cyclic RGD pentapeptides bearing NBD motifs (Fig. 46b).[265] The RGD peptide selectively binds to the integrin $\alpha_V\beta_3$ *via* interaction of the peptide and the Tyr^{122} of integrin β_3.[266] When treated with integrin $\alpha_V\beta_3$, probe **146** demonstrates a selective fluorescence decrease (Fig. 46c), due to PET quenching of NBD-NHR by the Tyr phenol.[122] Molecular mechanic investigations support that NBD and Tyr^{122} might be close (<10 Å) for efficient PET quenching. This sensing mechanism provides a method for investigating integrin–ligand interactions *via* NBD-based probes.

The binding between a hydropic pocket of proteins and NBD-modified lipids can also be used to sense the lipid–protein interactions (Fig. 47a). For example, Atkinson and coworkers developed phosphatidylcholine analogue **147** (Fig. 47b) for studying the effect of membrane concentration and composition on the transfer rate of phospholipids to small unilamellar vesicles (SUVs).[267] Binding of **147** to yeast phosphatidylinositol transfer protein (Sec14) resulted in a 50-fold fluorescence enhancement at 529 nm, and the associated dissociation constant (K_D) was determined to be 33 nM. Probe **147** was further applied to a FRET-based phospholipid transfer assay in which Sec14-bound **147** was rapidly mixed with SUVs

containing a FRET partner of NBD. In this assay, a fluorescence decrease was observed upon transfer of protein-bound **147** to vesicles, which suggests that this method may be conducive to understanding lipid transfer mechanisms.

In another study, Atkinson and coworkers developed **148a–148d**, which are fluorescent analogues of α-tocopherol, to investigate ligand binding and transfer by α-tocopherol transfer protein (α-TTP).[268] When comparing the fluorescence of **148a–148d** in ethanol *versus* aqueous buffer, each of the probes was significantly less fluorescent in water. For example, **148d** showed only 2% of the fluorescence in buffer compared to that observed in ethanol. The results suggested that probe **148d** has the most environmentally sensitive fluorescent response within this group of compounds. Upon addition of α-TTP protein, the fluorescence intensity of **148d** increased by 21-fold at 535 nm. In addition, probe **148d** binds specifically and reversibly to α-TTP with a K_D of 60 nM, which is comparable to the value of the natural ligand (K_D 25 nM), suggesting that **148d** may be a useful tool for investigating α-TTP activity at membranes.[268b]

Petry, Opatz, and coworkers developed fatty acid-bearing probes **149a–149f** with various chain lengths (Fig. 47b) for investigating lipid–HSA interactions.[269] Although the short chain conjugates **149a–149c** do not demonstrate fluorescence increase upon addition to HSA, the more lipophilic derivatives **149d–149f** all demonstrate a turn-on fluorescence response. Upon binding, probe **149f** generates a 4.5-fold fluorescence enhancement at 535 nm with a K_D of 27 μM. This response is consistent with the probe binding to HSA with a 1 : 1 binding stoichiometry, and the binding site was identified in a lipophilic region (subdomain IIA) of HSA using X-ray crystal structure analysis. In addition, FRET signals between Trp214 (donor) and NBD (acceptor) further confirmed the probe-protein binding. Importantly, the NBD-based probe enables the development of a fluorescent method to identify other ligands for HSA binding and to understand drug–protein interactions.

Chemical probes can help to clarify molecular mechanisms of sterol transport in mammalian cells. To this end, a series of NBD-modified cholesterol-like steroids (Fig. 47b) have been developed as probes for sensing cholesterol-binding proteins. For example, Sluchanko and coworkers reported probes **150–153** for binding steroidogenic acute regulatory protein (StAR),[270] which is a key factor in intracellular cholesterol transfer to mitochondria.[271] Of these compounds, probe **150** demonstrates the largest fluorescence enhancement during the binding with the apparent K_D of 26 nM. The NBD should be in close proximity to Trp241 in the **150**-StAR complex, leading to a FRET between the Trp residue and NBD, which also confirms the binding of **150** with StAR. These NBD-based probes should be useful tools for sensing StAR *in vitro*.

Cai and coworkers used the probe **151** for monitoring protein-mediated cholesterol monomerization from aggregates.[272] The fluorescence of **151** is strongly quenched in the aggregated state, but addition of the detergent sodium dodecylsulfate (SDS) results in a 32-fold fluorescence enhancement at 530 nm. Comparable dequenching is observed in the presence of proteins from enterocytes of hamster small intestine, which may help monomerization of the probe from its aggregated state. In addition, a ~140 kDa protein complex (p140) was identified to mediate the monomerization of **151**, and protein-disulfide

isomerase (PDI) is one of the components of the p140. The probe provides a rapid and sensitive assay for studying protein-assisted cholesterol monomerization.

Tontonoz and coworkers used probes **151** and **154** to study the cholesterol binding to ER-resident proteins (Aster).[273] All three Aster domains bound **151** with an accompanying significant fluorescence enhancement, but did not bind to **154** as no fluorescence change was observed during the binding study. Fluorescence competition assays revealed that the binding of **151** to Aster is inhibited by cholesterol, but not by several oxysterols. This study suggests that NBD-based probes are useful tools for studying sterol-binding proteins in mammalian cells.

NBD-*N*-ligand probes can also be applied for *in vivo* imaging. For example, Dhaliwal, Bradley, and coworkers developed a series of NBD-based probes **155a–155d** (Fig. 48a) for *in situ* and real-time visualization of Gram-negative bacterial species in human lungs.[274] These probes contain an NBD amine conjugated to the antimicrobial peptide polymyxin, which can selectively bind lipopolysaccharide (LPS) on the outer membrane of Gram-negative bacteria.[275] Among the probes, **155a** shows the best selectivity for Gram-negative over Gram-positive bacteria. Probe **155a** demonstrates a 3.5-fold fluorescence increase at 550 nm in nonpolar environments generated by increasing DMSO concentrations, forming the basis of its environmental sensitivity during bacterial membrane insertion. In addition, enrichment of the probe on bacteria may also contribute to the bright bioimaging. Probe **155a** was successfully used to label *P. aeruginosa* in a concentration-dependent manner. Furthermore, the probe could discriminate Gram-negative from Gram-positive bacteria with high signal-to-noise ratio. No labelling of human lung epithelial cells in a bacterial-human lung co-culture experiments was observed (Fig. 48b). Importantly, the probe was chemically stable, nontoxic, and used for the fast and selective detection of Gram-negative bacteria in patients (Fig. 48c). These results suggest that pulmonary molecular imaging using the NBD-based probes targeting bacterial lipid A may be applied for a fast diagnosis of bacterial infection.

5.2.2 Fluorogenic assays for detecting enzyme activity and inhibition.—

NBD-ligand probes have also been used to develop fluorogenic enzyme assays. For example, Peterson and coworkers developed probe **156** that mimics the Myr-Gly-Cys *N*-terminus of Src family proteins for assaying protein palmitoylation.[276] The observed PM fluorescence upon addition of **156** to cells (Fig. 49b) suggested that **156** is palmitoylated intracellularly. As expected, addition of inhibitor 2-bromopalmitic acid reduced the PM fluorescence of **156** (Fig. 49c). In addition, the cellular fluorescence was quantified by flow cytometry (Fig. 49d) and indicated that **156** can be used to detect the inhibition of palmitoylation with better sensitivity than previously reported assays.[276] These data suggest that probe **156** may provide an efficient method to carry out high-throughput assays for detection of protein palmitoylation.

Protein prenylation modifications in mammalian cells are catalyzed by three different prenyltransferases: farnesyltransferase (FTase), geranylgeranyl transferase-I (GGTase-I), and Rab (Ras-like protein from rat brain) geranylgeranyl transferase (RabGGTase).[277,278] In 2005, Alexandrov and coworkers developed fluorescent analogues **157a** and **157b** (Fig. 50a)

of farnesyl pyrophosphate (FPP) and geranylgeranyl pyrophosphate (GGPP), respectively, for assaying prenyltransferase activity and inhibition.[279–281] The small size of NBD enables the probes to be efficient lipid donors for prenyltransferases, as evidenced by significant fluorescence changes of **157b** in the presence of the enzymes (Fig. 50b). Such properties of the probes can be utilized for sensing the protein–ligand interactions (Fig. 50c).

Subsequently, an on-bead *in vitro* prenylation assay was developed based on the NBD-based probes (Fig. 50d).[279] In the assay, the substrate GTPase was attached to beads *via* a glutathione S-transferase (GST) tag. Upon mixing of prenyltransferase, probe **157a** or **157b**, and the substrate-loaded beads, the NBD fluorophore can be transferred to the beads after protein prenylation (Fig. 50e) to produce fluorescence-labelled beads. Prenyltransferase inhibitors can interrupt the transformation of NBD to the beads, which was employed for development of a high-throughput assay. Analysis of the prenylation by SDS-PAGE provided another assay for determination of the enzymatic activities and IC_{50} of inhibitors (Fig. 50f). When compared to small-molecule probe **157b**, the fluorescence intensity of the NBD-labelled Rab demonstrates an about 21-fold enhancement at 538 nm, which can be used to develop a fluorometric assay for RabGGTase.[280] In addition, analysis of interactions of the identified inhibitors with prenyltransferases can be achieved by using **157b** as a fluorescent reporter.[281] In summary, the NBD-based probes can be used as efficient substrates for the three prenyltransferases, providing efficient tools for the development of fluorogenic enzyme assays.

Commercial NBD-lipid probes can also be used to detect phospholipid scramblase activity.[282] For example, Menon and coworkers utilized the NBD-modified lipids to investigate the phospholipid scramblase activity of GPCRs (Fig. 51a). In this assay, the NBD acyl-labelled phospholipid probes can be distributed in both leaflets of large unilamellar vesicles. Dithionite ($S_2O_4^{2-}$) can irreversibly reduce NBD to non-fluorescent 7-amino-2,1,3-benzoxadiazol (ABD). $S_2O_4^{2-}$ will only eliminate the NBD fluorescence of the outer leaflet of the vesicles since it is negatively-charged and cannot cross membranes. In this case, ~50% of the NBD fluorescence is expected to be lost because NBD in the inner-leaflet lipids are protected from the reduction reaction. However, all fluorescence should be lost on adding $S_2O_4^{2-}$ in 'scramblase-active' vesicles, because the "flip-flop" process enables the access of inner-leaflet NBD lipids to the outer leaflet for the reduction. The results showed that about 80% of the fluorescence is lost for proteoliposomes (Fig. 51b and c), whereas about 50% of the fluorescence lost is observed for protein-free liposome. In addition, the assay revealed that scrambling is a constitutive activity of some rhodopsin-like GPCRs.[282]

5.2.3 Sensing protein–protein interactions.—Protein–protein interactions (PPIs) are involved in many biological processes including the assembly of enzymes,[283] regulation of enzymatic activity,[284] lipid transport,[285] gene expression,[286] and receptor–ligand interactions.[287] In addition, PPIs are employed as targets for therapeutic drug design.[288,289] Therefore, understanding the basics of PPIs can help reveal detailed biological mechanisms and also provide useful information or assay for designing therapeutic drugs.[290–292] The NBD-based protein probes can provide unique tools for sensing PPIs because of the small size of the NBD moiety, which minimizes potential interference in PPIs. In addition, the

environmental sensitivity and water solubility of the NBD moiety also make it an ideal fluorophore to study PPIs.

Prenylated Rab GTPases are involved in vesicle trafficking in eukaryotic cells and interact with a multitude of Rab-specific effectors including Rab escort protein (REP) and GDP dissociation inhibitor (GDI).[293] Biophysical analysis of the PPIs of prenylated Rabs is complicated by their low solubility in aqueous solutions. To solve this problem, Goody, Alexandrov, Wu, and coworkers developed semisynthetic fluorescent analogue **158** of prenylated Rab7 using expressed protein ligation (Fig. 52a).[294] The protein probe **158** is weakly fluorescent and water-soluble but has similar biological behaviours to naturally prenylated Rab7. As shown in Fig. 52b, addition of REP to **158** resulted in a 10-fold fluorescence increase at 525 nm. Consequently, probe **158** was successfully applied to study PPIs *in vitro*. Competitive fluorescence titrations indicated that REP shows about 20-fold stronger binding to monogeranylgeranylated Rab7 than that of doublyprenylated Rab7. Whereas GDI binds both prenylated forms of Rab7 with comparable affinities.[294] The protein probe helps to formulate a thermodynamic model for the extraction of Rab from membranes (Fig. 52c) and explain the need for both REP and GDI in Rab functions.

Goody, Wu, and coworkers further employed the protein probe **158** to study the mechanism of targeted membrane delivery of RabGTPases.[295] Fluorescence titrations revealed that REP or GDI demonstrates a three-order-of-magnitude greater affinity for GDP-bound Rab GTPase than for the GppNHp-bound protein (Fig. 52d and e). In addition, semi-synthetic NBD-labelled Rab probes were prenylated and then used for sensing the dissociation of Rab–REP or Rab–GDI complexes.[295] Furthermore, the reversible Rab–GDI interactions can be real-time monitored by the fluorescence change in the presence of guanine nucleotide exchange factors (GEFs). These protein probes help to produce detailed kinetic data of the PPIs, providing that nucleotide dissociation in the presence of a GEF can be very rapid, and once GDP–Rab dissociates from its complex with GDI, the nucleotide exchange reaction makes this dissociation essentially irreversible for the following membrane attachment (Fig. 52f).

Sommer and coworkers developed protein probes **159** for sensing PPIs by direct labelling of Cys residues in arrestin with NBD.[296] Specifically, multiple sites within the binding interface are individually mutated to Cys for NBD labelling (Fig. 53a). Of all the sites tested, only probes that have mutations on or near loop-72 (residues 68–78) or loop-344 (residues 336–344) demonstrate significant fluorescence increase when the probes bind to the dark-state rhodopsin (Fig. 53b). These results imply that the loop-72 and loop-344 are involved in PPIs. In addition, the PPI studies using **159** revealed that conformational changes in the loop-72 (*N*-domain) are coupled to the entry of agonist, whereas the loop-344 (*C*-domain) engages the apo-receptor even before agonist is added. Such a mechanism can protect the rod cells in bright light by concurrently sequestering toxic all-*trans*-retinol and allowing regeneration with 11-*cis*-retinal.[296b]

6. Self-assembled NBD-based probes

Self-assembly and disassembly of natural biomolecules play vital roles in regulating many biological processes and are responsible for various cellular functions.[297–299] Inspired by nature, many biomimic approaches have been developed and employed to construct supramolecular structures in a bottom-up manner.[300–302] Supramolecular self-assembly has emerged as an attractive approach due to its capacity for modifying the properties of supramolecular structures at the nanoscale. Various non-covalent interactions, including aromatic interactions, hydrogen bonds, electrostatic interactions, and hydrophobic contacts, contribute to the well-ordered nano- or micro-structures in self-assembled systems. Self-assembly approaches have been widely utilized in numerous applications, including enzyme activity assays,[303] cellular imaging,[304] drug delivery,[305] controlled release,[306] immune modulation,[307] and tissue engineering.[308]

NBD-containing motifs have gained popularity in designing building blocks for self-assembled systems due to the advantages of environmental sensitivity, water solubility, and small size. The NBD group can provide a significantly enhanced fluorescent signal upon self-assembly, which provides a method for monitoring the formation of hydrogelation (nanofibers) in real time. The rigid and hydrophobic microenvironment within nanofibers reduces the diffusion-originated non-radiative decay pathways and increases the quantum yield of NBD. In addition, enrichment of NBD groups within the nanofibers further contributes to the bright fluorescence for bioimaging. In particular, Xu and coworkers have pioneered many different approaches focused on enzyme-instructed self-assembly (EISA) and recently reviewed enzymatic noncovalent synthesis.[309] In this section, we specially discuss the NBD-based self-assembled probes and related sensing strategies and bioimaging applications.

6.1 ALP-triggered self-assembled probes

Alkaline phosphatase (ALP), an ectoenzyme overexpressed in cancer cells and involved in immunosuppression in tumors, represents an interesting therapeutic target.[310,311] In the last decade, many NBD-based self-assembled probes have been developed using ALP as the trigger for assaying enzyme activities as well as for developing organelle-targeted imaging and related applications.

6.1.1 Self-assembled probes for enzymatic activity.—Xu and coworkers reported the first approach for imaging ALP-instructed self-assembly of NBD-based probes inside living cells (Fig. 54).[13] In their design, an NBD fluorophore was conjugated to a self-assembled peptide motif to prepare a precursor L-**160**. ALP triggers the transformation of the precursor to a hydrogelator by removing the hydrophilic phosphate group, which leads to the formation of a hydrogel *via* self-assembly. The fluorescent signal of NBD allowed for real-time monitoring the formation of nanofibers inside live cells (Fig. 54c). The studies revealed that the self-assembly of the fluorescent nanofibers occurred in the ER and nanofiber growth proceeded from the ER toward the edge of the cells. Subsequently, Xu and coworkers designed and studied an enantiomer D-**160** with higher proteolytic stability.[312] An intense fluorescence signal from D-**160** was observed near the nuclei of live HeLa cells

(Fig. 54d), suggesting again that the self-assembled nanofibers formed around the ER. In addition, these studies revealed that the precursor chirality had negligible effects on EISA. This work represents the first detailed study of enzymatic dephosphorylation of D-peptides and illustrates the generation of supramolecular hydrogels with improved biostability.

In a subsequent study, Xu and coworkers reported self-assembly of D-peptidic derivative **161** for screening activities of ALPs in live cells at the single-cell level (Fig. 55a).[313] ALP-triggered dephosphorylation of **161** leads to self-assembly and subsequent formation of fluorescent, non-diffusive nanofibrils. This strategy was also utilized to profile the activity of ALPs in various types of cell lines at a single-cell level (Fig. 55b). The study revealed dramatically higher activity of ALPs in cancer cells than stromal cells. Interestingly, drug-resistant and drug-sensitive cancer cells exhibit different inherent ALP activities. This work highlights the potential of NBD-based self-assembled probes for the detection of cancer stem cells.

To better understand the structure–activity relationship (SAR) of EISA for killing cancer cells, Xu and coworkers designed NBD-containing D-tetrapeptides **162a** and **162b** with one or two phosphotryosine residues, respectively.[314] Treatment of HeLa cells with diphosphorylated **162b** only led to faint yellow fluorescence, whereas addition of monophosphorylated **162a** resulted in strong fluorescence on the surface of the cells (Fig. 55c). Compared with **162b**, monophosphorylated **162a** could quickly self-assemble on the surface of cancer cells and produce an increased fluorescent response. In contrast to the results in HeLa cells, the addition of **162a** in Saos-2 cells led to a more significant fluorescent response (Fig. 55c) due to the overexpression of ALP in Saos-2 cells. Moreover, **162a** exhibits more potent inhibitory activity to cancer cells than **162b**, which is likely due to the increased self-assembly of nanofibers around the cells. This work provides insights into designing suitable precursors for supramolecular assemblies as potential antitumor therapy.

Self-assembled NBD-based probes can also be applied for detecting ALP activity in complex biological fluids such as blood. Yang, Wang, and coworkers developed an efficient strategy of surface-induced self-assembly (Fig. 56) for “visualization” of ALP activities.[315] This method utilized a glass surface to initiate the self-assembly of an ALP-mediated fluorescent probe **163**. The produced nanofibers could be separated from the sample fluids and enriched on the glass surfaces with enhanced fluorescence and color (Fig. 56c and d). By comparing the color depth or thickness of hydrogels on the glass surface, the enzyme activity could be estimated directly by the naked eye. The approach is easy and can be utilized for direct assay of ALP activity in blood and cell lysates.

6.1.2 Organelle-targeted self-assembled probes.—

Subcellular organelle-targeting has emerged as an efficient approach for drug delivery due to its enhanced inhibitory capacity and decrease of side effects and cytotoxicity.[316,317] Recently, self-assembled NBD-based probes have also been used in combination with organelle-targeting moieties or functional groups to selectively form nanofibers in specific organelles of cells for different applications (Fig. 57–60).

Xu and coworkers designed probe **164** (Fig. 57a) using a cholesterol moiety for directly profiling membrane dynamics at a cellular level.[318] The cholesterol motif enables the probe to rapidly accumulate on the membrane. After the dephosphorylation by ectophosphatases on membranes, these probes can then self-assemble to produce a strong fluorescence response (Fig. 57b). Cell imaging with Saos-2 cells showed that the probe fluorescence was primarily localized on the cell membrane and there were different intensities at different locations, which suggested a heterogeneity of the membrane at the nanoscale. The excellent resolution of these imaging experiments also confirmed the membrane interconnectivity between live cells.

Similarly, the selective pericellular hydrogelation of probe **165b** (Fig. 57a) by ALP and membrane receptor cholecystokinin-2 (CCK2R) was reported by Yang and coworkers.[319] The probe is constructed by a self-assembled precursor NBD-GFFYp and a membrane-bound CCK-6 peptide fragment, which is a selective ligand of CCK2R. Probe **165b** can be efficiently converted to a hydrogelator by ALP. The resultant hydrogelator can then interact with CCK2R and self-assemble to form nanofibers around the cancer cells (Fig. 57c). In contrast, the control probe **165a** with a RGD moiety only exhibited faint fluorescent signal, implying essential roles of CCK2R for the formation of hydrogels. Moreover, the selectively formed hydrogels on the membrane efficiently inhibited the growth of cancer cells, which suggests its future potential for cancer therapy and diagnostics.

Targeting mitochondria and modulating mitochondrial redox potentials provides a promising strategy for killing cancer cells that minimizes drug resistance. To this end, Xu, Yang, and coworkers developed TPP-containing probe **166** for mitochondria-targeting self-assembly (Fig. 58a).[320] Upon dephosphorylation of D- or L-**166** by overexpressed ALP from cancer cells (*e.g.* Saos2), the peptide self-assembles to form nanostructures on the cellular surface, which can be uptaken *via* endocytosis and then localize to mitochondria (Fig. 58b). In addition, the intracellular self-assembly induced dysfunction of mitochondria and apoptosis. Importantly, this approach facilitates the spatial control of the self-assembly in mitochondria for selectively killing cancer cells. In another study, Ryu and coworkers also independently employed the TPP moiety to form nanofibers specifically on mitochondria for selectively killing cancer cells.[321]

Nuclear targeting of anticancer drugs is often important for cancer therapeutic efficacy since many of the drugs target the nucleus.[322,323] To this end, Yang, Li, and coworkers designed nucleus-directed probe **167a** by conjugating NBD-FFpYG with a dodecapeptide ligand (TSFAEYWNLLSP, PMI), which can accumulate in the nucleus (Fig. 59a).[324] For EISA at 4 °C or during a heating–cooling process (Fig. 59b), the peptides exhibited conformations similar to an α-helix. In contrast, the peptides adopted a β-sheet conformation during EISA at 37 °C. Despite these differences in conformation, the confocal images of HepG2 cells treated by the three methods (heating–cooling method of **167b**, EISA at 4 or 37 °C of **167a**) all exhibited bright yellow fluorescence, which overlapped with that labelled by the DAPI nuclear dye (Fig. 59c). In addition, the optimized nanomedicine formed by the EISA strategy at 4 °C exhibited improved nuclear accumulation and anticancer activity.

ER-targeting has emerged as an efficient strategy for cancer therapy.[325] For example, Xu and coworkers developed probe **168** by linking an L-Arg to the C-terminus of a D-tetrapeptide (Fig. 60a).[326] This probe could form crescent-shaped supramolecular assemblies (Fig. 60b) and disrupt cell membranes due to the positively charged L-Arg residue. Cell imaging experiments showed that the fluorescence from the self-assembly of **168** overlapped well with the signal from an ER-tracker (Fig. 60c), which indicated that **168** accumulated in the ER. In addition, the supramolecular assemblies induce ER stress and activate the caspase signaling cascade for apoptosis. Probe **168** also exhibited selective inhibition to cancer cells over normal cells due to the overexpression of ALP of cancer cells.

Furthermore, Xu and coworkers developed probe **169**, which contains the antagonistic motif (AVPI) of the inhibitors of apoptotic proteins (IAPs) for selectively killing cancer cells (Fig. 60a).[327] Probe **169** can enter cancer cells and normal cells through micropinocytosis and endocytosis, respectively. The assembled **169** mainly accumulated in the ER in cancer cells (Fig. 60d). Further immunofluorescence staining of XIAP (one of IAPs) showed that XIAP overlaps with the assembled **169** (Fig. 60e), suggesting that the **169** assemblies sequestrate and antagonize the IAPs in cancer cells. Conversely, **169** enters normal cells HS-5 through micropinocytosis, and the observed fluorescence barely colocalizes with the XIAP. In addition, the micelles of bortezomib (BTZ, a proteasome inhibitor) and **169** analogue can enter cancer cells and mainly assemble in the ER. Subsequently, the system releases BTZ to the cytosol, which induces apoptosis of cancer cells. Thus, the combination of BTZ and **169** analogue exhibited improved cytotoxicity against cancer cells, implying the potential of such approach for cancer therapy with enhanced selectivity and sensitivity.

6.2 Other enzyme-triggered self-assembled probes

6.2.1 Esterase-triggered self-assembled probes.—

D-Peptides have emerged as important platforms for biological applications, however, they often suffer from low cellular uptake due to weak interactions with endogenous transporters.[328] To address this problem, Xu and coworkers designed probe **170a** based on a D-peptide bearing a taurine moiety linked through an ester bond (Fig. 61a).[329] After being triggered by esterase, **170a** self-assembles to form nanofibers with bright fluorescence (Fig. 61b and c). The nanofiber formation could contribute to the accumulation of the D-peptide in live cells. More importantly, **170a** can boost the cellular uptake more than 10-fold compared to control compound **170b** without the taurine moiety. As shown in Fig. 61d, intense fluorescence from the assembled **170a** was observed in the cytoplasm, supporting the enhanced cellular uptake of the D-peptide. In contrast, only faint fluorescence from **170b** was observed, indicating its limited cellular uptake without a taurine moiety. This work provides a novel strategy to increase the cellular uptake of D-peptide-based self-assembled probes.

6.2.2 SIRT5-Triggered self-assembled probes.—

Very recently, Sun, Hu, and coworkers reported a strategy for utilizing SIRT5 with specific localization to achieve mitochondria-targeting self-assembly.[330] Probe **171** contains a self-assembled peptide fragment, a succinylated Lys as the enzyme trigger, and an NBD as the fluorescent reporter (Fig. 62a). Upon desuccinylation by the mitochondria-localized enzyme SIRT5, **171** could be transformed to a hydrogelator by removing hydrophilic succinylated groups, leading

to the formation of supramolecular nanofibers in mitochondria (Fig. 62b). The increased hydrophobicity that arose from the self-assembly significantly enhanced the fluorescence of NBD in the nanofibers. In contrast, control experiments using suramin (a SIRT5 inhibitor) exhibited negligible fluorescence. Further colocalization with Mito-tracker as well as cell fractionation experiments supported that the nanofibers were selectively formed in mitochondria (Fig. 62c). With this approach, Sun and coworkers provided activity-based imaging of SIRT5 in live cells for the first time. In addition, the self-assembly of **171** analogue in mitochondria was found to alter mitochondrial membrane potential and induce formation of ROS. Furthermore, synergistic anticancer effects between self-assembled **171** analogue and three different anticancer drugs were observed (Fig. 62d). This work provides a unique strategy for cellular SIRT5 imaging as well as a promising method for mitochondria-based cancer therapy.

6.2.3 Enterokinase-triggered self-assembled probe.—In general, most of the reported mitochondrial-targeting compounds are cationic and lipophilic, thereby exhibiting cytotoxicity to cells after mitochondrial accumulation. Alternatively, Xu and coworkers designed an enzymatic cleavage approach for branched peptidic probe **172** with negative charges for targeting mitochondria (Fig. 63a).[331] Probe **172** is constructed by a well-established protein FLAG-tag with an NBD-modified self-assembled motif. The cell-compatible probe could form micelles, which could be easily uptaken by cells. Upon cleavage of the hydrophilic FLAG-tag (DDDDK) by enterokinase (ENTK), **172** could rapidly self-assemble on mitochondria (Fig. 63b), whereas inhibiting ENTK proteolytic activity diminished mitochondria targeting ability. Moreover, the micelles formed by **172** were able to deliver a red-phycoerythrin (RPE) protein to mitochondria (Fig. 63c), as indicated by excellent co-localization of RPE and **172** in the mitochondria. This work illustrates the first example of mitochondrial targeting *via* enzymatic self-assembly and delivering cargo selectively to the mitochondria.

6.2.4 Caspase-triggered self-assembled probe.—Zhao, Wang, and coworkers developed a powerful probe **173**, which is responsive to caspase to form self-assembly *in vivo* (Fig. 64). The probe consists of an enzymatically cleavable linker (DEVD for caspase-3), a tumor-specific recognition motif (AVPIAQK for protein XIAP), a self-assembly motif (KLVFFAECG), an NBD group, and a functional molecule (NIR cyanine dye).[332] After entering cancer cells, the self-assembly of **173** can be triggered by caspase-3 to form intracellular nanofibrils. As expected, bright fluorescence was visible in H460 cells (human NSCLC cells with high XIAP expression). However, negligible fluorescence was observed for control groups of H460 cells treated with caspase-3 inhibitor or normal HEK293T cells with low XIAP levels. Furthermore, **173** showed enhanced accumulation in the tumor site of H460 xenograft mouse model (high expression of XIAP). After cleavage by enzyme, it undergoes self-assembly *in situ* and exhibits higher retention efficiency in the tumor region. This work provides an innovative strategy for *in vivo* self-assembly in tumors.

6.2.5 β-Galactosidase-triggered self-assembled probes.—Because β-galactosidase (β-Gal) is overexpressed in senescent cells, β-Gal-triggered self-assembly has been used for selectively identifying and removing senescent cells. For example, Yang,

Chen, and coworkers reported **174**, which is the first β-Gal responsive probe that could simultaneously detect and remove senescent cells (Fig. 64).[333] After enzymatic cleavage by β-Gal, **174** is transformed to a hydrogelator to form nanofibers in senescent cells associated with a bright fluorescence. In addition, the formed nanofibers could alleviate the senescence of endothelial cells and specifically remove senescent cells by inducing cell apoptosis. This work represents the first example of EISA *via* a sugar hydrolase, which may contribute to the development of biomedical applications related with sugar hydrolase.

6.2.6 Furin-triggered self-assembled probes.—

Yi, Zhou, and coworkers designed and synthesized a biocompatible probe **175**, which contains a gelator NBD-FFF and an RVRR motif for furin. Furin is a proprotein convertase to promote tumor progression (Fig. 64).[334] Probe **175** can self-assemble to stable micelles and demonstrates a rapid response toward furin with a 2.9-fold fluorescence enhancement at 549 nm in solution. Moreover, the probe exhibited bright fluorescence in furin-overexpressed breast adenocarcinoma cells (MDA-MB-231). However, the fluorescence of **175** in furin-deficient colorectal adenocarcinoma cells (LoVo) and normal macrophage cells (Raw 264.7) was negligible. This work represents the first strategy for selectively imaging furin-overexpressed cancer cells by the self-assembled probe.

6.2.7 Trypsin-triggered self-assembled probes.—

Xu and coworkers developed self-assembled probe **176**, which can be triggered by trypsin.[335] The probe contains an NBD fluorophore (Fig. 64), a self-assembled D-peptide backbone, and a branched peptide (KYDKKKKDG) that can be cleaved by trypsin. The probe could selectively form nanofibers in the ER of the high-grade serous ovarian cancer cell line (OVSAHO) that over-expresses trypsin. In addition, the fluorescence response of NBD in this system enabled the analysis of trypsin activity and also investigations of the dynamics and localization of the self-assembly in live cells. Moreover, the self-assembled **176** analogue resulted in ER stress and cancer cell death, but no cytotoxicity for normal cells due to low levels of intracellular trypsin. This work illustrates the first example of *in situ* trypsin-triggered self-assembly in the ER and provides an efficient strategy for targeting organelles with the potential for cancer therapy.

6.3 Nonenzyme-triggered self-assembled probes

Self-assembled NBD-based probes can be triggered by not only enzymes, but also environmental stimuli such as pH, temperature, and even bacterial surfaces. For instance, Zhong and coworkers reported a pH-triggered probe **177a** for accurate and reversible pH measurement.[336] The probe is constructed by a peptide fragment (VVAADD) and an NBD fluorophore linked by a C_{12}-alkyl-chain (Fig. 65a). At pH 7.0, the self-assembly of **177a** leads to a supramolecular hydrogel with β-sheet structures. When the pH was shifted to strongly alkaline solution, a gel-to-sol transition occurs rapidly. The fluorescence intensity of **177a** showed a sigmoidal relationship with the basic pH values, which provides an accurate pH detection assay regardless of ionic strength or salt identity. Control compound **177b**, which lacks the peptide motif, fails to self-assemble and only generated minimal fluorescence under similar conditions (Fig. 65b). Moreover, the fluorescence of **177a**

was fully reversible during cycles of pH at 7.0–11.2, which validated the design of pH-responsive sensors and *in situ* pH detection systems for numerous applications.

Yang and coworkers developed probe **178** for spatiotemporal control of the self-assembly (Fig. 65c).[337] The probe can form different aggregation states through controlling enzymatic activity at different temperatures, which led to the formation of nanoparticles at 37 °C with weak fluorescence but nanofibers (hydrogel) at 4 °C with bright fluorescence. Notably, confocal images showed that cells incubated with nanofibers exhibited an intense yellow fluorescence, whereas cells treated by nanoparticles only showed weak fluorescence. The results indicated that the nanofibers exhibited much higher cellular uptake (~10×) than nanoparticles in 3T3 cells. Moreover, the NBD fluorescence colocalized well with the red fluorescence from Lyso-Tracker, suggesting that the uptake of the nanofibers was through endocytosis. This work illustrates a new strategy for controlling the morphology and properties of nanomaterials in a spatiotemporal manner. Furthermore, Yang and coworkers reported a strategy to construct a thermogel system of self-assembled probe **179** through enzymatic dephosphorylation (Fig. 65c).[338] Unlike **178**, the EISA of **179** at 4 °C fails to form a hydrogel, but undergoes a sol-to-gel transition at 37 °C. The group further applied this thermogel system of **179** analogues for 3D cell culture due to their good bioactivity and biocompatibility. A hydrogel-cell structure was formed within 15 minutes. Moreover, the cells could spread well inside the thermogel and proliferate about 1.5 times during 5 days culture. This strategy holds great potential for tissue engineering and regenerative medicine.

The antibiotic vancomycin (Van) can tightly bind to the Gram-positive bacterial cell wall and result in bacterial death. Yang and coworkers developed NBD-Van conjugates that can self-assemble at the bacterial surface for simultaneous bacterial detection and inhibition, which is mediated by the interaction between the Van molecule and the terminal peptides at the bacteria surface (Fig. 66).[339] Both **180a** and **180b** show higher antimicrobial ability against *E. faecalis* than Van alone. The mixture of bacteria with probes **180a** or **180b** results in a fluorescence response of 2.3- or 1.4-fold at 550 nm in solution, respectively. The stronger fluorescence response of **180a** compared to **180b** may be due to its lower CMC value. Confocal images of bacteria treated with **180a** showed intense yellow fluorescence, indicating the self-assembly of **180a** at the surface of the bacteria. This work represents the first example of bacterial surface-induced self-assembly *via* the specific peptide–antibiotic interaction.

6.4 Dual-triggered self-assembled probes

Dual-triggered self-assembled probes allow the detection of multiple cancer biomarkers, which can dramatically improve diagnostic accuracy. For example, the Yang group designed a series of NBD-based probes that can be triggered by a combination of chemical and enzymatic reactions.[340–342] These systems allowed for the development of biomaterials that can detect multiple analytes and improve cancer therapy performance.

Yang, Wang, and coworkers developed self-assembled NBD-based probes for sensing both Cu^{2+} and caspase-3 or GSH.[340] Probe **181** was designed with a caspase-cleavable DEVD peptide placed between a self-assembly motif NBD-FFF and a Cu^{2+}-binding tripeptide GGH

(Fig. 67a). The fluorescence of self-assembled **181** was quenched by Cu^{2+} in aqueous buffer and live cells. After caspase-3 treatment, the GGH in probe **181** could be cleaved to restore a 12-fold fluorescence enhancement at 550 nm (Fig. 67b). Therefore, this property could be utilized for detecting caspase-3 activity *in vitro* and in cells. To demonstrate the universality of self-assembled nanofibers in multiple-analyte detection, probe **182** was also developed to sense GSH and Cu^{2+} (Fig. 67a). In the presence of Cu^{2+}, the fluorescence of **182** was significantly quenched, but could be restored by addition of GSH due to the removal of GGH (Fig. 67c). This work highlights that self-assembled NBD-based probes can be used to detect multiple biological analytes.

Later, Yang and coworkers developed probe **183**, which can be dual-activated by ALP and GSH (Fig. 68a).[341] The tandem self-assembly of **183** in the presence of ALP and GSH led to hydrogel formation *in vitro* (Fig. 68b), which was further characterized and verified by TEM (Fig. 68c). In addition, probe **183** first formed nanoparticles around the cells after activation by ALP and then self-assembled into nanofibers inside the cells due to GSH. As shown in Fig. 68d, after 0.5 h incubation of **183** in HepG2 cells, yellow fluorescent signals on the cell membrane were observed. When the incubation time was prolonged to 4 h, the yellow fluorescence expanded to a dense fiber network inside cancer cells. The strong fluorescence was also observed in OGY7703 cells. In contrast, only negligible fluorescence was observed in normal cell lines. Owing to the higher levels of ALP and GSH in liver cancer cells, probe **183** could self-assemble into nanofibers and exhibit enhanced cell killing activity in liver cancer cells than normal cells. Such dual-activated self-assembly might lead to new approaches for liver cancer diagnosis and therapy.

Yang, Li, and coworkers also developed probe **184** that can be dual-activated by ALP and reductase with tandem self-assembly behaviours in liver cancer cells (Fig. 69a).[342] After the reaction with extracellular ALP, probe **184** formed nanoparticles or short nanofibers and subsequently self-assembled into nanofibers after reaction with reductase on the mitochondrial membrane (Fig. 69b and c). The NBD fluorescence colocalized with the signal from Lyso-Tracker in A549 cells after 1 h incubation, suggesting efficient cellular uptake of the NBD-peptide by endocytosis (Fig. 69d). After 8 h incubation, the NBD fluorescence colocalized with the signal from Mito-tracker, indicating that the NBD-peptide had moved from the lysosomes to the mitochondria. Moreover, the accumulation of nanofibers in the mitochondria led to disruption of the mitochondrial membrane, ER stress, and consequently the apoptosis of A549 cells. This work provides a dual-triggered strategy for directing self-assembly in lung cancer cells, which may facilitate lung cancer diagnosis and therapy.

Very recently, Huang, Cai, and coworkers developed peptide probe **185** (Fig. 70a) that can self-assemble by tandem change in pH and treatment with legumain in glioma cells.[343] The probe contains a gelator NBD-FFY linked with an enzymatic cleavage site (ANN, triggered by legumain in lysosomes) followed by a RGD motif (for targeting integrin). The dual-responsive self-assembly of **185** led to a 12.3-fold fluorescent enhancement at 550 nm in legumain-containing solution at pH 5 (Fig. 70b). TEM images indicated that **185** can form nanodots at pH 5.0 (Fig. 70c) and then nanofibers after further incubation with legumain (Fig. 70d). In addition, such self-assembly in glioma cells allowed prolonged retention time

(48 h) in lysosomes (Fig. 70e). Importantly, the self-assembly blocked the degradation of HIF-1α in lysosomes, decreased DNA replication, and induced cell cycle arrest, which subsequently inhibited glioma cell growth. Furthermore, inhibition of tumor growth by **185** was confirmed in mice. This work suggests that the disruption of lysosomal functions by self-assembly might serve as an efficient strategy for inhibiting cancer cell growth.

7. Conclusions and future prospects

The above examples highlight the recently reported NBD-based probes and outline selected design strategies, detection mechanisms, and biological applications. These NBD-based tools have enabled significant progress in chemical and bioanalyte analysis and have advanced associated chemical biology investigations. Many of these studies are facilitated by the prominent photophysical properties of NBD-based fluorescent probes, namely environmental sensitivity, small size, high selectivity and reliable reactivity. In general, NBD-NHR compounds exhibit weak to moderate fluorescence, whereas other NBD derivatives (*i.e.* NBD-OR, NBD-SR, NBD-NRR′) range from being non-fluorescent to weakly fluorescent. NBD derivatives have also been incorporated as fluorescence quenchers by using PET and FRET effects. When combined, these properties lead to four major approaches that are commonly used in the design of NBD-based turn-on fluorescent probes (Fig. 71): (1) chemical cleavage of a quenched NBD-fluorophore to release the fluorophore and generate a fluorescence response (*e.g.* cleavage of NBD-NRR′ to form NBD-SH); (2) chemical transformation of weakly fluorescent NBD derivatives to brighter NBD derivatives (*e.g.* from NBD-SR to NBD-NHR); (3) ligand-exchange reactions to convert non-fluorescent NBD-OR to fluorescent NBD-NHR compounds; (4) changes in the local polarity environment to increase the fluorescence of NBD amines. In addition to these primary approaches, there are also instances in which PET groups can be used to further tune the fluorescence properties of NBD-NHR probes (*e.g.* **104**, **146**).

These sensing strategies have distinct intrinsic impacts on the maximal fluorescence enhancement of NBD-based systems. For example, in the thiolysis of NBD amines, the resultant fluorescent probes have different quenching mechanisms and efficiencies that depend on the emission profiles of the attached fluorophores (Fig. 71). In general, probes that use dual-quenching FRET-PET effects exhibit larger turn-on responses after activation (6.5–200 fold) than those of probes that rely on PET quenching alone (4.5–160 fold). NBD-amine-based probes are used widely in bioimaging and prodrug design. In general, NBD-*O*/*S*-fluorophore probes are efficiently quenched by PET or ICT effects from the NBD moiety. These probes can react with H_2S or biothiols and then release the fluorophore with large fluorescence enhancement (17–1000 fold). For example, the thiolysis of NBD (thio)ethers with Cys/Hcy, followed by rapid intramolecular Smiles rearrangement to generate fluorescent NBD-NHR compounds, results in large fluorescence responses at 540–550 nm (3.6–745 fold). This general approach can be used to improve selectivity on the thiol sensing systems and result in discriminative detection between biothiols. Similarly, direct aminolysis of NBD-*O*-ligand probes generates NBD-NHR fluorescent products with typical turn-on ranges of 5.2–60 fold. Related NBD-*NH*-ligand probes can bind target proteins with a hydrophobic microenvironment, which results in a similar fluorescence enhancement of the NBD fluorophore (2.4–50 fold). The small size of the NBD chromophore minimizes the

impact of the probes ligated or bound to target proteins. In addition, NBD-*NH*-precursor systems can self-assemble to enhance the fluorescence signal of NBD (less than 13 fold) in the presence of specific triggers. Although such fluorescence enhancement is fairly minimal by comparison to other NBD-based probes, the enrichment effects of NBD fluorophores within the nanofibers appear very useful for bright imaging in live systems.

Based on these NBD-based synthetic probes, significant progress has been made toward different bioapplications and new directions, including: (1) NIR NBD-based probes for tumor imaging; (2) NBD-based probes to selectively detect Cys or Hcy; (3) chemical-enzymatic dual-activated probes for differentiating cancer cells; (4) multi-reactable and multi-quenching probes for simultaneous discrimination of all biothiols; (5) thiolysis of NBD dyes for prodrug design; (6) direct aminolysis of NBD-based probes for site-specific fluorescent labelling of proteins; (7) NBD-based probes for sensing biomolecular interactions; (8) NBD-based probes for enzymatic assay and inhibitor screening; and (9) self-assembled NBD-based probes for various biomedical applications.

Building from these broad applications, the development of NBD-based synthetic probes is still in its infancy. New chemical probes are still needed to image and measure biological analytes dynamically with high efficiency and accuracy. For example, key unmet needs remain in monitoring changes of endogenous bioanalytes in real time and *in situ*. Additionally, the development of NBD-based cell-trappable probes can provide opportunities for further investigations into cell biochemistry. An additional opportunity lies in the area of PA and NIR-II fluorescent probe development, which can be used to improve imaging quality with deep tissue penetration ability. Additionally, many of the environment-sensitive NBD-NHR probes suffer from relatively small fluorescent enhancements, and the reactivity and selectivity of some NBD-based probes could also be improved. Therefore, continued efforts are needed to optimize the core scaffold of NBD fluorophores, which may be a promising approach to develop new probes with specific properties to adapt to different complex conditions.

We view that expansion of NBD-based probes with different substitution at the oxygen atom of the oxazole group, and/or electron-withdrawing groups at the 7-position are an additional area of likely future investigation (Fig. 72). To obtain different reactivity and selectivity, modifications of the 4-position of NBD with different linking groups[344] as well as replacement of the oxygen atom of the oxazole moiety[190] are efficient strategies. In addition, altering the electron-withdrawing group in the 7-position also contributes to the regulation of photophysical properties and environmental sensitivity. For example, sulfonamide substituted benzoxadiazole (SBD) is more sensitive to change in polarity and the hydrogen-bonding ability of a solvent than NBD.[345–349] In contrast to the less basic nitro (NBD) and sulfonamide (SBD) groups, cyanide substituted benzoxadiazole (CBD) with the greater basicity would confer even greater sensitivity and response of the emission to changes in polarity and solvation, but also may be more susceptible to nucleophilic attack.[350,351] In addition, SBD contains two reactive sites for facile development of dual-functional probes.[352–355] A practical limitation of many NBD-based systems is that the fluorescence is centered at 540 nm, which often overlaps with commonly-used green fluorescent reporters, and has minimal tissue penetration depth. Atomic substitution by a

chalcogen group has previously been used to shift the absorption and emission spectra of oxygen-containing dyes.[356–358] Similarly, the oxygen atom of the oxazole moiety in NBD could also be substituted by different groups for enhanced bioimaging performance, such as aliphatic amine (NBD(N)), sulfur (NBD(S)), selenium (NBD(Se)) and geminal dimethyl group (NBD(C)).[10,190,359,360] For example, Vendrell and coworkers developed the smallest fluorophores (NBD(C)) emitting in the NIR window (650–900 nm) reported to date.[360] We expect that various BD derivatives can be further developed for SBD(N), SBD(S), SBD(C), CBD(N), CBD(S), and CBD(C) (Fig. 72). Beyond the spectral properties, BD(N) derivatives provide two additional sites for modification, which can expand the functions for BD probes. BD dyes with other push–pull pairs[361–363] and even other isobenzofuran scaffolds[364] may also find use in the development of probes with different properties. Moreover, these modifications would impact the degree of aromaticity in the parent dye platform due to the different electronegativity of atomic substitution, which should result in additional tunable reactivities. These and other future modifications should provide a broad landscape for continued development and advancement of these synthetic probes to generate systems with specific tunable properties in the future.

The NBD-based multi-reactable probes described in this review have enabled the highly specific detection of H_2S as well as the simultaneous discrimination of biothiols. Despite great progress, we proposed that combining NBD with other receptors and reporters could be further used to advance the simultaneous detection of multiple analytes. In addition, future modifications of BD derivatives should also provide new opportunities for developing multi-reactable and multi-quenching probes for diverse future applications. As a whole, we expect that NBD-based probes will become increasingly important tools in revealing different biological mechanisms as well as in the diagnosis and treatment of diseases.

Acknowledgements

We thank all the excellent authors whose names appear in the references. We acknowledge the support of the National Key R&D Program of China (2017YFD0200501), NSFC (21877008, 21837001, and 21778044), the NIH (R01GM113030), Beijing Natural Science Foundation (2192038), and the Science Technology and Innovation Committee of Shenzhen Municipality (JCYJ20180507181654823).

Biographies

From left to right: Chenyang Jiang, Haojie Huang, Xueying Kang and Long Yi

From left to right: Chenyang Jiang, Haojie Huang and Xueying Kang received their BS degree at Beijing University of Chemical Technology (BUCT). They are currently PhD, MS, and PhD candidates at BUCT, respectively, with Long Yi. Long got his BS and MS from Nankai University, and earned his doctoral degree from Max-Planck Institute of Molecular Physiology under the joint direction of Prof. Roger S. Goody and Prof. Herbert Waldmann. In 2013, Long took a scientific research position at BUCT, and he also performed some experiments himself in Prof. Zhen Xi's group during 2013–2017. His current research

interests include NBD-based chemical tools for H_2S biology as well as chemical labelling of biomolecules.

Liu Yang

Liu Yang received her BS and MS degrees from Central South University in 2014 and 2017. After she obtained her PhD degree in 2020 from City University of Hong Kong under the supervision of Dr Hongyan Sun, she is currently a Postdoctoral Fellow in the group of Dr Sun. Her current research focuses on designing fluorescent probes and enzyme-instructed self-assembly.

Zhen Xi

Prof. Dr Zhen Xi got a BS in Chemistry from Central China Normal University (1979–1983), MS in Organometallic Chemistry from Nankai University (1985–1988), and PhD in Bioorganic Chemistry from Uppsala University (Sweden) under the supervision of Professor Jyoti Chattopadhyaya (1990–1994). He was a Postdoc Research Associate in the Department of Biological Chemistry & Molecular Pharmacology in Harvard Medical School with Professor Irvine H. Goldberg (1994–2001). He joined Nankai Faculty as a Changjiang Professor (specially appointed by the Ministry of Education, China) in 2001. Currently he is a Chairman of Department of Chemical Biology, Nankai University, and the Director of National Engineering Research Center on Pesticide (Tianjin). His research interests include chemical biology of nucleic acids and pesticide science.

Hongyan Sun

Dr Sun received her BS from Wuhan University and PhD from National University of Singapore. Her PhD research focused on systematic enzyme profiling under the supervision of Professor Shao Qin Yao. After receiving her doctorate, she was granted a fellowship by Humboldt Foundation and carried out postdoc research with Professor Herbert Waldmann at Max Planck Institute of Molecular Physiology. She joined the City University of Hong

Kong in 2011 and was promoted to associate professor in 2017. Her current research interests include developing chemical tools for studying protein PTMs and designing novel biosensors/biomaterials for biological applications.

Michael D. Pluth

Michael D. Pluth earned his BS in chemistry and applied mathematics from the University of Oregon in 2004 where he conducted undergraduate research with Prof. David Tyler. He earned his PhD in 2008 from UC Berkeley as an NSF predoctoral fellow under the joint direction of Profs. Robert Bergman and Kenneth Raymond in the area of supramolecular chemistry. Mike then moved to MIT as an NIH NRSA and later NIH Pathway to Independence Postdoctoral Fellow with Prof. Stephen Lippard. Mike began his independent career at the University of Oregon in 2011. His research interests are thematically based on different aspects of chemical biology and physical organic chemistry. Much of his lab focuses on investigations into reactive sulfur species relevant to biology.

Notes and references

1. Ghosh PB and Whitehouse MW, 7-Chloro-4-nitrobenzo-2-oxa-1,3-diazole: A new fluorigenic reagent for amino acids and other amines, Biochem. J, 1968, 108, 155–156. [PubMed: 5657448]
2. Imai K, Uzu S and Toyo'oka T, Fluorogenic reagents, having benzofurazan structure, in liquid chromatography, J. Pharm. Biomed. Anal, 1989, 7, 1395–1403. [PubMed: 2490525]
3. Imai K, Uzu S, Kanda S and Baeyems WRG, Availability of fluorogenic reagents having a benzofurazan structure in the biosciences, Anal. Chim. Acta, 1994, 290, 3–20.
4. Uchiyama S, Santa T, Okiyama N, Fukushima T and Imai K, Fluorogenic and fluorescent labelling reagents with a benzofurazan skeleton, Biomed. Chromatogr, 2001, 15, 295–318. [PubMed: 11507712]
5. Santa T, Fukushima T, Ichibangase T and Imai K, Recent progress in the development of derivatization reagents having a benzofurazan structure, Biomed. Chromatogr, 2008, 22, 343–353. [PubMed: 18059058]
6. Pidgeon SE, Fura JM, Leon W, Birabaharan M, Vezenov D and Pires MM, Metabolic profiling of bacteria by unnatural C-terminated D-amino acids, Angew. Chem., Int. Ed, 2015, 54, 6158–6162.
7. Akram AR, Avlonitis N, Lilienkampf A, Perez-Lopez AM, McDonald N, Chankeshwara SV, Scholefield E, Haslett C, Bradley M and Dhaliwal K, A labelled-ubiquicidin antimicrobial peptide for immediate *in situ* optical detection of live bacteria in human alveolar lung tissue, Chem. Sci, 2015, 6, 6971–6979. [PubMed: 29861935]
8. Tan HY, Eskandari R, Shen D, Zhu Y, Liu T-W, Willems LI, Alteen MG, Madden Z and Vocadlo DJ, Direct one-step fluorescent labelling of *O*-GlcNAc-modified proteins in live cells using metabolic intermediates, J. Am. Chem. Soc, 2018, 140, 15300–15308. [PubMed: 30296064]
9. Uchiyama S, Santa T, Fukushima T, Homma H and Imai K, Effects of the substituent groups at the 4- and 7-positions on the fluorescence characteristics of benzofurazan compounds, J. Chem. Soc., Perkin Trans 2, 1998, 2165–2174.
10. Uchiyama S, Kimura K, Gota C, Okabe K, Kawamoto K, Inada N, Yoshihara T and Tobita S, Environment-sensitive fluorophores with benzothiadiazole and benzoselenadiazole structures as

candidate components of a fluorescent polymeric thermometer, Chem. – Eur. J, 2012, 18, 9552–9563. [PubMed: 22760959]

11. Singha S, Kim D, Roy B, Sambasivan S, Moon H, Rao AS, Kim JY, Joo T, Park JW, Rhee YM, Wang T, Kim KH, Shin YH, Jung J and Ahn KH, A structural remedy toward bright dipolar fluorophores in aqueous media, Chem. Sci, 2015, 6, 4335–4342. [PubMed: 29218204]
12. Brunsveld L, Kuhlmann J, Alexandrov K, Wittinghofer A, Goody RS and Waldmann H, Lipidated ras and rab peptides and proteins–synthesis, structure, and function, Angew. Chem., Int. Ed, 2006, 45, 6622–6646.
13. Gao Y, Shi J, Yuan D and Xu B, Imaging enzyme-triggered self-assembly of small molecules inside live cells, Nat. Commun, 2012, 3, 1033. [PubMed: 22929790]
14. Kand D, Saha T and Talukdar P, Off-on type fluorescent NBD-probe for selective sensing of cysteine and homocysteine over glutathione, Sens. Actuators, B, 2014, 196, 440–449.
15. Khalili F, Henni A and East ALL, p*K*a Values of some piperazines at (298, 303, 313, and 323) K, J. Chem. Eng. Data, 2009, 54, 2914–2917.
16. Song F, Li Z, Li J, Wu S, Qiu X, Xi Z and Yi L, Investigation of thiolysis of NBD amines for the development of H_2S probes and evaluating the stability of NBD dyes, Org. Biomol. Chem, 2016, 14, 11117–11124. [PubMed: 27853796]
17. de Almeida RFM, Santos TCB, da Silva LC, Suchodolski J, Krasowska A, Stokowa-Sołtys K, Puchalska M and Starosta R, NBD derived diphenyl(aminomethyl)phosphane – a new fluorescent dye for imaging of low pH regions and lipid membranes in live cells, Dyes Pigm, 2021, 184, 108771.
18. Wada M, Hirose M, Kuroki M, Ikeda R, Sekitani Y, Takamura N, Kuroda N and Nakashima K, Simultaneous determination of homocysteine, methionine and cysteine in maternal plasma after delivery by HPLC-fluorescence detection with DBD-F as a label, Biomed. Chromatogr, 2013, 27, 708–713. [PubMed: 23225528]
19. Zivanovic J, Kouroussis E, Kohl JB, Adhikari B, Bursac B, Schott-Roux S, Petrovic D, Miljkovic JL, Thomas-Lopez D, Jung Y, Miler M, Mitchell S, Milosevic V, Gomes JE, Benhar M, Gonzalez-Zorn B, Ivanovic-Burmazovic I, Torregrossa R, Mitchell JR, Whiteman M, Schwarz G, Snyder SH, Paul BD, Carroll KS and Filipovic MR, Selective persulfide detection reveals evolutionarily conserved antiaging effects of *S*-sulfhydration, Cell Metab, 2019, 30, 1152–1170. [PubMed: 31735592]
20. Ellis HR and Poole LB, Novel application of 7-chloro-4-nitrobenzo-2-oxa-1,3-diazole to identify cysteine sulfenic acid in the ahpC component of alkyl hydroperoxide reductase, Biochemistry, 1997, 36, 15013–15018. [PubMed: 9398227]
21. Sigg RH, Luisi PL and Aboderin AA, Alkaline structural transition of 4-nitrobenz-2-oxa-1,3-diazolyl-Lysozyme. Kinetic and spectroscopic investigations, J. Biol. Chem, 1977, 252, 2507–2514. [PubMed: 15990]
22. Montoya LA, Pearce TF, Hansen RJ, Zakharov LN and Pluth MD, Development of selective colorimetric probes for hydrogen sulfide based on nucleophilic aromatic substitution, J. Org. Chem, 2013, 78, 6550–6557. [PubMed: 23735055]
23. Wei C, Wei L, Xi Z and Yi L, A FRET-based fluorescent probe for imaging H_2S in live cells, Tetrahedron Lett, 2013, 54, 6937–6939.
24. Wei C, Zhu Q, Liu WW, Chen WB, Xi Z and Yi L, NBD-based colorimetric and fluorescent turn-on probes for hydrogen sulfide, Org. Biomol. Chem, 2014, 12, 479–485. [PubMed: 24276473]
25. Montoya LA and Pluth MD, Hydrogen sulfide deactivates common nitrobenzofurazan-based fluorescent thiol labelling reagents, Anal. Chem, 2014, 86, 6032–6039. [PubMed: 24852143]
26. Xie Y, Ge J, Lei H, Peng B, Zhang H, Wang D, Pan S, Chen G, Chen L, Wang Y, Hao Q, Yao SQ and Sun H, Fluorescent probes for single-step detection and proteomic profiling of histone deacetylases, J. Am. Chem. Soc, 2016, 138, 15596–15604. [PubMed: 27805808]
27. Yamaguchi T, Asanuma M, Nakanishi S, Saito Y, Okazaki M, Dodo K and Sodeoka M, Turn-on fluorescent affinity labelling using a small bifunctional *O*-nitrobenzoxadiazole unit, Chem. Sci, 2014, 5, 1021–1029.

28. Lin VS, Chen W, Xian M and Chang CJ, Chemical probes for molecular imaging and detection of hydrogen sulfide and reactive sulfur species in biological systems, Chem. Soc. Rev, 2015, 44, 4596–4618. [PubMed: 25474627]
29. Yi L and Xi Z, Thiolysis of NBD-based dyes for colorimetric and fluorescence detection of H_2S and biothiols: Design and biological applications, Org. Biomol. Chem, 2017, 15, 3828–3839. [PubMed: 28358164]
30. Wallace JL and Wang R, Hydrogen sulfide-based therapeutics: Exploiting a unique but ubiquitous gasotransmitter, Nat. Rev. Drug Discovery, 2015, 14, 329–345. [PubMed: 25849904]
31. Kimura H, Hydrogen sulfide: From brain to gut, Antioxid. Redox Signaling, 2010, 12, 1111–1123.
32. Wang R, Physiological implications of hydrogen sulfide: A whiff exploration that blossomed, Physiol. Rev, 2012, 92, 791–896. [PubMed: 22535897]
33. Szabo C, A timeline of hydrogen sulfide (H_2S) research: From environmental toxin to biological mediator, Biochem. Pharmacol, 2018, 149, 5–19. [PubMed: 28947277]
34. Hartle MD and Pluth MD, A practical guide to working with H_2S at the interface of chemistry and biology, Chem. Soc. Rev, 2016, 45, 6108–6117. [PubMed: 27167579]
35. Stipanuk MH and Beck PW, Characterization of the enzymic capacity for cysteine desulphhydration in liver and kidney of the rat, Biochem. J, 1982, 206, 267–277. [PubMed: 7150244]
36. Shibuya N, Koike S, Tanaka M, Ishigami-Yuasa M, Kimura Y, Ogasawara Y, Fukui K, Nagahara N and Kimura H, A novel pathway for the production of hydrogen sulfide from D-cysteine in mammalian cells, Nat. Commun, 2013, 4, 1366. [PubMed: 23340406]
37. Kabil O and Banerjee R, Enzymology of H_2S biogenesis, decay and signaling, Antioxid. Redox Signaling, 2014, 20, 770–782.
38. Kimura H, Hydrogen sulfide: Its production, release and functions, Amino Acids, 2011, 41, 113–121. [PubMed: 20191298]
39. Mani S, Cao W, Wu L and Wang R, Hydrogen sulfide and the liver, Nitric Oxide, 2014, 41, 62–71. [PubMed: 24582857]
40. Feng X, Zhang H, Shi M, Chen Y, Yang T and Fan H, Toxic effects of hydrogen sulfide donor NaSH induced liver apoptosis is regulated by complex IV subunits and reactive oxygen species generation in rats, Environ. Toxicol, 2020, 35, 322–332. [PubMed: 31680430]
41. Yan Y, Chen C, Zhou H, Gao H, Chen L, Chen L, Gao L, Zhao R and Sun Y, Endogenous hydrogen sulfide formation mediates the liver damage in endotoxemic rats, Res. Vet. Sci, 2013, 94, 590–595. [PubMed: 23151462]
42. Huang CY, Yao WF, Wu WG, Lu YL, Wan H and Wang W, Endogenous CSE/H_2S system mediates TNF-α-induced insulin resistance in 3T3-L1 adipocytes, Cell Biochem. Funct, 2013, 31, 468–475. [PubMed: 23080424]
43. Cao X, Ding L, Xie ZZ, Yang Y, Whiteman M, Moore PK and Bian JS, A review of hydrogen sulfide synthesis, metabolism, and measurement: Is modulation of hydrogen sulfide a novel therapeutic for cancer?, Antioxid. Redox Signaling, 2019, 31, 1–38.
44. Hellmich MR, Coletta C, Chao C and Szabo C, The therapeutic potential of cystathionine β-synthetase/hydrogen sulfide inhibition in cancer, Antioxid. Redox Signaling, 2015, 22, 424–448.
45. Szabo C and Papapetropoulos A, International union of basic and clinical pharmacology. CII: Pharmacological modulation of H_2S levels: H_2S donors and H_2S biosynthesis inhibitors, Pharmacol. Rev, 2017, 69, 497–564. [PubMed: 28978633]
46. Szabo C, Coletta C, Chao C, Modis K, Szczesny B, Papapetropoulos A and Hellmich MR, Tumor-derived hydrogen sulfide, produced by cystathionine-beta-synthase, stimulates bioenergetics, cell proliferation, and angiogenesis in colon cancer, Proc. Natl. Acad. Sci. U. S. A, 2013, 110, 12474–12479. [PubMed: 23836652]
47. Untereiner AA, Olah G, Modis K, Hellmich MR and Szabo C, H_2S-induced *S*-sulfhydration of lactate dehydrogenase a (LDHA) stimulates cellular bioenergetics in HCT116 colon cancer cells, Biochem. Pharmacol, 2017, 136, 86–98. [PubMed: 28404377]
48. Phillips CM, Zatarain JR, Nicholls ME, Porter C, Widen SG, Thanki K, Johnson P, Jawad MU, Moyer MP, Randall JW, Hellmich JL, Maskey M, Qiu S, Wood TG, Druzhyna N, Szczesny B, Modis K, Szabo C, Chao C and Hellmich MR, Upregulation of cystathionine-β-synthase in

colonic epithelia reprograms metabolism and promotes carcinogenesis, Cancer Res, 2017, 77, 5741–5754. [PubMed: 28923859]

49. Fan K, Li N, Qi J, Yin P, Zhao C, Wang L, Li Z and Zha X, Wnt/beta-catenin signaling induces the transcription of cystathionine-gamma-lyase, a stimulator of tumor in colon cancer, Cell. Signalling, 2014, 26, 2801–2808. [PubMed: 25193114]
50. Szabo C, Gasotransmitters in cancer: From pathophysiology to experimental therapy, Nat. Rev. Drug Discovery, 2016, 15, 185–203. [PubMed: 26678620]
51. Sekoguchi F, Sekimoto T, Ogura A and Kawabata A, Endogenous hydrogen sulfide enhances cell proliferation of human gastric cancer AGS cells, Biol. Pharm. Bull, 2016, 39, 887–890. [PubMed: 27150157]
52. You J, Shi X, Liang H, Ye J, Wang L, Han H, Fang H, Kang W and Wang T, Cystathionine-γ-lyase promotes process of breast cancer in association with STAT3 signaling pathway, Oncotarget, 2017, 8, 65677–65686. [PubMed: 29029463]
53. Wang L, Shi H, Liu Y, Zhang W, Duan X, Li M, Shi X and Wang T, Cystathionine-γ-lyase promotes the metastasis of breast cancer *via* the VEGF signaling pathway, Int. J. Oncol, 2019, 55, 473–487. [PubMed: 31173185]
54. Ismail I, Wang D, Wang Z, Wang D, Zhang C, Yi L and Xi Z, A julolidine-fused coumarin-NBD dyad for highly selective and sensitive detection of H_2S in biological samples, Dyes Pigm, 2019, 163, 700–706.
55. Yang L, Wang F, Luo X, Kong X, Sun Z and You J, A FRET-based ratiometric fluorescent probe for sulfide detection in actual samples and imaging in *Daphnia magna*, Talanta, 2020, 209, 120517. [PubMed: 31892092]
56. Kim HM and Cho BR, Small-molecule two-photon probes for bioimaging applications, Chem. Rev, 2015, 115, 5014–5055. [PubMed: 25938620]
57. Zheng Z, Liu H, Zhai S, Zhang H, Shan G, Kwok RTK, Ma C, Sung HHY, Williams ID, Lam JWY, Wong KS, Hu X and Tang BZ, Highly efficient singlet oxygen generation, two-photon photodynamic therapy and melanoma ablation by rationally designed mitochondria-specific near-infrared AIEgens, Chem. Sci, 2020, 11, 2494–2503. [PubMed: 34084415]
58. Tang Y and Jiang G-F, A novel two-photon fluorescent probe for hydrogen sulfide in live cells using an acedan-NBD amine dyad based on FRET process with high selectivity and sensitivity, New J. Chem, 2017, 41, 6769–6774.
59. Roubinet B, Bailly L, Petit E, Renard P-Y and Romieu A, A FRET-based probe for fluorescence sensing of sulfide/sulfite analytes, using a novel long-wavelength water-soluble 7-hydroxycoumarin as reporter fluorophore, Tetrahedron Lett, 2015, 56, 1015–1019.
60. Filipovic MR, Zivanovic J, Alvarez B and Banerjee R, Chemical biology of H_2S signaling through persulfidation, Chem. Rev, 2018, 118, 1253–1337. [PubMed: 29112440]
61. May PM, Batka D, Hefter G, Königsberger E and Rowland D, Goodbye to S^{2-} in aqueous solution, Chem. Commun, 2018, 54, 1980–1983.
62. Huang Y, Zhang C, Xi Z and Yi L, Synthesis and characterizations of a highly sensitive and selective fluorescent probe for hydrogen sulfide, Tetrahedron Lett, 2016, 57, 1187–1191.
63. Wang RY, Li ZF, Zhang CY, Li YY, Xu GC, Zhang QZ, Li LY, Yi L and Xi Z, Fast-response turn-on fluorescent probes based on thiolysis of NBD amine for H_2S bioimaging, ChemBioChem, 2016, 17, 962–968. [PubMed: 26952316]
64. Sureshkumar K, Ramakrishnappa T and Samrat D, Piperazine appended napthalimide scaffold as turn on fluorescent probe for hydrogen sulfide, Microchem. J, 2020, 157, 105019.
65. Zhu H, Fan J, Du J and Peng X, Fluorescent probes for sensing and imaging within specific cellular organelles, Acc. Chem. Res, 2016, 49, 2115–2126. [PubMed: 27661761]
66. Zhu J-L, Xu Z, Yang Y and Xu L, Small-molecule fluorescent probes for specific detection and imaging of chemical species inside lysosomes, Chem. Commun, 2019, 55, 6629–6671.
67. Zheng X, Zhu W, Ni F, Ai H, Gong S, Zhou X, Sessler JL and Yang C, Simultaneous dual-colour tracking lipid droplets and lysosomes dynamics using a fluorescent probe, Chem. Sci, 2019, 10, 2342–2348. [PubMed: 30881662]
68. Zhang J, Wang RY, Zhu ZT, Yi L and Xi Z, A FRET-based ratiometric fluorescent probe for visualizing H_2S in lysosomes, Tetrahedron, 2015, 71, 8572–8576.

69. Ou-Yang J, Jiang W-L, Tan K-Y, Liu H-W, Li S-J, Liu J, Li Y-F and Li C-Y, Two-photon fluorescent probe for precisely detecting endogenous H_2S in lysosome by employing a dual lock system, Sens. Actuators, B, 2018, 260, 264–273.
70. Pak YL, Li J, Ko KC, Kim G, Lee JY and Yoon J, Mitochondria-targeted reaction-based fluorescent probe for hydrogen sulfide, Anal. Chem, 2016, 88, 5476–5481. [PubMed: 27094621]
71. Jia X, Li W, Guo Z, Guo Z, Li Y, Zhang P, Wei C and Li X, An NBD-based mitochondrial targeting ratiometric fluorescent probe for hydrogen sulfide detection, Chemistry-Select, 2019, 4, 8671–8675.
72. Zhang H, Chen J, Xiong H, Zhang Y, Chen W, Sheng J and Song X, An endoplasmic reticulum-targetable fluorescent probe for highly selective detection of hydrogen sulfide, Org. Biomol. Chem, 2019, 17, 1436–1441. [PubMed: 30672561]
73. Ismail I, Chen Z, Sun L, Ji X, Ye H, Kang X, Huang H, Song H, Bolton SG, Xi Z, Pluth MD and Yi L, Highly efficient H_2S scavengers *via* thiolysis of positively-charged NBD amines, Chem. Sci, 2020, 11, 7823–7828. [PubMed: 34094155]
74. Ismail I, Wang D, Wang D, Niu C, Huang H, Yi L and Xi Z, A mitochondria-targeted red-emitting probe for imaging hydrogen sulfide in live cells and zebrafish, Org. Biomol. Chem, 2019, 17, 3389–3395. [PubMed: 30860220]
75. Zhang Y, Chen H, Chen D, Wu D, Chen X, Liu SH and Yin J, A fluorescent turn-on H_2S-responsive probe: Design, synthesis and application, Org. Biomol. Chem, 2015, 13, 9760–9766. [PubMed: 26252421]
76. Wei H-G, Liu Y-J and Zhao X-D, Methylene blue-based 7-nitro-1,2,3-benzoxadiazole NIR fluorescent probe triggered by H_2S, Bioorg. Med. Chem. Lett, 2020, 30, 127221. [PubMed: 32386977]
77. Wang Y, Lv X and Guo W, A reaction-based and highly selective fluorescent probe for hydrogen sulfide, Dyes Pigm, 2017, 139, 482–486.
78. Guo Z, Park S, Yoon J and Shin I, Recent progress in the development of near-infrared fluorescent probes for bioimaging applications, Chem. Soc. Rev, 2014, 43, 16–29. [PubMed: 24052190]
79. Zhang J, Chai X, He X-P, Kim H-J, Yoon J and Tian H, Fluorogenic probes for disease-relevant enzymes, Chem. Soc. Rev, 2019, 48, 683–722. [PubMed: 30520895]
80. Ismail I, Chen Z, Ji X, Sun L, Yi L and Xi Z, A fast-response red shifted fluorescent probe for detection of H_2S in live cells, Molecules, 2020, 25, 437.
81. Huang X, Liu H, Zhang J, Xiao B, Wu F, Zhang Y, Tan Y and Jiang Y, A novel near-infrared fluorescent hydrogen sulfide probe for live cell and tissue imaging, New J. Chem, 2019, 43, 6848–6855.
82. Zhang K, Zhang J, Xi Z, Li L-Y, Gu X, Zhang Q-Z and Yi L, A new H_2S-specific near-infrared fluorescence-enhanced probe that can visualize the H_2S level in colorectal cancer cells in mice, Chem. Sci, 2017, 8, 2776–2781. [PubMed: 28553513]
83. Yang X, Zhang C, Shen L, Bao H, Xu J, Fang X, Zhao Y and Yang W, A near-infrared fluorescent probe for sulfide detection, Sens. Actuators, B, 2017, 242, 332–337.
84. Xiong J, Xia L, Huang Q, Huang J, Gu Y and Wang P, Cyanine-based NIR fluorescent probe for monitoring H_2S and imaging in live cells and *in vivo*, Talanta, 2018, 184, 109–114. [PubMed: 29674020]
85. Wu MX, Sha XL, Wei XR, Sun R, Chen Y, Gao J, Xu YJ and Ge JF, Fluorescent hydrogen sulfide probes based on azonia-cyanine dyes and their imaging applications in organelles, Anal. Chim. Acta, 2019, 1068, 60–69. [PubMed: 31072478]
86. Xu Z-Y, Wu Z-Y, Tan H-Y, Yan J-W, Liu X-L, Li J-Y, Xu Z-Y, Dong C-Z and Zhang L, Piperazine-tuned NBD-based colorimetric and fluorescent turn-off probes for hydrogen sulfide, Anal. Methods, 2018, 10, 3375–3379.
87. Huang J, Qu W, Zhu J, Liu H, Wen W, Zhang X and Wang S, Electrochemiluminescent sensor based on $Ru(bpy)_3^{2+}$-doped silica nanoprobe by incorporating a new co-reactant NBD-amine for selective detection of hydrogen sulfide, Sens. Actuators, B, 2019, 284, 451–455.
88. Cheng H-B, Li Y, Tang BZ and Yoon J, Assembly strategies of organic-based imaging agents for fluorescence and photoacoustic bioimaging applications, Chem. Soc. Rev, 2020, 49, 21–31. [PubMed: 31799523]

89. Zhang J, Wen G, Wang W, Cheng K, Guo Q, Tian S, Liu C, Hu H, Zhang Y, Zhang H, Wang L and Sun H, Controllable cleavage of C-N bond-based fluorescent and photoacoustic dual-modal probes for the detection of H_2S in live mice, ACS Appl. Bio Mater, 2021, 4, 2020–2025.

90. Xie Y, Huang H, Ismail I, Sun H, Yi L and Xi Z, A fluorogenic H_2S-triggered prodrug based on thiolysis of the NBD amine, Bioorg. Med. Chem. Lett, 2019, 29, 126627. [PubMed: 31444083]

91. (a)Huang Z, Ding S, Yu D, Huang F and Feng G, Aldehyde group assisted thiolysis of dinitrophenyl ether: A new promising approach for efficient hydrogen sulfide probes, Chem. Commun, 2014, 50, 9185–9187;(b)Ding SS, Feng WY and Feng GQ, Rapid and highly selective detection of H_2S by nitrobenzofurazan (NBD) ether-based fluorescent probes with an aldehyde group, Sens. Actuators, B, 2017, 238, 619–625.

92. Hou P, Li HM and Chen S, A highly selective and sensitive 3-hydroxyflavone-based colorimetric and fluorescent probe for hydrogen sulfide with a large Stokes shift, Tetrahedron, 2016, 72, 3531–3534.

93. Chen Q, Yang J, Li Y, Zheng J and Yang R, Sensitive and rapid detection of endogenous hydrogen sulfide distributing in different mouse viscera *via* a two-photon fluorescent probe, Anal. Chim. Acta, 2015, 896, 128–136. [PubMed: 26481996]

94. Jeong YA, Chang IJ and Chang S-K, Discriminative sensing of sulfide and azide ions in solution by anitro-benzoxadiazole-dansyl dyad by simply tuning the water content, Sens. Actuators, B, 2016, 224, 73–80.

95. Boens N, Leen V and Dehaen W, Fluorescent indicators based on BODIPY, Chem. Soc. Rev, 2012, 41, 1130–1172. [PubMed: 21796324]

96. Shi Z, Han X, Hu W, Bai H, Peng B, Ji L, Fan Q, Li L and Huang W, Bioapplications of small molecule Aza-BODIPY: From rational structural design to *in vivo* investigations, Chem. Soc. Rev, 2020, 49, 7533–7567. [PubMed: 32996497]

97. Wang JM, Yu H, Li Q and Shao SJ, A BODIPY-based turn-on fluorescent probe for the selective detection of hydrogen sulfide in solution and cells, Talanta, 2015, 144, 763–768. [PubMed: 26452888]

98. Kang J, Huo FJ, Ning P, Meng XM, Chao JB and Yin CX, Two red-emission single and double ‘arms’ fluorescent materials stemed from ‘one-pot’ reaction for hydrogen sulfide *vivo* imaging, Sens. Actuators, B, 2017, 250, 342–350.

99. Gong SY, Zhou EB, Hong JX and Feng GQ, Nitrobenzoxadiazole ether-based near-infrared fluorescent probe with unexpected high selectivity for H_2S imaging in live cells and mice, Anal. Chem, 2019, 91, 13136–13142. [PubMed: 31550882]

100. (a)Jin X, Zhao S, Wang T, Si L, Liu Y, Zhao C, Zhou H, Leng X and Zhang X, Near-infrared fluorescent probe for selective detection of H_2S and its application in live animals, Anal. Bioanal. Chem, 2019, 411, 5985–5992; [PubMed: 31236651] (b)Zhu HC, Liu CY, Yuan RF, Wang RK, Zhang HM, Li ZL, Jia P, Zhu BC and Sheng WL, A simple highly specific fluorescent probe for simultaneous discrimination of cysteine/homocysteine and glutathione/hydrogen sulfide in live cells and zebrafish using two separated fluorescence channels under single wavelength excitation, Analyst, 2019, 144, 4258–4265. [PubMed: 31215916]

101. Kim HW, Choi MG, Park H, Lee JW and Chang S-K, Single molecular multianalyte signaling of sulfide and azide ions by a nitrobenzoxadiazole-based probe, RSC Adv, 2015, 5, 4623–4627.

102. (a)Lan LA, Wu SY, Meng XG, Jiang JJ, Zheng MY and Fan GR, A simple liquid chromatography tandem mass spectrometric method for fast detection of hydrogen sulfide based on thiolysis of 7-nitro-2, 1, 3-benzoxadiazole ether, J. Chromatogr. A, 2020, 1625, 461243; [PubMed: 32709315] (b)Bae J, Choi J, Park TJ and Chang S-K, Reaction-based colorimetric and fluorogenic signaling of hydrogen sulfide using a 7-nitro-2,1,3-benzoxadiazole-coumarin conjugate, Tetrahedron Lett., 2014, 55, 1171–1174.

103. Zhai L, Shi Z, Tu Y and Pu S, A dual emission fluorescent probe enables simultaneous detection and discrimination of Cys/Hcy and GSH and its application in cell imaging, Dyes Pigm, 2019, 165, 164–171.

104. Ghanizadeh A, Akhondzadeh S, Hormozi M, Makarem A, Abotorabi-Zarchi M and Firoozabadi A, Glutathione-related factors and oxidative stress in autism, a review, Curr. Med. Chem, 2012, 19, 4000–4005. [PubMed: 22708999]

105. Maher P, The effects of stress and aging on glutathione metabolism, Ageing Res. Rev, 2005, 4, 288–314. [PubMed: 15936251]
106. Paul BD, Sbodio JI and Snyder SH, Cysteine metabolism in neuronal redox homeostasis, Trends Pharmacol. Sci, 2018, 39, 513–524. [PubMed: 29530337]
107. Cotgreave IA and Gerdes RG, Recent trends in glutathione biochemistry – glutathione-protein interactions: A molecular link between oxidative stress and cell proliferation?, Biochem. Biophys. Res. Commun, 1998, 242, 1–9. [PubMed: 9439600]
108. Lu SC, Glutathione synthesis, Biochim. Biophys. Acta, Gen. Subj, 2013, 1830, 3143–3153.
109. Stipanuk MH, Sulfur amino acid metabolism: Pathways for production and removal of homocysteine and cysteine, Annu. Rev. Nutr, 2004, 24, 539–577. [PubMed: 15189131]
110. Yin J, Ren WK, Yang G, Duan JL, Huang XG, Fang RJ, Li CY, Li TJ, Yin YL, Hou YQ, Kim S and Wu GY, L-Cysteine metabolism and its nutritional implications, Mol. Nutr. Food Res, 2016, 60, 134–146. [PubMed: 25929483]
111. Qu K, Lee SW, Bian JS, Low CM and Wong PT, Hydrogen sulfide: Neurochemistry and neurobiology, Neurochem. Int, 2008, 52, 155–165. [PubMed: 17629356]
112. Paulsen CE and Carroll KS, Cysteine-mediated redox signaling: Chemistry, biology, and tools for discovery, Chem. Rev, 2013, 113, 4633–4679. [PubMed: 23514336]
113. Lehmann A, Alterations in hippocampal extracellular amino acids and purine catabolites during limbic seizures induced by folate injections into the rabbit amygdala, Neuroscience, 1987, 22, 573–578. [PubMed: 3670597]
114. Heafield MT, Fearn S, Steventon GB, Waring RH, Williams AC and Sturman SG, Plasma cysteine and sulphate levels in patients with motor neurone, Parkinson's and Alzheimer's disease, Neurosci. Lett, 1990, 110, 216–220. [PubMed: 2325885]
115. Schnelldorfer T, Gansauge S, Gansauge F, Schlosser S, Beger HG and Nussler AK, Glutathione depletion causes cell growth inhibition and enhanced apoptosis in pancreatic cancer cells, Cancer, 2000, 89, 1440–1447. [PubMed: 11013356]
116. Gorrini C, Harris IS and Mak TW, Modulation of oxidative stress as an anticancer strategy, Nat. Rev. Drug Discovery, 2013, 12, 931–947. [PubMed: 24287781]
117. Hudson VM, Rethinking cystic fibrosis pathology: The critical role of abnormal reduced glutathione (GSH) transport caused by CFTR mutation, Free Radical Biol. Med, 2001, 30, 1440–1461. [PubMed: 11390189]
118. Chen Y, Dong H, Thompson DC, Shertzer HG, Nebert DW and Vasiliou V, Glutathione defense mechanism in liver injury: Insights from animal models, Food Chem. Toxicol, 2013, 60, 38–44. [PubMed: 23856494]
119. Saharan S and Mandal PK, The emerging role of glutathione in Alzheimer's disease, J. Alzheimer's Dis, 2014, 40, 519–529. [PubMed: 24496077]
120. Jacobsen JP, Rodriguiz RM, Mørk A and Wetsel WC, Monoaminergic dysregulation in glutathione-deficient mice: Possible relevance to schizophrenia?, Neuroscience, 2005, 132, 1055–1072. [PubMed: 15857710]
121. Hwang C, Sinskey AJ and Lodish HF, Oxidized redox state of glutathione in the endoplasmic reticulum, Science, 1992, 257, 1496–1502. [PubMed: 1523409]
122. Cairns RA, Harris IS and Mak TW, Regulation of cancer cell metabolism, Nat. Rev. Cancer, 2011, 11, 85–95. [PubMed: 21258394]
123. Petras M, Tatarkova Z, Kovalska M, Mokra D, Dobrota D, Lehotsky J and Drgova A, Hyperhomocysteinemia as a risk factor for the neuronal system disorders, J. Physiol. Pharmacol, 2014, 65, 15–23. [PubMed: 24622826]
124. Robinson K, Gupta A, Dennis V, Arheart K, Chaudhary D, Green R, Vigo P, Mayer EL, Selhub J, Kutner M and Jacobsen DW, Hyperhomocysteinemia confers an independent increased risk of atherosclerosis in end-stage renal disease and is closely linked to plasma folate and pyridoxine concentrations, Circulation, 1996, 94, 2743–2748. [PubMed: 8941098]
125. de Carvalho SCR, Muniz MTC, Siqueira MDV, Siqueira ERF, Gomes AV, Silva KA, Bezerra LCL, D'Almeida V, de Oliveira CPMS and Pereira LMMB, Plasmatic higher levels of homocysteine in non-alcoholic fatty liver disease (NAFLD), Nutr. J, 2013, 12, 37. [PubMed: 23547829]

126. Debreceni B and Debreceni L, The role of homocysteine-lowering B-vitamins in the primary prevention of cardiovascular disease, Cardiovasc. Ther, 2014, 32, 130–138. [PubMed: 24571382]

127. Krishna SM, Dear A, Craig JM, Norman PE and Golledge J, The potential role of homocysteine mediated DNA methylation and associated epigenetic changes in abdominal aortic aneurysm formation, Atherosclerosis, 2013, 228, 295–305. [PubMed: 23497786]

128. Sharma M, Tiwari M and Tiwari RK, Hyperhomocysteinemia: Impact on neurodegenerative diseases, Basic Clin. Pharmacol. Toxicol, 2015, 117, 287–296. [PubMed: 26036286]

129. Steegers-Theunissen RP, Boers GH, Trijbels FJ and Eskes TK, Neural-tube defects and derangement of homocysteine metabolism, N. Engl. J. Med, 1991, 324, 199–200. [PubMed: 1984202]

130. Seshadri S, Beiser A, Selhub J, Jacques PF, Rosenberg IH, D'Agostino RB, Wilson PW and Wolf PA, Plasma homocysteine as a risk factor for dementia and Alzheimer's disease, N. Engl. J. Med, 2002, 346, 476–483. [PubMed: 11844848]

131. Refsum H, Ueland P, Nygård O and Vollset SE, Homocystein and cardiovascular disease, Annu. Rev. Med, 1998, 49, 31–62. [PubMed: 9509248]

132. Karmin O and Siow YL, Metabolic imbalance of homocysteine and hydrogen sulfide in kidney disease, Curr. Med. Chem, 2018, 25, 367–377. [PubMed: 28486919]

133. van Meurs JBJ, Dhonukshe-Rutten RAM, Pluijm SMF, van der Klift M, de Jonge R, Lindemans J, de Groot LCPGM, Hofman A, Witteman JCM, van Leeuwen JPTM, Breteler MMB, Lips P, Pols HAP and Uitterlinden AG, Homocysteine levels and the risk of osteoporotic fracture, N. Engl. J. Med, 2004, 350, 2033–2041. [PubMed: 15141041]

134. Behera J, Bala J, Nuru M, Tyagi SC and Tyagi N, Homocysteine as a pathological biomarker for bone disease, J. Cell. Physiol, 2017, 232, 2704–2709. [PubMed: 27859269]

135. Wang JM, Shao XM, Wang JH and Shao SJ, An NBD-based fluorescent turn-on probe for the detection of homocysteine over cysteine and its imaging applications, Chem. Lett, 2017, 46, 442–445.

136. Gu X-H, Lei Y, Wang S, Cao F, Zhang Q, Chen SJ, Wang K-P and Hu Z-Q, Tetrahydro[5]helicene fused nitrobenzoxadiazole as a fluorescent probe for hydrogen sulfide, cysteine/homocysteine and glutathione, Spectrochim. Acta, Part A, 2020, 229, 118003.

137. Zhu HC, Zhang HM, Liang CX, Liu CY, Jia P, Li ZL, Yu YM, Zhang X, Zhu BC and Sheng WL, A novel highly sensitive fluorescent probe for bioimaging biothiols and its applications in distinguishing cancer cells from normal cells, Analyst, 2019, 144, 7010–7016. [PubMed: 31647063]

138. Zhang D, Du W, Peng B, Ni Y, Fang H, Qiu X, Zhang G, Wu Q, Yu C, Li L and Huang W, Two-photon small molecular fluorogenic probe visualizing biothiols and sulfides in live cells, mice brain slices and zebrafish, Sens. Actuators, B, 2020, 323, 128673.

139. Qiu XY, Jiao XJ, Liu C, Zheng DS, Huang K, Wang Q, He S, Zhao LC and Zeng XS, A selective and sensitive fluorescent probe for homocysteine and its application in live cells, Dyes Pigm, 2017, 140, 212–221.

140. Hammers MD and Pluth MD, Ratiometric measurement of hydrogen sulfide and cysteine/homocysteine ratios using a dual-fluorophore fragmentation strategy, Anal. Chem, 2014, 86, 7135–7140. [PubMed: 24934901]

141. Song XF, Tu YY, Wang RJ and Pu SZ, A lysosome-targetable fluorescent probe for simultaneous detection and discrimination of Cys/Hcy and GSH by dual channels, Dyes Pigm, 2020, 177, 108270.

142. Jing XY, Yu FQ and Lin WY, A fluorescent probe for specific detection of cysteine in lysosomes *via* dual-color mode imaging, Spectrochim. Acta, Part A, 2020, 240, 118555.

143. Zhang YB, Wang JF, Yue YK, Chao JB, Huo FJ and Yin CX, A new strategy for the fluorescence discrimination of Cys/Hcy and GSH/H_2S simultaneously colorimetric detection for H_2S, Spectrochim. Acta, Part A, 2020, 227, 117537.

144. Odyniec ML, Park S-J, Gardiner JE, Webb EC, Sedgwick AC, Yoon J, Bull SD, Kim HM and James TD, A fluorescent ESIPT-based benzimidazole platform for the ratiometric two-photon imaging of ONOO– *in vitro* and *ex vivo*, Chem. Sci, 2020, 11, 7329–7334. [PubMed: 33033609]

145. Zhu ZT, Liu W, Cheng LH, Li ZF, Xi Z and Yi L, New NBD-based fluorescent probes for biological thiols, Tetrahedron Lett, 2015, 56, 3909–3912.

146. Men YW, Li ZF, Zhang J, Tong ZZ, Xi Z, Qiu XB and Yi L, Rational design and synthesis of fast-response NBD-based fluorescent probes for biothiols, Tetrahedron Lett, 2015, 56, 5781–5786.

147. Zhou ZY, Duan GF, Wang YY, Yang SK, Liu XY, Zhang LY, Sun RN, Xu YG, Gu YQ and Zha XM, A highly sensitive fluorescent probe for selective detection of cysteine/homocysteine from glutathione and its application in live cells and tissues, New J. Chem, 2018, 42, 18172–18181.

148. Lu Z, Lu Y, Fan C, Sun X, Zhang M and Lu Y, A two-separated-emission fluorescent probe for simultaneous discrimination of Cys/Hcy and GSH upon excitation of two different wavelengths, J. Mater. Chem. B, 2018, 6, 8221–8227. [PubMed: 32254942]

149. Lu ZL, Lu Y, Sun X, Fan CH, Long ZY and Gao LY, A dual-emission fluorescent probe for discriminating cysteine from homocysteine and glutathione in live cells and zebrafish models, Bioorg. Chem, 2019, 92, 103215. [PubMed: 31541803]

150. Sharma P, Kumar K, Kaur S, Kaur S, Bhargava G, Kumar S and Singh P, Near-IR discriminative detection of H_2S and Cysteine with 7-nitro-2,1,3-benzoxadiazole-perylenediimide conjugate in water, live cells and solid state: Mimicking IMP, INH and NOR/OR complimentary logic, J. Photochem. Photobiol., A, 2020, 388, 112151.

151. Gao XH, Li XH, Li LH, Zhou J and Ma HM, A simple fluorescent off-on probe for the discrimination of cysteine from glutathione, Chem. Commun, 2015, 51, 9388–9390.

152. Zhang J, Miao YQ, Cheng Z, Liang LL, Ma XY and Liu CY, A paper-based colorimetric assay system for sensitive cysteine detection using a fluorescent probe, Analyst, 2020, 145, 1878–1884. [PubMed: 31971166]

153. Yang MW, Fan JL, Sun W, Du JJ, Long S and Peng XJ, Simultaneous visualization of cysteine/homocysteine and glutathione in live cells and *Daphnia magna via* dual-signaling fluorescent chemosensor, Dyes Pigm, 2019, 168, 189–196.

154. Ren XJ, Tian HH, Yang L, He L, Geng YN, Liu XJ and Song XZ, Fluorescent probe for simultaneous discrimination of Cys/Hcy and GSH in pure aqueous media with a fast response under a single-wavelength excitation, Sens. Actuators, B, 2018, 273, 1170–1178.

155. Chen WQ, Luo HC, Liu XJ, Foley JW and Song XZ, Broadly applicable strategy for the fluorescence based detection and differentiation of glutathione and cysteine/homocysteine: Demonstration *in vitro* and *in vivo*, Anal. Chem, 2016, 88, 3638–3646. [PubMed: 26911923]

156. Niu HW, Ni BW, Chen KK, Yang XP, Cao WB, Ye Y and Zhao YF, A long-wavelength-emitting fluorescent probe for simultaneous discrimination of H_2S/Cys/GSH and its bio-imaging applications, Talanta, 2019, 196, 145–152. [PubMed: 30683344]

157. Huang YF, Zhang YB, Huo FJ, Liu YM and Yin CX, Dual-channel red fluorescent probe for detection of Cys/Hcy and GSH in plants, Sens. Actuators, B, 2019, 301, 127123.

158. Ren XJ, Zhang Y, Zhang F, Zhong H, Wang JP, Liu XJ, Yang ZG and Song XZ, Red-emitting fluorescent probe for discrimination of Cys/Hcy and GSH with a large Stokes shift under a single-wavelength excitation, Anal. Chim. Acta, 2020, 1097, 245–253. [PubMed: 31910966]

159. Pan J, Zhang Y, Xu JC, Liu JB, Zeng LT and Bao G-M, A smart fluorescent probe for simultaneous detection of GSH and Cys in human plasma and cells, RSC Adv, 2015, 5, 97781–97787.

160. Xia X and Qian Y, NIR two-photon fluorescent probe for biothiol detection and imaging of live cells *in vivo*, Analyst, 2018, 143, 5218–5224. [PubMed: 30270379]

161. Zhang J, Ji X, Zhou JL, Chen ZJ, Dong XC and Zhao WL, Pyridinium substituted BODIPY as NIR fluorescent probe for simultaneous sensing of hydrogen sulphide/glutathione and cysteine/homocysteine, Sens. Actuators, B, 2018, 257, 1076–1082.

162. Ye Z, Duan C, Hu Q, Zhang Y, Qin CQ and Zeng LT, A dual-channel responsive near-infrared fluorescent probe for multicolour imaging of cysteine in live cells, J. Mater. Chem. B, 2017, 5, 3600–3606. [PubMed: 32264297]

163. Xiang H-J, Tham HP, Nguyen MD, Phua SZF, Lim WQ, Liu J-G and Zhao YL, An aza-BODIPY based near-infrared fluorescent probe for sensitive discrimination of cysteine/homocysteine and glutathione in live cells, Chem. Commun, 2017, 53, 5220–5223.

164. (a)Xu S, Zhou J, Dong X, Zhao W and Zhu Q, Fluorescent probe for sensitive discrimination of Hcy and Cys/GSH in live cells *via* dual-emission, Anal. Chim. Acta, 2019, 1074, 123–130; [PubMed: 31159932] (b)Zhang H, Xia X, Zhao H, Zhang G-N, Jiang D-Y, Xue X-Y and Zhang J, A near-infrared fluorescent probe based on S_NAr reaction for H_2S/GSH detection in live cells and zebrafish, Dyes Pigm., 2019, 163, 183–189.

165. Wang P, Wang Y, Li N, Huang J, Wang QQ and Gu YQ, A novel DCM-NBD conjugate fluorescent probe for discrimination of Cys/Hcy from GSH and its bioimaging applications in live cells and animals, Sens. Actuators, B, 2017, 245, 297–304.

166. Xu JC, Pan J, Zhang Y, Liu JB, Zeng LT and Liu XG, Ultrasensitive near-infrared fluorescence-enhanced probe for discriminative detection of GSH and Cys from different emission channels, Sens. Actuators, B, 2017, 238, 58–65.

167. Hu QH, Yu CM, Xia XT, Zeng F and Wu SZ, A fluorescent probe for simultaneous discrimination of GSH and Cys/Hcy in human serum samples *via* distinctly-separated emissions with independent excitations, Biosens. Bioelectron, 2016, 81, 341–348. [PubMed: 26991600]

168. Bai J, Yang X and Qian Y, A ratiometric and near-infrared fluorescent probe for discrimination of Cys/Hcy/GSH in aqueous solution and its intracellular imaging in live cells, J. Lumin, 2020, 221, 117055.

169. Yang XL, He LW, Xu KX and Lin WY, A fluorescent dyad with large emission shift for discrimination of cysteine/homocysteine from glutathione and hydrogen sulfide and the application of bioimaging, Anal. Chim. Acta, 2017, 981, 86–93. [PubMed: 28693733]

170. Wei Y, Cheng D, Ren T, Li Y, Zeng Z and Yuan L, Design of NIR chromenylium-cyanine fluorophore library for “Switch-ON” and ratiometric detection of bio-active species *in vivo*, Anal. Chem, 2016, 88, 1842–1849. [PubMed: 26730493]

171. Huang HJ, Ji XR, Jiang YQ, Zhang CY, Kang XY, Zhu JQ, Sun L and Yi L, NBD-based fluorescent probes for separate detection of cysteine and biothiols *via* different reactivities, Org. Biomol. Chem, 2020, 18, 4004–4008. [PubMed: 32419001]

172. Yang XF, Guo YX and Strongin RM, Conjugate addition/cyclization sequence enables selective and simultaneous fluorescence detection of cysteine and homocysteine, Angew. Chem., Int. Ed, 2011, 50, 10690–10693.

173. An JM, Kang S, Huh E, Kim Y, Lee D, Jo H, Joung J, Kim VJ, Lee JY, Dho YS, Jung Y, Hur JK, Park C, Jung J, Huh Y, Ku J-L, Kim S, Chowdhury T, Park S, Kang JS, Oh MS, Park CK and Kim D, Penta-fluorophenol: A Smiles rearrangement-inspired cysteine-selective fluorescent probe for imaging of human glioblastoma, Chem. Sci, 2020, 11, 5658–5668. [PubMed: 32874505]

174. Zhong KL, Zhou SY, Yan XM, Hou SH, Li XP and Tang LJ, A novel D-**π**-A type NBD-based fluorescent probe for ultrafast and distinguishable detection of Hcy/Cys and its bioimaging application, J. Lumin, 2020, 224, 117330.

175. Steiger AK, Pardue S, Kevil CG and Pluth MD, Self-immolative thiocarbamates provide access to triggered H_2S donors and analyte replacement fluorescent probes, J. Am. Chem. Soc, 2016, 138, 7256–7259. [PubMed: 27218691]

176. Chen Y-H, Tsai J-C, Cheng T-H, Yuan S-S and Wang Y-M, Sensitivity evaluation of NBD-SCN towards cysteine/homocysteine and its bioimaging applications, Biosens. Bioelectron, 2014, 56, 117–123. [PubMed: 24480131]

177. Wang JM, Liao Y and Shao SJ, An NBD-based fluorescent probe with high selectivity to cysteine over homocysteine under neutral physiological conditions, Chem. Lett, 2015, 44, 1437–1439.

178. Yu H, Liu Y, Wang J, Liang Q, Liu H, Xu J and Shao S, A gold nanocluster-based ratiometric fluorescent probe for cysteine and homocysteine detection in live cells, New J. Chem, 2017, 41, 4416–4423.

179. Wang JM, Niu LQ, Huang J, Yan ZJ and Wang JH, A novel NBD-based fluorescent turn-on probe for the detection of cysteine and homocysteine in live cells, Spectrochim. Acta, Part A, 2018, 192, 52–58.

180. Wang JM, Niu LQ, Huang J, Yan ZJ, Zhou XM and Wang JH, Thiazolyl substituted NBD as fluorescent probe for the detection of homocysteine and cysteine, Dyes Pigm, 2018, 158, 151–156.

181. Li M, Kang N, Zhang CH, Liang WT, Zhang GM, Jia JP, Yao QJ, Shuang SM and Dong C, A turn-on fluorescent probe for cysteine/homocysteine based on the nucleophilic-induced rearrangement of benzothiazole thioether, Spectrochim. Acta, Part A, 2019, 222, 117262.
182. Zhang CY, Wu S, Xi Z and Yi L, Design and synthesis of NBD-*S*-dye dyads for fluorescently discriminative detection of biothiols and Cys/Hcy, Tetrahedron, 2017, 73, 6651–6656.
183. Sun L, Jiang YQ, Zhang CY, Ji XR, Lv DQ, Xi Z and Yi L, An NBD-*S*-rhodamine dyad for dual-color discriminative imaging of biothiols and Cys/Hcy, New J. Chem, 2018, 42, 15277–15283.
184. Li R, Kassaye H, Pan Y, Shen Y, Li W, Cheng Y, Guo J, Xu Y, Yin H and Yuan Z, A visible and near-infrared dual-fluorescent probe for discrimination of Cys/Hcy and GSH and its application in bioimaging, Biomater. Sci, 2020, 8, 5994–6003. [PubMed: 32990301]
185. Lee D, Jeong K, Luo X, Kim G, Yang Y, Chen X, Kim S and Yoon J, Near-infrared fluorescent probes for the detection of glutathione and their application in the fluorescence imaging of live cells and tumor-bearing mice, J. Mater. Chem. B, 2018, 6, 2541–2546. [PubMed: 32254472]
186. (a)Bae J, Choi MG, Choi J and Chang S-K, Colorimetric signaling of hydrogen sulfide by reduction of a phenylseleno-nitrobenzoxadiazole derivative, Dyes Pigm., 2013, 99, 748–752; (b)Bae J, Choi MG, Choi J and Chang S-K, Corrigendum to “Colorimetric signaling of hydrogen sulfide by reduction of a phenylseleno-nitrobenzoxadiazole derivative” [Dyes Pigments 99 (2013) 748–752], Dyes Pigm., 2014, 103, 228–229.
187. Kim NY, Choi MG, Lee KM, Hong S and Chang S-K, Colorimetric analysis of malononitrile *via* the formation of a novel NBD-based CH-acidic dye, Dyes Pigm, 2020, 174, 108034.
188. (a)Shen Y, Zhang X, Huang X, Wen S, Liu M, Deng Y, Zhang Y, Zhang C, Jin J, Li H and Yao S, A simple and reversible fluorescent probe based on NBD for rapid detection of hypochlorite and its application for bioimaging, RSC Adv., 2015, 5, 79519–79524;(b)Fang L and Watkinson M, Subcellular localised small molecule fluorescent probes to image mobile Zn^{2+}, Chem. Sci, 2020, 11, 11366–11379. [PubMed: 34094379]
189. Zhou GD, Wang HL, Ma Y and Chen XQ, An NBD fluorophore-based colorimetric and fluorescent chemosensor for hydrogen sulfide and its application for bioimaging, Tetrahedron, 2013, 69, 867–870.
190. Lee D, Kim G, Yin J and Yoon J, An aryl-thioether substituted nitrobenzothiadiazole probe for the selective detection of cysteine and homocysteine, Chem. Commun, 2015, 51, 6518–6520.
191. Long GL and Winefordner JD, Limit of detection a closer look at the IUPAC definition, Anal. Chem, 1983, 55, 712A–724A.
192. Zhang CY, Wang RY, Cheng LH, Li BJ, Xi Z and Yi L, A redox-nucleophilic dual-reactable probe for highly selective and sensitive detection of H_2S: Synthesis, spectra and bioimaging, Sci. Rep, 2016, 6, 30148. [PubMed: 27440747]
193. Zhang CY, Wei L, Zhang J, Wang RY, Xi Z and Yi L, A FRET-ICT dual-quenching fluorescent probe with large off-on response for H_2S: Synthesis, spectra and bioimaging, Chem. Commun, 2015, 51, 7505–7508.
194. Wei C, Wang RY, Zhang CY, Xu GC, Li YY, Zhang QZ, Li L-Y, Yi L and Xi Z, Dual-reactable fluorescent probes for highly selective and sensitive detection of biological H_2S, Chem. – Asian J, 2016, 11, 1376–1381. [PubMed: 26955779]
195. Ma C, Wei C, Li X, Zheng X, Chen B, Wang M, Zhang P and Li X, A mitochondria-targeted dual-reactable fluorescent probe for fast detection of H_2S in live cells, Dyes Pigm, 2019, 162, 624–631.
196. Kim HJ, Kim T and Hong J-I, Selective electrochemiluminescent detection of sulfide based on a dual-quenching cyclometalated Ir(III) complex, Sens. Actuators, B, 2020, 307, 127656.
197. Zhang H, Zhang C, Liu R, Yi L and Sun H, A highly selective and sensitive fluorescent thiol probe through dual-reactive and dual-quenching groups, Chem. Commun, 2015, 51, 2029–2032.
198. Tong H, Zhao J, Li X, Zhang Y, Ma S, Lou K and Wang W, Orchestration of dual cyclization processes and dual quenching mechanisms for enhanced selectivity and drastic fluorescence turn-on detection of cysteine, Chem. Commun, 2017, 53, 3583–3586.

199. Wang F-F, Liu Y-J, Wang B-B, Gao L-X, Jiang F-L and Liu Y, A BODIPY-based mitochondria-targeted turn-on fluorescent probe with dual response units for the rapid detection of intracellular biothiols, Dyes Pigm., 2018, 152, 29–35.

200. Wang B-J, Liu R-J, Fang J, Wang Y-W and Peng Y, A water-soluble dual-site fluorescent probe for the rapid detection of cysteine with high sensitivity and specificity, Chem. Commun, 2019, 55, 11762–11765.

201. Jiang Y, Zheng G, Duan Q, Yang L, Zhang J, Zhang H, He J, Sun H and Ho D, Ultra-sensitive fluorescent probes for hypochlorite acid detection and exogenous/endogenous imaging of live cells, Chem. Commun, 2018, 54, 7967–7970.

202. Zheng G, Li Z, Duan Q, Cheng K, He Y, Huang S, Zhang H, Jiang Y, Jia Y and Sun H, Two quenching groups are better than one: A robust strategy for constructing HOCl fluorescent probe with minimized background fluorescence and ultra-high sensitivity and its application of HOCl imaging in live cells and tissues, Sens. Actuators, B, 2020, 310, 127890.

203. Duan Q, Zheng G, Li Z, Cheng K, Zhang J, Yang L, Jiang Y, Zhang H, He J and Sun H, An ultra-sensitive ratiometric fluorescent probe for hypochlorous acid detection by the synergistic effect of AIE and TBET and its application of detecting exogenous/endogenous HOCl in live cells, J. Mater. Chem. B, 2019, 7, 5125–5131. [PubMed: 31363729]

204. Jiang Y, Ji X, Zhang C, Xi Z, Sun L and Yi L, Dual-quenching NBD-based fluorescent probes for separate detection of H_2S and Cys/Hcy in live cells, Org. Biomol. Chem, 2019, 17, 8435–8442. [PubMed: 31465085]

205. Zhang H, Li W, Chen J, Li G, Yue X, Zhang L, Song X and Chen W, Simultaneous detection of Cys/Hcy and H_2S through distinct fluorescence channels, Anal. Chim. Acta, 2020, 1097, 238–244. [PubMed: 31910965]

206. Yue X, Li W, Chen W, Zhang L, Li G and Sheng J, A dual-response naphthofluorescein-based fluorescent probe for multiple-channel imaging of cysteine/homocysteine in live cells, Tetrahedron Lett, 2018, 59, 2232–2237.

207. Qiao D, Shen T, Zhu M, Liang X, Zhang L, Yin Z, Wang B and Shang L, A highly selective and sensitive fluorescent probe for simultaneously distinguishing and sequentially detecting H_2S and various thiol species in solution and live cells, Chem. Commun, 2018, 54, 13252–13255.

208. He L, Yang X, Xu K, Kong X and Lin W, A multi-signal fluorescent probe for simultaneously distinguishing and sequentially sensing cysteine/homocysteine, glutathione, and hydrogen sulfide in live cells, Chem. Sci, 2017, 8, 6257–6265. [PubMed: 28989659]

209. Qi F, Zhang Y, Wang B, Chen W, Yang L, Yang Z and Song X, A fluorescent probe for the dicriminatory detecion of Cys/Hcy, GSH and H_2S in live cells and zebrafish, Sens. Actuators, B, 2019, 296, 126533.

210. (a)Yang L, Su Y, Geng Y, Zhang Y, Ren X, He L and Song X, A triple-emission fluorescent probe for discriminatory detection of cysteine/homocysteine, glutathione/hydrogen sulfide, and thiophenol in live cells, ACS Sens., 2018, 3, 1863–1869; [PubMed: 30132654] (b)Cao X, Lin W, Zheng K and He L, A near-infrared fluorescent turn-on probe for fluorescence imaging of hydrogen sulfide in live cells based on thiolysis of dinitrophenyl ether, Chem. Commun, 2012, 48, 10529–10531;(c)Li J, Yin C and Huo F, Chromogenic and fluorogenic chemosensors for hydrogen sulfide: Review of detection mechanisms since the year 2009, RSC Adv., 2015, 5, 2191–2206;(d)Liu Y, Yu Y, Zhao Q, Tang C, Zhang H, Qin Y, Feng X and Zhang J, Fluorescent probes based on nucleophilic aromatic substitution reactions for reactive sulfur and selenium species: Recent progress, applications, and design strategies, Coord. Chem. Rev, 2021, 427, 213601. [PubMed: 33024340]

211. He L, Yang X, Xu K, Yang Y and Lin W, A multifunctional logic gate by means of a triple-chromophore fluorescent biothiol probe with diverse fluorescence signal patterns, Chem. Commun, 2017, 53, 13168–13171.

212. Zhu N, Guo X, Pang S, Chang Y, Liu X, Shi Z and Feng S, Mitochondria-immobilized unimolecular fluorescent probe for multiplexing imaging of live cancer cells, Anal. Chem, 2020, 92, 11103–11110. [PubMed: 32662262]

213. Zhai L, Tu Y, Shi Z and Pu S, A colorimetric and fluorescent chemosensor based on diarylethene for simultaneous detection and discrimination of biothiols, Spectrochim. Acta, Part A, 2019, 218, 171–177.

214. Zhang C, Zhang Q-Z, Zhang K, Li L-Y, Pluth MD, Yi L and Xi Z, Dual-biomarker-triggered fluorescent probes for differentiating cancer cells and revealing synergistic antioxidant effects under oxidative stress, Chem. Sci, 2019, 10, 1945–1952. [PubMed: 30931093]

215. Tamura T and Hamachi I, Chemistry for covalent modification of endogenous/native proteins: From test tubes to complex biological systems, J. Am. Chem. Soc, 2019, 141, 2782–2799. [PubMed: 30592612]

216. Zhang Y, Park K-Y, Suazo KF and Distefano MD, Recent progress in enzymatic protein labelling techniques and their applications, Chem. Soc. Rev, 2018, 47, 9106–9136. [PubMed: 30259933]

217. Wang J, Liu Y, Liu Y, Zheng S, Wang X, Zhao J, Yang F, Zhang G, Wang C and Chen PR, Time-resolved protein activation by proximal decaging in living systems, Nature, 2019, 569, 509–513. [PubMed: 31068699]

218. Shiraiwa K, Cheng R, Nonaka H, Tamura T and Hamachi I, Chemical tools for endogenous protein labelling and profiling, Cell Chem. Biol, 2020, 27, 970–985. [PubMed: 32679042]

219. Boutureira O and Bernardes GJL, Advances in chemical protein modification, Chem. Rev, 2015, 115, 2174–2195. [PubMed: 25700113]

220. Hofmann R, Akimoto G, Wucherpfennig TG, Zeymer C and Bode JW, Lysine acylation using conjugating enzymes for site-specific modification and ubiquitination of recombinant proteins, Nat. Chem, 2020, 12, 1008–1015. [PubMed: 32929246]

221. Xue D, Ye L, Zheng J, Wu Y, Zhang X, Xu Y, Li T, Stevens RC, Xu F, Zhuang M, Zhao S, Zhao F and Tao H, The structure-based traceless specific fluorescence labelling of the smoothened receptor, Org. Biomol. Chem, 2019, 17, 6136–6142. [PubMed: 31180094]

222. Gober IN and Waters ML, Supramolecular affinity labelling of histone peptides containing trimethyllysine and its application to histone deacetylase assays, J. Am. Chem. Soc, 2016, 138, 9452–9459. [PubMed: 27387477]

223. Sundaresan NR, Bindu S, Pillai VB, Samant S, Pan Y, Huang J-Y, Gupta M, Nagalingam RS, Wolfgeher D, Verdin E and Gupta MP, SIRT3 blocks aging-associated tissue fibrosis in mice by deacetylating and activating glycogen synthase kinase 3β, Mol. Cell. Biol, 2015, 36, 678–692. [PubMed: 26667039]

224. Ross S, Cheung E, Petrakis TG, Howell M, Kraus WL and Hill CS, Smads orchestrate specific histone modifications and chromatin remodeling to activate transcription, EMBO J, 2006, 25, 4490–4502. [PubMed: 16990801]

225. Kong P, Christia P and Frangogiannis NG, The pathogenesis of cardiac fibrosis, Cell. Mol. Life Sci, 2014, 71, 549–574. [PubMed: 23649149]

226. Dompierre JP, Godin JD, Charrin BC, Cordelières FP, King SJ, Humbert S and Saudou F, Histone deacetylase 6 inhibition compensates for the transport deficit in Huntington's disease by increasing tubulin acetylation, J. Neurosci, 2007, 27, 3571–3583. [PubMed: 17392473]

227. Saba NF, Magliocca KR, Kim S, Muller S, Chen ZJ, Owonikoko TK, Sarlis NJ, Eggers C, Phelan V, Grist WJ, Chen AY, Ramalingam SS, Chen ZG, Beitler JJ, Shin DM, Khuri FR and Marcus AI, Acetylated tubulin (AT) as a prognostic marker in squamous cell carcinoma of the head and neck, Head Neck Pathol., 2014, 8, 66–72. [PubMed: 23881549]

228. Boggs AE, Vitolo MI, Whipple RA, Charpentier MS, Goloubeva OG, Ioffe OB, Tuttle KC, Slovic J, Lu YL, Mills GB and Martin SS, α-Tubulin acetylation elevated in metastatic and basal-like breast cancer cells promotes microtentacle formation, adhesion, and invasive migration, Cancer Res, 2015, 75, 203–215. [PubMed: 25503560]

229. Das C, Lucia MS, Hansen KC and Tyler JK, CBP/p300-mediated acetylation of histone H3 on lysine 56, Nature, 2009, 459, 113–117. [PubMed: 19270680]

230. McLendon PM, Ferguson BS, Osinska H, Bhuiyan MS, James J, McKinsey TA and Robbins J, Tubulin hyperacetylation is adaptive in cardiac proteotoxicity by promoting autophagy, Proc. Natl. Acad. Sci. U. S. A, 2014, 111, E5178–E5186. [PubMed: 25404307]

231. Li P, Ge JB and Li H, Lysine acetyltransferases and lysine deacetylases as targets for cardiovascular disease, Nat. Rev. Cardiol, 2020, 17, 96–115. [PubMed: 31350538]

232. McEnery MW, Snowman AM, Trifiletti RR and Snyder SH, Isolation of the mitochondrial benzodiazepine receptor: Association with the voltage-dependent anion channel and the adenine nucleotide carrier, Proc. Natl. Acad. Sci. U. S. A, 1992, 89, 3170–3174. [PubMed: 1373486]

233. Veenman L, Shandalov Y and Gavish M, VDAC activation by the 18 kDa translocator protein (TSPO), implications for apoptosis, J. Bioenerg. Biomembr, 2008, 40, 199–205. [PubMed: 18670869]

234. Primofiore G, Settimo FD, Taliani S, Simorini F, Patrizi MP, Novellino E, Greco G, Abignente E, Costa B, Chelli B and Martini C, *N,N*-dialkyl-2-phenylindol-3-ylglyoxylamides. A new class of potent and selective ligands at the peripheral benzodiazepine receptor, J. Med. Chem, 2004, 47, 1852–1855. [PubMed: 15027878]

235. Briscoe J and Thérond PP, The mechanisms of Hedgehog signalling and its roles in development and disease, Nat. Rev. Mol. Cell Biol, 2013, 14, 416–429. [PubMed: 23719536]

236. Wakagi T and Ohta T, Implications of the existence of two states of beef liver mitochondrial adenosine triphosphatase as revealed by kinetic studies, J. Biochem, 1981, 90, 1205–1211. [PubMed: 7309716]

237. Cole PA, Chemical probes for histone-modifying enzymes, Nat. Chem. Biol, 2008, 4, 590–597. [PubMed: 18800048]

238. He M, Han Z, Liu L and Zheng YG, Chemical biology approaches for investigating the functions of lysine acetyltransferases, Angew. Chem., Int. Ed, 2018, 57, 1162–1184.

239. He M, Han Z, Qiao J, Ngo L, Xiong MP and Zheng YG, A bioorthogonal turn-on fluorescent strategy for the detection of lysine acetyltransferase activity, Chem. Commun, 2018, 54, 5594–5597.

240. Xie Y, Chen L, Wang R, Wang J, Li J, Xu W, Li Y, Yao SQ, Zhang L, Hao Q and Sun H, Chemical probes reveal Sirt2's new function as a robust "Eraser" of lysine lipoylation, J. Am. Chem. Soc, 2019, 141, 18428–18436. [PubMed: 31644285]

241. Li R, Xue F, Cao C, Wei P, Zhong Y, Xiao S, Li F and Yi T, A near infrared fluorescent probe for one-step detection of histone deacetylase activity based on an intramolecular FRET, Sens. Actuators, B, 2019, 297, 126791.

242. Okada K, Yamaguchi T, Dodo K, Sodeoka M and Obika S, Detection of esterase activity by chromogenic and fluorogenic probe based on an *O*-nitrobenzoxadiazole (*O*-NBD) unit, Bioorg. Med. Chem, 2019, 27, 1444–1448. [PubMed: 30795989]

243. Pagano RE and Sleight RG, Defining lipid transport pathways in animal cells, Science, 1985, 229, 1051–1057. [PubMed: 4035344]

244. Sasaki H and White SH, A novel fluorescent probe that senses the physical state of lipid bilayers, Biophys. J, 2009, 96, 4631–4641. [PubMed: 19486685]

245. Matosevic S and Paegel BM, Layer-by-layer cell membrane assembly, Nat. Chem, 2013, 5, 958–963. [PubMed: 24153375]

246. Brunner JD, Lim NK, Schenck S, Duerst A and Dutzler R, X-ray structure of a calcium-activated TMEM16 lipid scramblase, Nature, 2014, 516, 207–212. [PubMed: 25383531]

247. Vanni S, Hirose H, Barelli H, Antonny B and Gautier R, A sub-nanometre view of how membrane curvature and composition modulate lipid packing and protein recruitment, Nat. Commun, 2014, 5, 4916. [PubMed: 25222832]

248. François-Martin C, Rothman JE and Pincet F, Low energy cost for membrane fusion, Proc. Natl. Acad. Sci. U. S. A, 2017, 114, 1238–1241. [PubMed: 28115718]

249. Lipp N-F, Gautier R, Magdeleine M, Renard M, Albanèse V, Čopič A and Drin G, An electrostatic switching mechanism to control the lipid transfer activity of Osh6p, Nat. Commun, 2019, 10, 3926. [PubMed: 31477717]

250. Lakomek N-A, Yavuz H, Jahn R and Peŕez-Lara Á, Structural dynamics and transient lipid binding of synaptobrevin-2 tune SNARE assembly and membrane fusion, Proc. Natl. Acad. Sci. U. S. A, 2019, 116, 8699–8708. [PubMed: 30975750]

251. Kaur U and Lee JC, Unroofing site-specific α-synuclein-lipid interactions at the plasma membrane, Proc. Natl. Acad. Sci. U. S. A, 2020, 117, 18977–18983. [PubMed: 32719116]

252. Sasmal M, Islam ASM, Bhowmick R, Maiti D, Dutta A and Ali M, Site-selective interaction of human serum albumin with 4-chloro-7-nitro-1,2,3-benzoxadiazole modified olanzapine derivative and effect of β-cyclodextrin on binding: In the light of spectroscopy and molecular docking, ACS Appl. Bio Mater, 2019, 2, 3551–3561.

253. Qin X, Ma Z, Yang X, Hu S, Chen X, Liang D, Lin Y, Shi X, Du L and Li M, Discovery of environment-sensitive fluorescent agonists for alpha1-adrenergic receptors, Anal. Chem, 2019, 91, 12173–12180. [PubMed: 31321979]

254. Taliani S, Simorini F, Sergianni V, La Motta C, Da Settimo F, Cosimelli B, Abignente E, Greco G, Novellino E, Rossi L, Gremigni V, Spinetti F, Chelli B and Martini C, New fluorescent 2-phenylindolglyoxylamide derivatives as probes targeting the peripheral-type benzodiazepine receptor: Design, synthesis, and biological evaluation, J. Med. Chem, 2007, 50, 404–407. [PubMed: 17228885]

255. Taliani S, Da Pozzo E, Bellandi M, Bendinelli S, Pugliesi I, Simorini F, La Motta C, Salerno S, Marini AM, Da Settimo F, Cosimelli B, Greco G, Novellino E and Martini C, Novel irreversible fluorescent probes targeting the 18 kDa translocator protein: Synthesis and biological characterization, J. Med. Chem, 2010, 53, 4085–4093. [PubMed: 20438080]

256. Milite C, Barresi E, Da Pozzo E, Costa B, Viviano M, Porta A, Messere A, Sbardella G, Da Settimo F, Novellino E, Cosconati S, Castellano S, Taliani S and Martini C, Exploiting the 4-phenylquinazoline scaffold for the development of high affinity fluorescent probes for the translocator protein (TSPO), J. Med. Chem, 2017, 60, 7897–7909. [PubMed: 28858490]

257. Dong G, Chen L, Zhang J, Liu T, Du L, Sheng C and Li M, Discovery of turn-on fluorescent probes for detecting PDEdelta protein in live cells and tumor slices, Anal. Chem, 2020, 92, 9516–9522. [PubMed: 32571022]

258. Chandra A, Grecco HE, Pisupati V, Perera D, Cassidy L, Skoulidis F, Ismail SA, Hedberg C, Hanzal-Bayer M, Venkitaraman AR, Wittinghofer A and Bastiaens PI, The GDI-like solubilizing factor PDEδ sustains the spatial organization and signalling of Ras family proteins, Nat. Cell Biol, 2012, 14, 148–158.

259. Winzker M, Friese A, Koch U, Janning P, Ziegler S and Waldmann H, Development of a PDEδ-targeting PROTACs that impair lipid metabolism, Angew. Chem., Int. Ed, 2020, 59, 5595–5601.

260. (a)Kubiasová K, Mik V, Nisler J, Hönig M, Husičková A, Spíchal L, Pěkná Z, Šamajová O, Doležal K, Plíhal O, Benková E, Strnad M and Plíhalová L, Design, synthesis and perception of fluorescently labelled isoprenoid cytokinins, Phytochemistry, 2018, 150, 1–11; [PubMed: 29524794] (b)Kubiasova K, Montesinos JC, Samajova O, Nisler J, Mik V, Semeradova H, Plihalova L, Novak O, Marhavy P, Cavallari N, Zalabak D, Berka K, Dolezal K, Galuszka P, Samaj J, Strnad M, Benkova E, Plihal O and Spichal L, Cytokinin fluoroprobe reveals multiple sites of cytokinin perception at plasma membrane and endoplasmic reticulum, Nat. Commun, 2020, 11, 4285. [PubMed: 32855390]

261. Tsutsumi H, Nomura W, Abe S, Mino T, Masuda A, Ohashi N, Tanaka T, Ohba K, Yamamoto N, Akiyoshi K and Tamamura H, Fluorogenically active leucine zipper peptides as tag-probe pairs for protein imaging in live cells, Angew. Chem., Int. Ed, 2009, 48, 9164–9166.

262. Srinivasan M and Lahiri DK, Glucocorticoid-induced leucine zipper in central nervous system health and disease, Mol. Neurobiol, 2017, 54, 8063–8070. [PubMed: 27889894]

263. Myung JH, Launiere CA, Eddington DT and Hong S, Enhanced tumor cell isolation by a biomimetic combination of E-selectin and anti-EpCAM: Implications for the effective separation of circulating tumor cells (CTCs), Langmuir, 2010, 26, 8589–8596. [PubMed: 20155985]

264. Tara Bahadur KC, Suga K, Isoshima T, Aigaki T, Ito Y, Shiba K and Uzawa T, Wash-free and selective imaging of epithelial cell adhesion molecule (EpCAM) expressing cells with fluorogenic peptide ligands, Biochem. Biophys. Res. Commun, 2018, 500, 283–287. [PubMed: 29660346]

265. Komatsu T, Takeda A, Hanaoka K, Terai T, Ueno T, Tada Y, Nagano T and Urano Y, Fluorometric assay of integrin activity with a small-molecular probe that senses the binding site microenvironment, Chem. Commun, 2014, 50, 15894–15896.

266. Haubner R, Gratias R, Diefenbach B, Goodman SL, Jonczyk A and Kessler H, Structural and functional aspects of RGD-containing cyclic pentapeptides as highly potent and selective integrin $\alpha_V\beta_3$ antagonists, J. Am. Chem. Soc, 1996, 118, 7461–7472.

267. Panagabko C, Baptist M and Atkinson J, *In vitro* lipid transfer assays of phosphatidylinositol transfer proteins provide insight into the *in vivo* mechanism of ligand transfer, Biochim. Biophys. Acta, Biomembr, 2019, 1861, 619–630. [PubMed: 30543784]

268. (a)Nava P, Cecchini M, Chirico S, Gordon H, Morley S, Manor D and Atkinson J, Preparation of fluorescent tocopherols for use in protein binding and localization with the alpha-tocopherol transfer protein, Bioorg. Med. Chem, 2006, 14, 3721–3736; [PubMed: 16481173] (b)Morley S, Cross V, Cecchini M, Nava P, Atkinson J and Manor D, Utility of a fluorescent vitamin E analogue as a probe for tocopherol transfer protein activity, Biochemistry, 2006, 45, 1075–1081. [PubMed: 16430203]

269. Wenskowsky L, Schreuder H, Derdau V, Matter H, Volkmar J, Nazaré M, Opatz T and Petry S, Identification and characterization of a single high-affinity fatty acid binding site in human serum albumin, Angew. Chem., Int. Ed, 2018, 57, 1044–1048.

270. Tugaeva KV, Faletrov YV, Allakhverdiev ES, Shkumatov VM, Maksimov EG and Sluchanko NN, Effect of the NBD-group position on interaction of fluorescently-labelled cholesterol analogues with human steroidogenic acute regulatory protein STARD1, Biochem. Biophys. Res. Commun, 2018, 497, 58–64. [PubMed: 29408456]

271. Stocco DM, StAR protein and the regulation of steroid hormone biosynthesis, Annu. Rev. Physiol, 2001, 63, 193–213. [PubMed: 11181954]

272. Cai T-Q, Guo Q, Wong B, Milot D, Zhang L and Wright SD, Protein-disulfide isomerase is a component of an NBD-cholesterol monomerizing protein complex from hamster small intestine, Biochim. Biophys. Acta, Mol. Cell Biol. Lipids, 2002, 1581, 100–108.

273. Sandhu J, Li S, Fairall L, Pfisterer SG, Gurnett JE, Xiao X, Weston TA, Vashi D, Ferrari A, Orozco JL, Hartman CL, Strugatsky D, Lee SD, He C, Hong C, Jiang H, Bentolila LA, Gatta AT, Levine TP, Ferng A, Lee R, Ford DA, Young SG, Ikonen E, Schwabe JWR and Tontonoz P, Aster proteins facilitate nonvesicular plasma membrane to ER cholesterol transport in mammalian cells, Cell, 2018, 175, 514–529. [PubMed: 30220461]

274. Akram AR, Chankeshwara SV, Scholefield E, Aslam T, McDonald N, Megia-Fernandez A, Marshall A, Mills B, Avlonitis N, Craven TH, Smyth AM, Collie DS, Gray C, Hirani N, Hill AT, Govan JR, Walsh T, Haslett C, Bradley M and Dhaliwal K, *In situ* identification of Gram-negative bacteria in human lungs using a topical fluorescent peptide targeting lipid A, Sci. Transl. Med, 2018, 10, eaal0033. [PubMed: 30355797]

275. Velkov T, Thompson PE, Nation RL and Li J, Structure-activity relationships of polymyxin antibiotics, J. Med. Chem, 2010, 53, 1898–1916. [PubMed: 19874036]

276. Creaser SP and Peterson BR, Sensitive and rapid analysis of protein palmitoylation with a synthetic cell-permeable mimic of Src oncoproteins, J. Am. Chem. Soc, 2002, 124, 2444–2445. [PubMed: 11890786]

277. Ismail SA, Chen YX, Rusinova A, Chandra A, Bierbaum M, Gremer L, Triola G, Waldmann H, Bastiaens PI and Wittinghofer A, Arl2-GTP and Arl3-GTP regulate a GDI-like transport system for farnesylated cargo, Nat. Chem. Biol, 2011, 7, 942–949. [PubMed: 22002721]

278. Casey PJ and Seabra MC, Protein prenyltransferases, J. Biol. Chem, 1996, 271, 5289–5292. [PubMed: 8621375]

279. Dursina B, Reents R, Delon C, Wu Y, Kulharia M, Thutewohl M, Veligodsky A, Kalinin A, Evstifeev V, Ciobanu D, Szedlacsek SE, Waldmann H, Goody RS and Alexandrov K, Identification and specificity profiling of protein prenyltransferase inhibitors using new fluorescent phosphoisoprenoids, J. Am. Chem. Soc, 2006, 128, 2822–2835. [PubMed: 16506760]

280. Wu YW, Alexandrov K and Brunsveld L, Synthesis of a fluorescent analogue of geranylgeranyl pyrophosphate and its use in a high-throughput fluorometric assay for Rab geranylgeranyltransferase, Nat. Protoc, 2007, 2, 2704–2711. [PubMed: 18007605]

281. Guo Z, Wu YW, Tan KT, Bon RS, Guiu-Rozas E, Delon C, Nguyen TU, Wetzel S, Arndt S, Goody RS, Blankenfeldt W, Alexandrov K and Waldmann H, Development of selective RabGGTase inhibitors and crystal structure of a RabGGTase-inhibitor complex, Angew. Chem., Int. Ed, 2008, 47, 3747–3750.

282. Goren MA, Morizumi T, Menon I, Joseph JS, Dittman JS, Cherezov V, Stevens RC, Ernst OP and Menon AK, Constitutive phospholipid scramblase activity of a G protein-coupled receptor, Nat. Commun, 2014, 5, 5115. [PubMed: 25296113]

283. Brzovic PS, Keeffe JR, Nishikawa H, Miyamoto K, Fox D, Fukuda M, Ohta T and Klevit R, Binding and recognition in the assembly of an active BRCA1/BARD1 ubiquitin-ligase complex, Proc. Natl. Acad. Sci. U. S. A, 2003, 100, 5646. [PubMed: 12732733]

284. Sengupta N and Seto E, Regulation of histone deacetylase activities, J. Cell. Biochem, 2004, 93, 57–67. [PubMed: 15352162]

285. Rone MB, Fan J and Papadopoulos V, Cholesterol transport in steroid biosynthesis: Role of protein-protein interactions and implications in disease states, Biochim. Biophys. Acta, Mol. Cell Biol. Lipids, 2009, 1791, 646–658.

286. Jansen R, Greenbaum D and Gerstein M, Relating whole-genome expression data with protein-protein interactions, Genome Res, 2002, 12, 37–46. [PubMed: 11779829]

287. Özkan E, Carrillo RA, Eastman CL, Weiszmann R, Waghray D, Johnson KG, Zinn K, Celniker SE and Garcia KC, An extracellular interactome of immunoglobulin and LRR proteins reveals receptor-ligand networks, Cell, 2013, 154, 228–239. [PubMed: 23827685]

288. Arkin MR, Tang Y and Wells JA, Small-molecule inhibitors of protein-protein interactions: Progressing toward the reality, Chem. Biol, 2014, 21, 1102–1114. [PubMed: 25237857]

289. Alexander VV and Alexander IA, Inhibitors of protein-protein interactions as potential drugs, Curr. Comput.- Aided Drug Des, 2007, 3, 51–58.

290. Ozawa T and Umezawa Y, Detection of protein-protein interactions *in vivo* based on protein splicing, Curr. Opin. Chem. Biol, 2001, 5, 578–583. [PubMed: 11578933]

291. Rosenbaum MI, Clemmensen LS, Bredt DS, Bettler B and Stromgaard K, Targeting receptor complexes: A new dimension in drug discovery, Nat. Rev. Drug Discovery, 2020, 19, 884–901. [PubMed: 33177699]

292. Cui Y, Zhang X, Yu M, Zhu Y, Xing J and Lin J, Techniques for detecting protein-protein interactions in live cells: Principles, limitations, and recent progress, Sci. China: Life Sci, 2019, 62, 619–632. [PubMed: 30877434]

293. Müller MP and Goody RS, Molecular control of Rab activity by GEFs, GAPs and GDI, Small GTPases, 2018, 9, 5–21. [PubMed: 28055292]

294. Wu Y-W, Tan K-T, Waldmann H, Goody RS and Alexandrov K, Interaction analysis of prenylated Rab GTPase with Rab escort protein and GDP dissociation inhibitor explains the need for both regulators, Proc. Natl. Acad. Sci. U. S. A, 2007, 104, 12294–12299. [PubMed: 17640890]

295. Wu YW, Oesterlin LK, Tan KT, Waldmann H, Alexandrov K and Goody RS, Membrane targeting mechanism of Rab GTPases elucidated by semisynthetic protein probes, Nat. Chem. Biol, 2010, 6, 534–540. [PubMed: 20512138]

296. (a)Sommer ME, Hofmann KP and Heck M, Arrestin-rhodopsin binding stoichiometry in isolated rod outer segment membranes depends on the percentage of activated receptors, J. Biol. Chem, 2011, 286, 7359–7369; [PubMed: 21169358] (b)Sommer ME, Hofmann KP and Heck M, Distinct loops in arrestin differentially regulate ligand binding within the GPCR opsin, Nat. Commun, 2012, 3, 995. [PubMed: 22871814]

297. van den Ent F, Amos LA and Löwe J, Prokaryotic origin of the actin cytoskeleton, Nature, 2001, 413, 39–44. [PubMed: 11544518]

298. Whitesides GM and Grzybowski B, Self-assembly at all scales, Science, 2002, 295, 2418–2421. [PubMed: 11923529]

299. Tanaka S, Kerfeld CA, Sawaya MR, Cai F, Heinhorst S, Cannon GC and Yeates TO, Atomic-level models of the bacterial carboxysome shell, Science, 2008, 319, 1083–1086. [PubMed: 18292340]

300. Rogers WB, Shih WM and Manoharan VN, Using DNA to program the self-assembly of colloidal nanoparticles and microparticles, Nat. Rev. Mater, 2016, 1, 16008.

301. Seeman NC and Sleiman HF, DNA nanotechnology, Nat. Rev. Mater, 2017, 3, 17068.

302. Levin A, Hakala TA, Schnaider L, Bernardes GJL, Gazit E and Knowles TPJ, Biomimetic peptide self-assembly for functional materials, Nat. Rev. Chem, 2020, 4, 615–634.

303. Wang Y, Hu X, Weng J, Li J, Fan Q, Zhang Y and Ye D, A photoacoustic probe for the imaging of tumor apoptosis by caspase-mediated macrocyclization and self-assembly, Angew. Chem., Int. Ed, 2019, 58, 4886–4890.

304. Jiao J-B, Wang G-Z, Hu X-L, Zang Y, Maisonneuve S, Sedgwick AC, Sessler JL, Xie J, Li J, He X-P and Tian H, Cyclodextrin-based peptide self-assemblies (Spds) that enhance peptide-based fluorescence imaging and antimicrobial efficacy, J. Am. Chem. Soc, 2020, 142, 1925–1932. [PubMed: 31884796]

305. Zheng J, Fan R, Wu H, Yao H, Yan Y, Liu J, Ran L, Sun Z, Yi L, Dang L, Gan P, Zheng P, Yang T, Zhang Y, Tang T and Wang Y, Directed self-assembly of herbal small molecules into sustained release hydrogels for treating neural inflammation, Nat. Commun, 2019, 10, 1604. [PubMed: 30962431]
306. Deng R, Derry MJ, Mable CJ, Ning Y and Armes SP, Using dynamic covalent chemistry to drive morphological transitions: Controlled release of encapsulated nanoparticles from block copolymer vesicles, J. Am. Chem. Soc, 2017, 139, 7616–7623. [PubMed: 28497960]
307. Li T, Pan S, Gao S, Xiang W, Sun C, Cao W and Xu H, Diselenide–pemetrexed assemblies for combined cancer immuno-, radio-, and chemotherapies, Angew. Chem., Int. Ed, 2020, 59, 2700–2704.
308. Wang Y, Xu Z, Lovrak M, le Sage VAA, Zhang K, Guo X, Eelkema R, Mendes E and van Esch JH, Biomimetic strain-stiffening self-assembled hydrogels, Angew. Chem., Int. Ed, 2020, 59, 4830–4834.
309. He H, Tan W, Guo J, Yi M, Shy AN and Xu B, Enzymatic noncovalent synthesis, Chem. Rev, 2020, 120, 9994–10078. [PubMed: 32812754]
310. Heinrich D, Bruland Ø, Guise TA, Suzuki H and Sartor O, Alkaline phosphatase in metastatic castration-resistant prostate cancer: Reassessment of an older biomarker, Future Oncol., 2018, 14, 2543–2556. [PubMed: 29925281]
311. Ferreira LB, Gimba E, Vinagre J, Sobrinho-Simões M and Soares P, Molecular aspects of thyroid calcification, Int. J. Mol. Sci, 2020, 21, 7718.
312. Li J, Gao Y, Kuang Y, Shi J, Du X, Zhou J, Wang H, Yang Z and Xu B, Dephosphorylation of D-peptide derivatives to form biofunctional, supramolecular nanofibers/hydrogels and their potential applications for intracellular imaging and intratumoral chemotherapy, J. Am. Chem. Soc, 2013, 135, 9907–9914. [PubMed: 23742714]
313. Zhou J, Du X, Berciu C, He H, Shi J, Nicastro D and Xu B, Enzyme-instructed self-assembly for spatiotemporal profiling of the activities of alkaline phosphatases on live cells, Chem, 2016, 1, 246–263. [PubMed: 28393126]
314. Zhou J, Du X, Yamagata N and Xu B, Enzyme-instructed self-assembly of small D-peptides as a multiple-step process for selectively killing cancer cells, J. Am. Chem. Soc, 2016, 138, 3813–3823. [PubMed: 26966844]
315. Xu T, Liang C, Ji S, Ding D, Kong D, Wang L and Yang Z, Surface-induced hydrogelation for fluorescence and naked-eye detections of enzyme activity in blood, Anal. Chem, 2016, 88, 7318–7323. [PubMed: 27345959]
316. Pan L, Liu J and Shi J, Cancer cell nucleus-targeting nanocomposites for advanced tumor therapeutics, Chem. Soc. Rev, 2018, 47, 6930–6946. [PubMed: 30062349]
317. Rajendran L, Knölker H-J and Simons K, Subcellular targeting strategies for drug design and delivery, Nat. Rev. Drug Discovery, 2010, 9, 29–42. [PubMed: 20043027]
318. Wang H, Feng Z, Del Signore SJ, Rodal AA and Xu B, Active probes for imaging membrane dynamics of live cells with high spatial and temporal resolution over extended time scales and areas, J. Am. Chem. Soc, 2018, 140, 3505–3509. [PubMed: 29481071]
319. Wang Y, Zhan J, Chen Y, Ai S, Li L, Wang L, Shi Y, Zheng J and Yang Z, Selective pericellular hydrogelation by the overexpression of an enzyme and a membrane receptor, Nanoscale, 2019, 11, 13714–13719. [PubMed: 31314031]
320. Wang H, Feng Z, Wang Y, Zhou R, Yang Z and Xu B, Integrating enzymatic self-assembly and mitochondria targeting for selectively killing cancer cells without acquired drug resistance, J. Am. Chem. Soc, 2016, 138, 16046–16055. [PubMed: 27960313]
321. Jeena MT, Palanikumar L, Go EM, Kim I, Kang MG, Lee S, Park S, Choi H, Kim C, Jin SM, Bae SC, Rhee HW, Lee E, Kwak SK and Ryu JH, Mitochondria localization induced self-assembly of peptide amphiphiles for cellular dysfunction, Nat. Commun, 2017, 8, 26. [PubMed: 28638095]
322. Kenny RG and Marmion CJ, Toward multi-targeted platinum and ruthenium drugs-a new paradigm in cancer drug treatment regimens, Chem. Rev, 2019, 119, 1058–1137. [PubMed: 30640441]

323. Sedgwick AC, Brewster JT, Harvey P, Iovan DA, Smith G, He X-P, Tian H, Sessler JL and James TD, Metal-based imaging agents: Progress towards interrogating neurodegenerative disease, Chem. Soc. Rev, 2020, 49, 2886–2915. [PubMed: 32226991]

324. Liang C, Yan X, Zhang R, Xu T, Zheng D, Tan Z, Chen Y, Gao Z, Wang L, Li X and Yang Z, Enhanced cellular uptake and nuclear accumulation of drug-peptide nanomedicines prepared by enzyme-instructed self-assembly, J. Controlled Release, 2020, 317, 109–117.

325. King AP and Wilson JJ, Endoplasmic reticulum stress: An arising target for metal-based anticancer agents, Chem. Soc. Rev, 2020, 49, 8113–8136. [PubMed: 32597908]

326. Feng Z, Wang H, Wang S, Zhang Q, Zhang X, Rodal AA and Xu B, Enzymatic assemblies disrupt the membrane and target endoplasmic reticulum for selective cancer cell death, J. Am. Chem. Soc, 2018, 140, 9566–9573. [PubMed: 29995402]

327. He H, Liu S, Wu D and Xu B, Enzymatically formed peptide assemblies sequestrate proteins and relocate inhibitors to selectively kill cancer cells, Angew. Chem., Int. Ed, 2020, 59, 16445–16450.

328. Funkea SA and Willbold D, Mirror image phage display-a method to generate D-peptide ligands for use in diagnostic or therapeutical applications, Mol. BioSyst, 2009, 5, 783–786. [PubMed: 19603110]

329. Zhou J, Du X, Li J, Yamagata N and Xu B, Taurine boosts cellular uptake of small D-peptides for enzyme-instructed intracellular molecular self-assembly, J. Am. Chem. Soc, 2015, 137, 10040–10043. [PubMed: 26235707]

330. Yang L, Peltier R, Zhang M, Song D, Huang H, Chen G, Chen Y, Zhou F, Hao Q, Bian L, He ML, Wang Z, Hu Y and Sun H, Desuccinylation-triggered peptide self-assembly: Live cell imaging of SIRT5 activity and mitochondrial activity modulation, J. Am. Chem. Soc, 2020, 142, 18150–18159. [PubMed: 32991157]

331. He H, Wang J, Wang H, Zhou N, Yang D, Green DR and Xu B, Enzymatic cleavage of branched peptides for targeting mitochondria, J. Am. Chem. Soc, 2018, 140, 1215–1218. [PubMed: 29328651]

332. An H-W, Li L-L, Wang Y, Wang Z, Hou D, Lin Y-X, Qiao S-L, Wang M-D, Yang C, Cong Y, Ma Y, Zhao X-X, Cai Q, Chen W-T, Lu C-Q, Xu W, Wang H and Zhao Y, A tumor-selective cascade activatable self-detained system for drug delivery and cancer imaging, Nat. Commun, 2019, 10, 4861. [PubMed: 31649241]

333. Xu T, Cai Y, Zhong X, Zhang L, Zheng D, Gao Z, Pan X, Wang F, Chen M and Yang Z, β-Galactosidase instructed supramolecular hydrogelation for selective identification and removal of senescent cells, Chem. Commun, 2019, 55, 7175–7178.

334. Li X, Cao C, Wei P, Xu M, Liu Z, Liu L, Zhong Y, Li R, Zhou Y and Yi T, Self-assembly of amphiphilic peptides for recognizing high furin-expressing cancer cells, ACS Appl. Mater. Interfaces, 2019, 11, 12327–12334. [PubMed: 30864434]

335. Kim BJ, Fang Y, He H and Xu B, Trypsin-instructed self-assembly on endoplasmic reticulum for selectively inhibiting cancer cells, Adv. Healthcare Mater, 2020, 9, 2000416.

336. Mei L, He S, Zhang L, Xu K and Zhong W, Supramolecular self-assembly of fluorescent peptide amphiphiles for accurate and reversible pH measurement, Org. Biomol. Chem, 2019, 17, 939–944. [PubMed: 30629073]

337. Zhan J, Cai Y, Ji S, He S, Cao Y, Ding D, Wang L and Yang Z, Spatiotemporal control of supramolecular self-assembly and function, ACS Appl. Mater. Interfaces, 2017, 9, 10012–10018. [PubMed: 28252276]

338. Shang Y, Wang Z, Zhang R, Li X, Zhang S, Gao J, Li X and Yang Z, A novel thermogel system of self-assembling peptides manipulated by enzymatic dephosphorylation, Chem. Commun, 2019, 55, 5123–5126.

339. Ren C, Wang H, Zhang X, Ding D, Wang L and Yang Z, Interfacial self-assembly leads to formation of fluorescent nanoparticles for simultaneous bacterial detection and inhibition, Chem. Commun, 2014, 50, 3473–3475.

340. Cai Y, Shi Y, Wang H, Wang J, Ding D, Wang L and Yang Z, Environment-sensitive fluorescent supramolecular nanofibers for imaging applications, Anal. Chem, 2014, 86, 2193–2199. [PubMed: 24467604]

341. Zhan J, Cai Y, He S, Wang L and Yang Z, Tandem molecular self-assembly in liver cancer cells, Angew. Chem., Int. Ed, 2018, 57, 1813–1816.
342. Zheng D, Chen Y, Ai S, Zhang R, Gao Z, Liang C, Cao L, Chen Y, Hong Z, Shi Y, Wang L, Li X and Yang Z, Tandem molecular self-assembly selectively inhibits lung cancer cells by inducing endoplasmic reticulum stress, Research, 2019, 2019, 4803624. [PubMed: 31912037]
343. Zhan J, Zhong J, Ma S, Ma W, Wang Y, Yu Z, Cai Y and Huang W, Dual-responsive self-assembly in lysosomes enables cell cycle arrest for locking glioma cell growth, Chem. Commun, 2020, 56, 6957–6960.
344. Li Y, Yang Y and Guan X, Benzofurazan sulfides for thiol imaging and quantification in live cells through fluorescence microscopy, Anal. Chem, 2012, 84, 6877–6883. [PubMed: 22794193]
345. Zhuang YD, Chiang PY, Wang CW and Tan KT, Environment-sensitive fluorescent turn-on probes targeting hydrophobic ligand-binding domains for selective protein detection, Angew. Chem., Int. Ed, 2013, 52, 8124–8128.
346. Liu Y, Fares M, Dunham NP, Gao Z, Miao K, Jiang X, Bollinger SS, Boal AK and Zhang X, AgHalo: A facile fluorogenic sensor to detect drug-induced proteome stress, Angew. Chem., Int. Ed, 2017, 56, 8672–8676.
347. Wang C-X, Sato Y, Kudo M, Nishizawa S and Teramae N, Ratiometric fluorescent signaling of small molecule, environmentally sensitive dye conjugates for detecting single-base mutations in DNA, Chem. – Eur. J, 2012, 18, 9481–9484. [PubMed: 22733702]
348. Liu TK, Hsieh PY, Zhuang YD, Hsia CY, Huang CL, Lai HP, Lin HS, Chen IC, Hsu HY and Tan KT, A rapid SNAP-tag fluorogenic probe based on an environment-sensitive fluorophore for no-wash live cell imaging, ACS Chem. Biol, 2014, 9, 2359–2365. [PubMed: 25105835]
349. Gota C, Uchiyama S, Yoshihara T, Tobita S and Ohwada T, Temperature-dependent fluorescence lifetime of a fluorescent polymeric thermometer, poly(*N*-isopropylacrylamide), labelled by polarity and hydrogen bonding sensitive 4-sulfamoyl-7-aminobenzofurazan, J. Phys. Chem. B, 2008, 112, 2829–2836. [PubMed: 18278900]
350. Thooft AM, Cassaidy K and VanVeller B, A small push-pull fluorophore for turn-on fluorescence, J. Org. Chem, 2017, 82, 8842–8847. [PubMed: 28714302]
351. Suarez SI, Warner CC, Brown-Harding H, Thooft AM, VanVeller B and Lukesh JC, Highly selective staining and quantification of intracellular lipid droplets with a compact push-pull fluorophore based on benzothiadiazole, Org. Biomol. Chem, 2020, 18, 495–499. [PubMed: 31850447]
352. Xu H, Zhu C, Chen Y, Bai Y, Han Z, Yao S, Jiao Y, Yuan H, He W and Guo Z, A FRET-based fluorescent Zn^{2+} sensor: 3D ratiometric imaging, flow cytometric tracking and cisplatin-induced Zn^{2+} fluctuation monitoring, Chem. Sci, 2020, 11, 11037–11041. [PubMed: 34123194]
353. Wu T-W, Lee F-H, Gao R-C, Chew CY and Tan K-T, Fluorescent probe encapsulated in avidin protein to eliminate nonspecific fluorescence and increase detection sensitivity in blood serum, Anal. Chem, 2016, 88, 7873–7877. [PubMed: 27459352]
354. He L, Yang X, Xu K and Lin W, Improved aromatic substitution – rearrangement-based ratiometric fluorescent cysteine-specific probe and its application of real-time imaging under oxidative stress in live zebrafish, Anal. Chem, 2017, 89, 9567–9573. [PubMed: 28791863]
355. Li K-B, Qu W-B, Han D-M, Zhang S, Shi W, Chen C-X and Liang X-X, A colorimetric/fluorescence dual-channel probe for highly discriminating detection of cysteine, Talanta, 2019, 194, 803–808. [PubMed: 30609609]
356. Conley NR, Dragulescu-Andrasi A, Rao J and Moerner WE, A Selenium analogue of firefly D-luciferin with red-shifted bioluminescence emission, Angew. Chem., Int. Ed, 2012, 51, 3350–3353.
357. Detty MR, Prasad PN, Donnelly DJ, Ohulchanskyy T, Gibson SL and Hilf R, Synthesis, properties, and photodynamic properties *in vitro* of heavy-chalcogen analogues of tetramethylrosamine, Bioorg. Med. Chem, 2004, 12, 2537–2544. [PubMed: 15110836]
358. Park YS, Kale TS, Nam C-Y, Choi D and Grubbs RB, Effects of heteroatom substitution in conjugated heterocyclic compounds on photovoltaic performance: From sulfur to tellurium, Chem. Commun, 2014, 50, 7964–7967.

359. Jenkinson DR, Cadby AJ and Jones S, The synthesis and photophysical analysis of a series of 4-nitrobenzo-chalcogenadiazoles for super-resolution microscopy, Chem. – Eur. J, 2017, 23, 12585–12592. [PubMed: 28703339]

360. Benson S, Fernandez A, Barth ND, de Moliner F, Horrocks MH, Herrington CS, Abad JL, Delgado A, Kelly L, Chang Z, Feng Y, Nishiura M, Hori Y, Kikuchi K and Vendrell M, SCOTfluors: Small, conjugatable, orthogonal, and tunable fluorophores for *in vivo* imaging of cell metabolism, Angew. Chem., Int. Ed, 2019, 58, 6911–6915.

361. Park SJ, Juvekar V, Jo JH and Kim HM, Combining hydrophilic and hydrophobic environment sensitive dyes to detect a wide range of cellular polarity, Chem. Sci, 2020, 11, 596–601. [PubMed: 32206276]

362. Onoda M, Tokuyama H, Uchiyama S, Mawatari K-I, Santa T, Kaneko K, Imai K and Nakagomi K, Fluorescence enhancement by hydroperoxides based on a change in the intramolecular charge transfer character of benzofurazan, Chem. Commun, 2005, 1848–1850.

363. Yang X, He L, Xu K, Yang Y and Lin W, The development of an ICT-based formaldehyde-responsive fluorescence turn-on probe with a high signal-to-noise ratio, New J. Chem, 2018, 42, 12361–12364.

364. Norris SR, Warner CC, Lampkin BJ, Bouc P and VanVeller B, Synthesis and spectral properties of push-pull dyes based on isobenzofuran scaffolds, Org. Lett, 2019, 21, 3817–3821. [PubMed: 31038316]

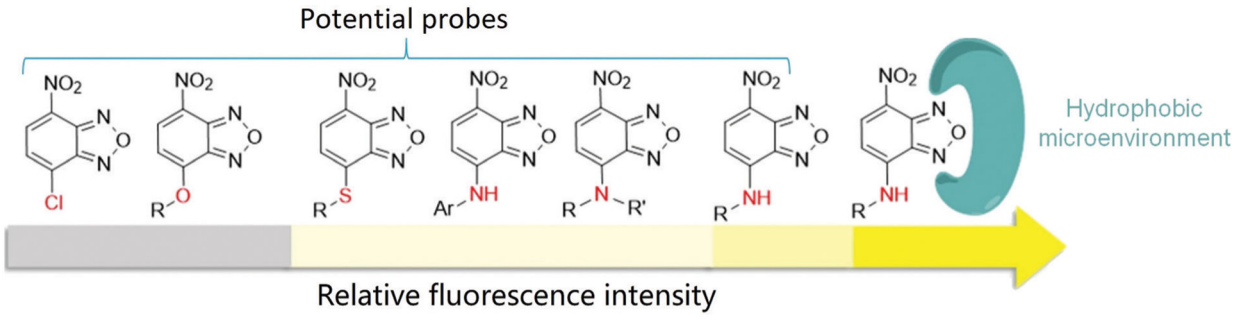

Fig. 1.

Illustration of relative fluorescence intensities of the NBD derivatives in aqueous solution. R = alkyl group.

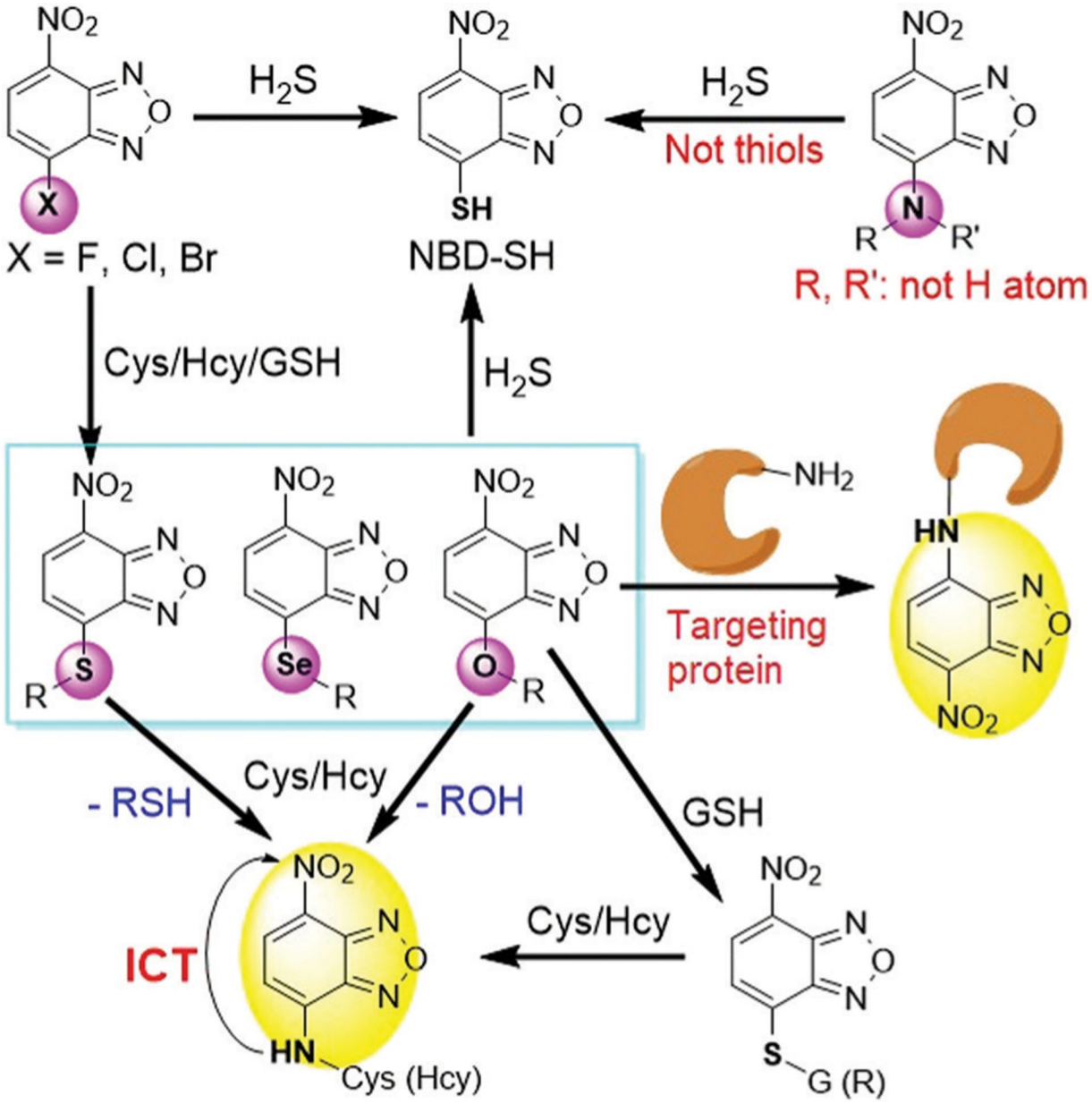

Fig. 2.

Illustration of chemical transformations between NBD probes and biothiols (including H_2S) or amines (including proteins). GSH, glutathione; Cys, cysteine; Hcy, homocysteine.

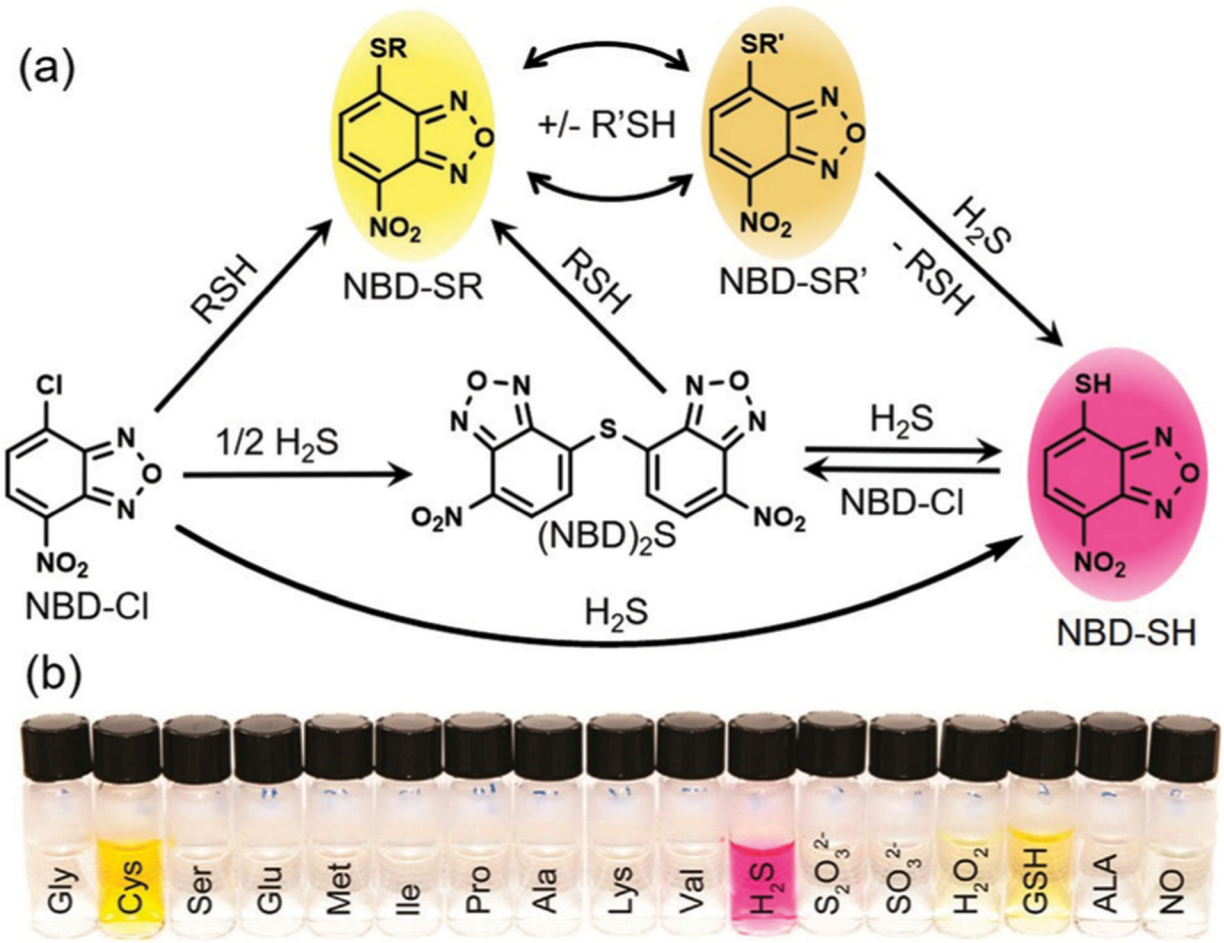

Fig. 3.

(a) Overall reactivity of NBD-Cl with H_2S and RSH compounds. (b) Photo of colorimetric response of NBD-Cl toward different reactive species as indicated. (b) Is adapted with permission from ref. 22. Copyright 2013 American Chemical Society.

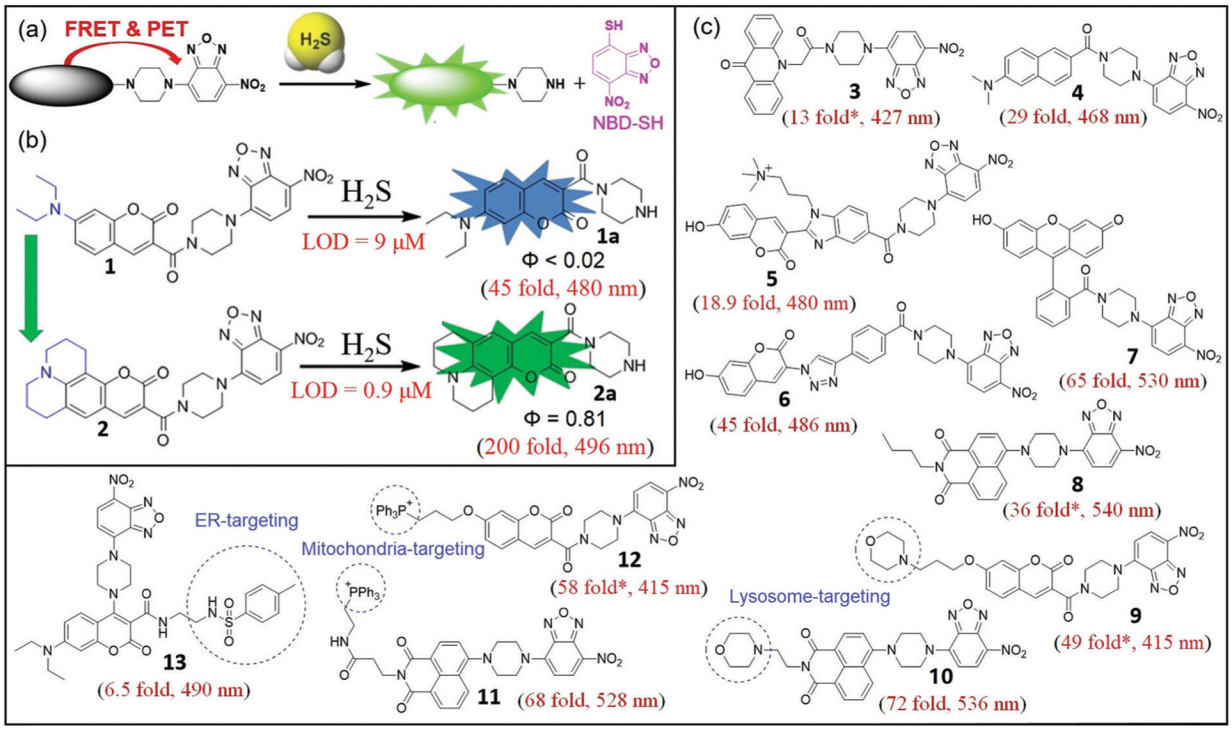

Fig. 4.

(a) The design strategy for H_2S probes with emission wavelength shorter than NBD. (b) Chemical structures of probes **1** and **2** and their associated reactions with H_2S. (c) Chemical structures of probes **3–13** and their associated fluorescence turn-on values after reaction with H_2S. * Represents estimated enhancement from the reported spectra.

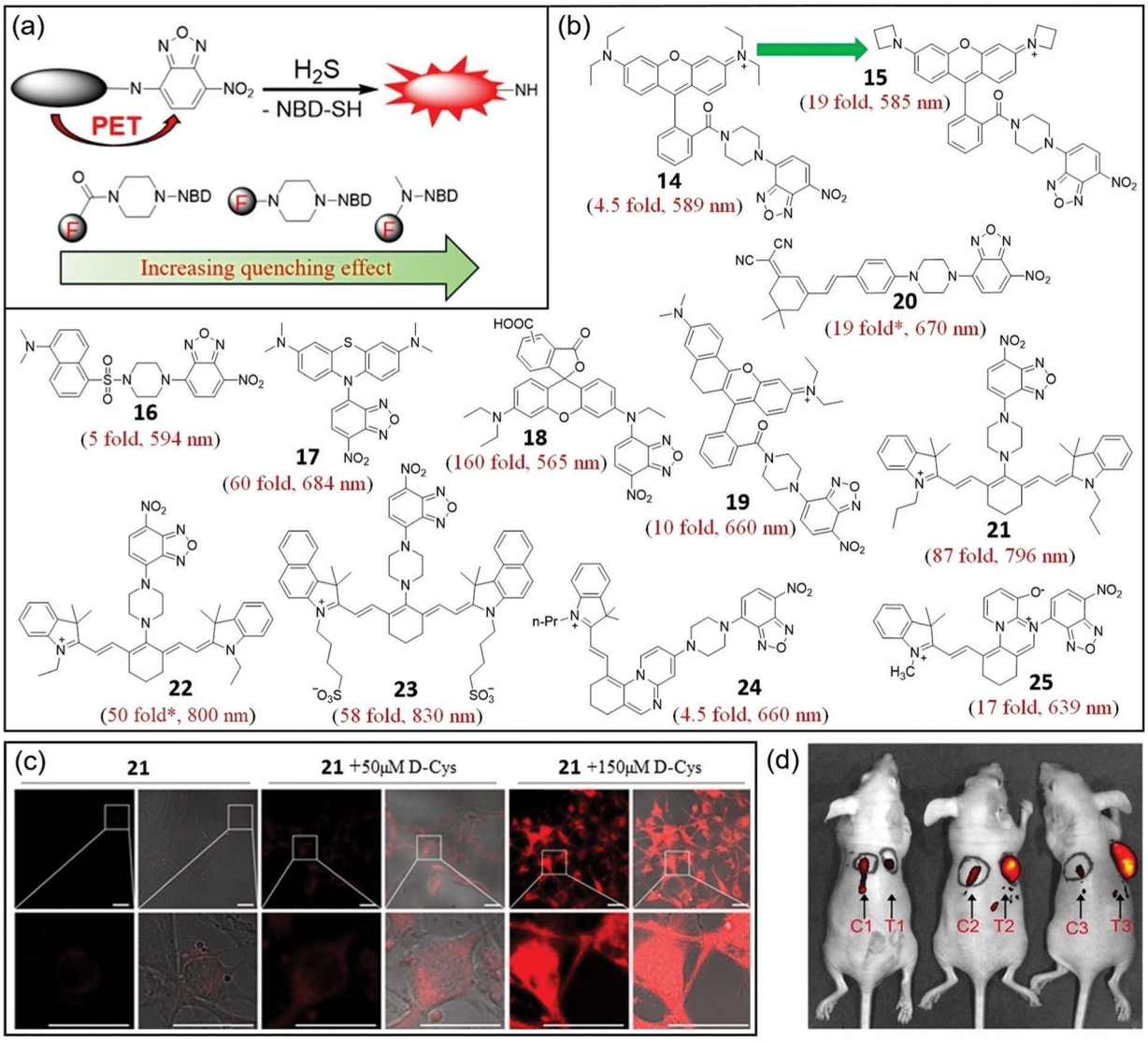

Fig. 5.

(a) The design strategy for probes with emission wavelengths greater than NBD. The distance-dependent quenching effects for the three types of NBD-fluorophore connections are shown at the bottom. (b) Chemical structures of **14–25** and their associated fluorescence turn-on after reaction with H_2S. * Represents estimated enhancement from the reported spectra. (c) Fluorescence images (left) and bright-field overlap images (right) of cells with **21** and D-Cys. (d) Fluorescence images of mice with skin-pop (left) or intratumoral (right) injection of probe **21**. The left injection positions (C1, C2, C3) were for control purposes, and the right injection positions (T1, T2, T3) were for FHC, HCT116, and HT29 grafted cell positions. Observed tumors were formed in the HCT116 (T2) and HT29 (T3) xenograft mice. (c) and (d) are adapted with permission from ref. 82. Copyright 2017 Royal Society of Chemistry.

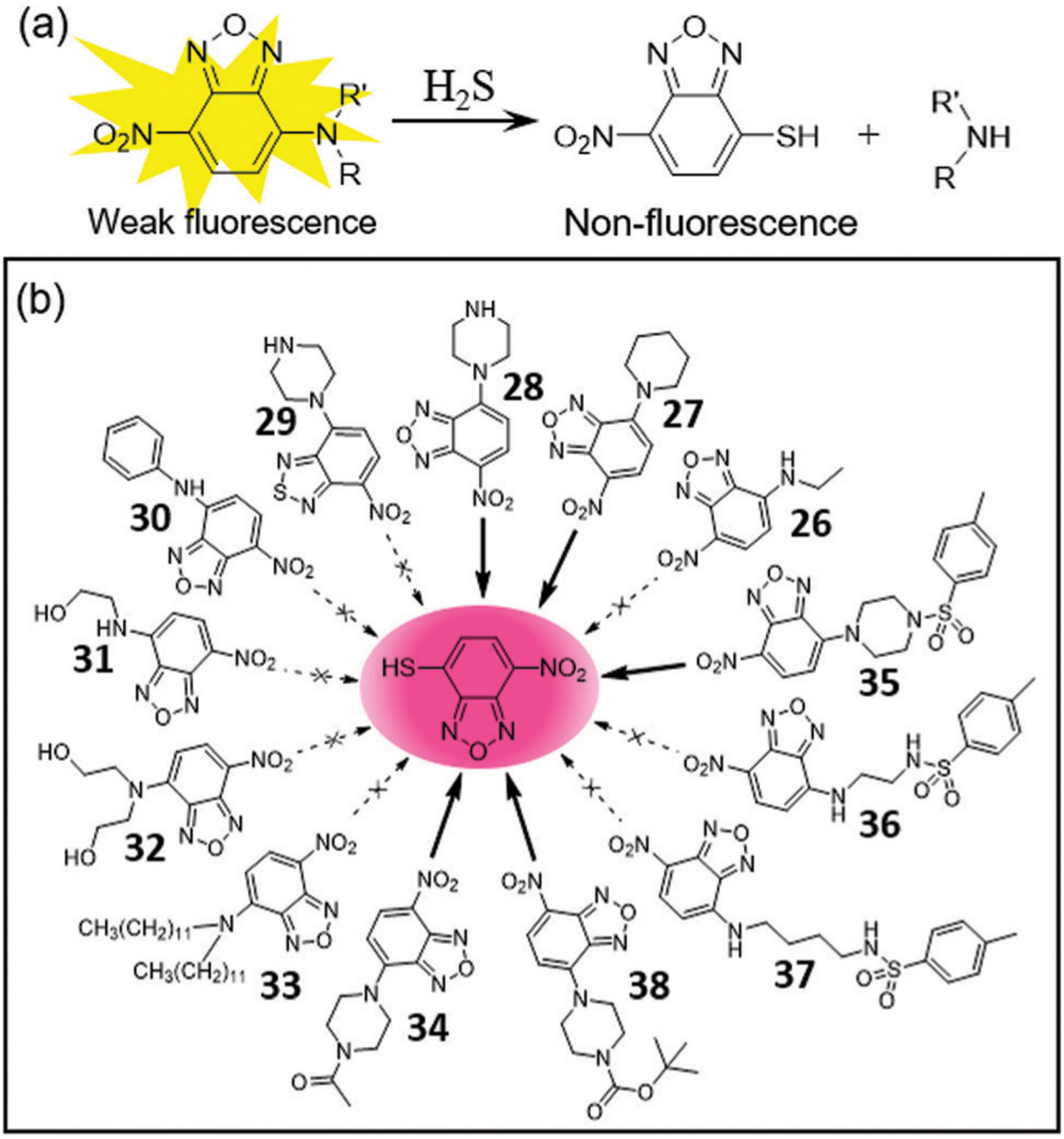

Fig. 6.

(a) The design strategy for turn-off H_2S probes. (b) Chemical structures of NBD amines **26–38** that react with micromolar H_2S to produce the purple NBD-SH.

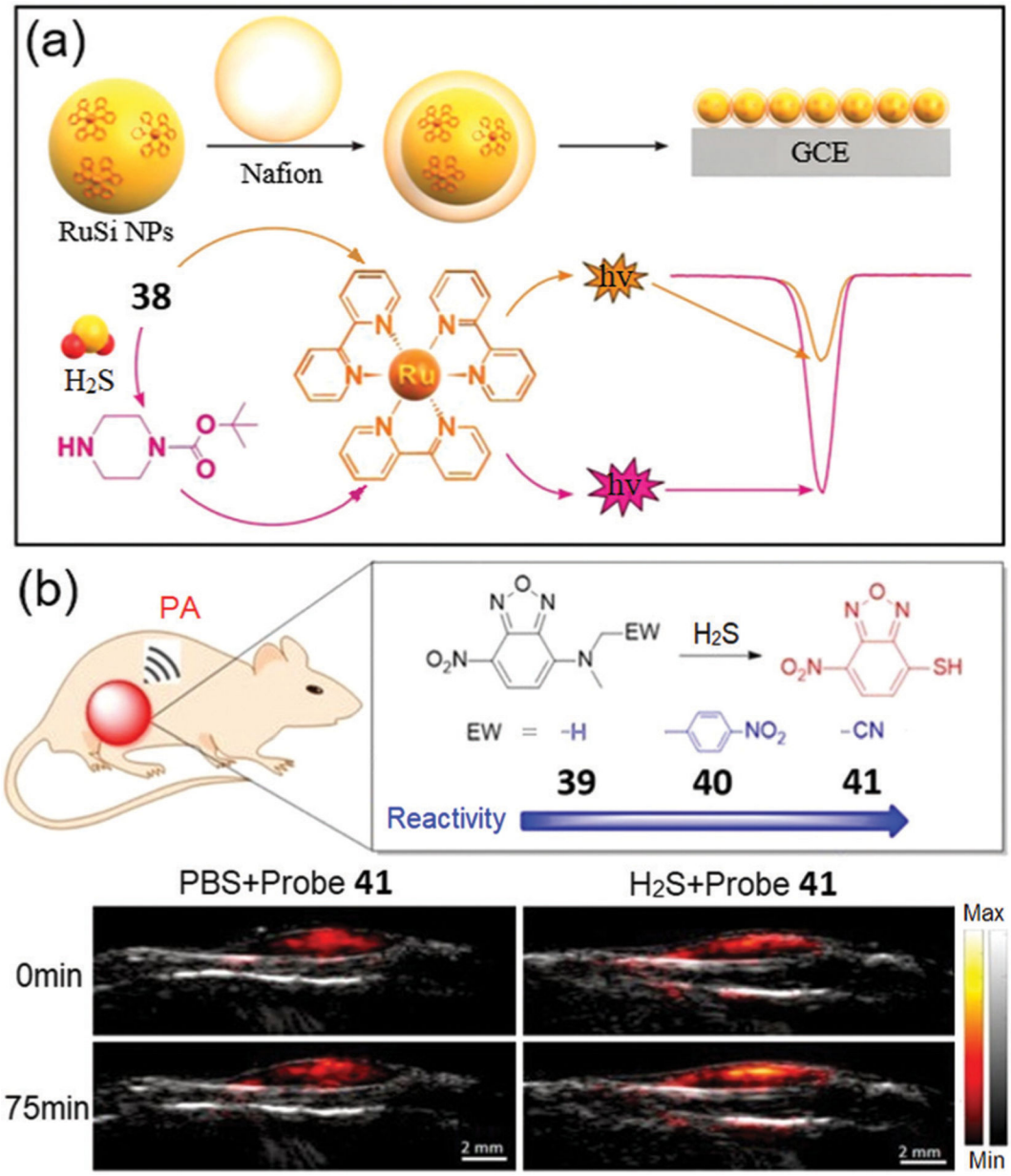

Fig. 7.

(a) Schematic diagram for fabrication of the electrochemiluminescent sensor based on a Ru complex and **38**. (b) Modular design of the fluorescent and PA dual-modal H_2S probes **39–41** and the PA imaging in matrigel. (a) and (b) are adapted with permission from ref. 87 and 89. Copyright 2019 Elsevier, 2020 American Chemical Society, respectively.

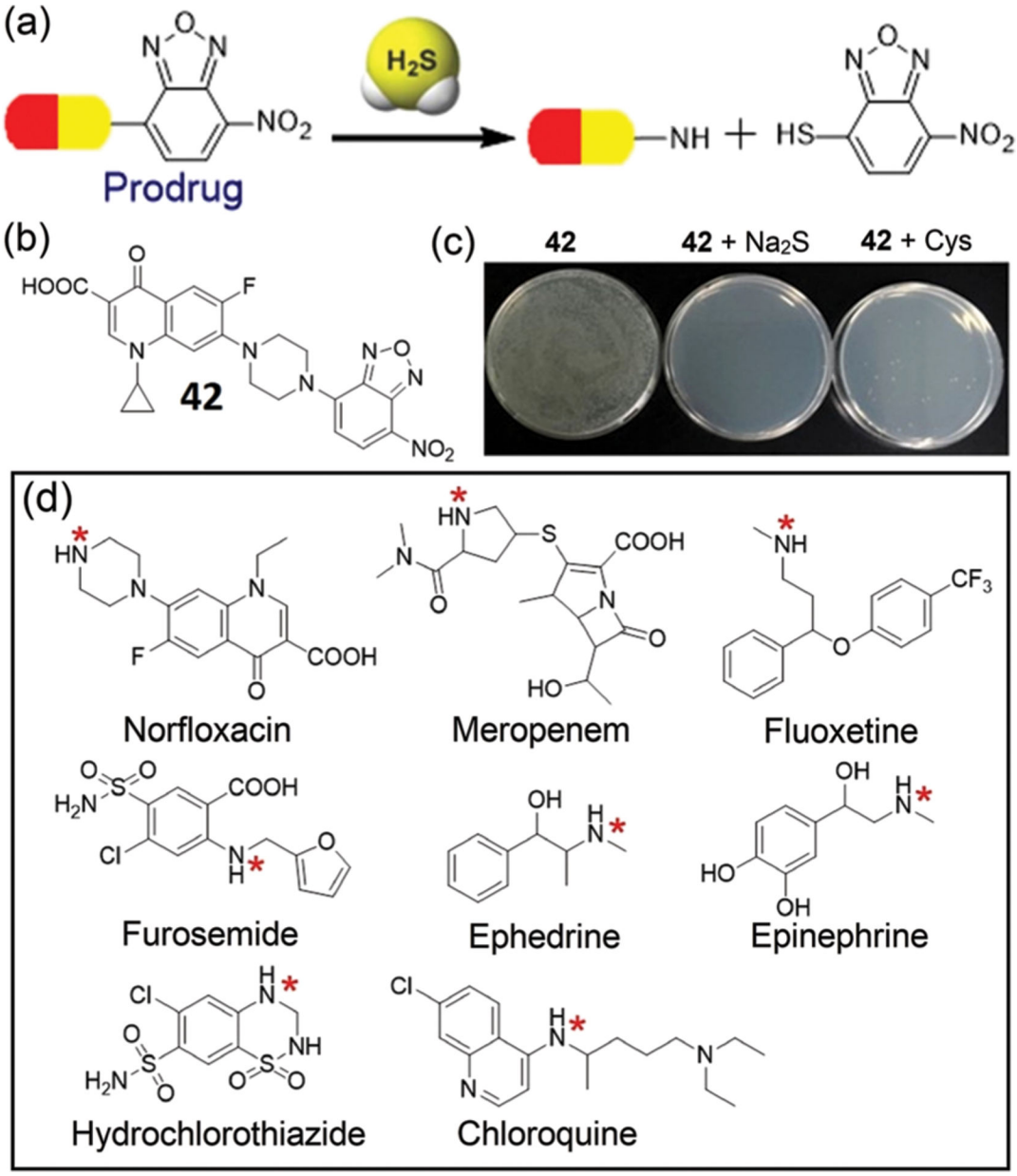

Fig. 8.

(a) Schematic illustration of H_2S-triggered release of prodrugs based on the thiolysis of NBD amines. (b) Chemical structure of a prodrug **42** and photo of bacterial growth inhibition for culture plates in the absence or presence of **42** and H_2S as indicated inset. (c) Concentration-dependent OD_{600} values of *E. coli* in different cultured conditions as indicated inset. (d) Chemical structures of drugs that contain amino groups (highlighted by red *). (b) and (c) are adapted with permission from ref. 90. Copyright 2019 Elsevier.

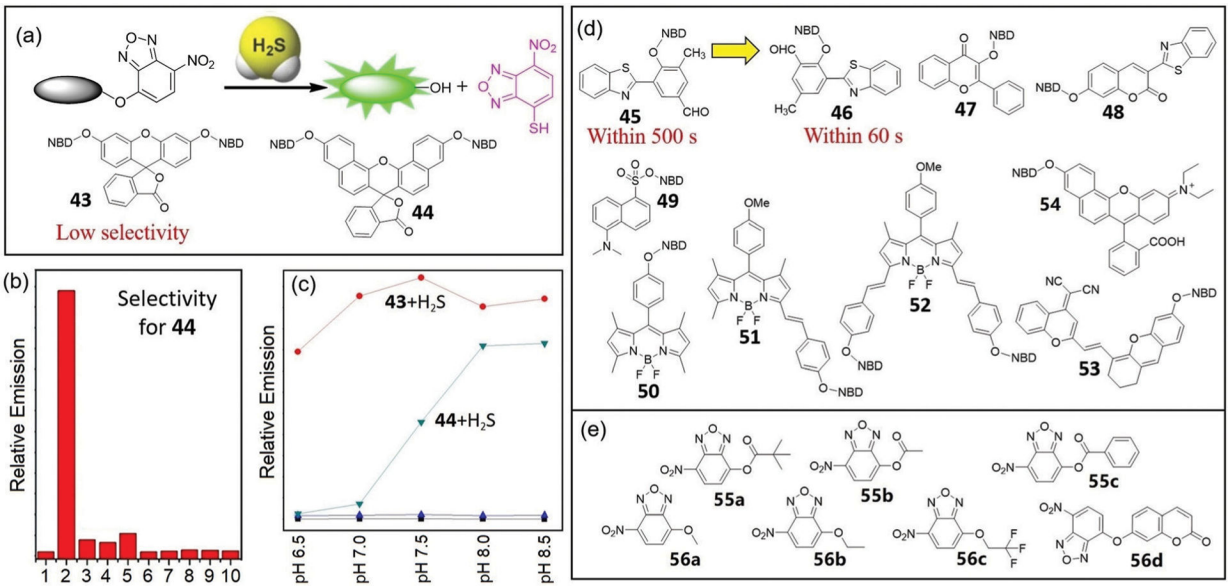

Fig. 9.

(a) The design strategy for H_2S-selective probes based on thiolysis of NBD ethers and chemical structures of **43** and **44**. (b) Fluorescence responses of **44** (10 μM) to various biologically relevant species (1 mM) in phosphate buffered saline (PBS, pH 7.4). Lane 1, probe **44** alone; 2, H_2S; 3, Cys; 4, GSH; 5, Zn^{2+}; 6, HCO_3^-; 7, CH_3COO^-; 8, I^-; 9, NO_2^-; 10, $C_2O_4^{2-}$. (c) The pH-dependent experiments of probe **43** (5 μM, ■) or probe **44** (10 μM, ▲) with H_2S (1 mM) at different pH values. Excitation 490 nm and emission 514 nm for **43**; excitation 600 nm and emission 662 nm for **44**. (d) Chemical structures of fluorescent probes **45–54**. (e) Chemical structures of colorimetric probes **55–56**. (b) and (c) are adapted with permission from ref. 24. Copyright 2014 Royal Society of Chemistry.

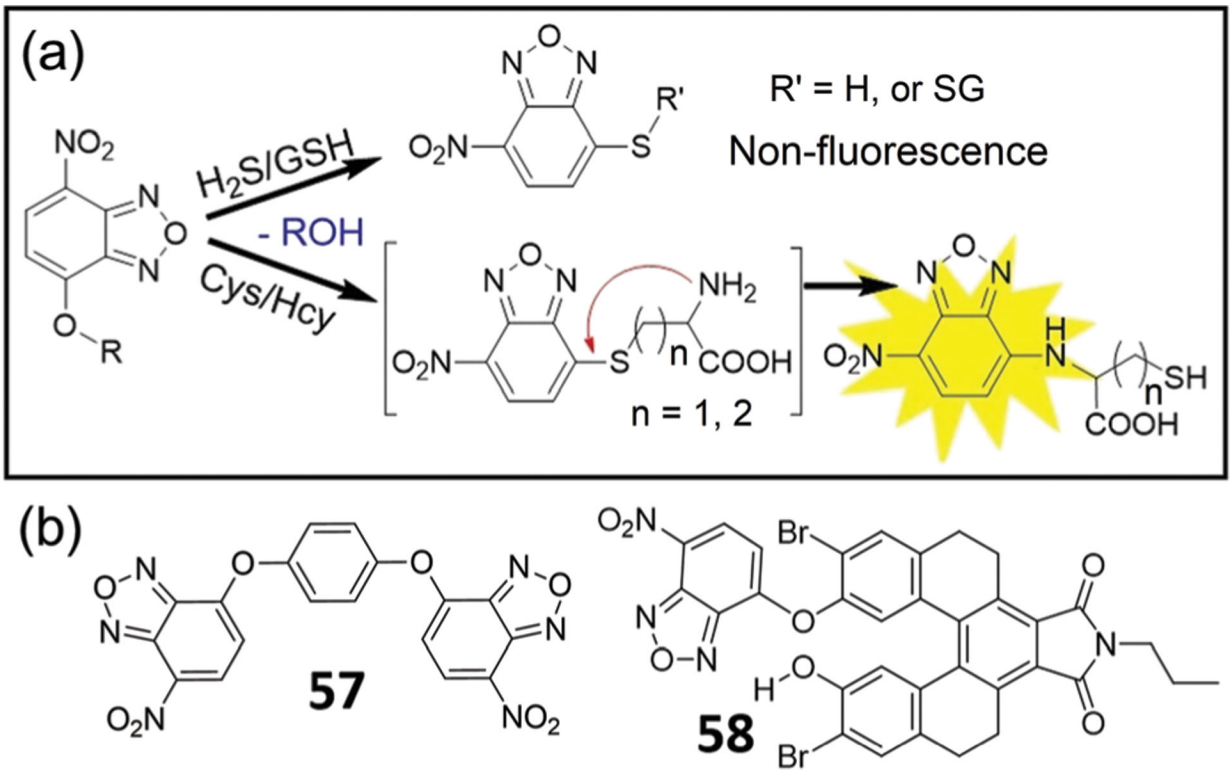

Fig. 10.

(a) Thiolysis of NBD-OR for fluorescent sensing of Cys/Hcy. (b) Chemical structures of probes **57** and **58**.

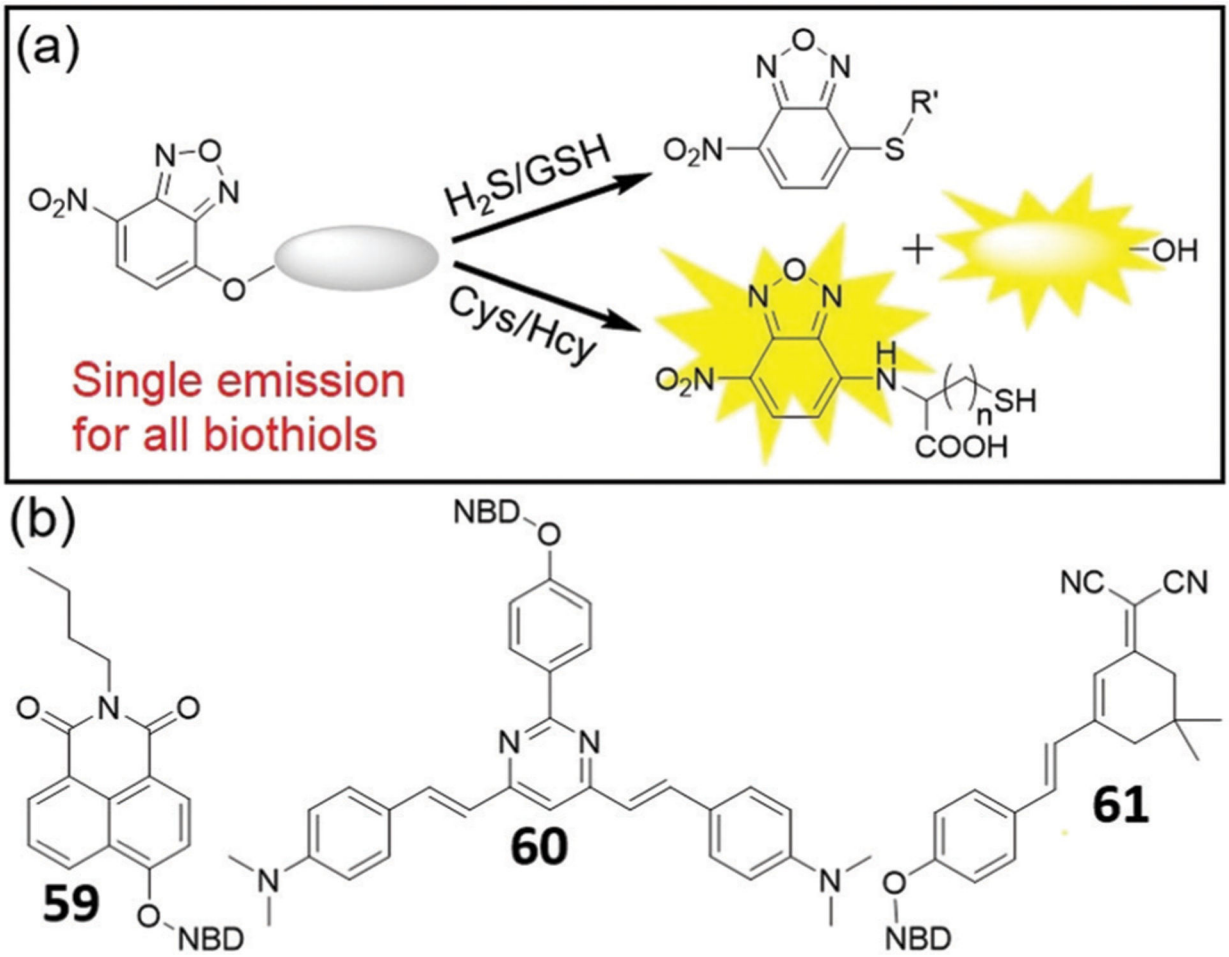

Fig. 11.

(a) A dual-fluorophore fragmentation strategy for generating a single emission for all biothiols and H_2S. (b) Chemical structures of probes **59–61**.

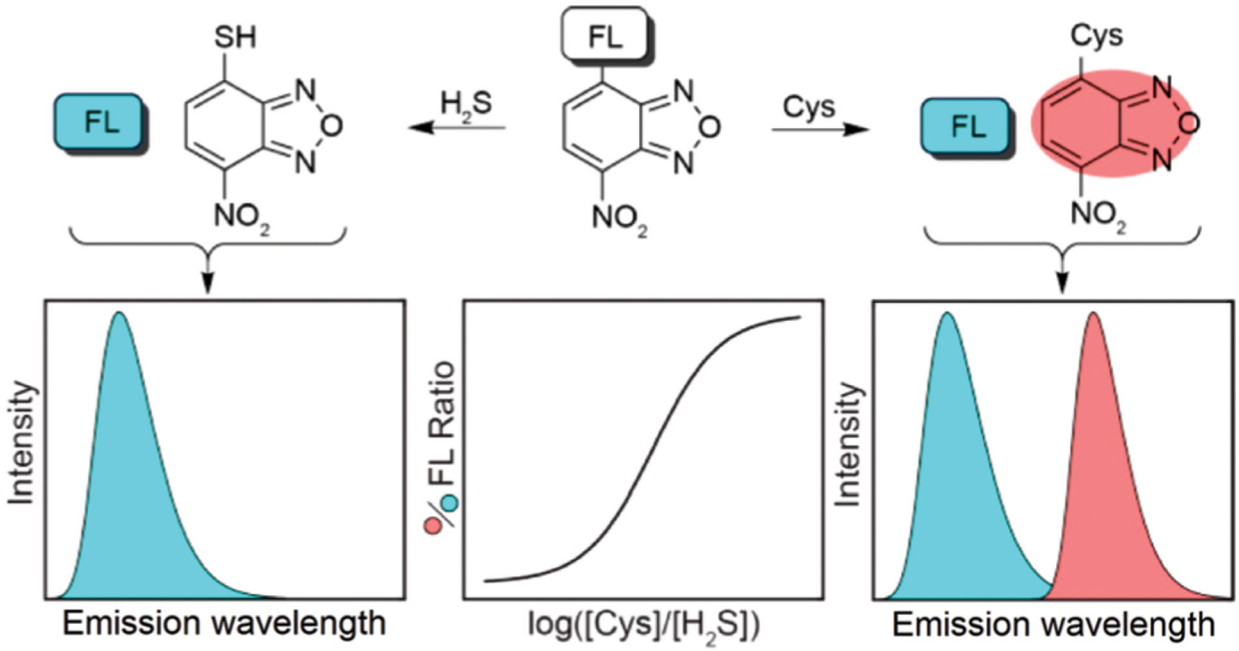

Fig. 12.

A dual-fluorophore fragmentation strategy for generating a ratiometric response to H_2S and Cys/Hcy levels. Adapted with permission from ref. 140. Copyright 2014 American Chemical Society.

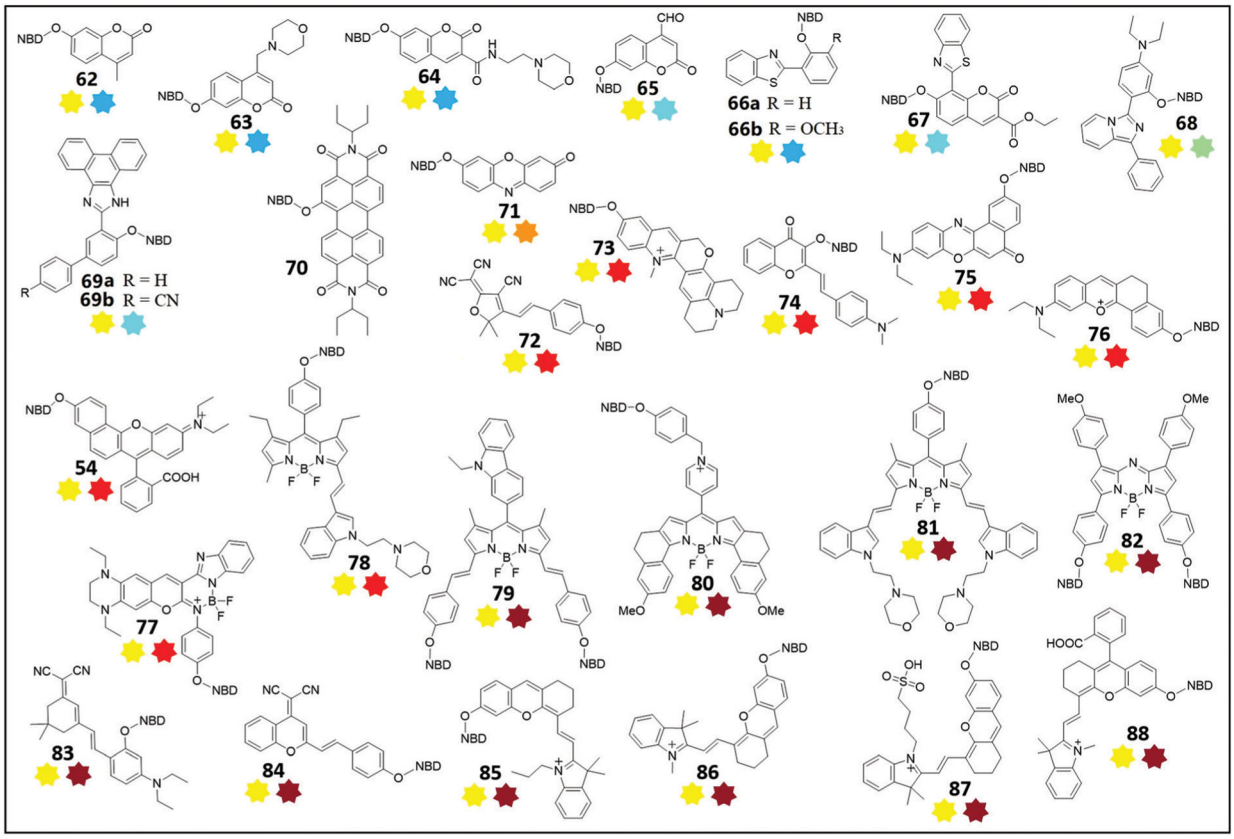

Fig. 13.

Chemical structures of thiol probes **54** and **62–88** based on the dual-fluorophore fragmentation strategy and the thiolysis of NBD ethers. The turn-on dual emissions are shown as colored stars below each structure; a dark red star represents NIR emission.

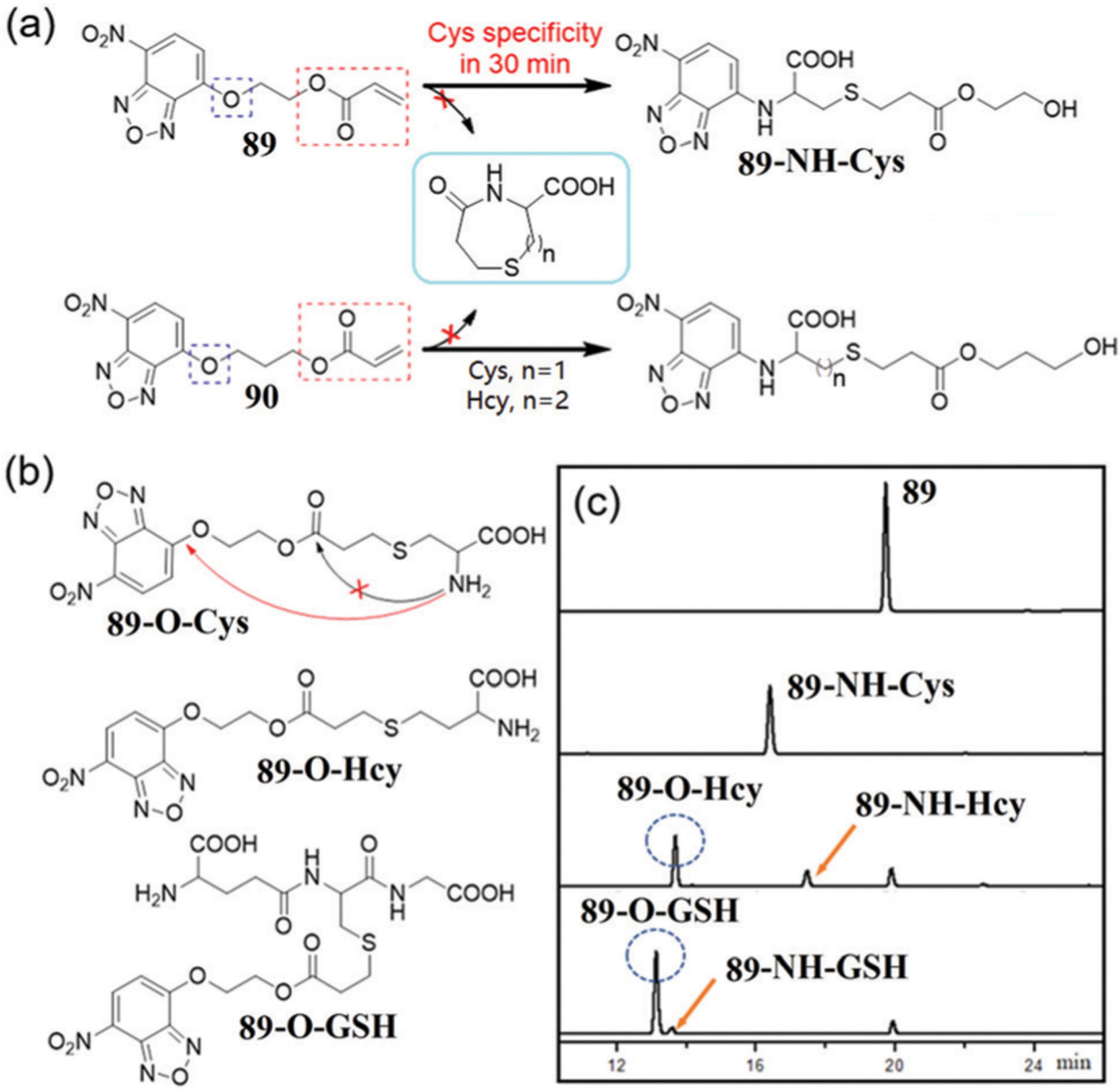

Fig. 14.

(a) Chemical structures and reactions of **89** and **90** with Cys/Hcy. (b) Chemical structures of reaction intermediates of **89** toward biothiols. (c) HPLC traces of **89** and its reaction with three biothiols for 42 min incubation. (c) is adapted with permission from ref. 171. Copyright 2020 Royal Society of Chemistry.

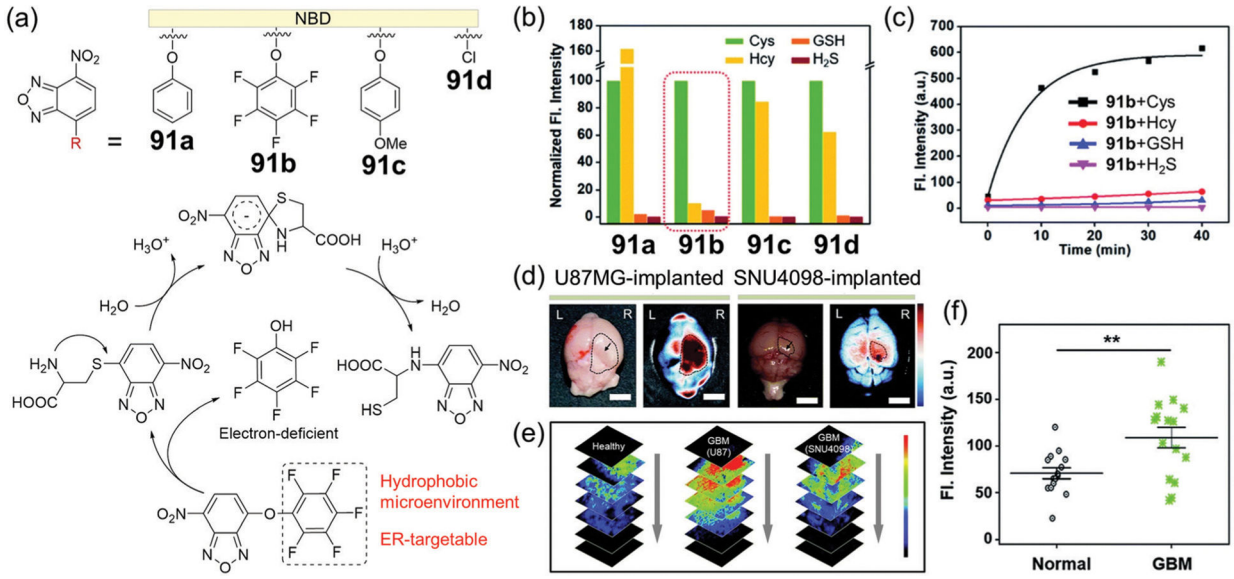

Fig. 15.

(a) Chemical structures of probes **91a–91d,** and the reaction mechanism of **91b** with Cys. (b) Normalized fluorescence intensity at 550 nm of probes **91a–91d** with biothiols and H_2S; excitation at 478 nm. (c) Time-dependent fluorescence intensity at 550 nm of **91b** with biothiols and H_2S. (d) *Ex vivo* bright-field (left) and FTIS (right) images of the brain for the U87MG- or SNU4098-implanted mouse. (e) TPM images of brain tissues at the normal and GBM site at the indicated depths (20–100 μm), after **91b** treatment. (f) Fluorescence intensity plots from TPM images of the brain tissues. (b)–(f) are adapted with permission from ref. 173. Copyright 2020 Royal Society of Chemistry.

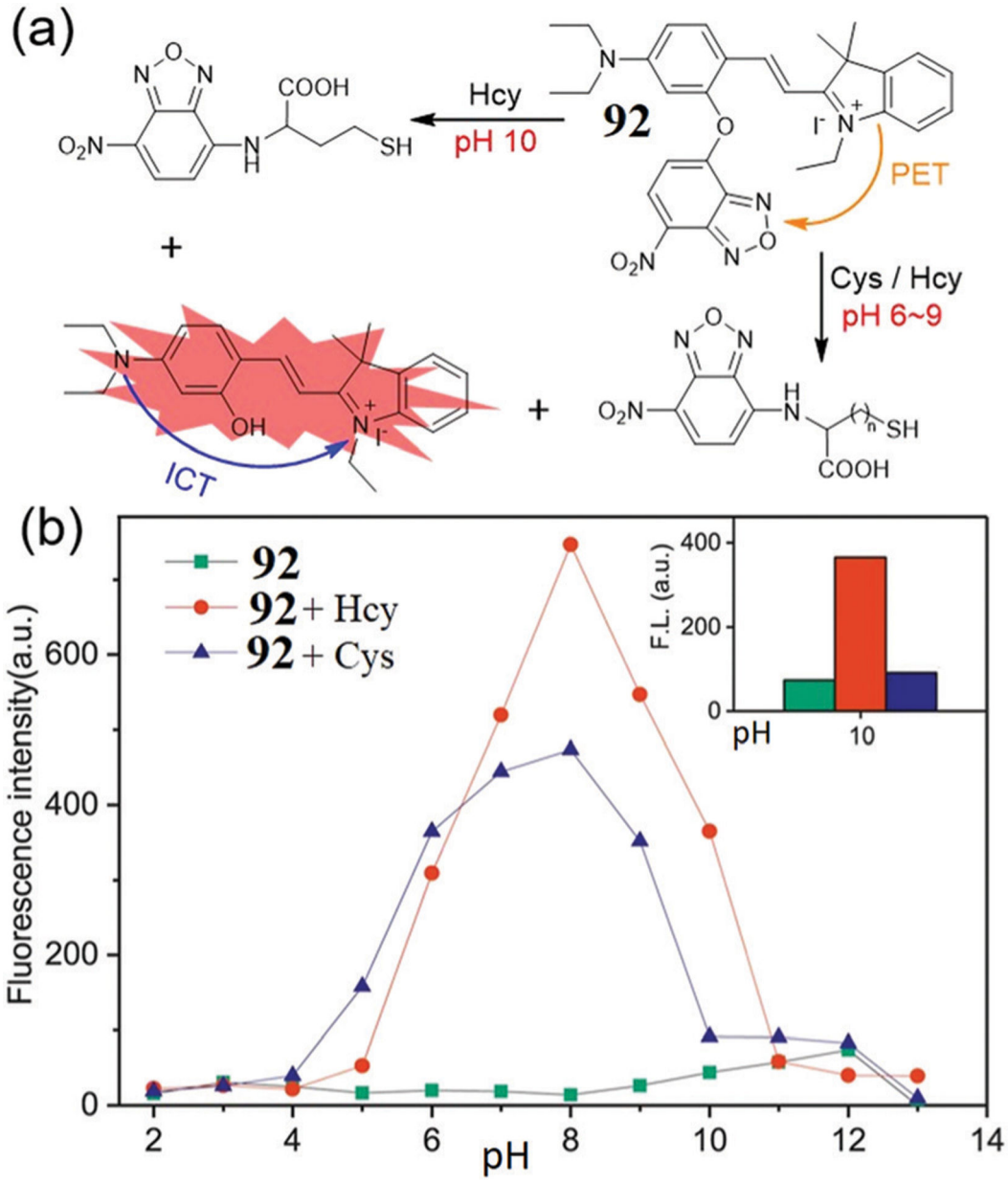

Fig. 16.

(a) The proposed response mechanism of probe **92** with Hcy/Cys. (b) The fluorescence intensity (592 nm) changes of **92** and **92** + Hcy/Cys at different pH values. (b) is adapted with permission from ref. 174. Copyright 2020 Elsevier.

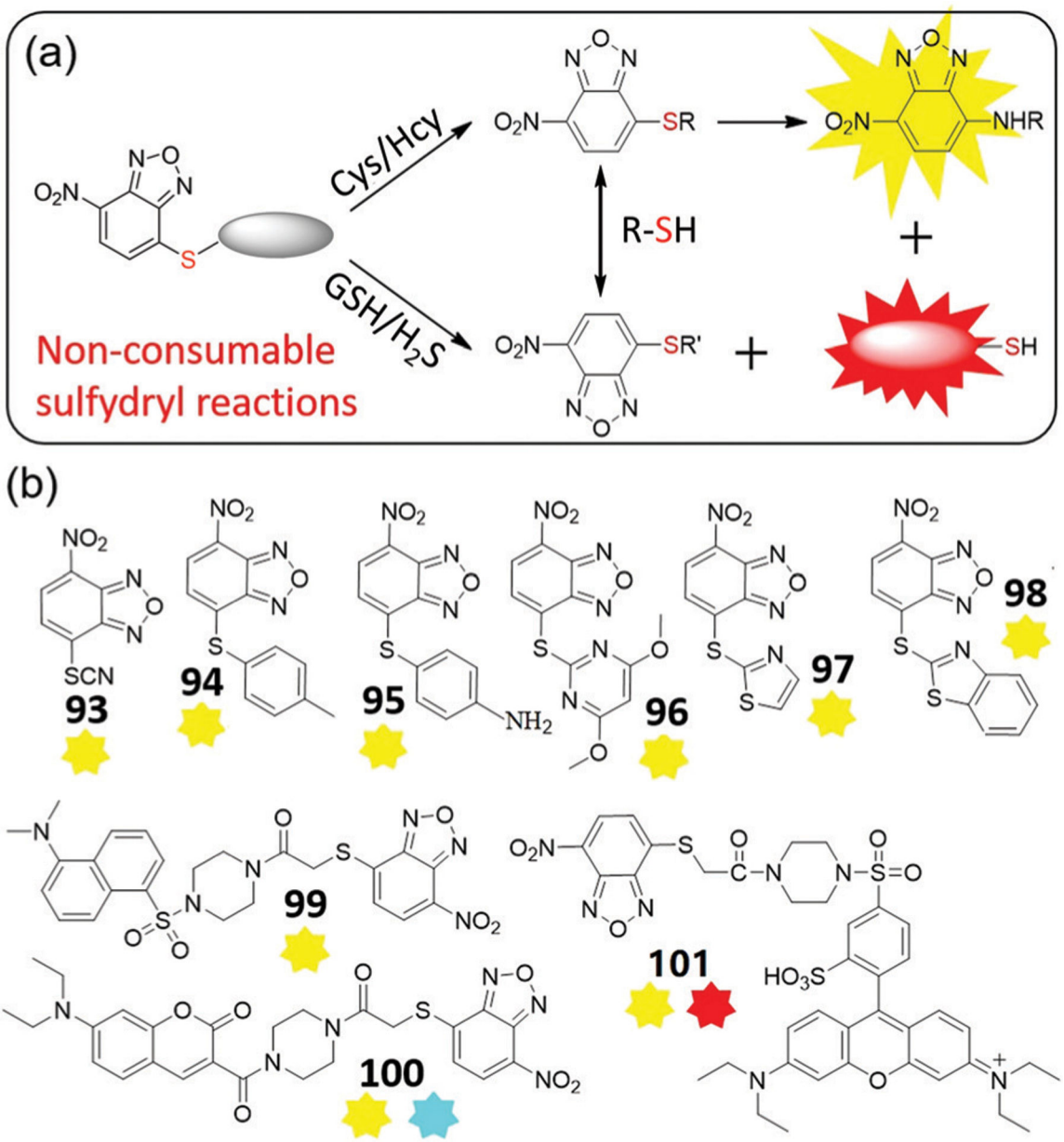

Fig. 17.

(a) The proposed response mechanism of dual-channel NBD thioether probes for biothiols and H_2S. (b) Chemical structures of probes **93–101**.

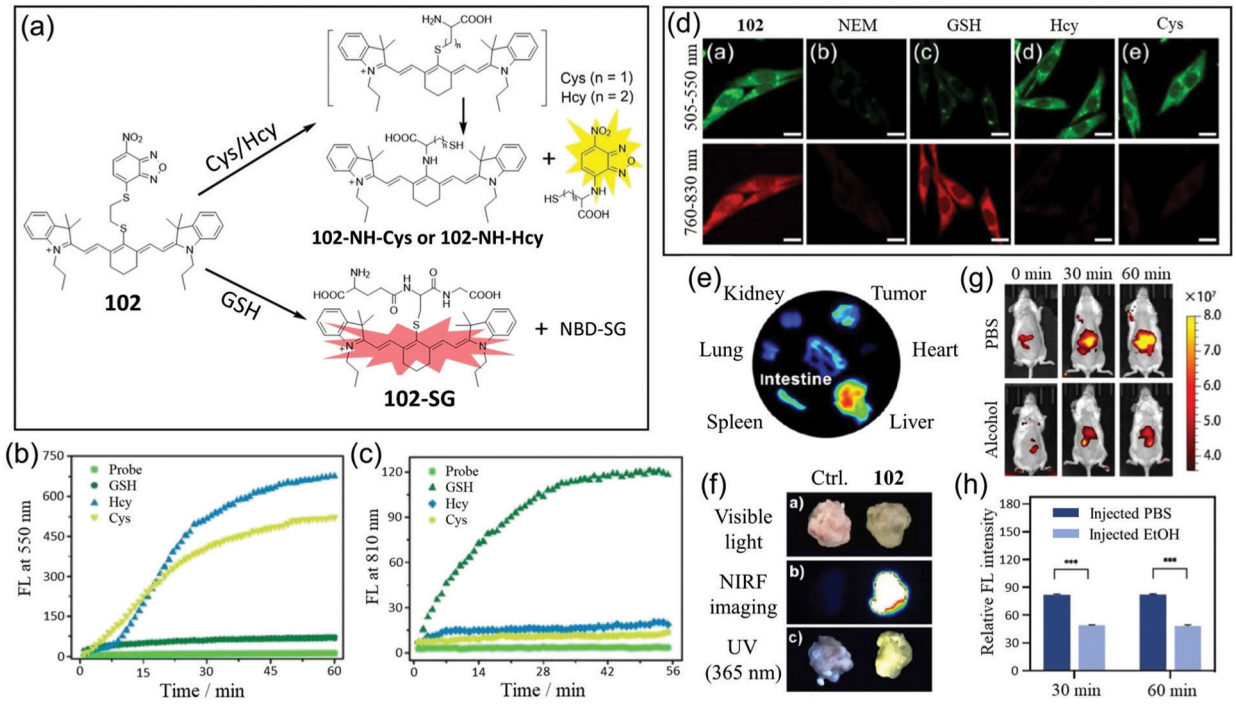

Fig. 18.

(a) Response mechanism of **102** for discriminating Cys/Hcy and GSH with two distinct emission patterns. (b and c) Time-dependent emission changes at 550 nm (b) and 810 nm (c) of **102** with the addition of GSH, Hcy and Cys, respectively. (d) Fluorescence images of U87 cells incubated with **102** (da); with *N*-ethylmaleimide (NEM) and then **102** (db); with NEM and then with GSH (dc), Hcy (dd), or Cys (de), followed by **102**. (e) *Ex vivo* fluorescence images of isolated organs from the tumor-bearing mice at 8 h post-injection of **102**. (f) Photos of tissue portions of tumors stained by PBS as control or **102**, respectively, under visible light, or fluorescence at 760 nm or 365 nm excitation. (g) Representative NIR fluorescence images of mice (oral gavage 2 g kg^{-1} alcohol) were collected at 0, 30, and 60 min post-injection of **102**. (h) Semi-quantitative analysis of the NIR fluorescence intensity of mice in (g). (b)–(h) are adapted with permission from ref. 184. Copyright 2020 Royal Society of Chemistry.

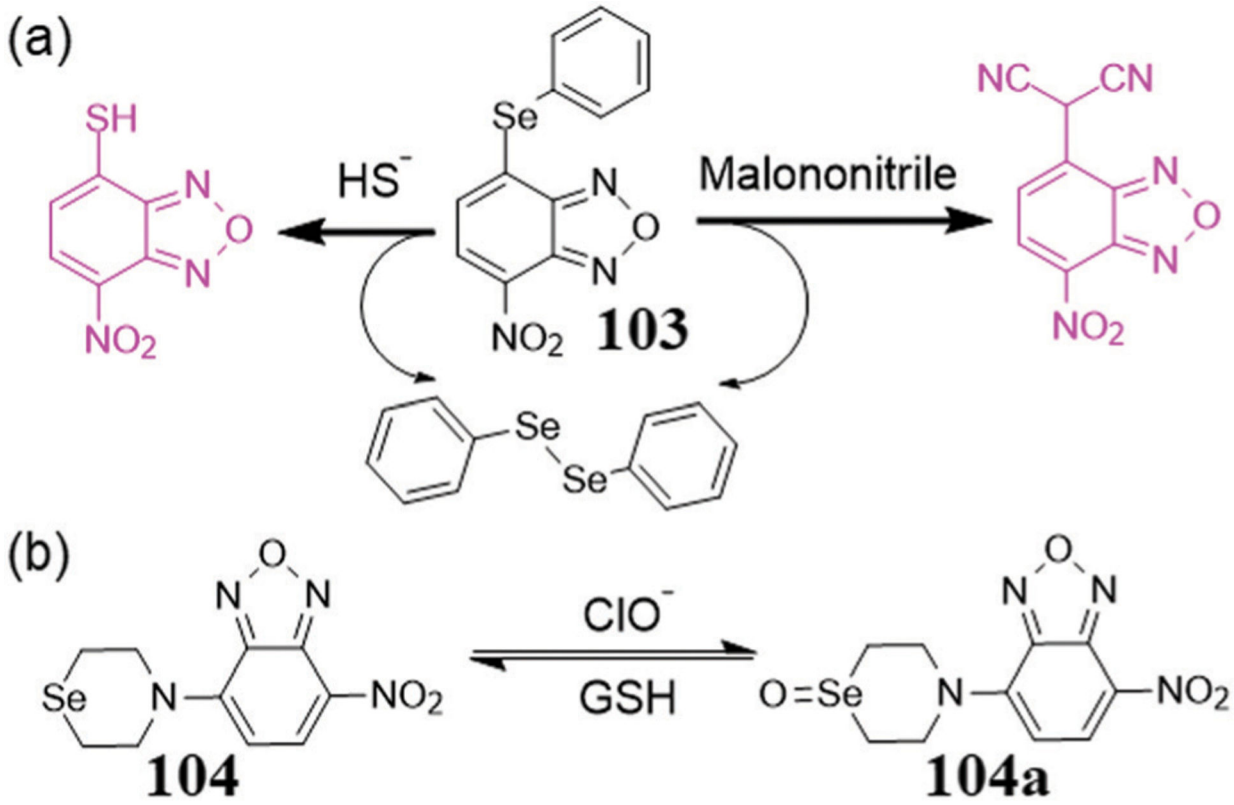

Fig. 19.

(a) Chemical structure of **103** and its reaction with H_2S or malononitrile. (b) Chemical structure of a chemically reversible probe **104** and its reaction with ClO^- and GSH.

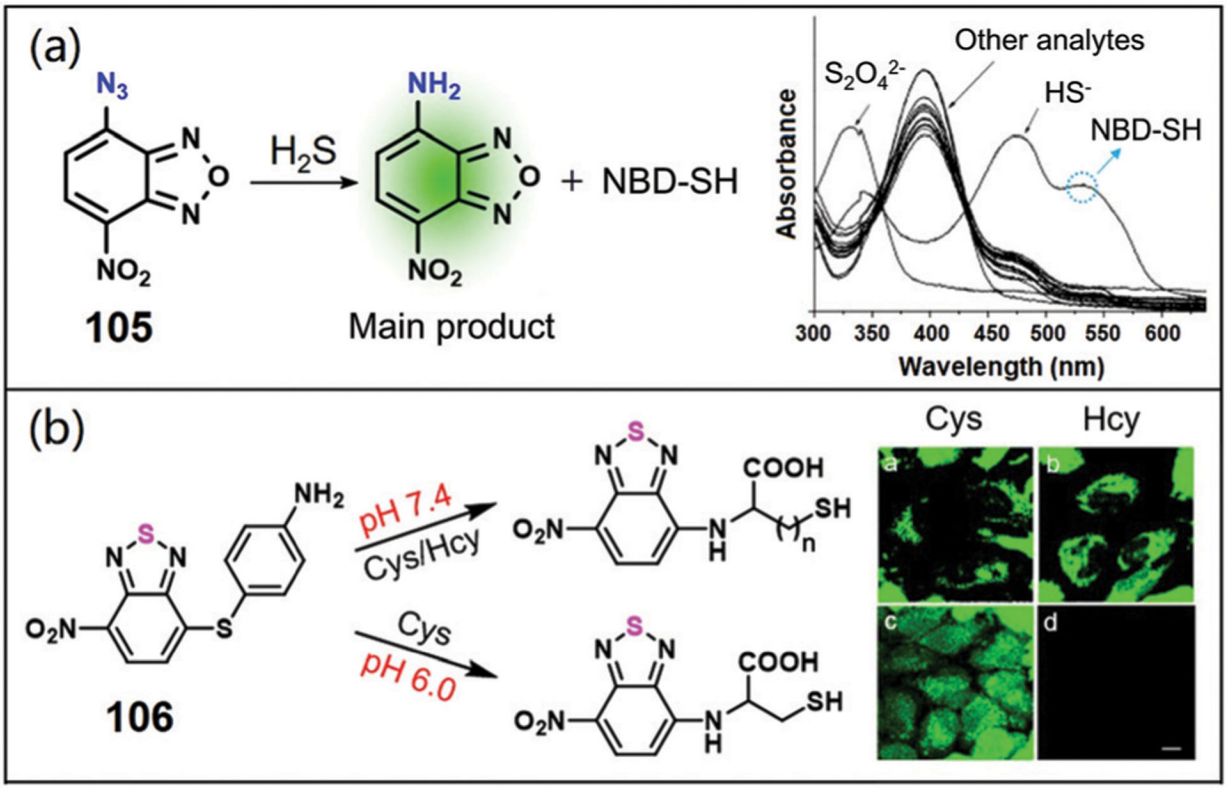

Fig. 20.

(a) Chemical structure of **105** and its reaction with H_2S (left); absorption spectra of **105** (10 μM) in the presence of 100 μM analytes upon 5 min incubation (right). (b) The sensing mechanism (left) and fluorescence images (right) of probe **106** for Cys/Hcy and Cys. (a) and (b) are adapted with permission from ref. 189 and 190. Copyright 2013 Elsevier, 2015 Royal Society of Chemistry, respectively.

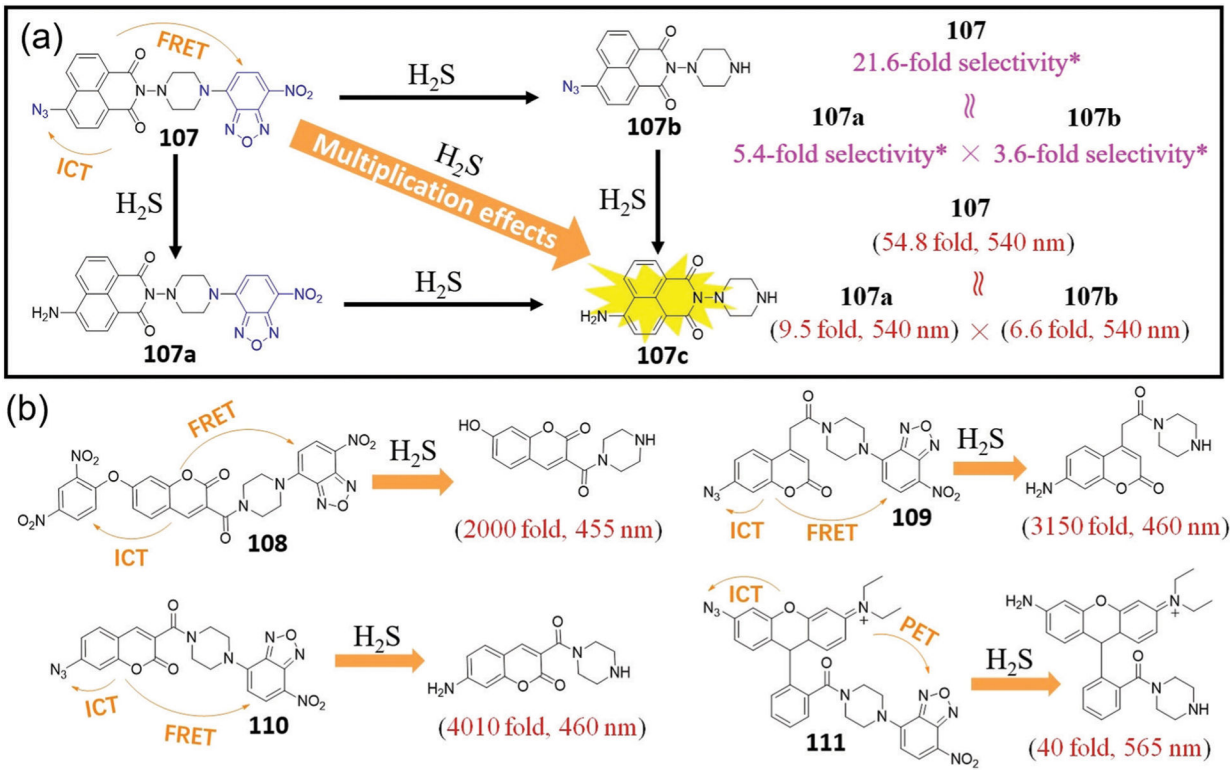

Fig. 21.

(a) Chemical structures of probes **107–107b** and their reactions with H_2S. * The selectivity is the 540 nm emission intensity ratio of the probe with 200 μM H_2S to with 1 mM Cys. (b) Chemical structures of **108–111** and their reactions with H_2S and their associated fluorescence turn-on values after reaction with H_2S.

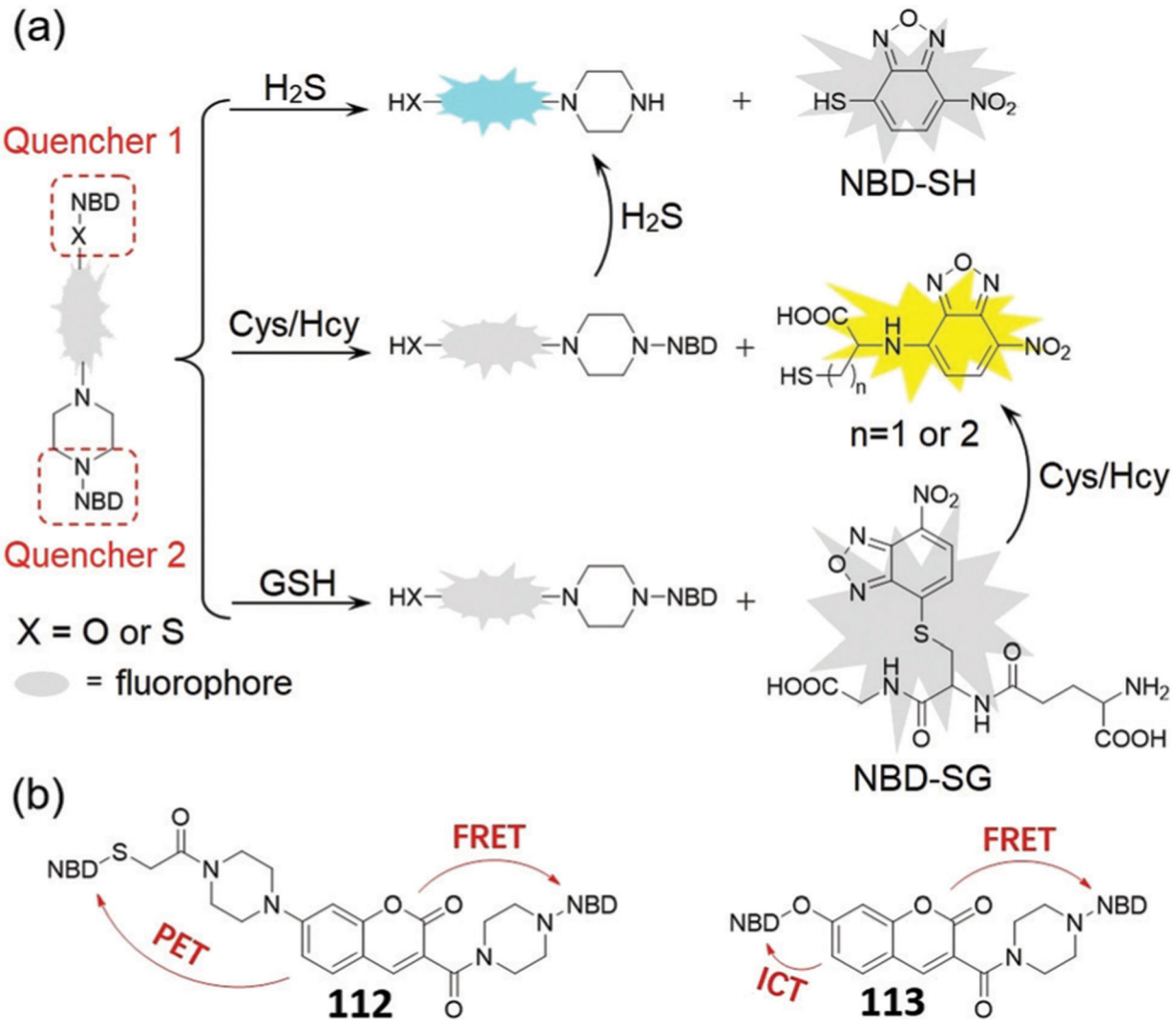

Fig. 22.

(a) Fluorescent sensing mechanism for H_2S, Cys/Hcy, and GSH. (b) Chemical structures of **112** and **113**, and their quenching effects.

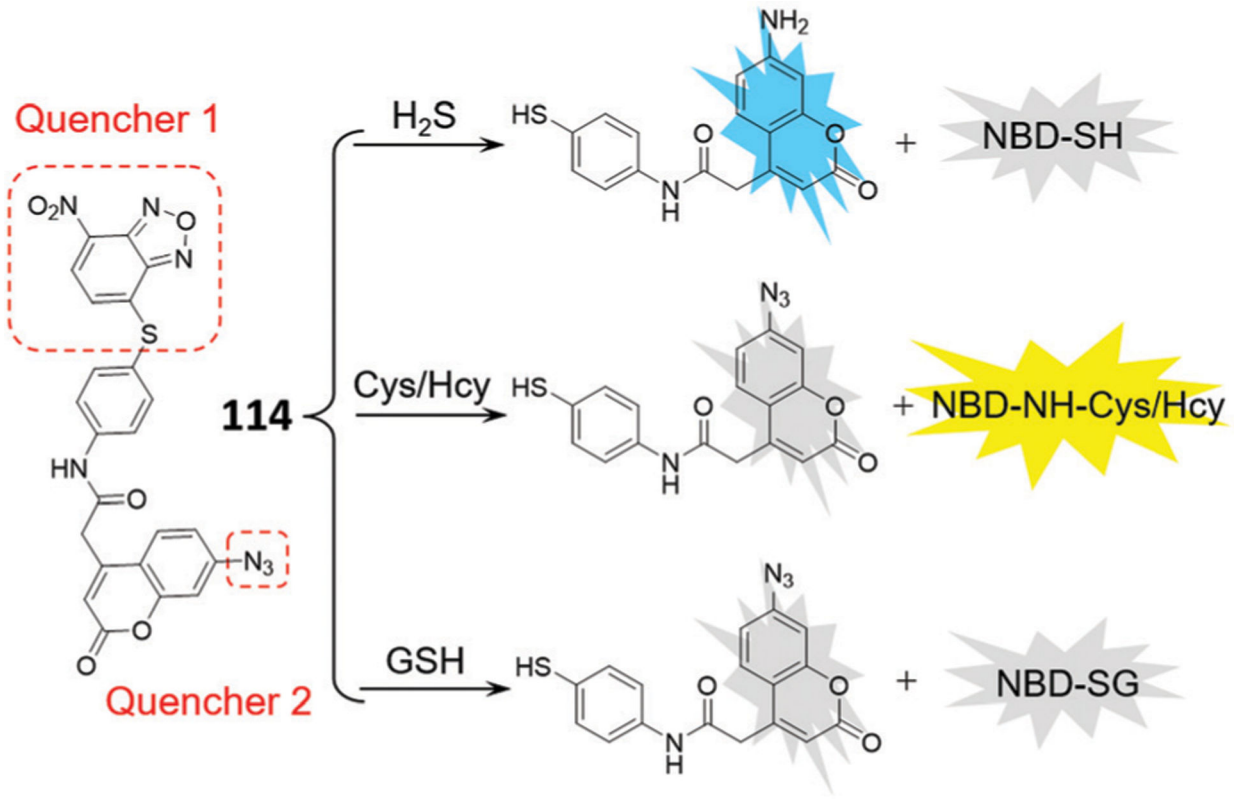

Fig. 23.
Chemical structure of probe **114** and its sensing mechanism for H_2S, Cys/Hcy, and GSH.

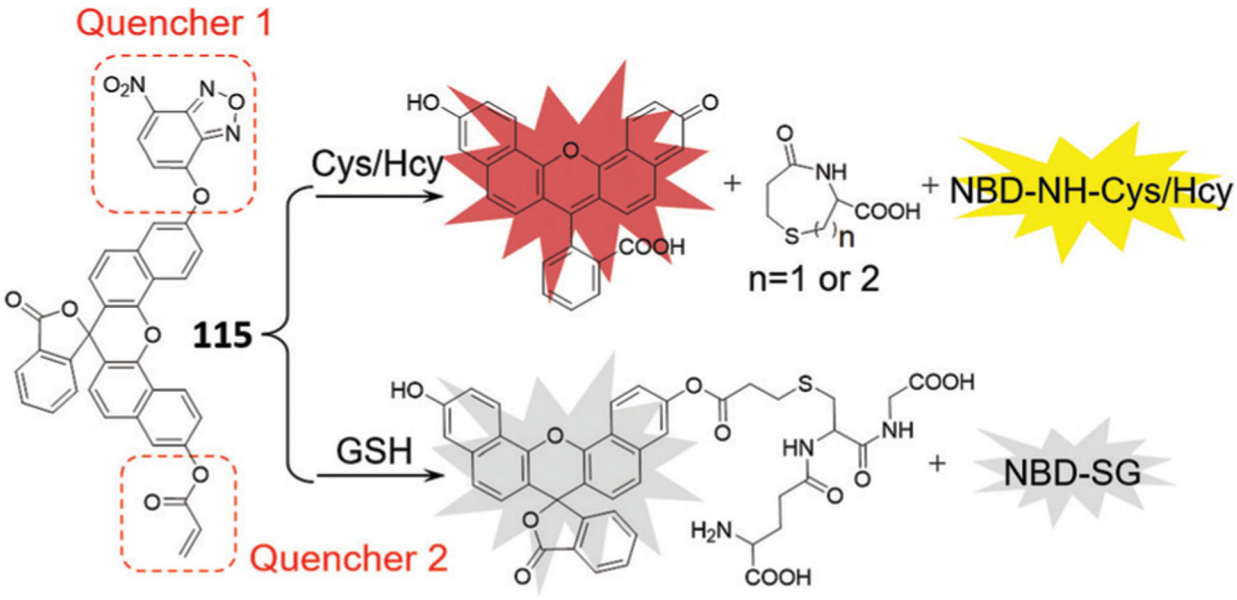

Fig. 24.

The chemical structure of probe **115** and its sensing mechanism for Cys/Hcy and GSH.

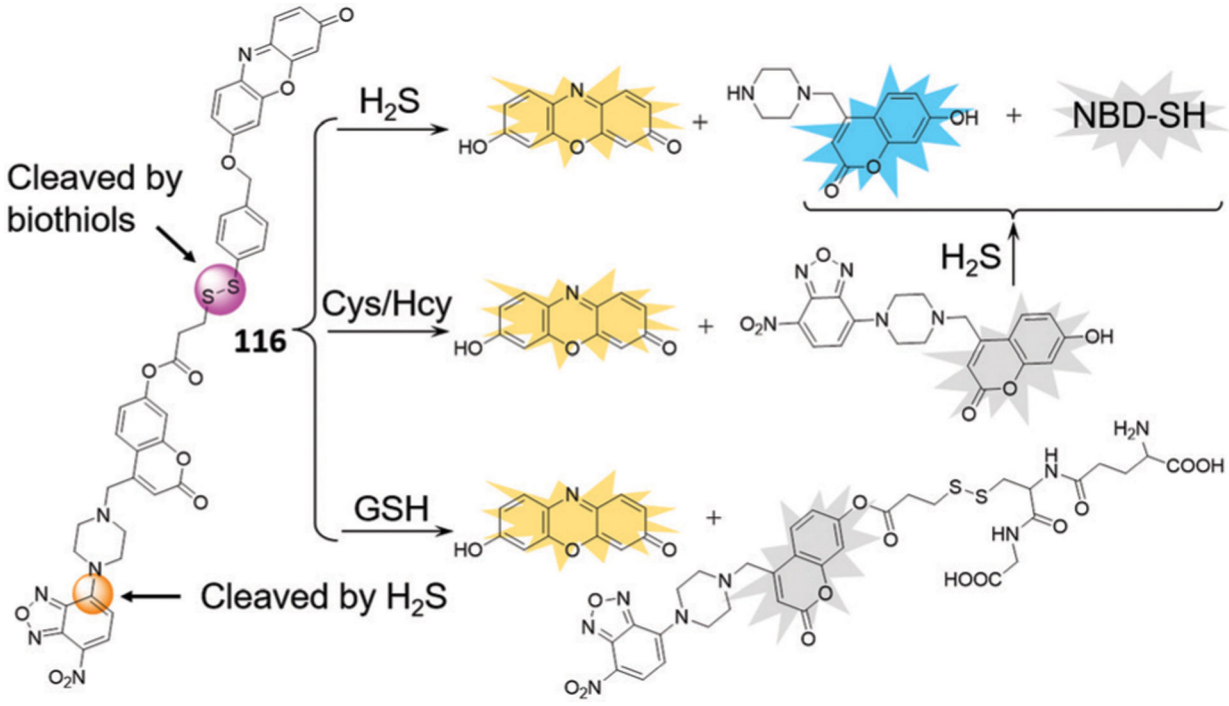

Fig. 25.

The chemical structure of probe **116** and its sensing mechanism for H_2S, Cys/Hcy, and GSH.

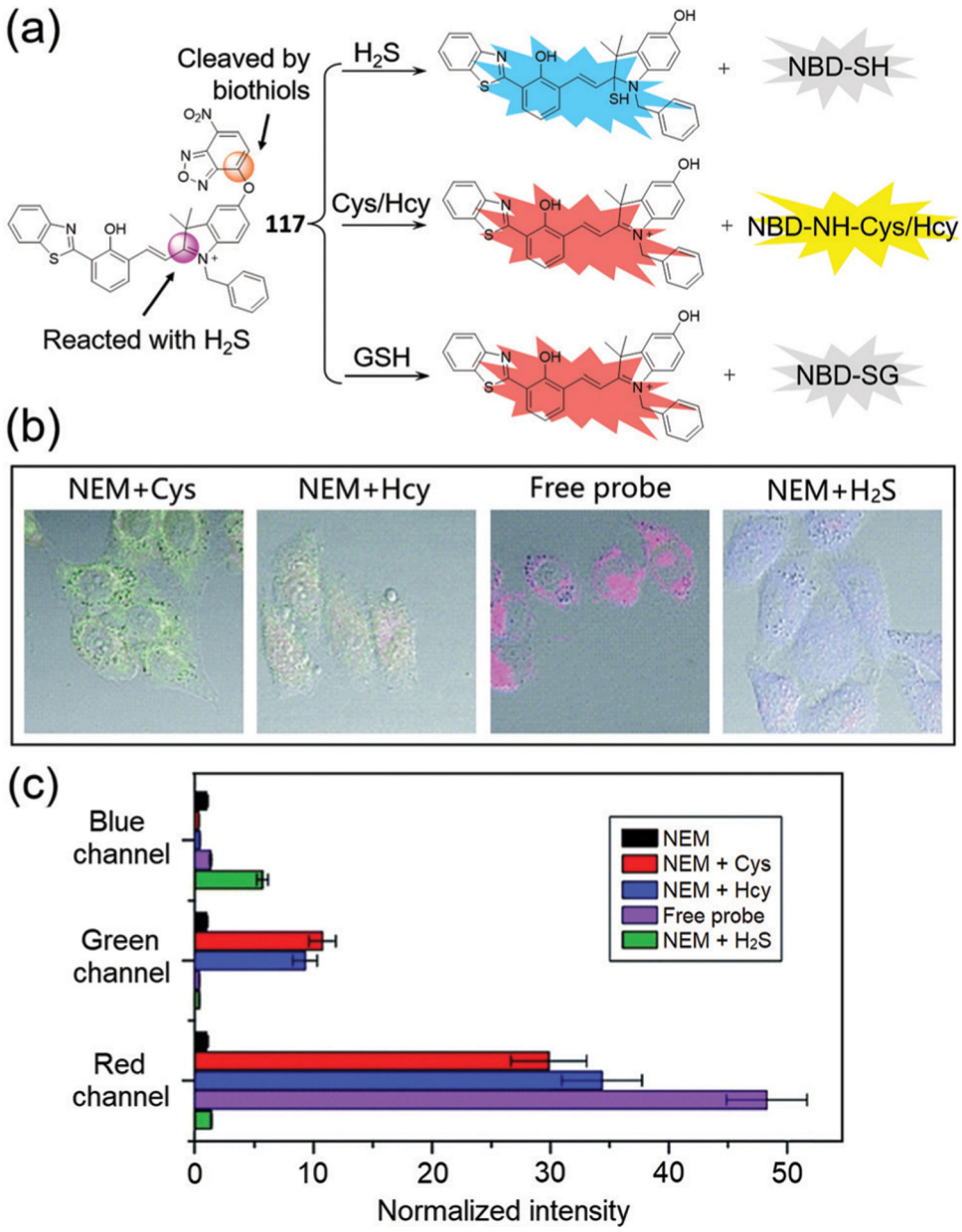

Fig. 26.

(a) Chemical structure of **117** and its sensing mechanism for H_2S, Cys/Hcy, and GSH. (b) Overlap of fluorescent and bright-field images of probe **117** responding to respective biothiols in live cells. (c) Normalized average fluorescence intensities of the blue, green, and red channels in (b). (b) and (c) are adapted with permission from ref. 208. Copyright 2017 Royal Society of Chemistry.

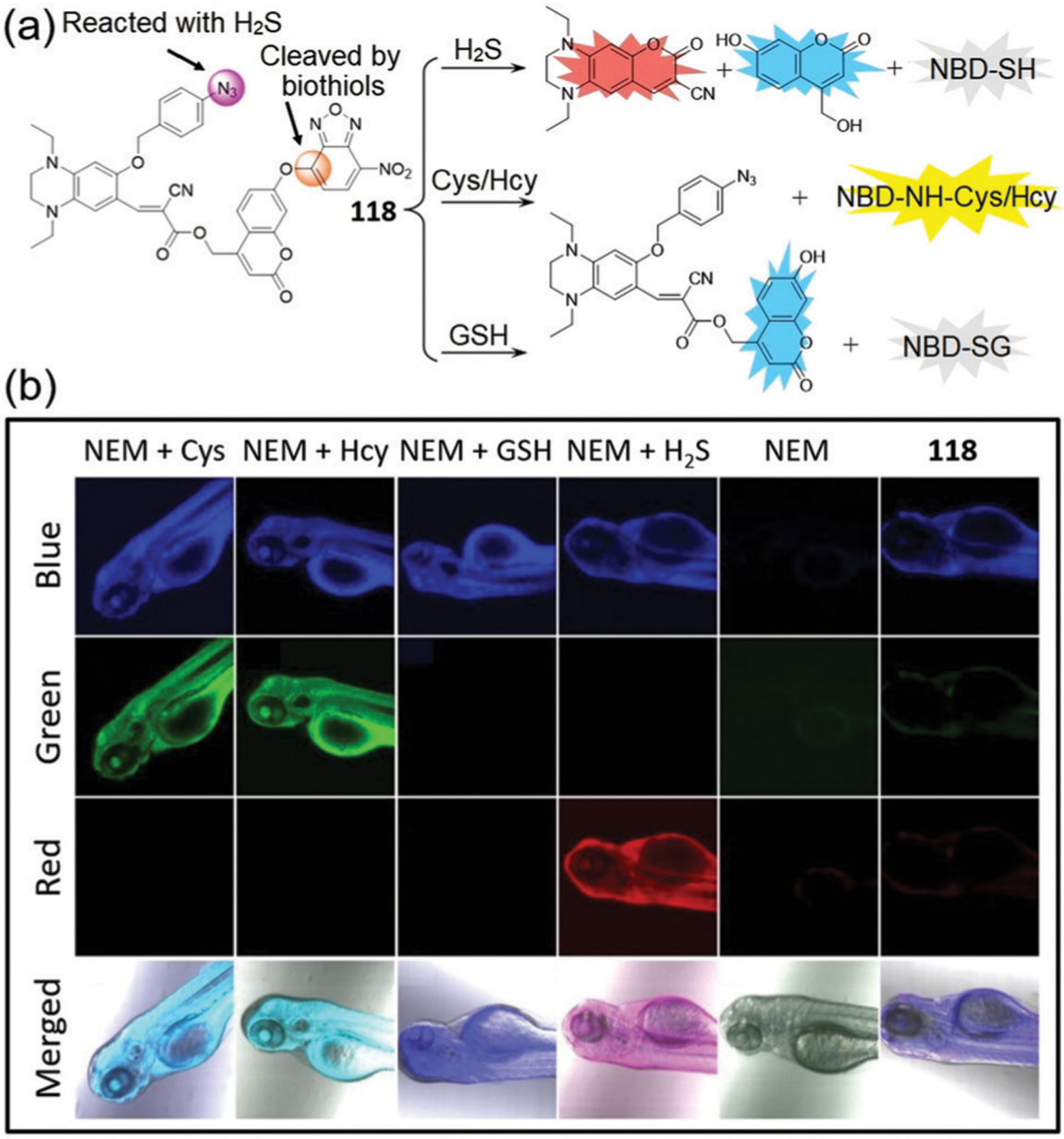

Fig. 27.

(a) The chemical structure of probe **118** and its sensing mechanism for H_2S, Cys/Hcy, and GSH. (b) Three-color fluorescent images and overlap fluorescent and bright-field images of zebrafish with different treatments as indicated in the inset. (b) is adapted with permission from ref. 209. Copyright 2019 Elsevier.

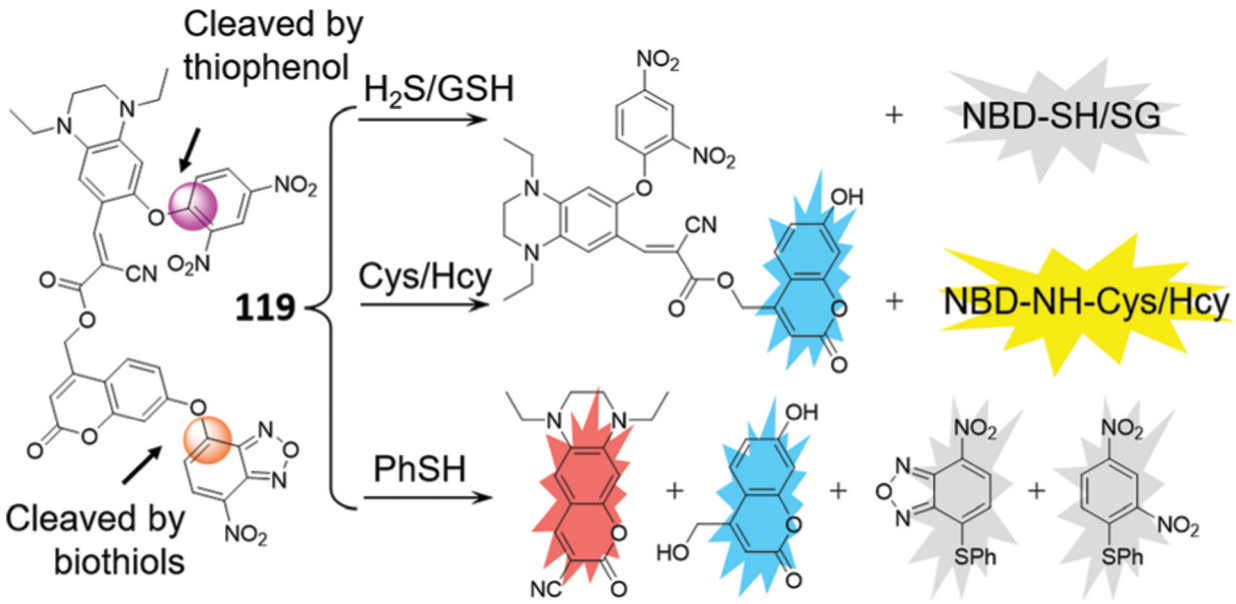

Fig. 28.

The chemical structure of probe **119** and its sensing mechanism for H_2S/GSH, Cys/Hcy, and PhSH.

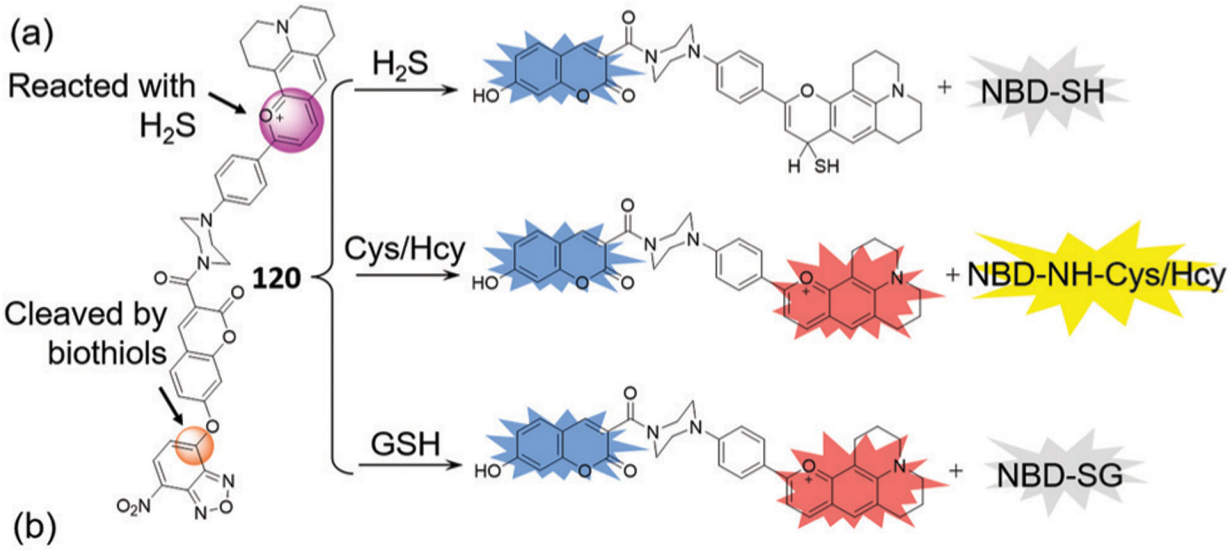

Inputs			Outputs		
Cys/Hcy	GSH	H_2S	Em_{453}	Em_{554}	Em_{658}
0	0	0	0	0	1
1	0	0	1	1	1
0	1	0	1	0	1
0	0	1	1	0	0
1	1	0	1	1	1
1	0	1	1	0	0
0	1	1	1	0	0
1	1	1	1	0	0

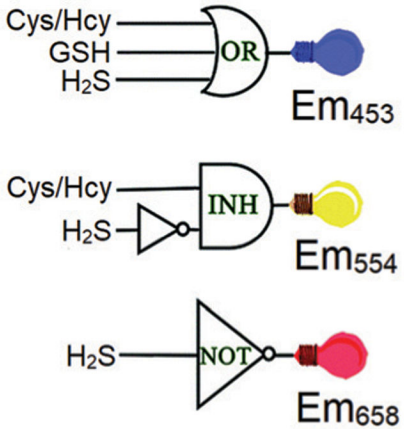

Fig. 29.

(a) The chemical structure of probe **120** and its sensing mechanism for H_2S, Cys/Hcy, GSH. (b) Illustration of three-input OR, two-input INH, and one-input NOT functions taking Em_{453}, Em_{554}, and Em_{658} as the outputs, respectively. The absence of inputs and the negative signal of outputs were considered to be 0, and the presence of inputs and the positive signal of outputs were considered to be 1. (b) is adapted with permission from ref. 211. Copyright 2017 Royal Society of Chemistry.

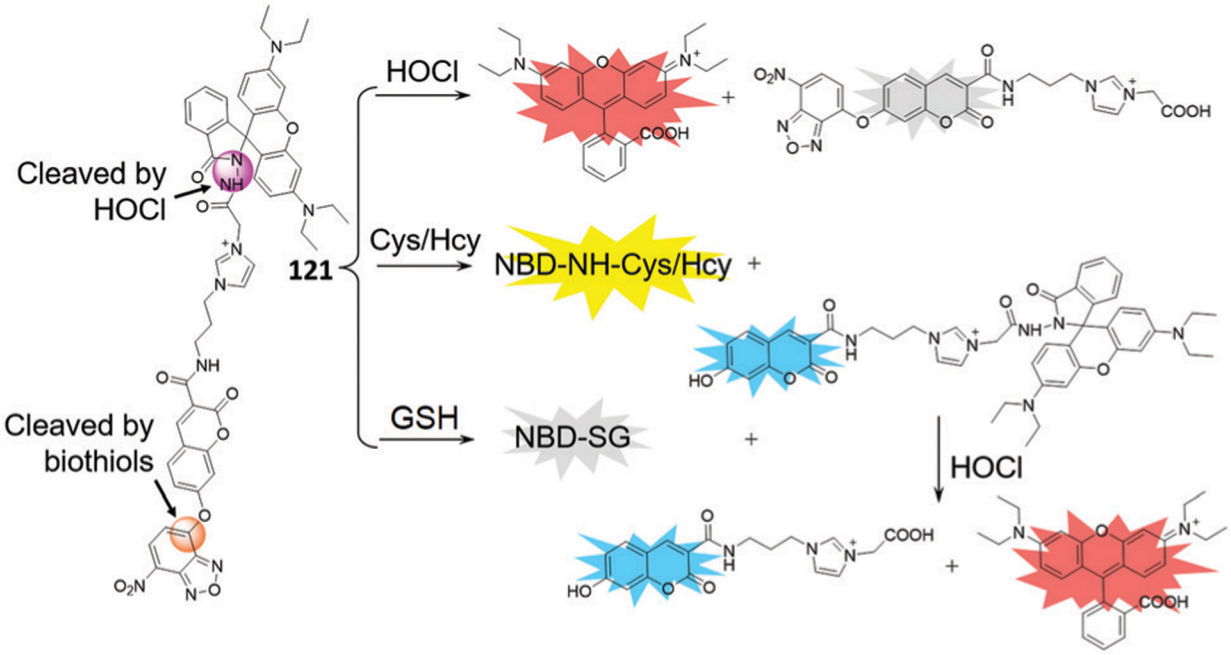

Fig. 30.

The chemical structure of probe **121** and its sensing mechanism for HOCl, Cys/Hcy, and GSH.

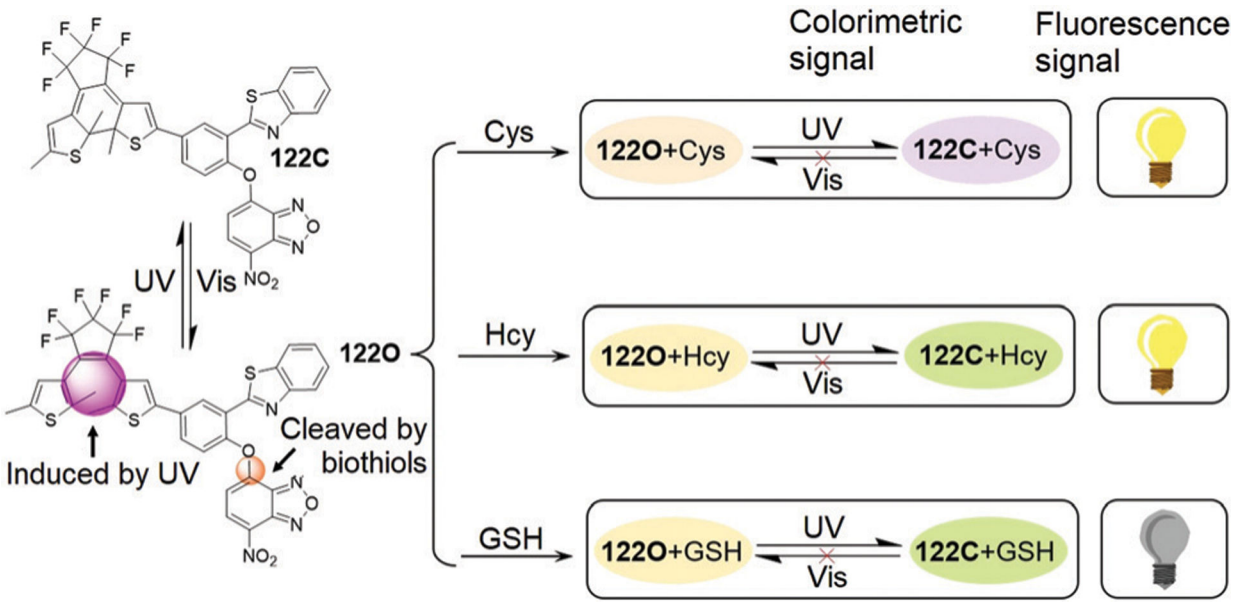

Fig. 31.

The chemical structure of probe **122** and its sensing mechanism for color and fluorescent distinguishing Cys/Hcy, GSH and H_2S.

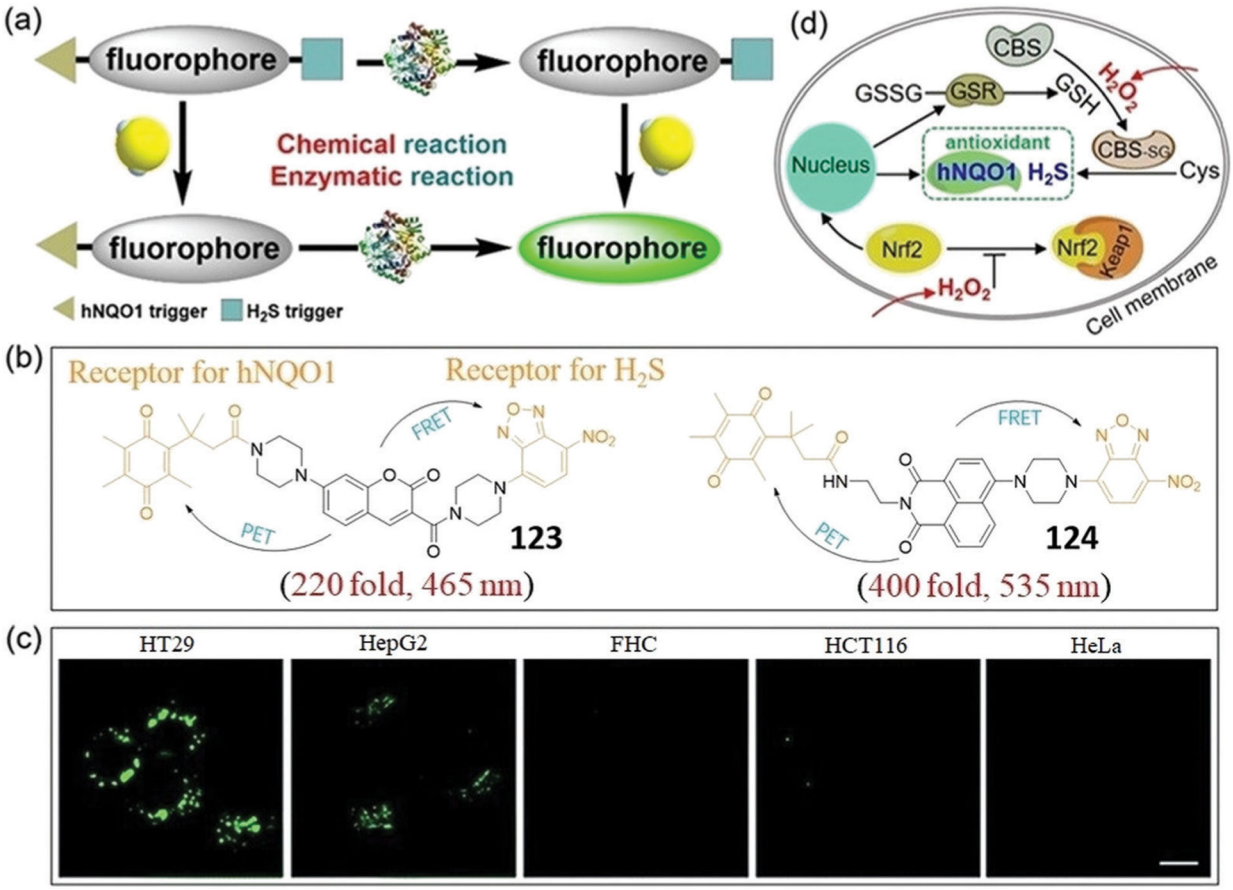

Fig. 32.

(a) Schematic illustration of the design for a dual-biomarker triggered fluorescent probe, which should only be activated by the synergistic chemical reaction with H_2S and enzymatic reaction with hNQO1. (b) Chemical structures of **123** and **124**. (c) Confocal microscopy images for endogenous H_2S and hNQO1 detection in different live cells using **124**. (d) A proposed mechanism of the synergistic antioxidant effect of H_2S and hNQO1 under oxidative stress. Keap1, Kelch-like ECH-associated protein 1; Nrf2, nuclear factor-erythroid 2-related factor 2. (a), (c) and (d) are adapted with permission from ref. 214. Copyright 2019 Royal Society of Chemistry.

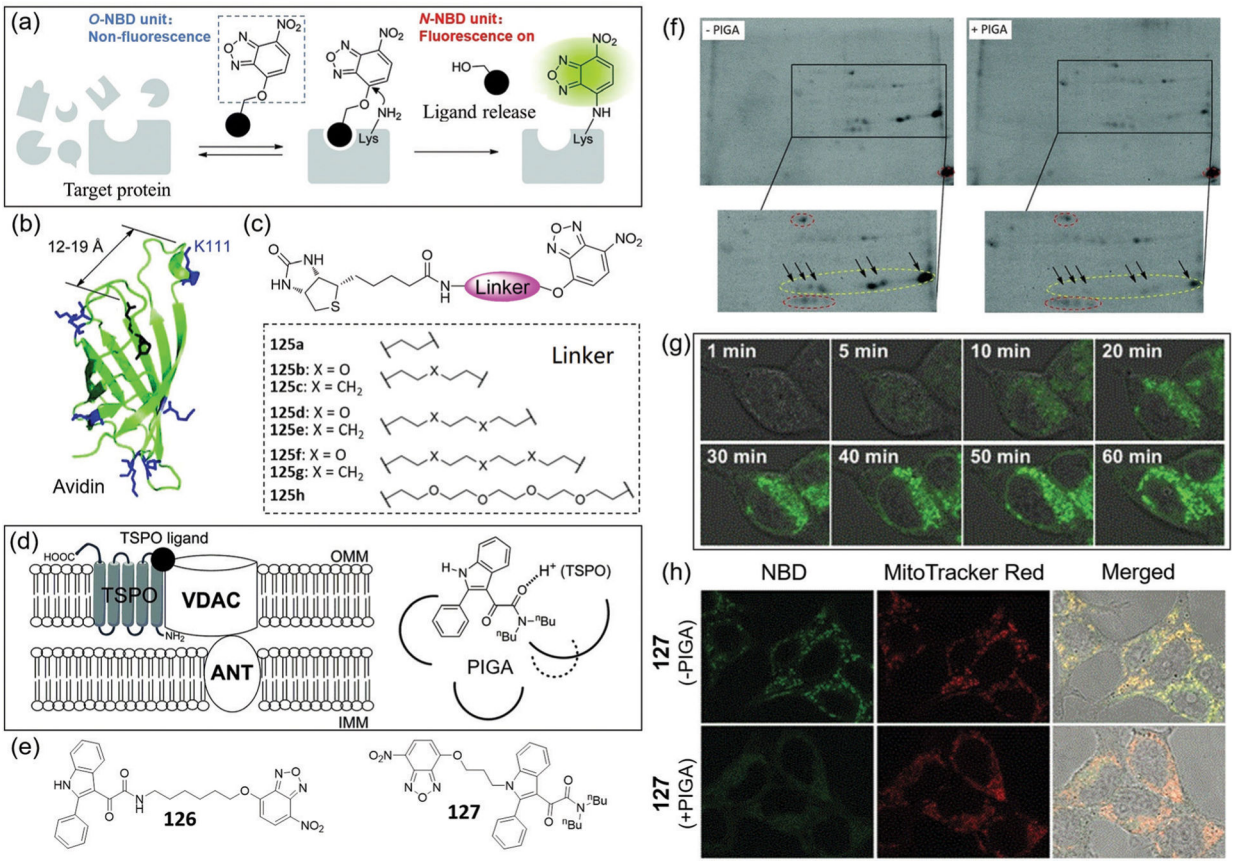

Fig. 33.

(a) Illustration of “turn-on” fluorescent labelling of a target protein by direct aminolysis of NBD-OR probes. (b) Structure model of the biotin–avidin complex. (c) Chemical structures of probes **125a–125h**. (d) A model of TSPO-multiprotein complex on the mitochondrial membrane, and the pharmacophore/topological model of ligand PIGA with TSPO. (e) Chemical structures of probes **126** and **127**. (f) 2D PAGE analysis of mouse kidney mitochondria labelled with **127** in the absence (left) or presence (right) of PIGA. The fluorescent spots circled in red show autofluorescent proteins. (g) Time-lapse fluorescence images of HEK293T cells after addition of **127**. (h) Fluorescence images of co-localization of **127** and Mito-Tracker Red in the absence and presence of PIGA. (a), (b), (d) and (f–h) are adapted with permission from ref. 27. Copyright 2014 Royal Society of Chemistry.

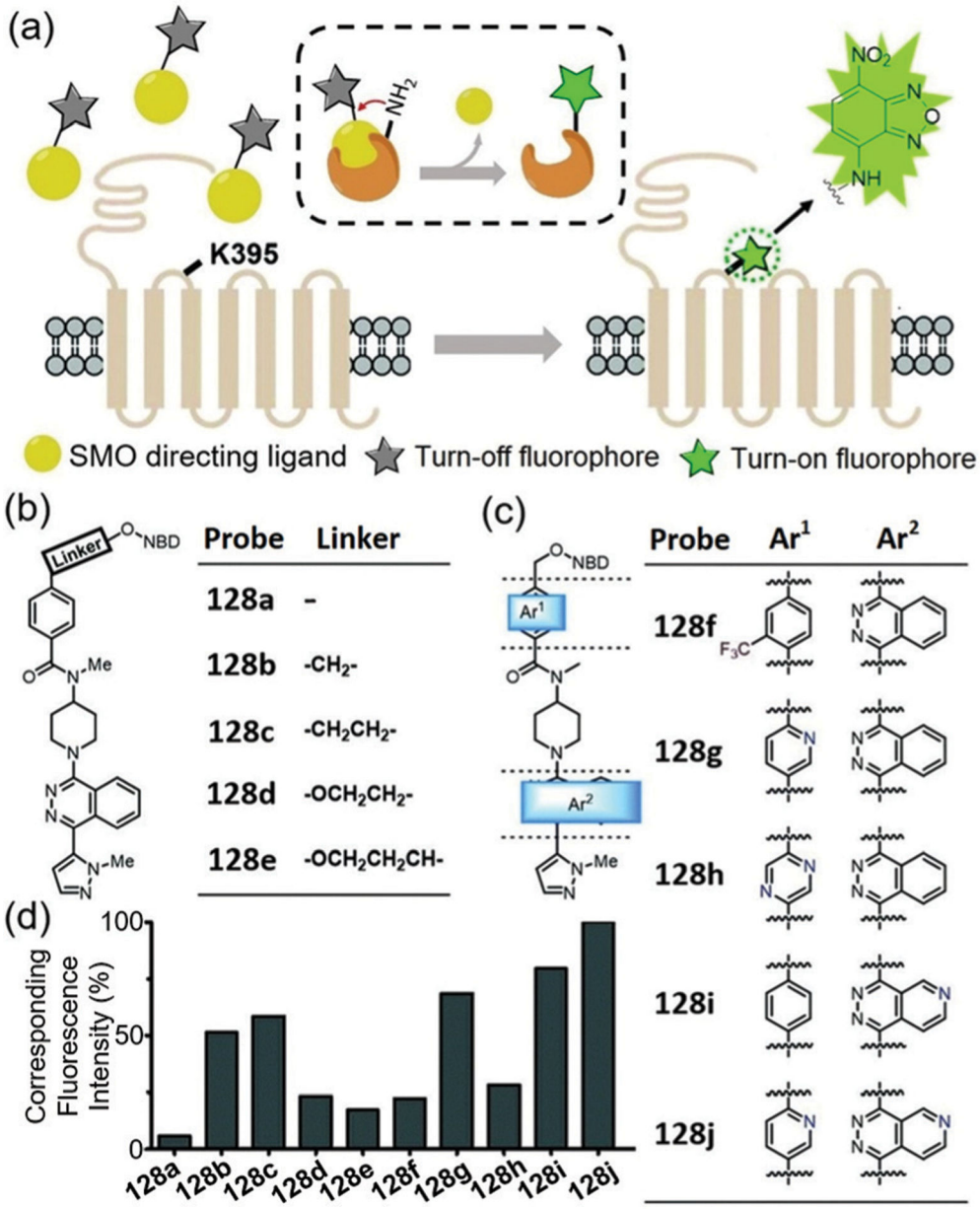

Fig. 34.

(a) Illustration of ligand-directed NBD modification on membrane. (b and c) Chemical structures of probes **128a–128e** with different linker lengths and probes **128f–128j** with different modifications in the ligand skeleton, respectively. (d) Normalized NBD fluorescence of PAGE bands of the SMO protein treated with probes **128a–128j**, respectively. Adapted with permission from ref. 221. Copyright 2019 Royal Society of Chemistry.

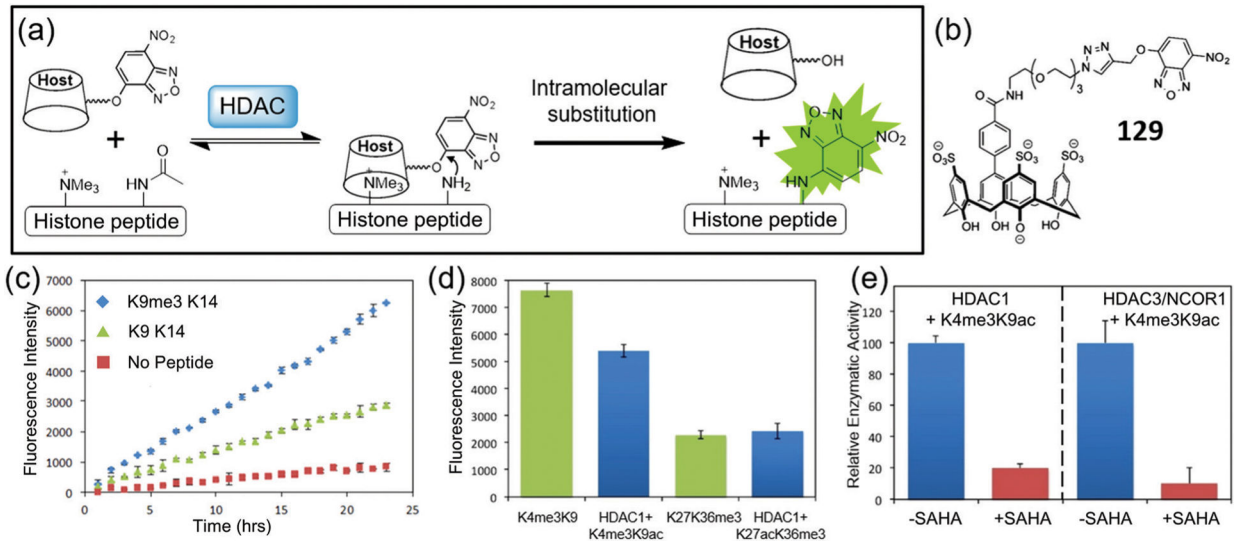

Fig. 35.

(a) General scheme for turn-on fluorescence affinity labelling of a histone Kme3 peptide using NBD-based probe after the cleavage of HDAC. (b) Chemical structure of **129**. (c) Turn-on fluorescence labelling of K9me3K14 and K9K14 peptides with **129**. (d and e) Fluorogenic assays of activity and inhibition, respectively. SAHA inhibitor vorinostat. Adapted with permission from ref. 222. Copyright 2016 American Chemical Society.

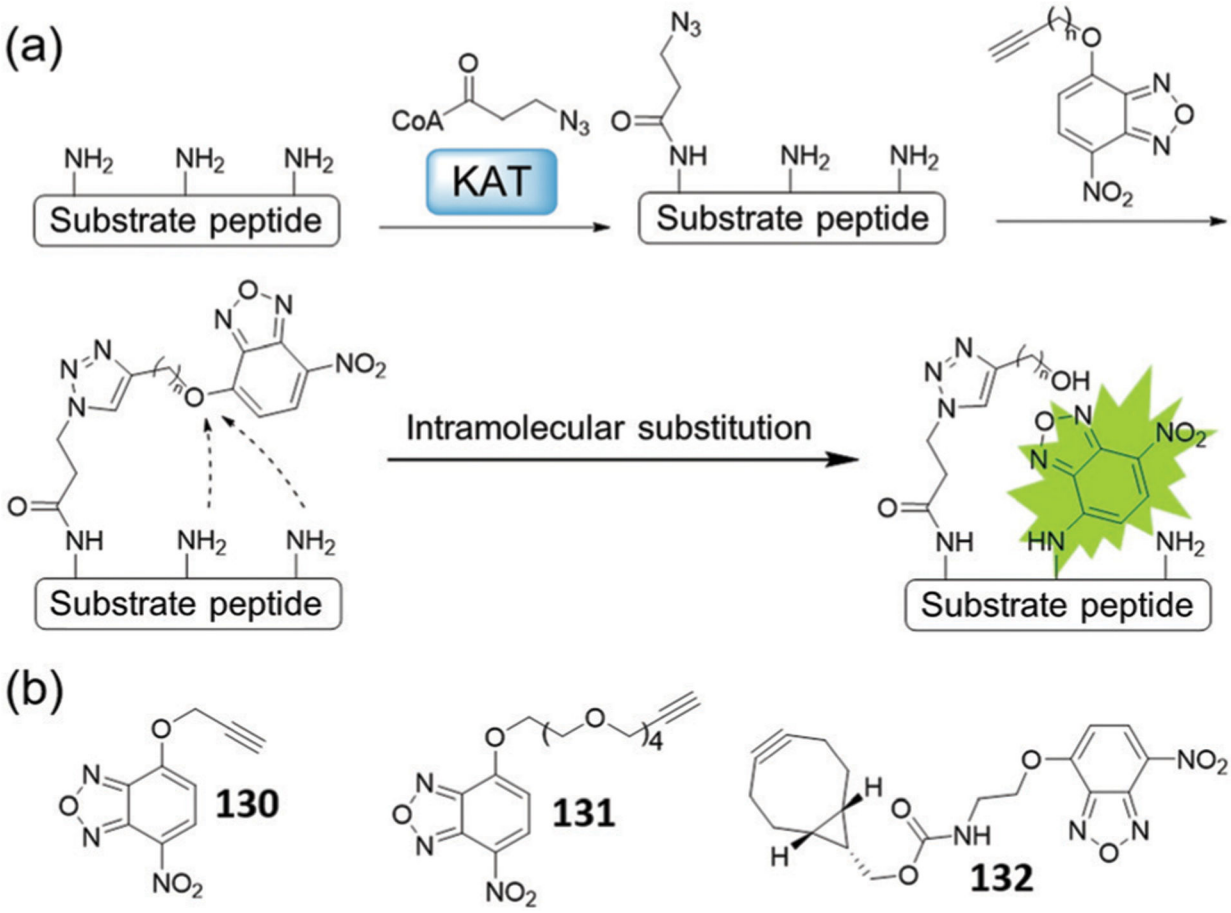

Fig. 36.

(a) Illustration of the bioorthogonal "turn-on" fluorescence strategy for KAT activity detection. (b) Chemical structures of **130–132**.

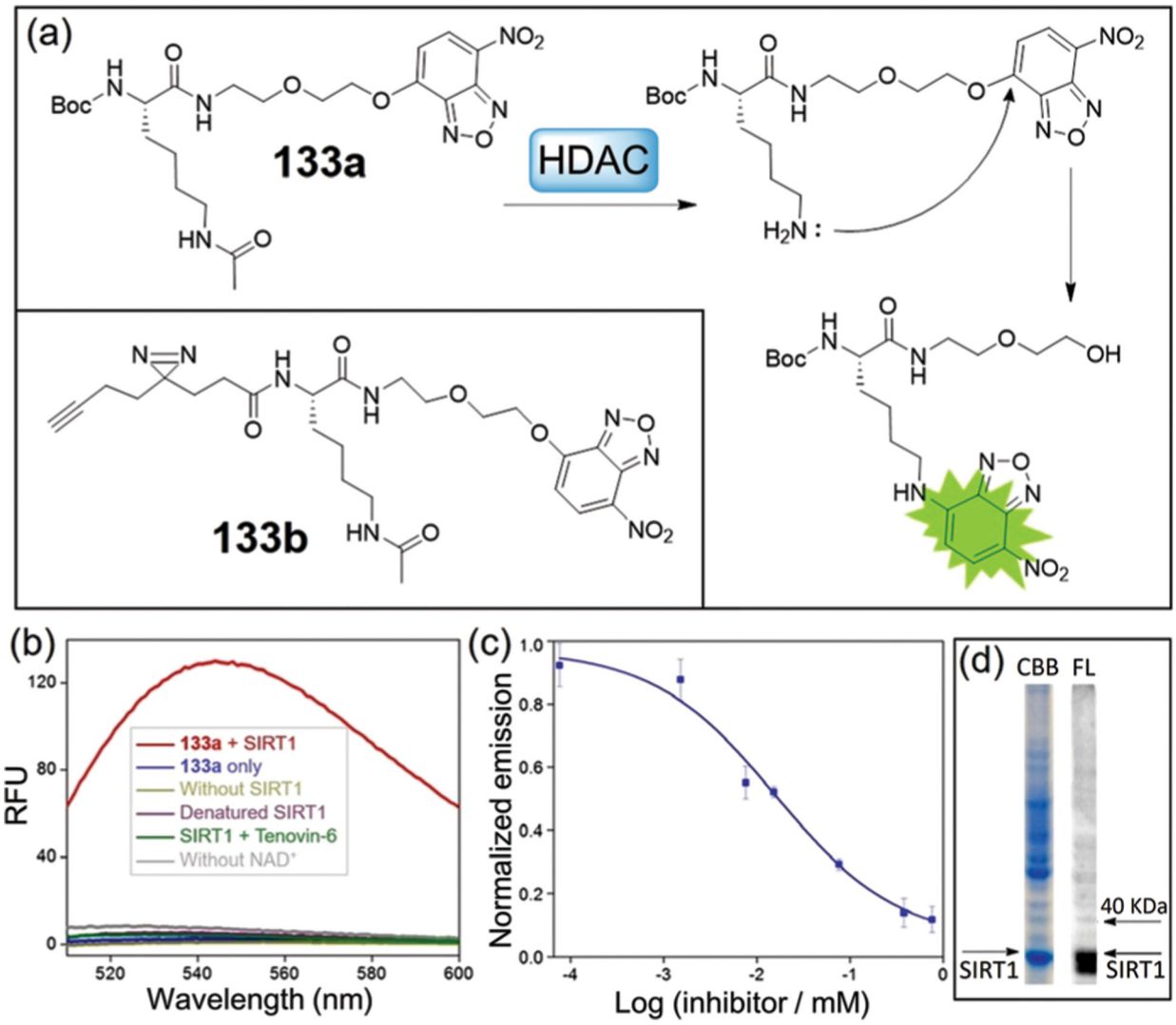

Fig. 37.

(a) Principle of strategy to detect HDAC by a fluorescent method and chemical structures of **133a–133b**. (b) Fluorescence spectra of **133a** with SIRT1 under various conditions (λ_{ex} = 480 nm). (c) Dose-response inhibition curve of SIRT2 by tenovin-6 using **133a**. (d) Labelling of SIRT1-spiked HeLa lysate by **133b**. (b)–(d) are adapted with permission from ref. 26. Copyright 2016 American Chemical Society.

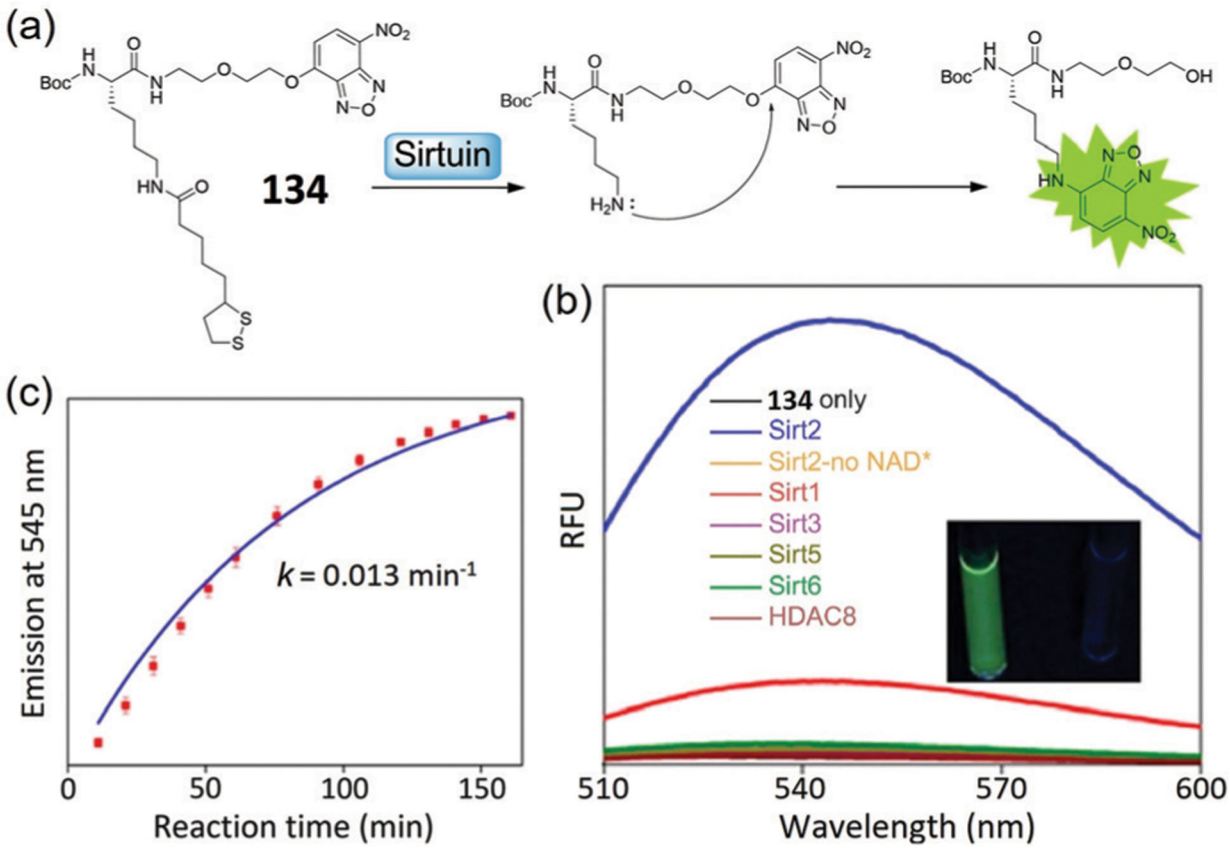

Fig. 38.

(a) Illustration of the fluorescence "turn-on" mechanism of probe **134** through a delipoylation reaction. (b) Fluorescence spectra of **134** with Sirtuins and HDAC8. The enzymatic reaction solution displayed green fluorescence color (inset). (c) Time-dependent emission of **134** with SIRT2. (b) and (c) are adapted with permission from ref. 240. Copyright 2019 American Chemical Society.

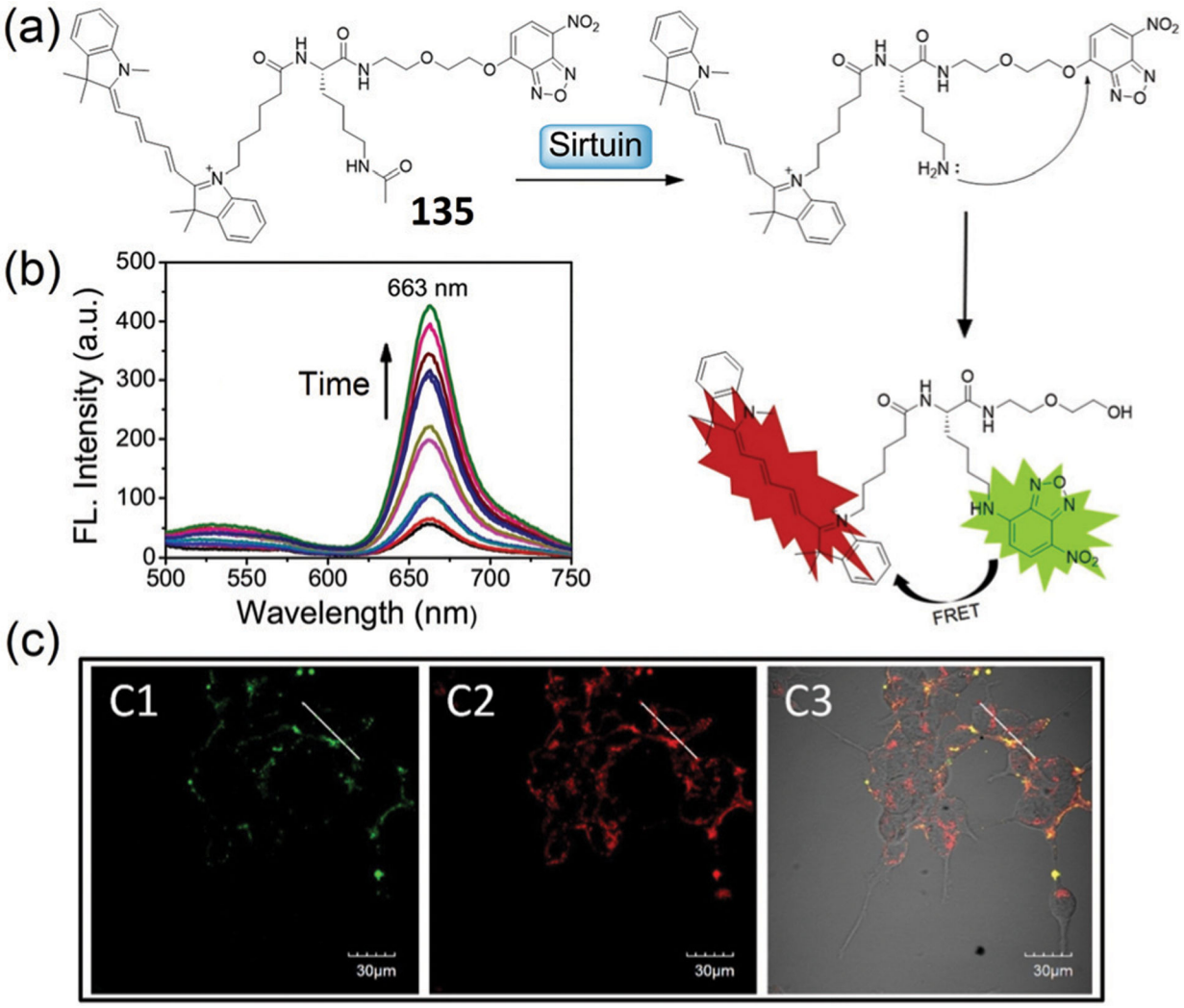

Fig. 39.

(a) Illustration of the detection mechanism of **135** towards Sirtuin. (b) Time-dependent fluorescence spectra of **135** in the presence of SIRT1. (c) Fluorescence images of cells pre-treated by serum starvation for 36 h, and then **135** for 2 h. C1: 520–560 nm, C2: 620–690 nm, C3: overlap. (b) and (c) are adapted with permission from ref. 241. Copyright 2019 Elsevier.

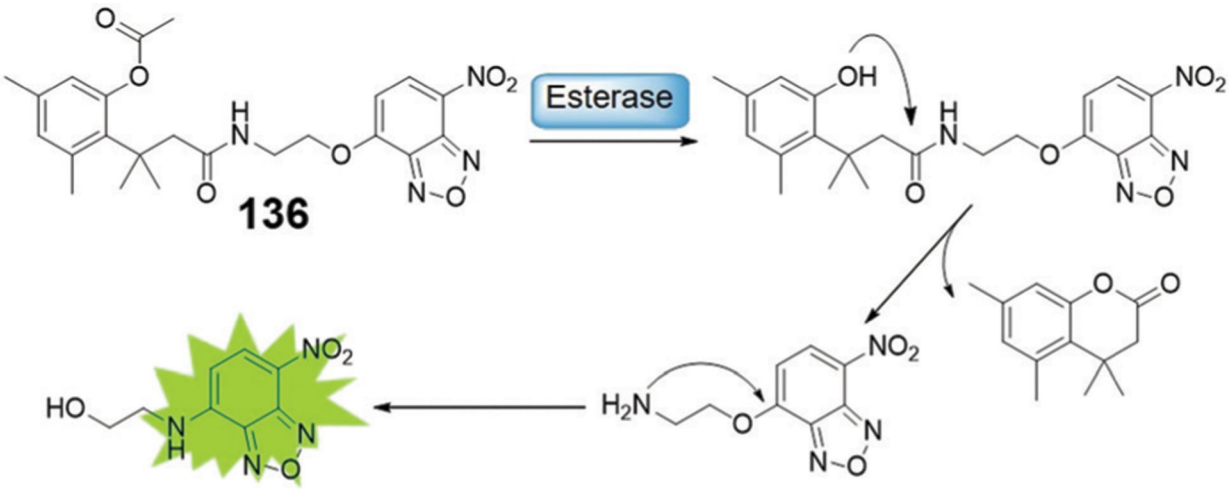

Fig. 40.
Illustration of an NBD-based fluorogenic probe **136** for the detection of esterase activity.

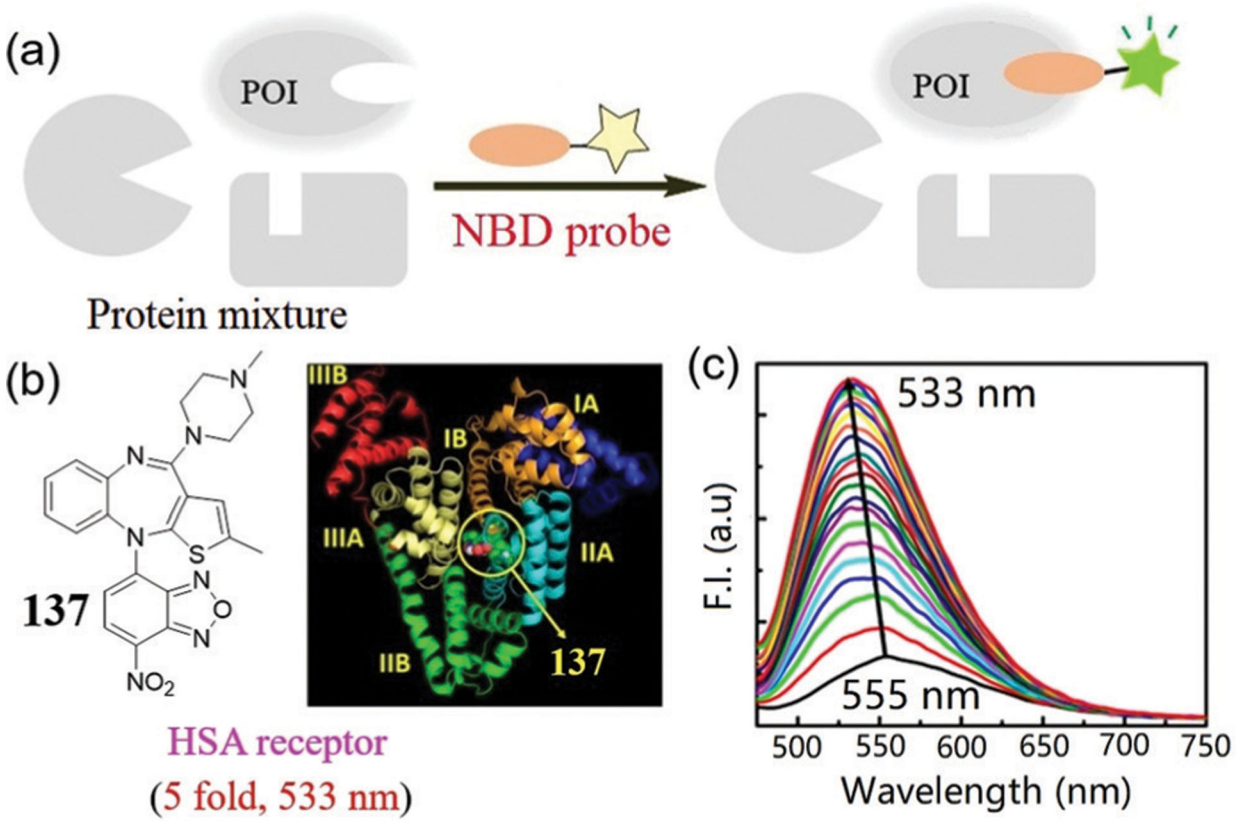

Fig. 41.

(a) The general design strategy of environment-sensitive NBD-*N*-ligand probe for selectively sensing POI. The probe exhibits weak yellow fluorescence, which turns to green fluorescence after protein binding. (b) Chemical structure of **137** (left) and stereo view of molecular docking posture of HSA protein (PDB ID: 1AO6) with **137** (right). (c) Emission spectra of probe **137** in the presence of increasing concentrations of HSA. (b) and (c) are adapted with permission from ref. 252. Copyright 2019 American Chemical Society.

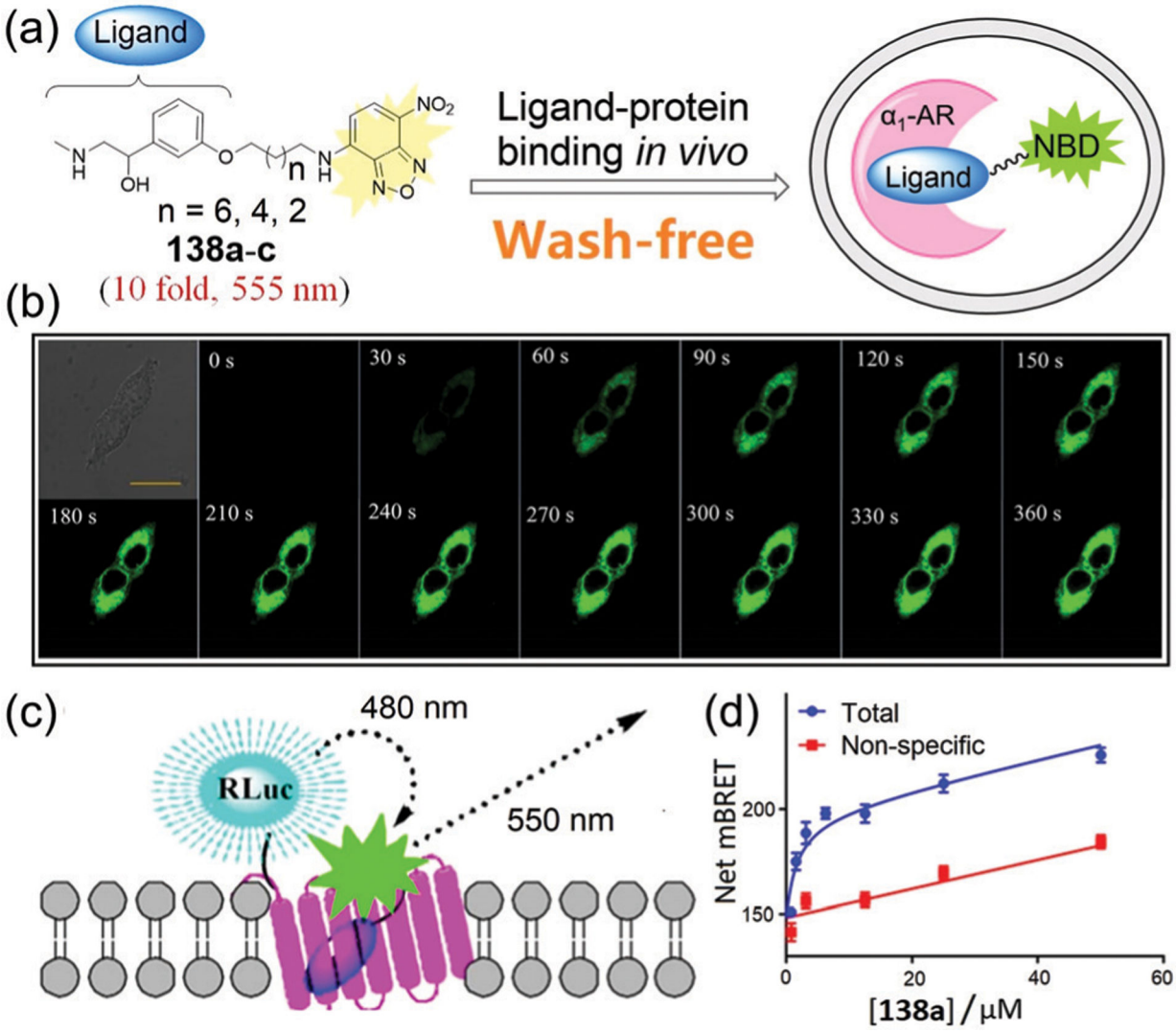

Fig. 42.

(a) The design strategy for wash-free imaging of ligand–protein binding and chemical structures of **138a–138c**. (b) Real-time fluorescence imaging of α_{1B}-AR transfected cells with **138a** without the washing step. (c) Illustration of the design principle of a BRET assay by using NBD probes and RLuc. (d) Representative saturation binding experiment tested with α_{1A}-AR and the BRET assay. (b)–(d) are adapted with permission from ref. 253. Copyright 2019 American Chemical Society.

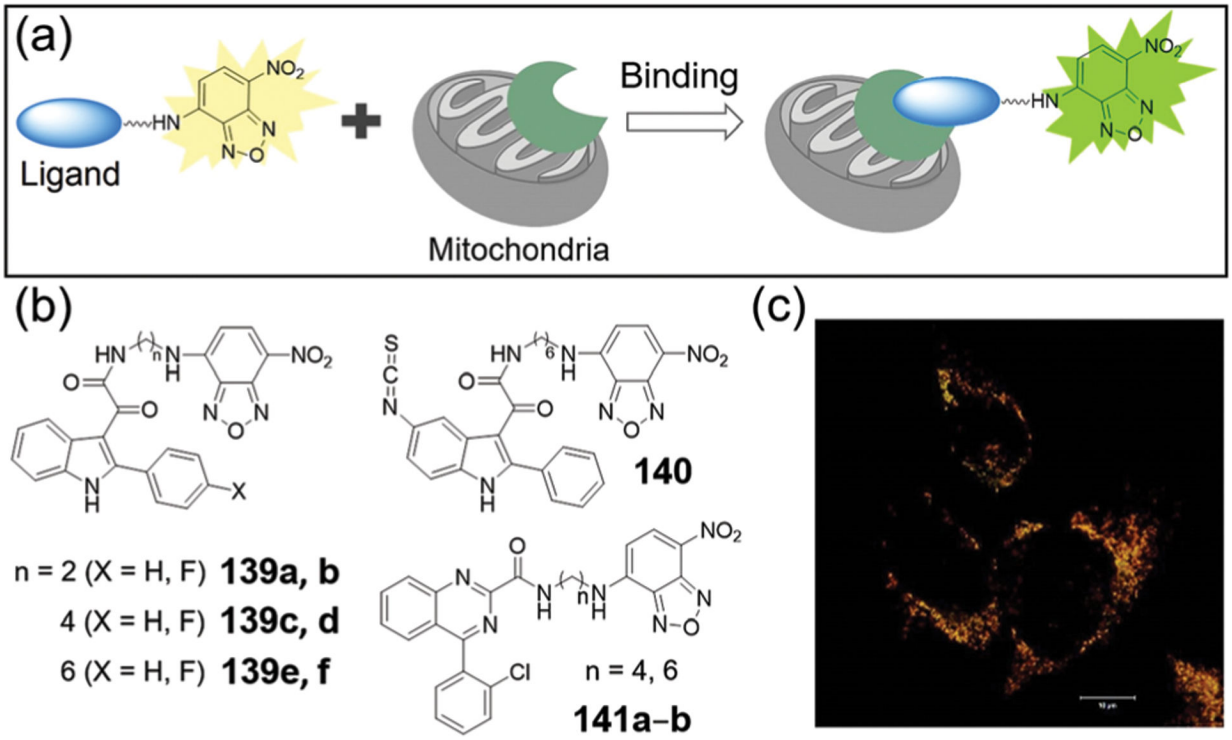

Fig. 43.

(a) Schematic illustration of NBD-ligand probes for labelling mitochondrial TSPO. (b) Chemical structures of **139a**–**141b**. (c) Probe **141a** specifically labelled the mitochondrial proteins inside cells. (c) is adapted with permission from ref. 256. Copyright 2017 American Chemical Society.

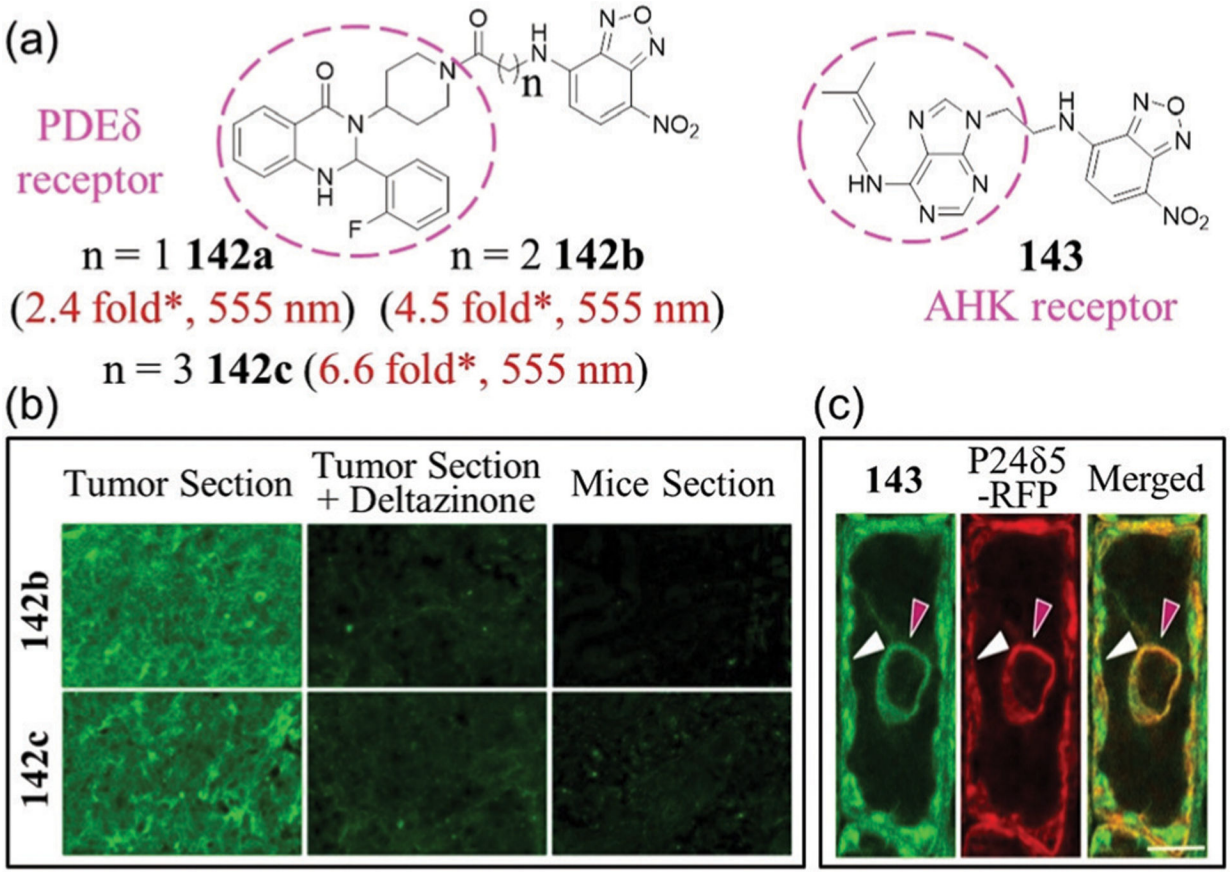

Fig. 44.

(a) Chemical structures of **142a–143**. * Represents estimated response from the reported spectra. (b) Tissue slice images using probes **142b** or **142c**. (c) Monitoring of **143** (green) and ER-marker p24δ5-RFP (red) in LRC cells. Probe **143** was found to partially co-localize with p24δ5-RFP in ER (red arrows) and non-ER cellular structures (white arrows). (b) and (c) are adapted with permission from ref. 257 and 260b. Copyright 2020 American Chemical Society, 2020 Nature Publishing Group, respectively.

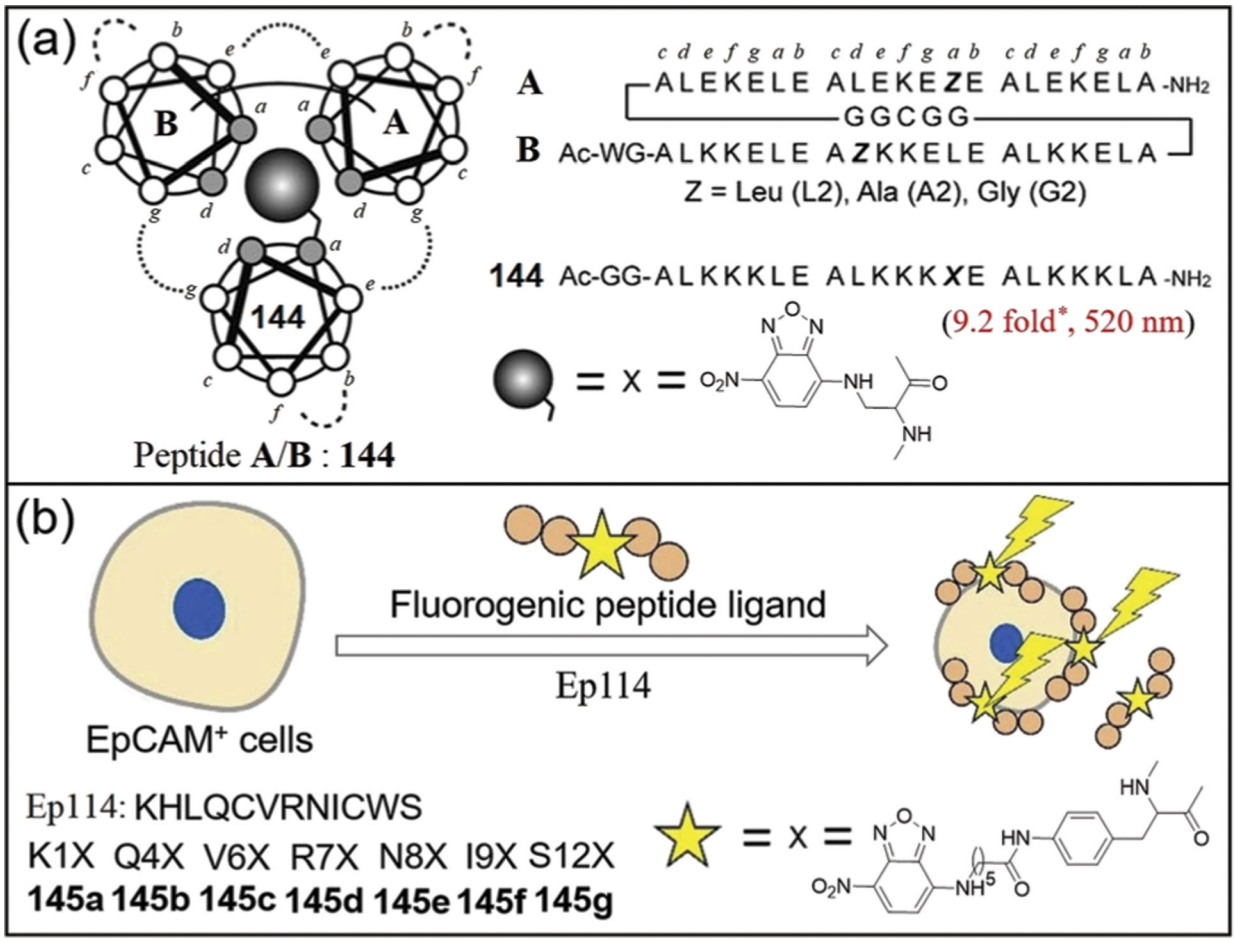

Fig. 45.

(a) Structures and peptide sequences of ZIP tag-probe pairs. * Represents estimated enhancement from the reported spectra. (b) Structure and peptide sequences of **145a–145g** and the strategy to detect EpCAM-positive cell. (a) and (b) are adapted with permission from ref. 261 and 264. Copyright 2009 Wiley-VCH, 2018 Elsevier, respectively.

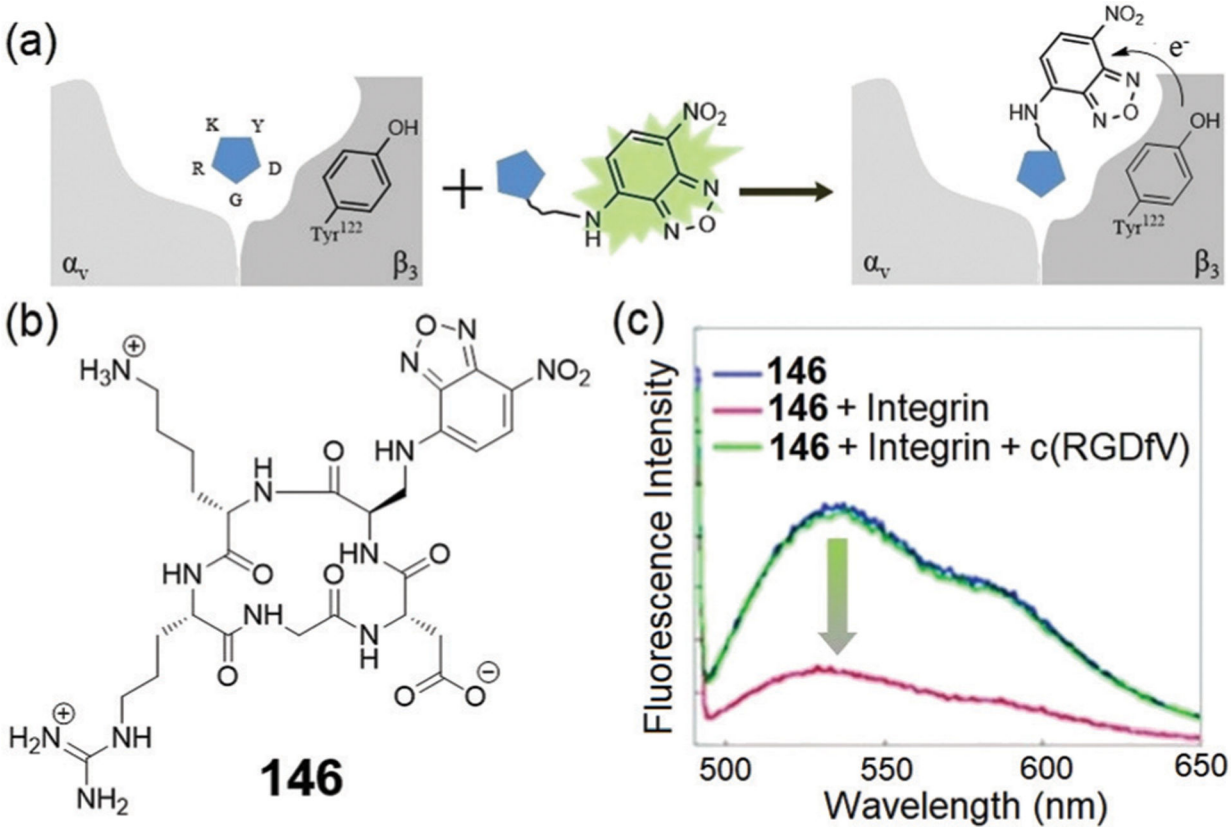

Fig. 46.

(a) The sensing mechanism for turn-off detection of protein–ligand interactions. (b) Chemical structure of **146** and (c) its fluorescence spectra change after addition of integrin $\alpha_v\beta_3$ with or without c(RGDfV). (a) and (c) are adapted with permission from ref. 265. Copyright 2014 Royal Society of Chemistry.

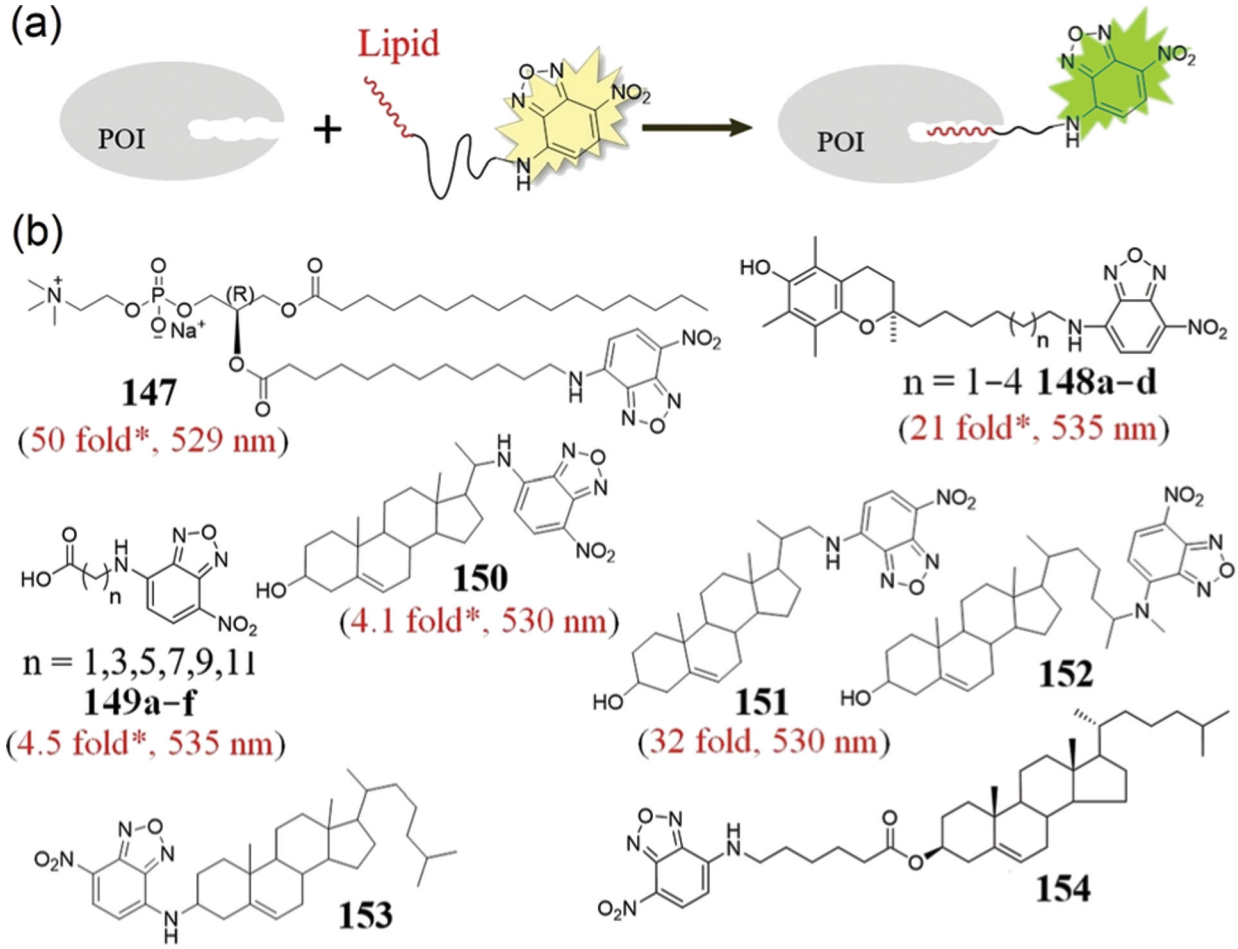

Fig. 47.

(a) General strategy of NBD-lipid probes for sensing POI. (b) Chemical structures of **147–154**. * Represents estimated enhancement from the reported spectra.

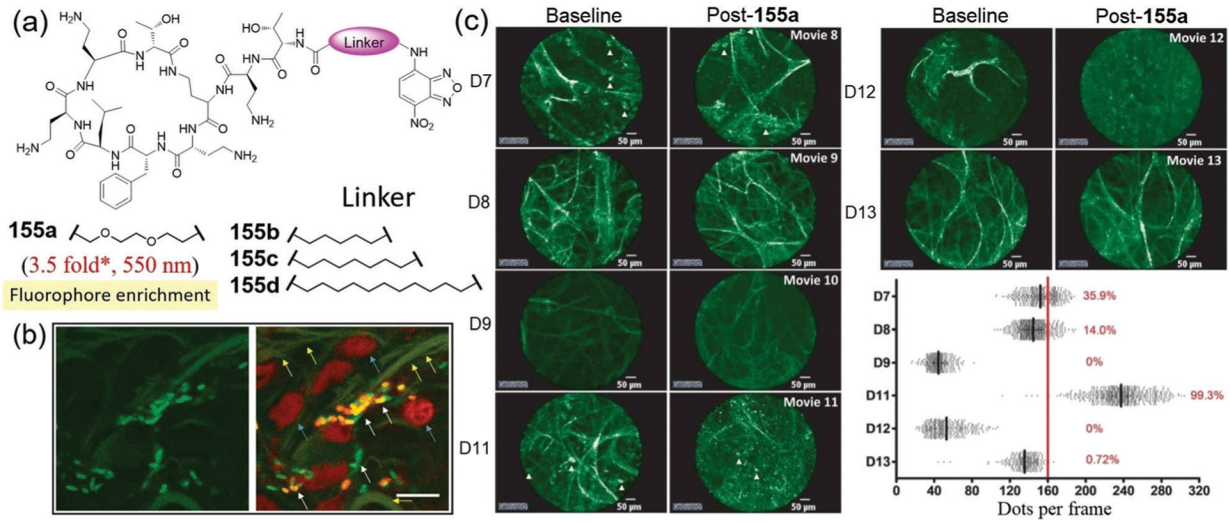

Fig. 48.

(a) Chemical structures of probes **155a–155d**. * Represents estimated response from the reported spectra. (b) Fluorescence image of human lung tissue cocultured with bacteria and treated with **155a**. Left: NBD and autofluorescence with excitation at 488 nm. Right: Merge with counterstain. White arrows indicate bacterial labelling, blue arrows demonstrate epithelial cells, and yellow arrows demonstrate elastin autofluorescence. (c) **155a** administration and imaging in six mechanically ventilated patients in intensive care unit (ICU) demonstrates a Gram-negative bacterial signal in two patients. Representative alveolar images of baseline imaging and after administration of **155a** in six patients with pulmonary infiltrates and suspected pneumonia. Cellular infiltrates are indicated by white arrowheads. Right-bottom graph demonstrates the frame-by-frame analysis of each video sequence after **155a** administration. (b) and (c) are adapted with permission from ref. 274. Copyright 2018 American Association for the Advancement of Science.

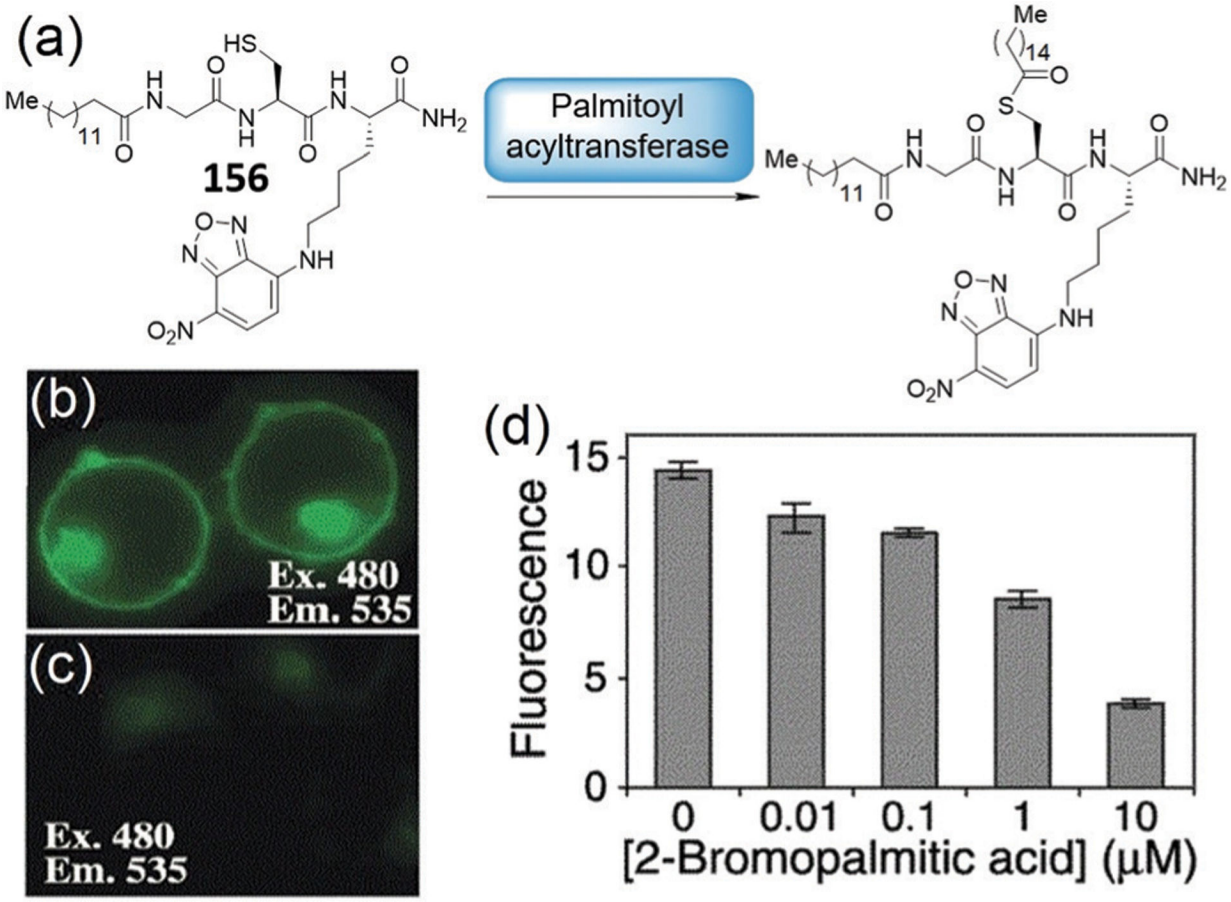

Fig. 49.

(a) Chemical structure of **156** and its palmitoylation. (b and c) Subcellular localization of **156** added to live cells treated without (b) or with (c) inhibitor 2-bromopalmitic acid. (d) Flow cytometry analysis of palmitoylation inhibition using **156**. (b)–(d) are adapted with permission from ref. 276. Copyright 2002 American Chemical Society.

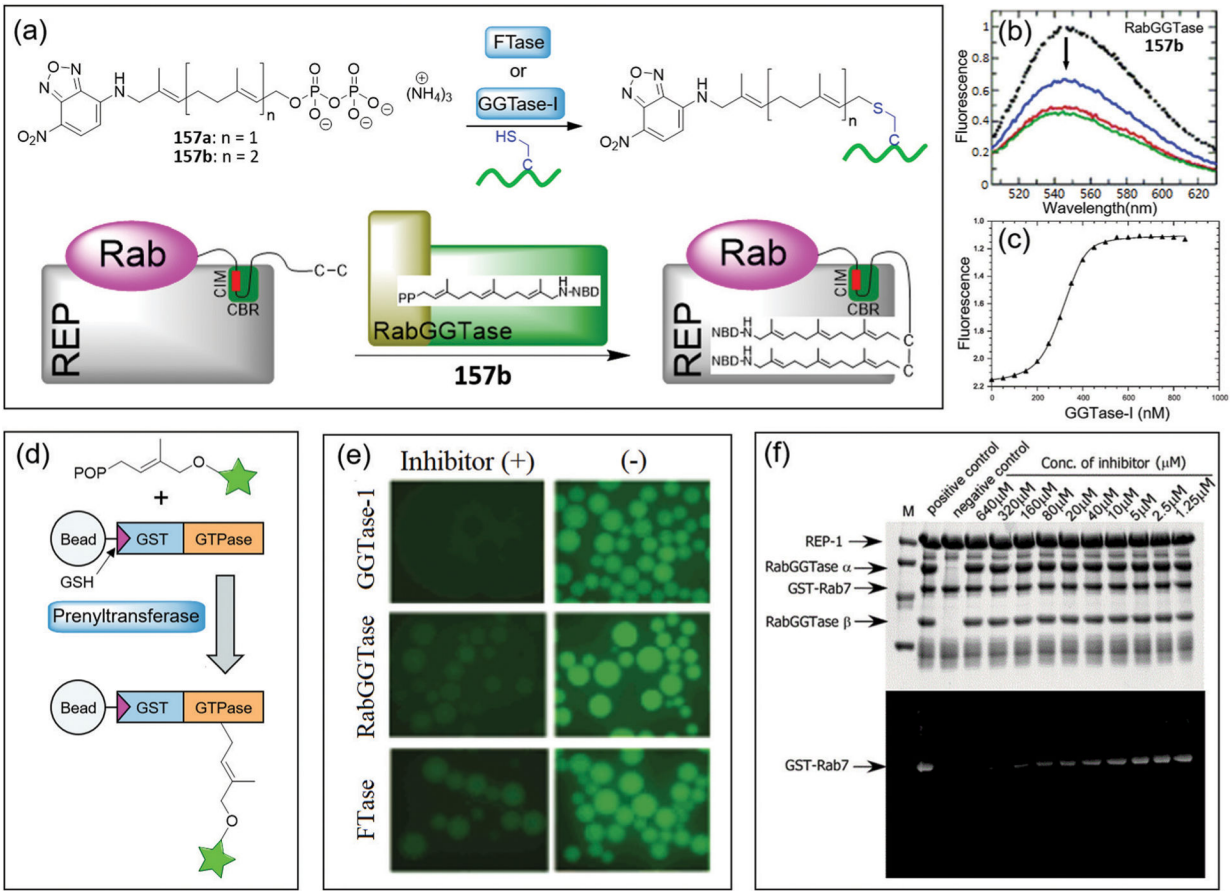

Fig. 50.

(a) Illustration of the prenylation reactions based on probes **157a–157b**. (b) Emission spectra of **157b** in the absence (black filled circles) and presence of RabGGTase (color lines). (c) Competitive titration of the **157b** and GGPP mixture with increasing concentrations of GGTase-I. (d) Principle of the on-bead microscopic assay for identification of prenyltransferse inhibitors. (e) Fluorescence of GST-GTPase loaded beads after prenylation with probes **157a–157b** in the presence or absence of putative inhibitors. (f) SDS-PAGE for the prenylation reactions containing various concentrations of inhibitor, or without RabGGTase as a negative control. The top and bottom panels for the gel after Coomassie blue staining and the fluorescent scan gel, respectively. (b)–(f) are adapted with permission from ref. 279. Copyright 2006 American Chemical Society.

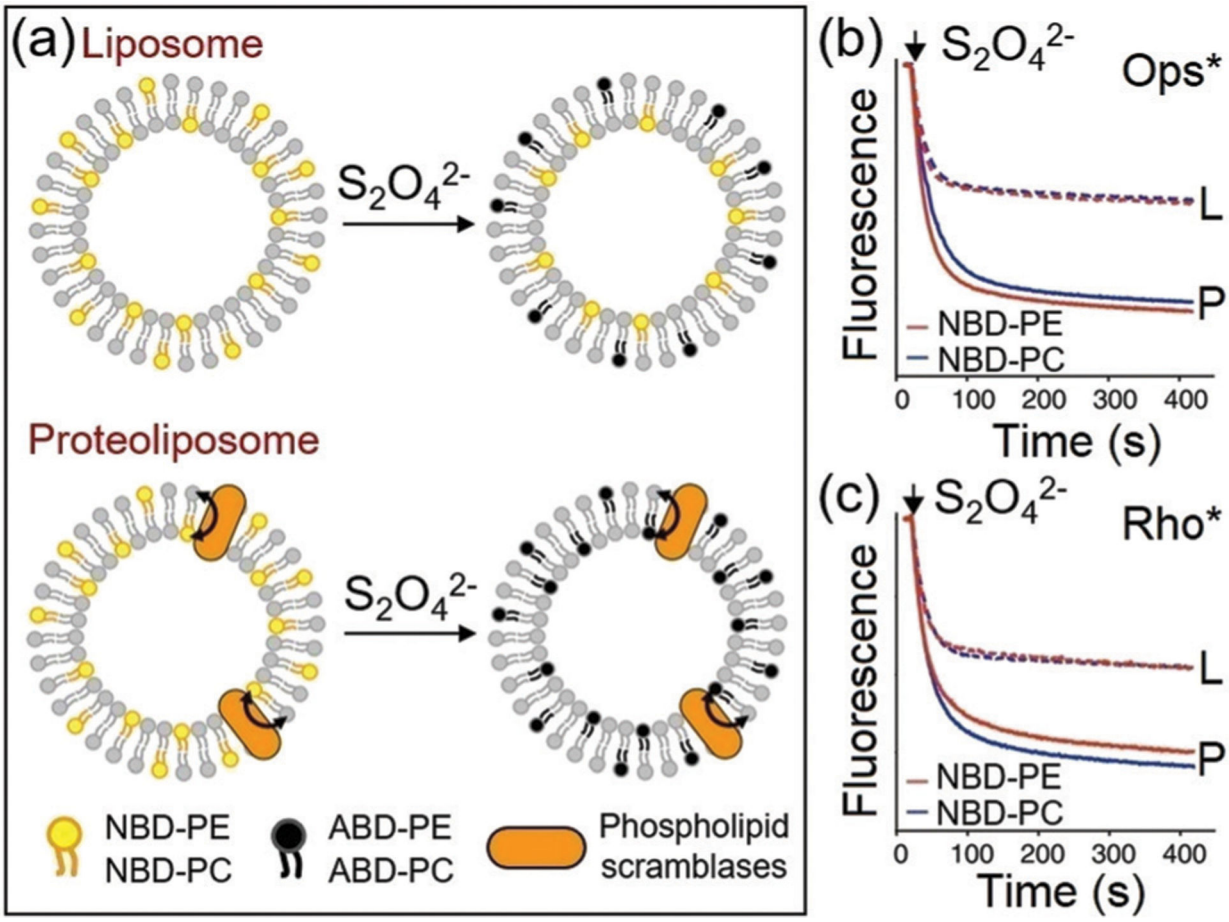

Fig. 51.

(a) Illustration of the strategy for the scramblase activity assay. (b and c) Scramblase activity of active opsin (Ops*) or metarhodopsin II (Rho*), respectively. Fluorescence traces corresponding to dithionite treatment of NBD-PE (red) and NBD-PC (blue) containing liposomes (L; dashed lines) and proteoliposomes (P; solid lines). (a)–(c) are adapted with permission from ref. 282. Copyright 2014 Nature Publishing Group.

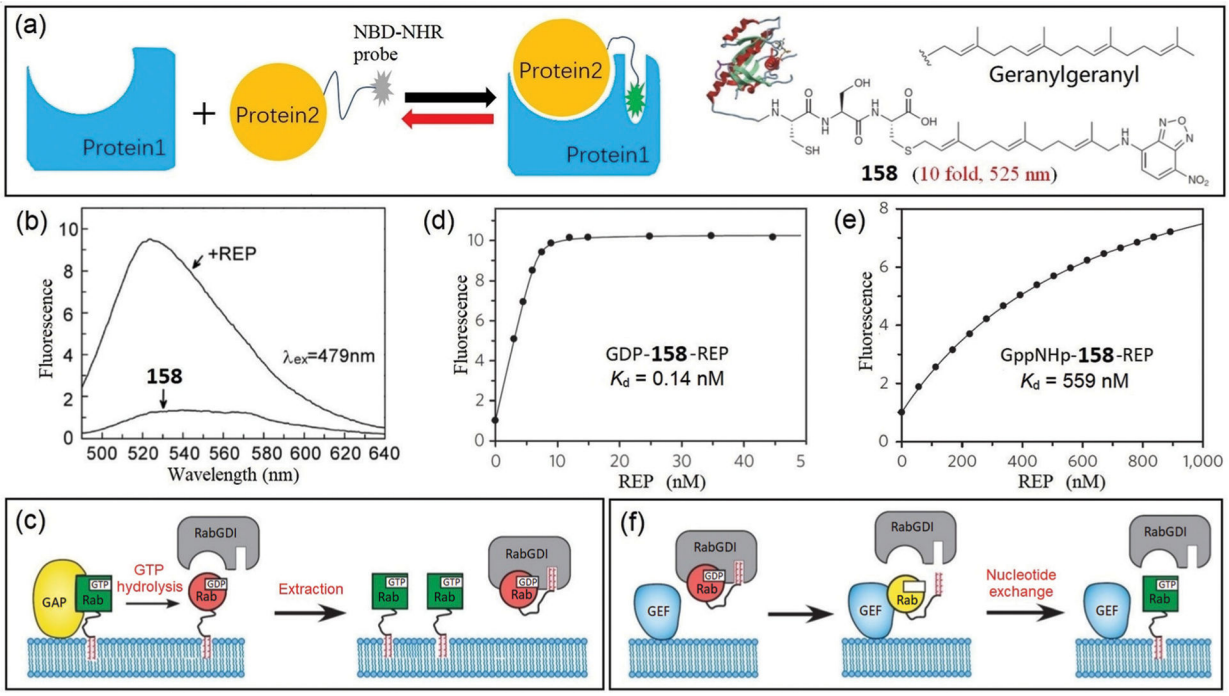

Fig. 52.

(a) Illustration of sensing PPIs *via* NBD-based probe protein **158**. (b) Emission spectra of **158** before and after addition of REP. (c) A model for the extraction of Rab from membranes. (d and e) Titration of REP to GDP-**158** or GppNHp-**158**, respectively. (f) A model for targeting of Rab to membranes. (b)–(f) are adapted with permission from ref. 294 and 295. Copyright 2007 The National Academy of Sciences of the USA, 2010 Nature Publishing Group, respectively.

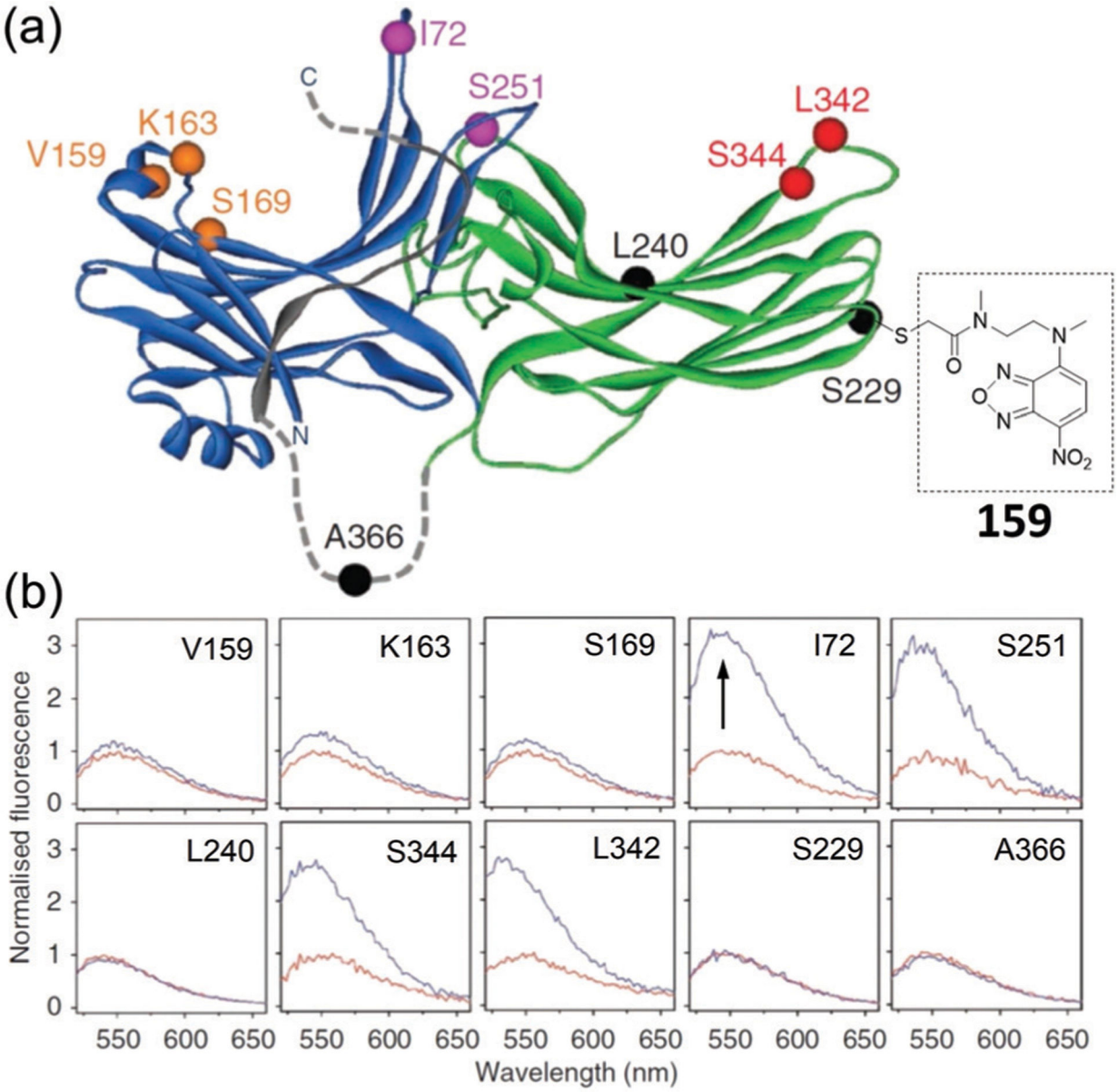

Fig. 53.

(a) Location of single Cys substitutions and chemical structure of the attached NBD fluorophore on a model of arrestin. (b) For each panel, NBD-labelled arrestin was mixed with a four-fold excess of dark-state rhodopsin. Adapted with permission from ref. 296b. Copyright 2012 Nature Publishing Group.

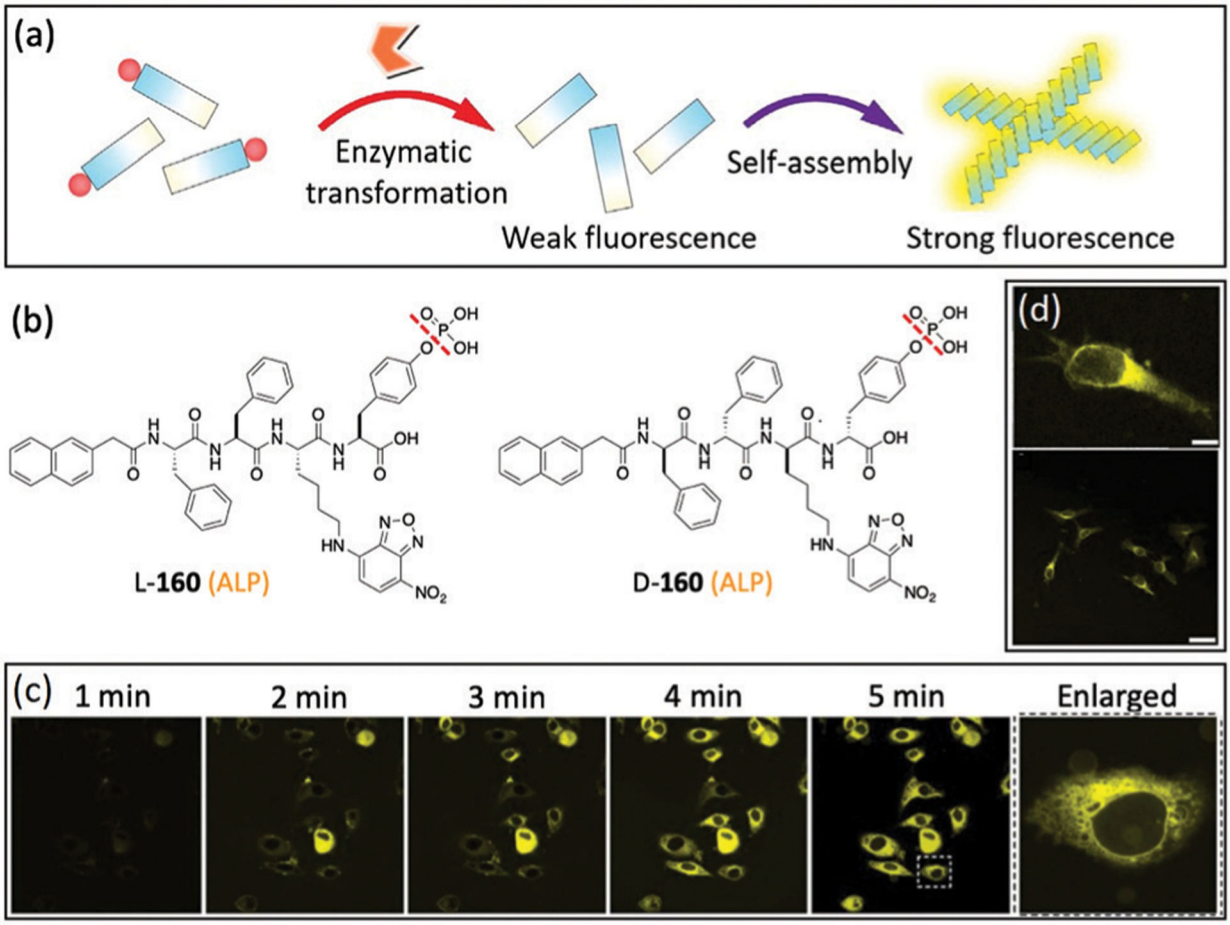

Fig. 54.

(a) Illustration of EISA for generating fluorescent nanofibrils from weakly-fluorescent precursors. (b) Chemical structures of L-**160** and D-**160**. (c) Time-dependent fluorescence images for EISA of L-**160** inside live cells. (d) Fluorescent image of HeLa cells incubated with D-**160** for 2 min. (a), (c) and (d) are adapted with permission from ref. 13 and 312. Copyright 2012 Nature Publishing Group, 2013 American Chemical Society, respectively.

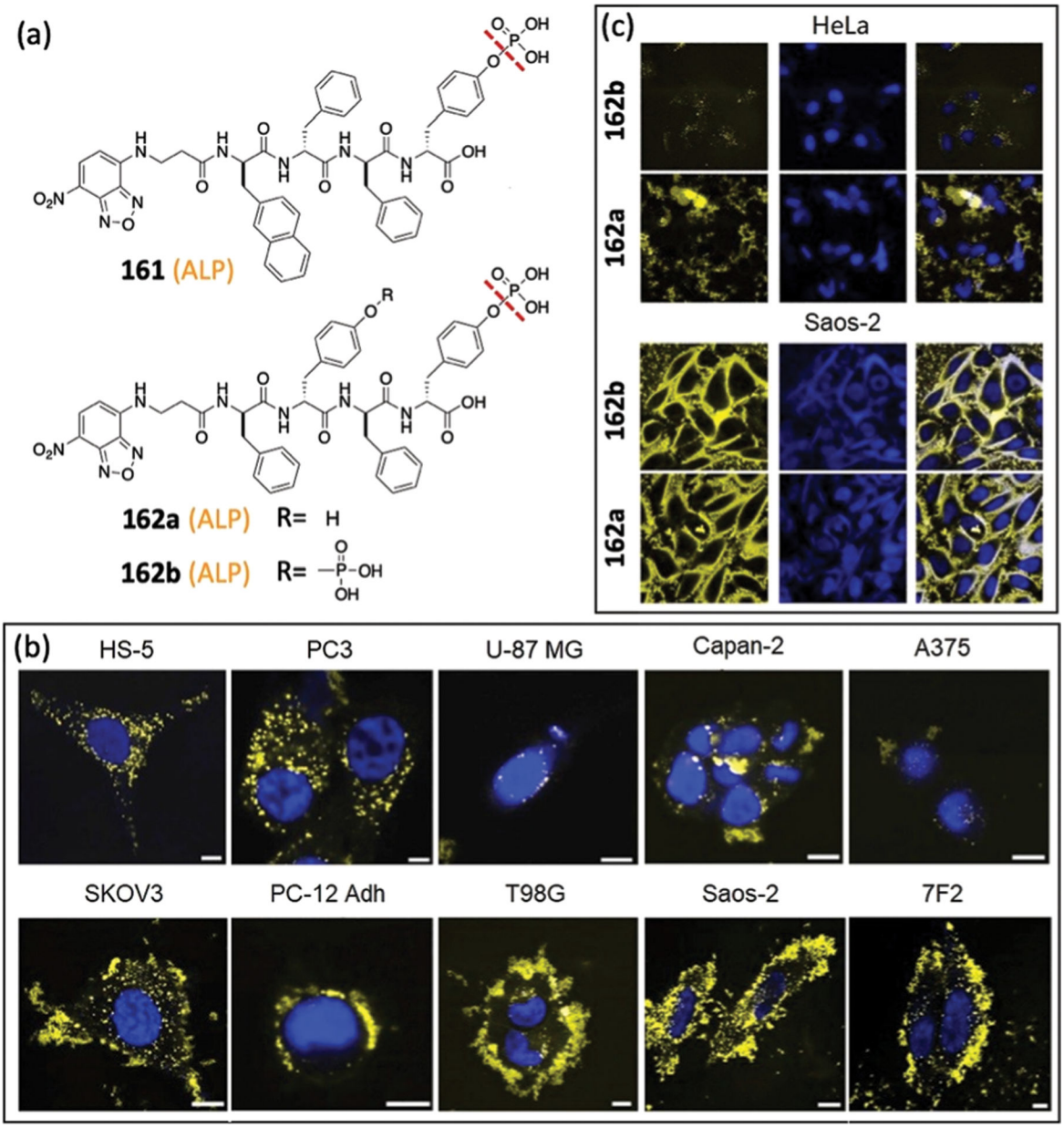

Fig. 55.

(a) Chemical structures of **161** and **162**. Fluorescence images of different cell lines incubated with (b) **161** and (c) **162**. Nuclei are stained by Hoechst 33342. (b) and (c) are adapted with permission from ref. 313 and 314. Copyright 2016 Elsevier, 2016 American Chemical Society, respectively.

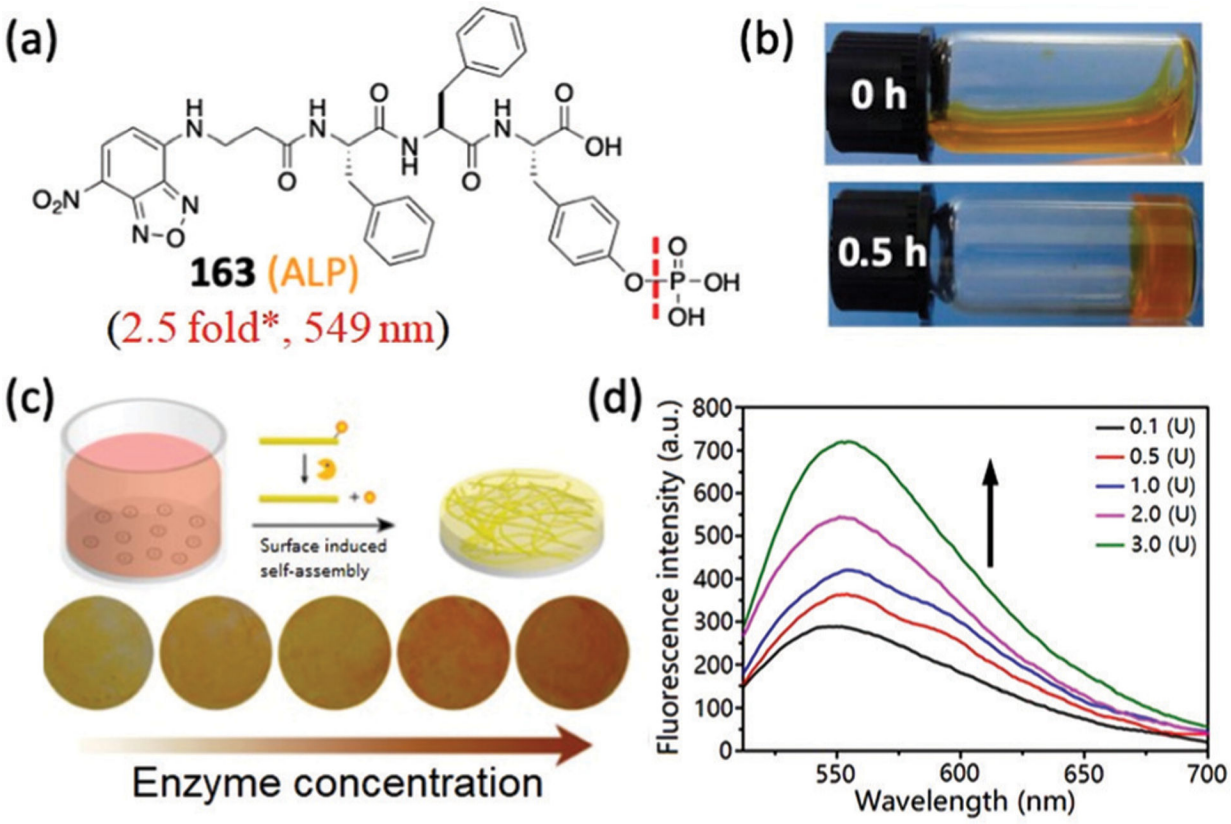

Fig. 56.

(a) Chemical structure of **163**. * Represents estimated response from the reported spectra. (b) Optical images of PBS solution of **163** by adding ALP for 0 h and 0.5 h. (c) Optical images of glass plates for samples after enzyme treatment. (d) Emission spectra of glass plates incubated with **163** and blood with different concentrations of ALP. (b)–(d) are adapted with permission from ref. 315. Copyright 2016 American Chemical Society.

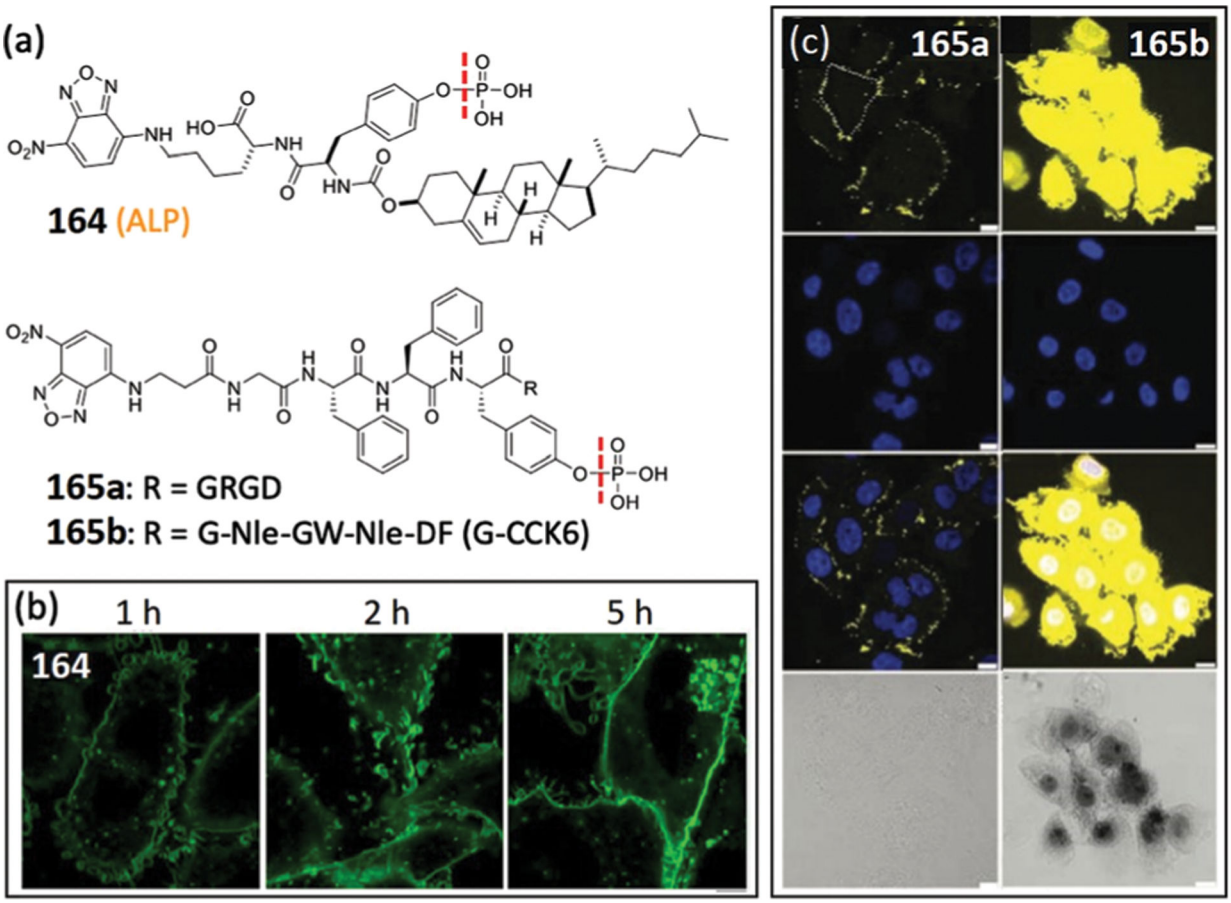

Fig. 57.

(a) Chemical structures of membrane-targeting probes **164–165b**. Confocal images of (b) Saos-2 cells treated with **164** and (c) HeLa cells treated with **165a** and **165b**. Nuclei are stained by DAPI. (b) and (c) are adapted with permission from ref. 318 and 319. Copyright 2018 American Chemical Society, 2019 Royal Society of Chemistry, respectively.

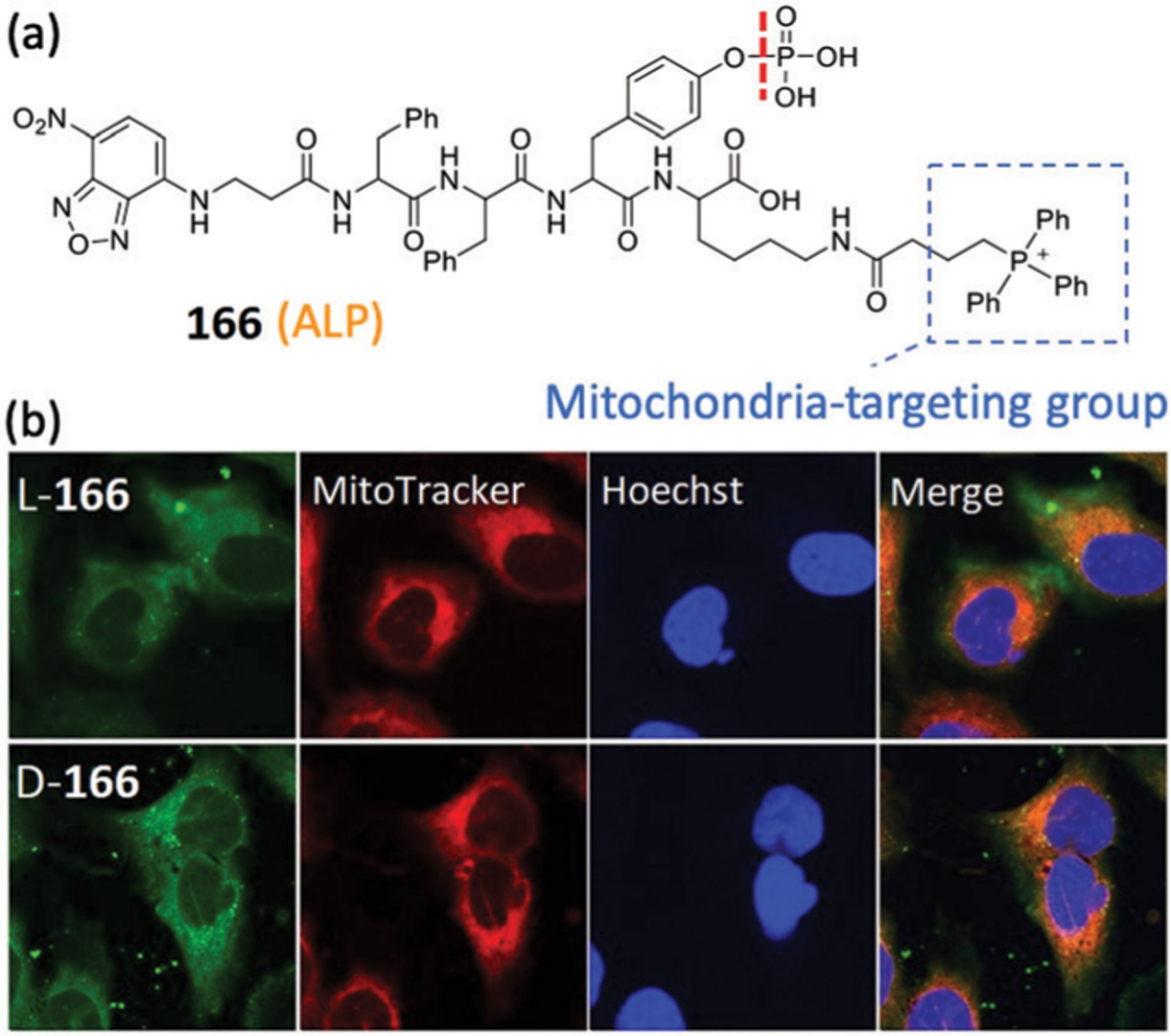

Fig. 58.

(a) Chemical structure of mitochondria-targeting probe **166**. (b) Confocal images of Saos-2 cells incubated with L-**166** and D-**166** and then stained with Mito-tracker. (b) is adapted with permission from ref. 320. Copyright 2016 American Chemical Society.

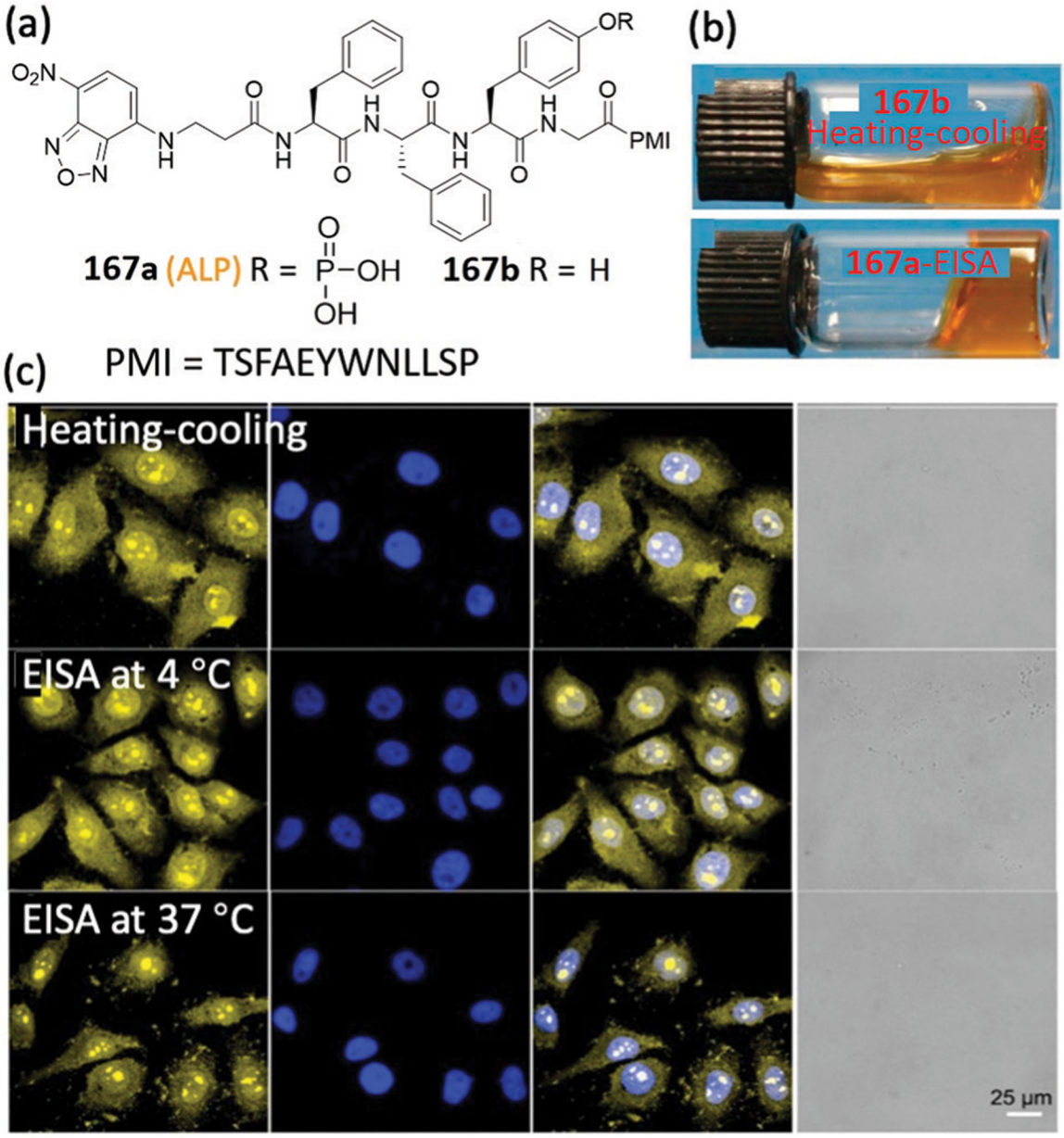

Fig. 59.

(a) Chemical structures of nuclear-targeting probes **167a–167b**. (b) Optical images of **167b** formed by the process of heating–cooling (top) and **167a** triggered by ALP (bottom). (c) Confocal images of HepG2 cells incubated with the different assemblies **167b** (top) and **167a** (middle and bottom). (b) and (c) are adapted with permission from ref. 324. Copyright 2020 Elsevier.

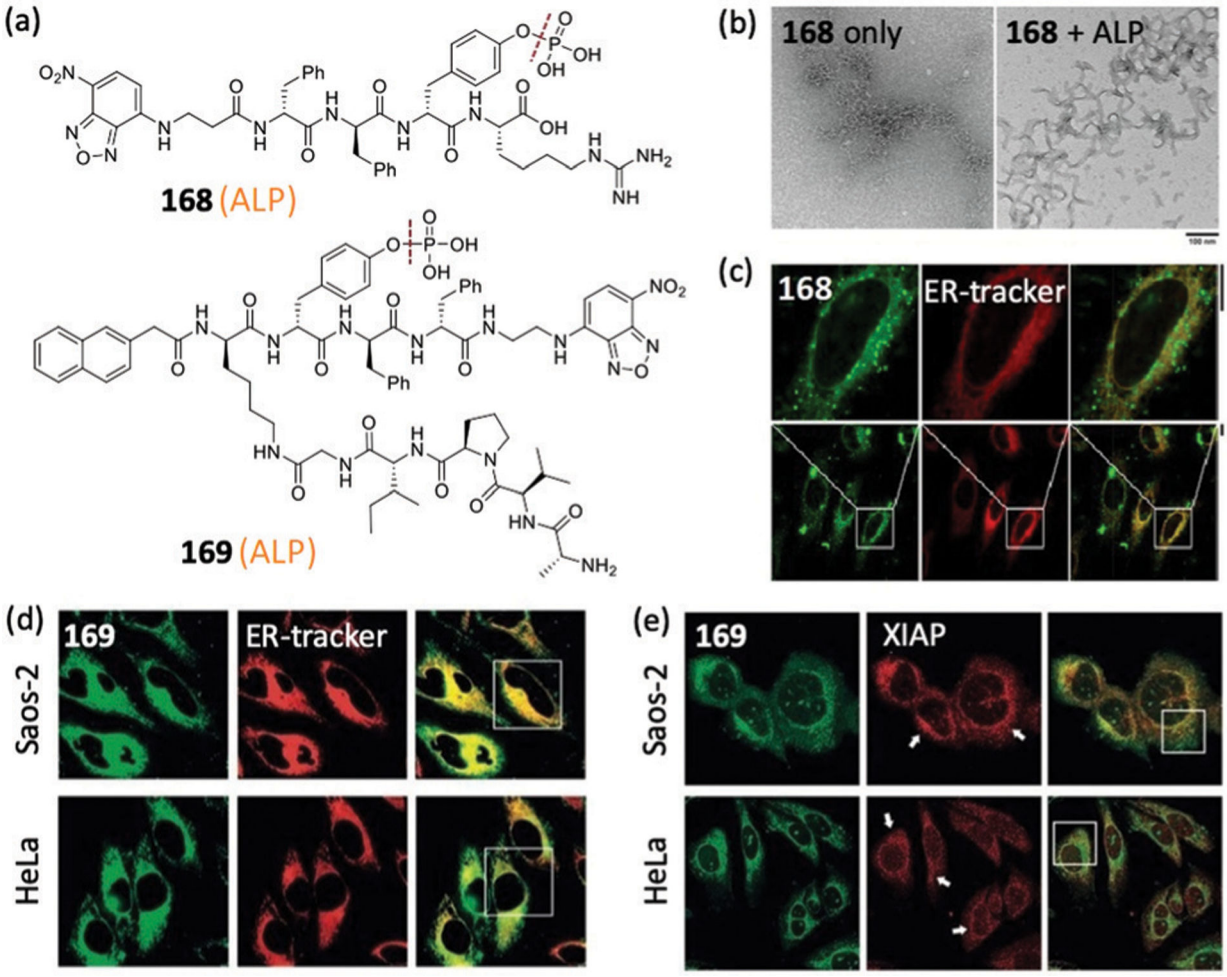

Fig. 60.

(a) Chemical structures of ER-targeting probes **168** and **169**. (b) TEM images of **168** before and after treating with ALP. (c) Confocal images of HeLa cells incubated with **168** and ER tracker. (d) Fluorescent images of HeLa and Saos-2 cells treated with **169** and ER tracker. (e) Immunofluorescence staining of XIAP in HeLa and Saos-2 cells treated with **169**. (b)–(e) are adapted with permission from ref. 326 and 327. Copyright 2018 American Chemical Society, 2020 Wiley-VCH, respectively.

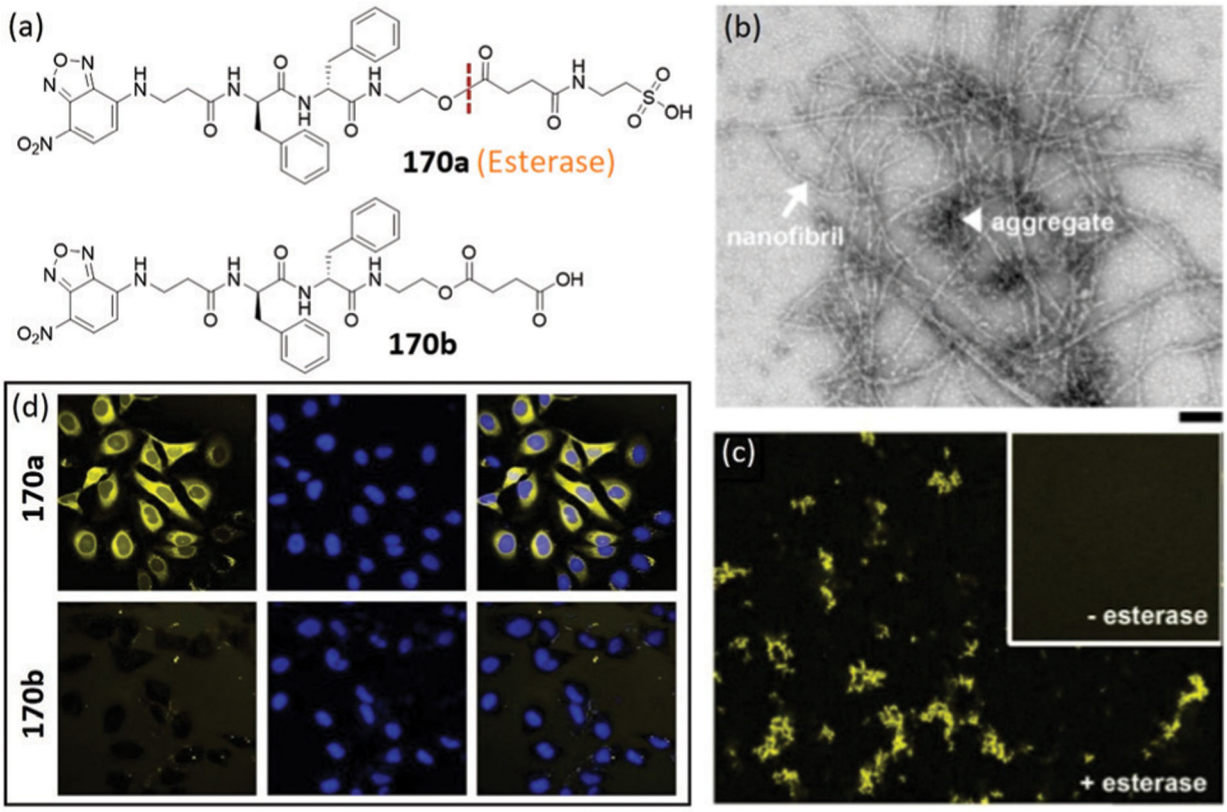

Fig. 61.

(a) Chemical structures of **170a-b**. (b) TEM image of **170a** after addition of esterase. (c) Fluorescent images of **170a** with or without esterase treatment. (d) Fluorescent images of HeLa cells treated with **170a** or **170b**. Nuclei are stained by Hoechst 33342. (b)–(d) are adapted with permission from ref. 329. Copyright 2015 American Chemical Society.

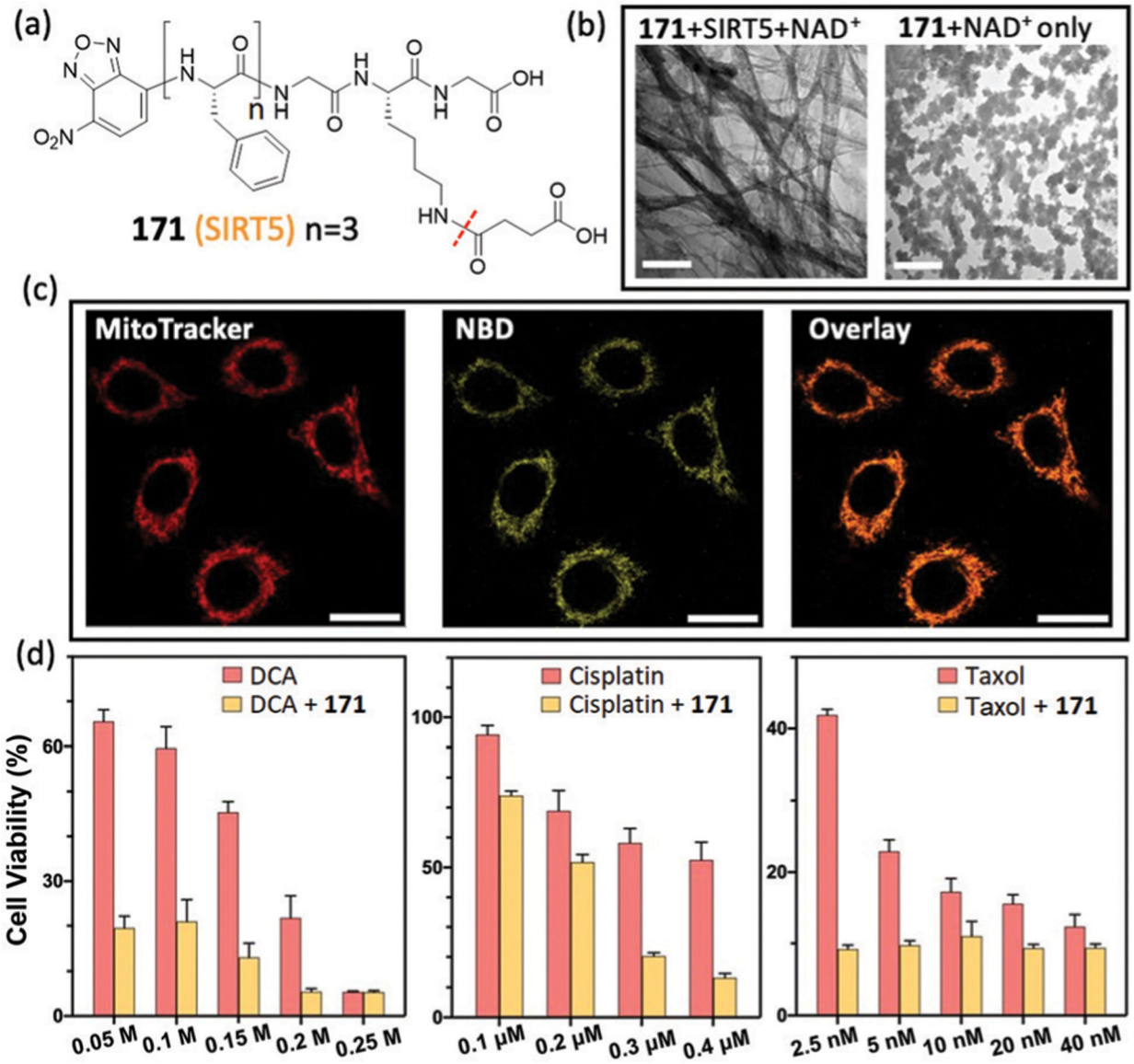

Fig. 62.

(a) Chemical structure of probe **171**. (b) TEM images of **171** incubated with or without SIRT5. (c) Fluorescence images of HeLa cells incubated with **171** and MitoTracker Red. (d) Cell viability assay of HeLa cells incubated with dichloroacetate (DCA), cisplatin and taxol with or without **171** analogue for 72 h. (b)–(d) are adapted with permission from ref. 330. Copyright 2020 American Chemical Society.

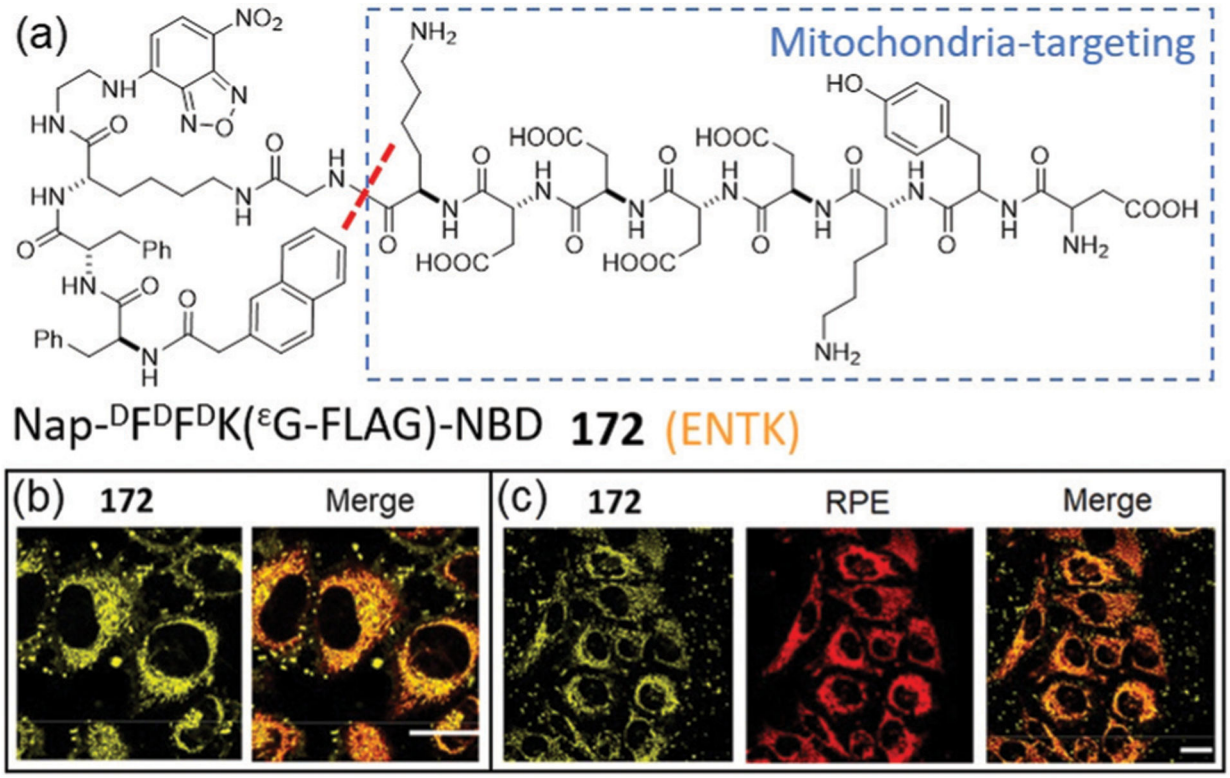

Fig. 63.

(a) Chemical structure of **172**. (b) Fluorescence images of **172** and its colocalization study with MitoTracker Red in HeLa cells. (c) Fluorescence images of cells treated by the mixture of RPE and **172**. (b) and (c) are adapted with permission from ref. 331. Copyright 2018 American Chemical Society.

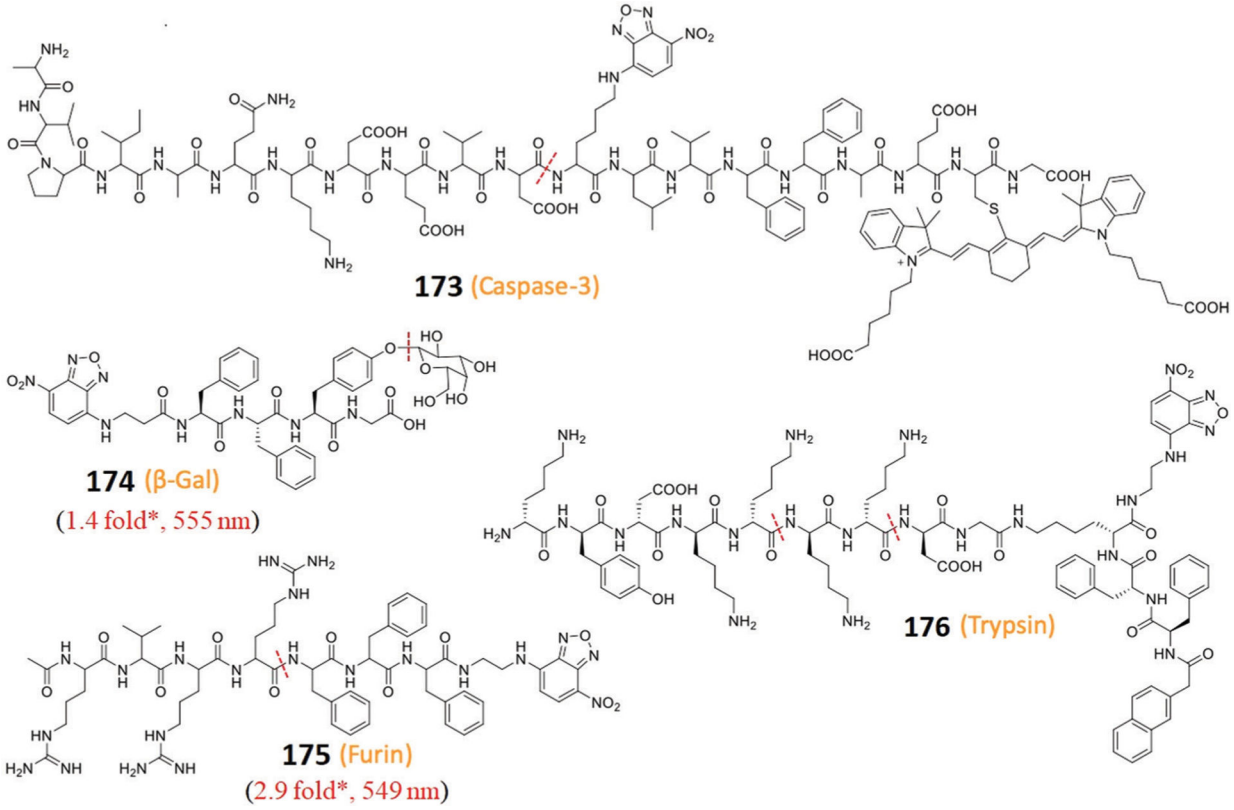

Fig. 64.

Chemical structures of self-assembled probes **173–176**. The enzymes for triggering the self-assembly are shown below each probe; all cleavage sites are highlighted by a red dotted line. * Represents estimated response from the reported spectra.

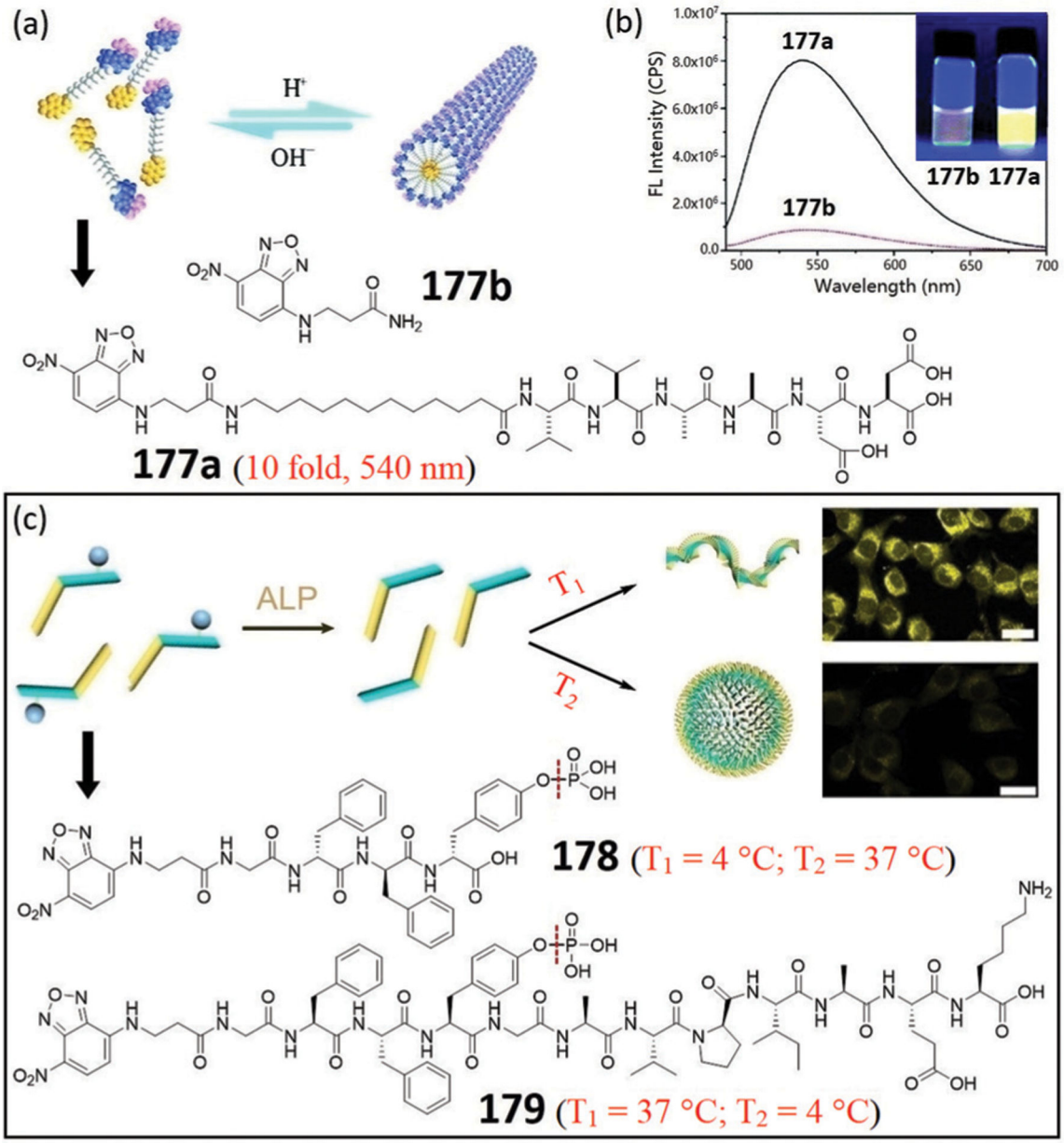

Fig. 65.

(a) Illustration of sol–gel transitions of **177a** *via* pH change. (b) Fluorescence spectra and photo (inset) of the probes under a 365 nm UV lamp. (c) Chemical structures of **178** and **179** and illustration of the self-assembly at different temperatures and the corresponding fluorescence images of cells. (a)–(c) are adapted with permission from ref. 336 and 337. Copyright 2019 Royal Society of Chemistry, 2017 American Chemical Society, respectively.

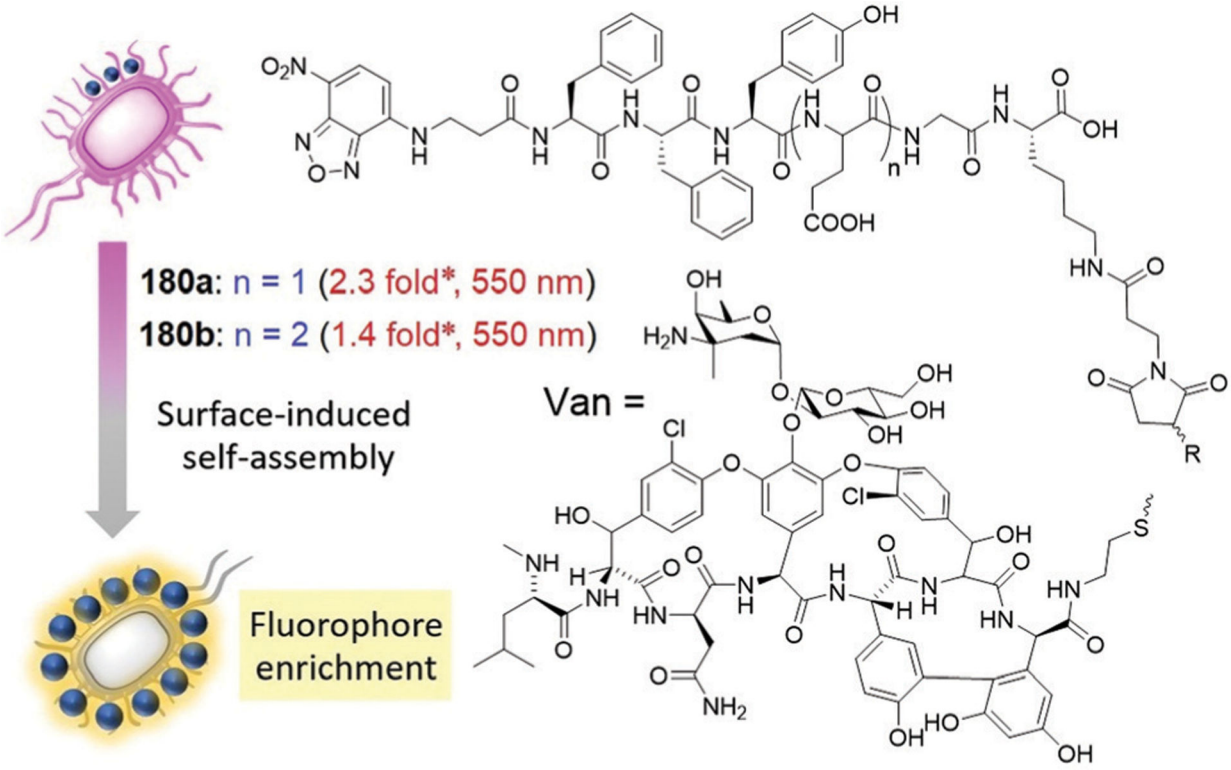

Fig. 66.

Chemical structures of **180a–180b** and illustration of bacterial surface-induced self-assembly. * Represents estimated response from the reported spectra.

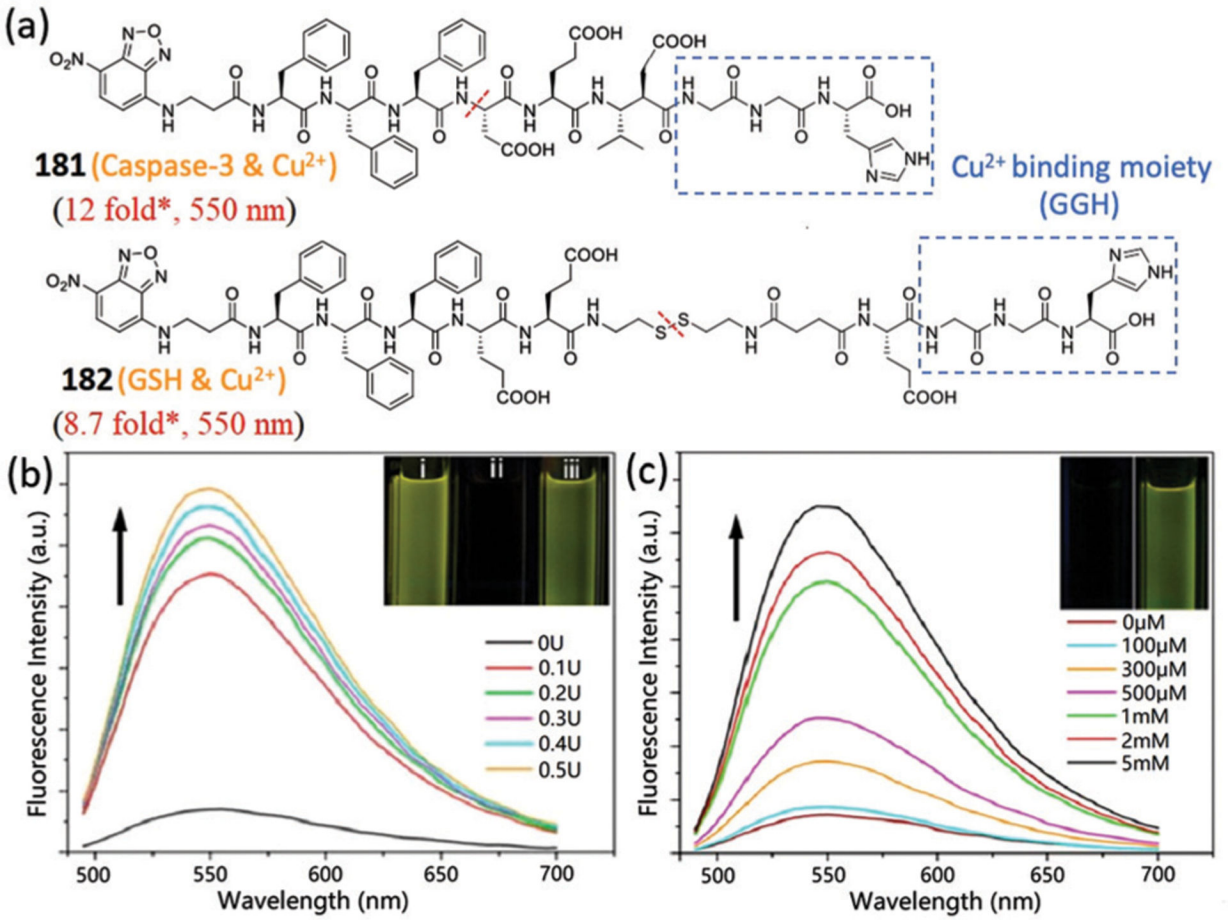

Fig. 67.

(a) Chemical structures of probes **181** and **182**. * Represents estimated response from the reported spectra. (b) Fluorescence spectra of **181**:Cu^{2+} upon treatment with different concentrations of caspase-3. Inset: Optical images of **181**, **181**:Cu^{2+}, **181**:Cu^{2+} with caspase-3, under a UV lamp. (c) Fluorescence spectra of **182**:Cu^{2+} upon treatment with different concentrations of GSH. Inset: Optical images of **182**:Cu^{2+} without and with GSH under a UV lamp. (b) and (c) are adapted with permission from ref. 340. Copyright 2014 American Chemical Society.

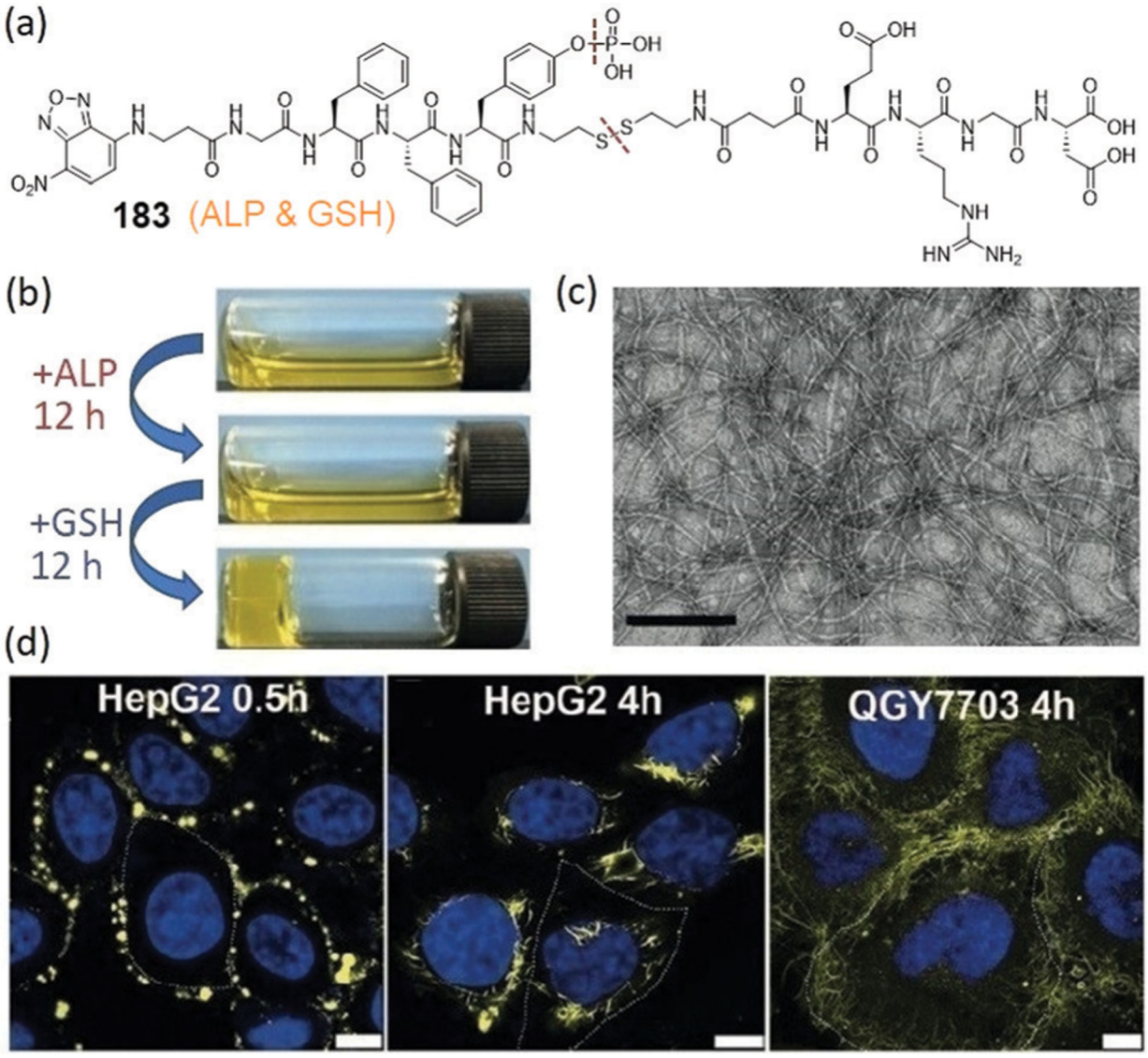

Fig. 68.

(a) Chemical structure of **183**. (b) Optical images of **183** after adding ALP and then GSH. (c) TEM image of **183** treated with both ALP and GSH. (d) Merged confocal images of HepG2 and QGY7703 cells incubated with **183** for different times. (b)–(d) are adapted with permission from ref. 341. Copyright 2018 Wiley-VCH.

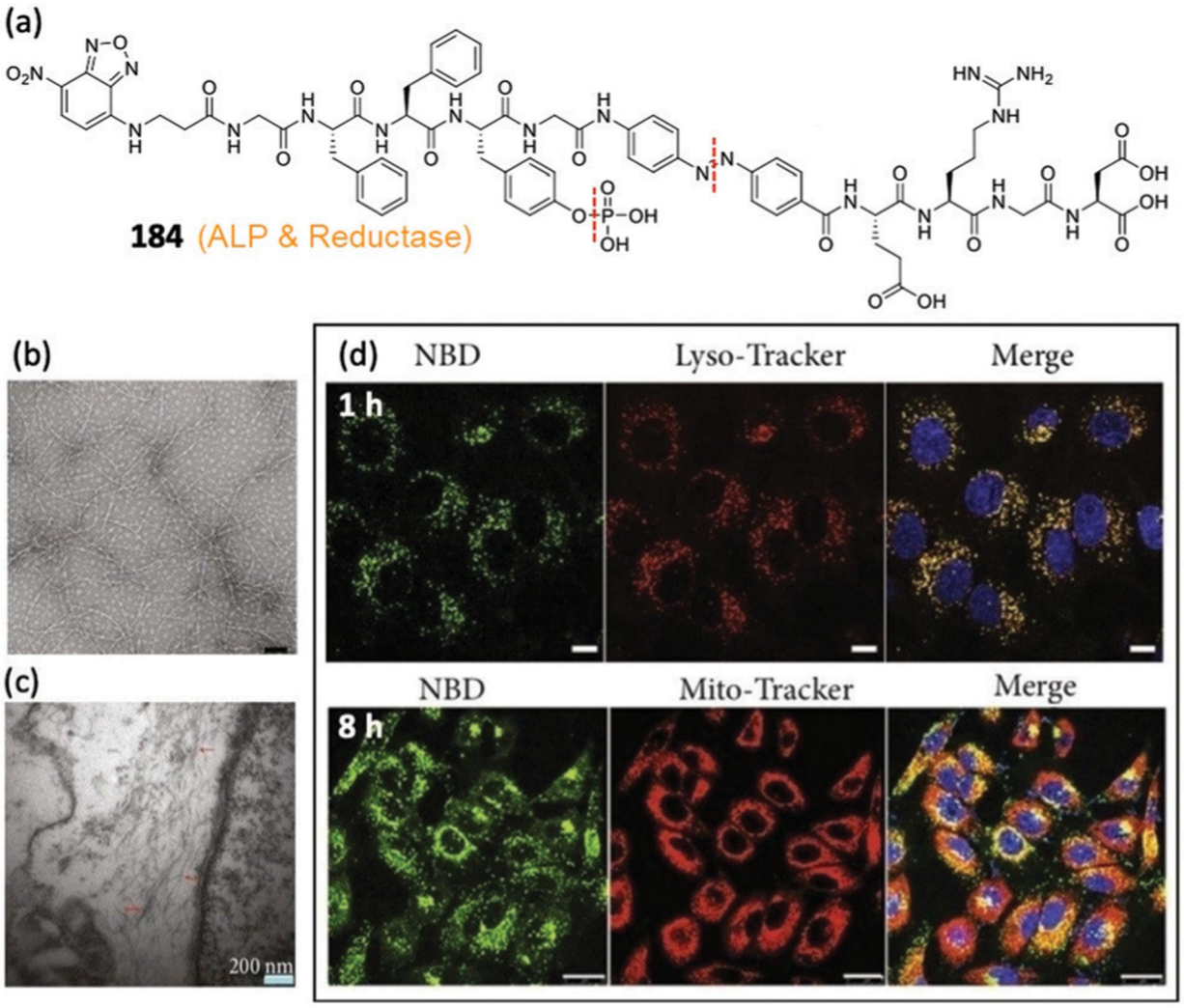

Fig. 69.

(a) Chemical structure of **184**. (b and c) TEM images of **184** treated with ALP for 24 h and ultrathin section of A549 cells at 6 h post administration of **184**, respectively. (d) Time-dependent confocal images of A549 cells treated with **184** and Lyso-tracker or Mito-tracker. (b)–(d) are adapted with permission from ref. 342. Copyright 2019 American Association for the Advancement of Science.

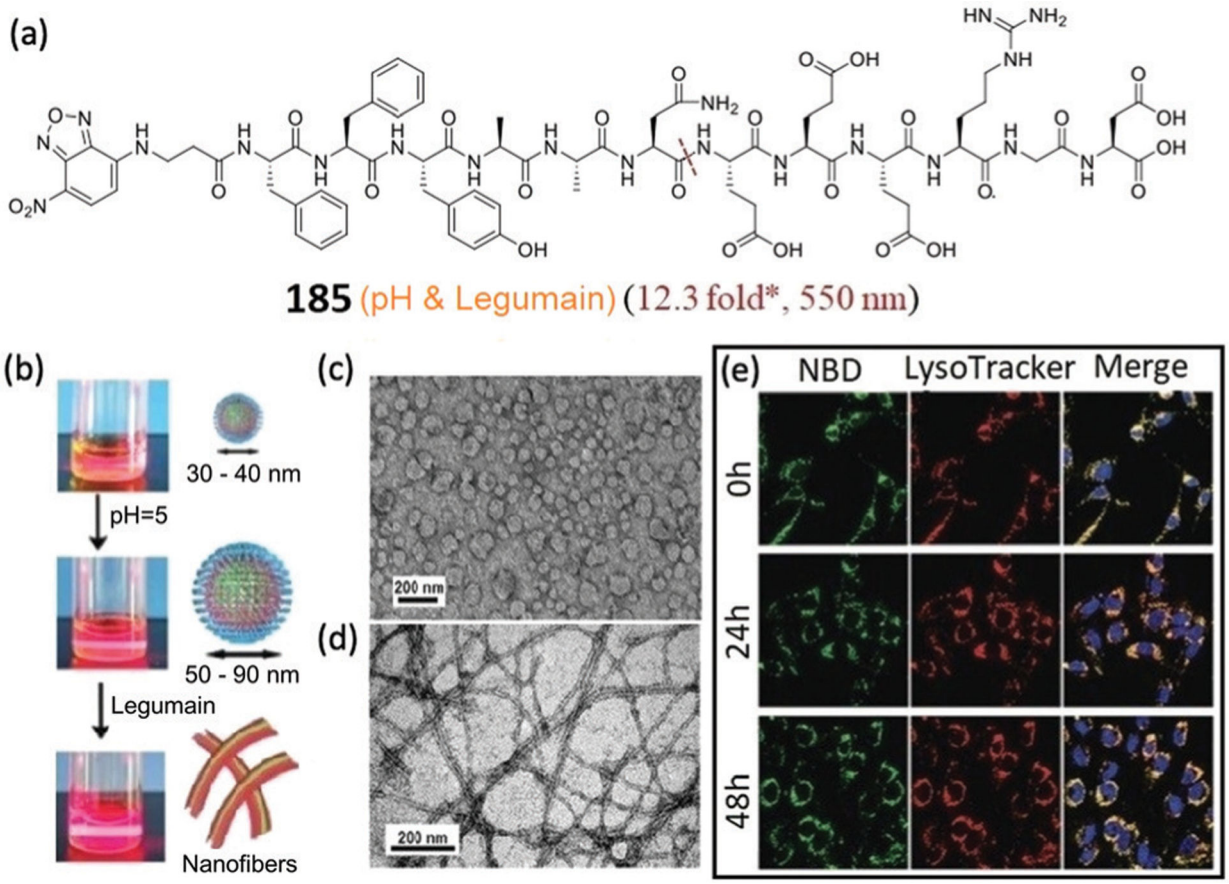

Fig. 70.

(a) Chemical structure of **185**. * Represents estimated response from the reported spectra. (b) Optical images with laser beam of **185** induced by pH change and then legumain. (c and d) TEM images of **185** at pH 5.0 for 2 h and then with legumain, respectively. (e) Confocal images of C6 cells incubated with **185** for 4 h, and then further cultured for 0–48 h. (b)–(e) are adapted with permission from ref. 343. Copyright 2020 Royal Society of Chemistry.

Fluorescent probes	Sensing mode	Change at maximum emission wavelength	Sensing mechanism	Properties of NBD	Applications
NBD–N(R)–Fluoro	Fluorophore < NBD H_2S (turn-on)	6.5~200 fold	FRET/PET	Electrophilicity; Quencher	Enzyme assay; Bioimaging; Prodrug
	Fluorophore > NBD H_2S (turn-on)	4.5~160 fold	PET		
NBD–N(R)(R')	H_2S (turn-off)	< 26 fold	NBD-NRR' ↓ NBD-SH	Electrophilicity	PA imaging; ECL sensor; H_2S scavenger
NBD–O/S–Fluoro	H_2S/GSH (turn-on)	17~1000 fold	PET/ICT	Electrophilicity; Quencher	Bioimaging
NBD–O/S–R	Cys/Hcy (turn-on)	3.6~745 fold	NBD-SR ↓ NBD-NHR	Electrophilicity	Bioimaging
NBD–O–ligand	Lys residues/ Intramolecular amino group (turn on)	5.2~60 fold	NBD-OR ↓ NBD-NHR	Electrophilicity; Small size	Bioimaging; Protein labeling; Enzyme assay
NBD–NH–ligand	Proteins (turn-on)	2.4~50 fold	Biomolecular interactions	Environmental sensitivity; Small size; Water solubility	Bioimaging; Sensing proteins; Enzyme assay
	Protein (turn-off)	3.3 fold	PET		Sensing protein
NBD–NH–precursor	Triggers (turn-on)	< 13 fold	Self-assembly; Fluorophore enrichment	Environmental sensitivity; Small size; Water solubility	Bioimaging; Drug delivery; Enzyme assay; Radiosensitizers •••••

Fig. 71.

Summary of properties and sensing mechanisms for major NBD-based synthetic probes and their applications.

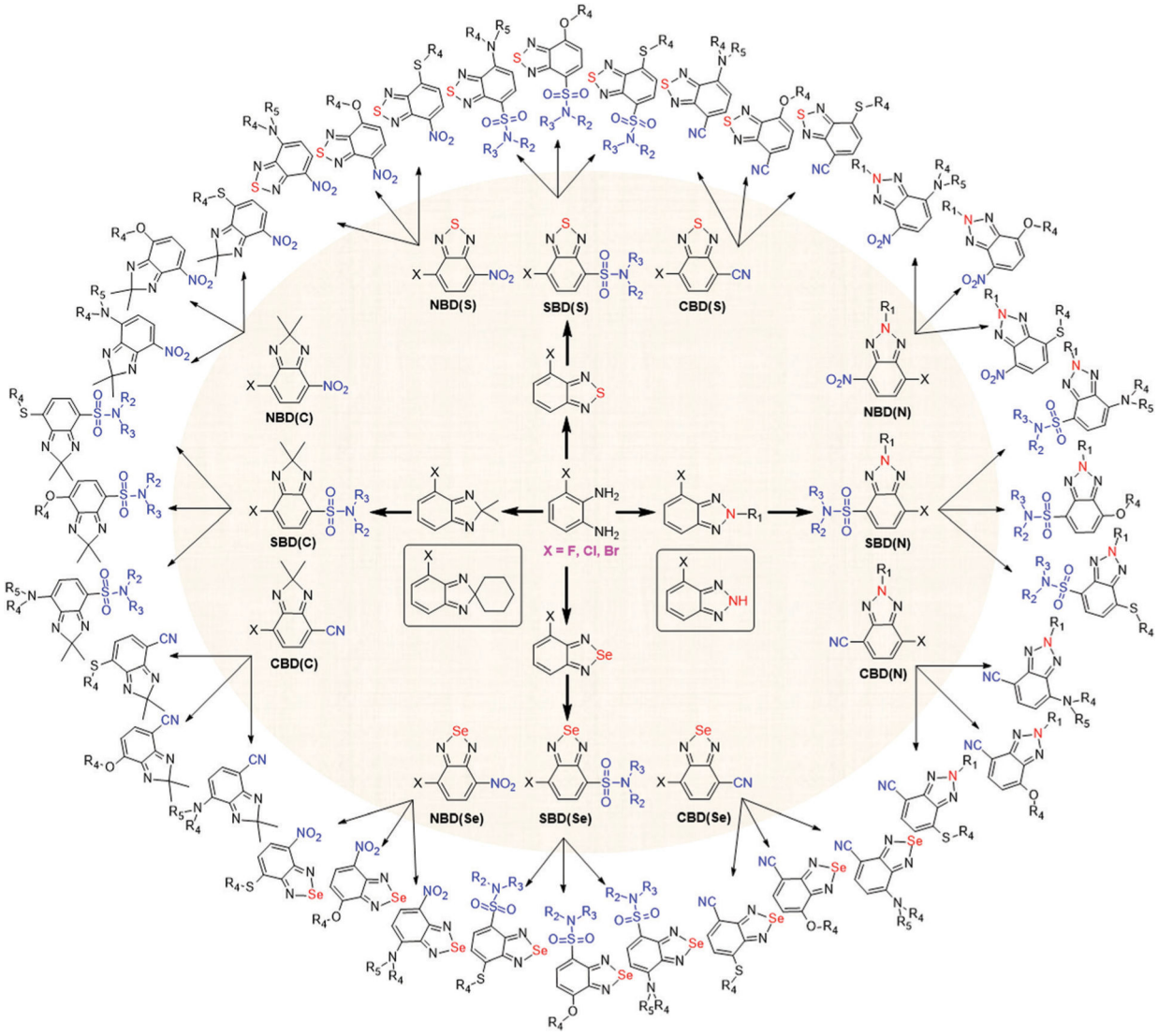

Fig. 72.

Chemical structures of potential BD derivatives with (1) different substitutions at the oxygen atom of the oxazole group; (2) different electron-withdrawing groups at the 7-position; and (3) different reactable groups at the 4-position.